

Production and Properties of Fibre Webs Containing Self-Assembling Peptides for Promotion of Hard Tissue Repair

Robabeh Gharaei

Submitted in accordance with the requirements for the degree of Doctor of
Philosophy

**The University of Leeds
School of Design**

January 2017

The candidate confirms that the work submitted is her own, except where work which has formed part of jointly authored publications has been included. The contribution of the candidate and the other authors to this work has been explicitly indicated below. The candidate confirms that appropriate credit has been given within the thesis where reference has been made to the work of others.

Parts of the work in Chapter 4 and Chapter 5 of the thesis has appeared in publications as follows:

1) Gharaei, R., Tronci, G., Davies, R. P., Goswami, P., & Russell, S. J. (2016). An investigation into the nano-/micro-architecture of electrospun poly (ϵ -caprolactone) and self-assembling peptide fibers. *MRS Advances*, 1(11), 711-716.

2) Gharaei, R., Tronci, G., Davies, R. P., Gough, C., Alazragi, R., Goswami, P., & Russell, S. J. (2016). A structurally self-assembled peptide nano-architecture by one-step electrospinning. *Journal of Materials Chemistry B*, 4(32), 5475-5485.

Robabeh Gharaei was solely responsible for performing the experiments and doing the analysis. The other authors assisted with the reading, reviewing and planning the layout of the papers.

This copy has been supplied on the understanding that it is copyright material and that no quotation from the thesis may be published without proper acknowledgement.

Acknowledgement

Undertaking this PhD has been a truly life-changing experience for me and it would not have been possible to do it without the help of my God and support and guidance that I received from many people.

Firstly I would like to say a very big thank you to both of my supervisors, Prof Stephen Russell and Dr. Parikshit Goswami for their continued support, enthusiasm and guidance throughout this PhD. This work would not have been achievable without their guidance and feedbacks.

Secondly I would like to thank Mr Mark Tucker, alumnus of the University of Leeds, for his financial contribution during this research.

I greatly appreciate the academic advice, help and supports received through the collaborative work undertaken with Dr. Giuseppe Tronci of the Nonwovens Research Group, Dr. Robert Davies, Sam Whitworth and Dr Caroline Gough from Biomaterials and Tissue Engineering Research Group and – thank to Dr. Reem Alazragi for her helps during the first few months of the study. I also would like to expand my thanks to Prof Jennifer Kirkham, Head of Oral Biology Department, for her invaluable supports and kind encouragements.

I wish to express my deepest appreciation and love to my parents, Gholamreza Gharaei and Sakineh Amini, and my beloved brother Ali Gharaei for their encouragement, inspiration and reassurance.

Finally a special thank to my loving husband, Hamidreza Arouni, for his endless love and supports that kept me strong and motivated throughout this journey.

Abstract

Self-assembling peptides (SAPs) have attracted interest due to their potential value in therapeutics. The 11-residue family of peptides (P₁₁-X), are able to self-assemble hierarchically into β -sheet tapes with higher order structures (ribbons, fibrils and fibres) being produced depending on peptide concentration. Previous studies of P₁₁-X peptides aimed at tissue repair focused on hydrogel formats where their potential for deposition of hard tissue minerals *in vivo* was demonstrated due in part to their ability to mimic the physiochemical properties of natural extracellular matrix (ECM) of bone. However, SAP hydrogels are often associated with inherently weak and transient mechanical properties, which make their handling and fixation challenging in large load-bearing tissue defects. Accordingly, to engineer a more robust scaffold, the present research demonstrates the feasibility of producing electrospun webs composed of a biodegradable polymer, poly (e-caprolactone) (PCL) commixed with either P₁₁-4 (Ac-QQRFWEFEQQ-Am) or P₁₁-8 (Ac QQRFOWOFEQQ-Am) self-assembling peptides. Morphological features of the electrospun webs investigated via scanning and transmission electron microscopies (SEM and TEM) revealed that PCL/P₁₁-4 and PCL/P₁₁-8 electrospun webs contain fibres in both nano- (10–100 nm) and submicron ranges (100–700 nm), whereas PCL fibre webs, produce a predominantly submicron fibre distribution. Homogeneous distribution of SAPs within the electrospun fibres was revealed via confocal microscopy. . Furthermore, it was discovered by spectroscopic analysis that SAPs exist entirely in their monomeric state in the electrospinning solution, and convert from monomeric form to β -sheet secondary conformation when converted into fibres. PCL/SAP fibres were shown to exhibit enhanced hydrophilicity compared to PCL-only fibres, and induce no cytotoxic response when cultured with L929 mouse fibroblasts. A study of the release kinetics of SAP from PCL fibres

in simulated conditions of biological pH (neutral pH of 7.4) after 7 days revealed at least 75% of P₁₁₋₄ and 45% of P₁₁₋₈ still remained, suggesting potential for long-term therapeutic delivery. Finally the ability of SAP embedded PCL fibrous scaffold to nucleate and support growth of bone minerals was investigated using two *in vitro* assays, specifically the simulated body fluid (SBF) method and the *in vitro* nucleation (IVN) tank method. PCL/SAP fibres were found to nucleate and support spheroidal growth of hydroxyapatite crystals and were capable of comparable mineral nucleation performance as SAP hydrogels.

Table of Contents

Chapter

Chapter 1: Introduction	1
1.1 General Tissue Engineering	2
1.2 Electrospun Polymer Webs as Tissue Engineering Scaffolds.....	3
1.3 Self-assembling Peptides.....	5
1.4 Aims and Objectives	6
Chapter 2: Review of Literature	8
2.1 Introduction	8
2.1.1 Principles of Mineral Crystal Nucleation and Secondary Crystal Growth	8
2.1.2 Biomineralisation.....	9
2.1.3 Biological Apatite	10
2.2 Mineralised Tissues.....	10
2.2.1 Bone	10
2.2.2 Teeth	12
2.2.3 Clinical Challenges in Mineralised Tissue Repair.....	13
2.3 Tissue Engineering.....	14
2.3.1 Engineering of Mineralised Tissues.....	15
2.3.2 Design of Scaffolds for Hard Tissue Engineering	17
2.3.2.1 Scaffold Structure	18
2.3.2.2 Biomaterials for Scaffolds	19

2.3.3	Biomimetic Approach.....	22
2.4	Self-assembling Peptides.....	22
2.4.1	Peptides and Protein.....	22
2.4.2	Peptide Self-assembly mechanism.....	25
2.4.3	P ₁₁ Peptides	25
2.4.3.1	P ₁₁ Peptides Background.....	26
2.4.3.2	Triggers to Peptide Self-assembly	28
2.4.4	Self-assembling Peptides Used in This Study	29
2.4.5	Peptides Investigated for Hard Tissue Engineering.....	30
2.5	Electrospun Scaffolds.....	32
2.5.1	Principles of Electrospinning	34
2.5.2	Electrospinning Parameters	36
2.5.2.1	Polymer Solution Parameters	36
2.5.2.2	Processing Parameters.....	38
2.5.2.3	Ambient Condition Parameters	42
2.5.3	Production of Electrospun Scaffolds Containing Self-assembling Peptides	43
2.6	Summary	44
Chapter 3: Materials and Methods		47
3.1	Materials.....	47
3.2	Experimental methods.....	49
3.2.1	Electrospinning Solution Preparation	49
3.2.2	Needle Electrospinning.....	50
3.2.3	Scanning Electron Microscopy (SEM)	52

3.2.4	Fibre Diameter Measurements	53
3.2.5	Transmission Electron Microscopy (TEM)	53
3.2.6	Environmental Scanning Electron Microscopy (ESEM).....	54
3.2.7	Confocal Laser Scanning Microscopy (CLSM)	55
3.2.8	Energy-Dispersive X-Ray Spectroscopy (EDX)	56
3.2.9	X-Ray Diffraction Crystallography (XRD)	56
3.2.10	Fourier Transform Infra-Red Spectroscopy (FTIR)	57
3.2.11	Circular Dichroism Spectroscopy (CD).....	58
3.2.12	Contact Angle Measurement.....	58
3.2.13	BS EN ISO 10993:2009 Biological Evaluation of Medical Devices (Cytotoxicity).....	59
3.2.13.1	Extract Cytotoxicity Method.....	59
3.2.13.2	Direct Cytotoxicity Method	62
3.2.14	BS ISO 23317:2014 <i>In Vitro</i> Evaluation for Apatite-Forming Ability of Materials Using Simulated Body Fluid (SBF).....	65
3.2.14.1	Preparation of Test Specimens.....	65
3.2.14.2	Preparation of Simulated Body Fluid (SBF).....	65
3.2.14.3	Calculation of Volume of SBF.....	68
3.2.15	Peptide Release from Electrospun PCL/SAPs Fibres in Water	69
3.2.15.1	Thermogravimetric Analysis (TGA).....	70
3.2.16	IVN Tank Apparatus.....	71
3.2.16.1	Preparation of Calcium and Phosphate Buffers	73
3.2.16.2	Preparation of Negative and Positive Control Samples	74
3.2.16.3	Assembling the Samples and the Controls for Testing	75
3.2.16.4	Phosphate Assay	78
3.2.16.5	Statistical Analysis of Data	78

Chapter 4: Characterisation of Electrospun PCL/SAPs Fibres.....79

4.1	Introduction	79
4.2	Experimental Details	79
4.2.1	100% PCL Electrospun Fibres	79
4.2.2	PCL/SAPs Electrospun Fibres	80
4.2.3	Influence of the Polarity of the High Voltage Power Supply during Electrospinning on Fibre Morphology	81
4.2.4	Effect of Concentrations of SAP in PCL/SAPs Electrospun Fibres	81
4.2.5	Peptide Presence in Fibres; Energy-Dispersive X-Ray Spectroscopy	82
4.2.6	Peptide Distribution in Fibres; Florescent Microscopy	82
4.2.7	Peptide Secondary Structures in Solution and in As-Spun Fibres	83
4.2.7.1	Peptides Secondary Structure in Spinning Solution.....	83
4.2.7.2	Peptides Secondary Structure in As-Spun Fibres.....	85
4.3	Results and Discussion.....	86
4.3.1	Fibre Morphological Results of 100% PCL Electrospinning	86
4.3.2	Fibre Morphological Results of PCL/SAPs Electrospinning.....	88
4.3.2.1	SEM of As-Spun Fibre Webs.....	88
4.3.2.2	Fibre Diameter in the PCL/SAPs Electrospun Webs	89
4.3.2.3	SEM Of Fibres Produced with Different Electrode Polarities in the Electrospinning Setup	91
4.3.2.4	TEM of As-Spun Electrospun Fibre Webs	92
4.3.2.5	ESEM of PCL/SAPs Multi-Scale Fibrous Structure.....	93
4.3.3	Effect of Peptide Concentration on Fibre Morphology and Diameter.....	96
4.3.3.1	Effect of P ₁₁ -8 Concentration on PCL/P ₁₁ -8 Fibre Morphology	96
4.3.3.2	Effect of P ₁₁ -4 Concentration on PCL/P ₁₁ -4 Fibre Morphology	96
4.3.4	Peptide Presence and Distribution in Fibres	99

4.3.4.1	Elemental Analysis on PCL/SAPs Fibre Webs by SEM-EDX	99
4.3.4.2	Elemental Analysis on PCL/P ₁₁ -8 Fibre Webs by TEM-EDX.....	100
4.3.4.3	SAPs distribution analysis on PCL/SAPs fibre webs by CLSM.....	102
4.3.5	Peptide Secondary State in PCL/SAPs Solutions	104
4.3.5.1	Peptide Secondary Structure in PCL/SAPs Solutions by CD Analysis	104
4.3.5.2	Peptide Secondary Structure in PCL/SAPs Solutions by FTIR Analysis	106
4.3.6	Peptide Secondary State in PCL/SAPs As-Spun Fibres	108
4.3.6.1	Peptide Secondary Structure in PCL/SAPs Fibre Webs by ATR-FTIR Analysis ..	108
4.4	Summary	110

Chapter 5: Biological Properties of Electrospun PCL/SAPs Fibre Webs.112

5.1	Introduction	112
5.2	Experimental Details	112
5.2.1	Wettability of PCL/SAPs Fibre Webs	112
5.2.2	Cytotoxicity Evaluation of PCL/SAPs Fibre Webs	114
5.2.2.1	Extract Cytotoxicity Method.....	114
5.2.2.2	Direct Cytotoxicity Method	116
5.2.3	Peptide Release Behaviour of PCL/SAPs Fibre Webs into Aqueous Solution	117
5.3	Results and Discussion.....	120
5.3.1	Wettability Behaviour of Electrospun PCL/SAPs Fibre Webs.....	120
5.3.1.1	Contact Angle of Water on PCL/SAPs Electrospun Fibres	120
5.3.1.2	Contact Angle of DMEM on PCL/SAPs Electrospun Fibres	124
5.3.1.3	Contact Angle of Water on PCL/SAP Films.....	127
5.3.2	Cytotoxicity Assessment of PCL/SAPs Electrospun Fibres.....	129
5.3.2.1	Result of Extract Cytotoxicity assessment of PCL/SAPs Fibres	129
5.3.2.2	Results of Direct Cytotoxicity assessment of PCL/SAPs Fibres	132
5.3.3	Peptide Release Behaviour of PCL/SAPs Fibres.....	135
5.3.3.1	Mass Loss of Electrospun Fibres after Dissolution.....	135

5.3.3.2	Effect of Peptide Release on the Morphology of PCL/SAPs Fibres	140
5.3.3.3	Peptide Release into Solution by CD analysis	146
5.4	Summary	149

Chapter 6: In Vitro Evaluations for Apatite Forming Ability of PCL/SAPs

Fibre Webs.....151

6.1	Introduction	151
6.2	Experimental Details	152
6.2.1	Nucleation of Apatite in Simulated Body Fluid (SBF).....	152
6.2.2	Nucleation of Apatite in the <i>In Vitro</i> Nucleation (IVN) Tank.....	153
6.3	Results and Discussion.....	156
6.3.1	Apatite Forming Ability of PCL/SAPs Fibres in SBF.....	156
6.3.1.1	SBF Method - First Experiment.....	156
6.3.1.2	SBF method - Second Experiment.....	158
6.3.2	IVN Tank Results	173
6.4	Summary	182

7 Conclusions.....184

7.1	General Conclusions	184
7.2	Recommendations for Further Work.....	190

References.....192

List of Figures

Figure 2-1. Schematic diagram indicating the main tissues of tooth (70).	13
Figure 2-2. Cell based bone tissue engineering, involving the application of metabolically active cells and growth factors using a 3D scaffold for functional bone tissue regeneration (12).	16
Figure 2-3: Molecular repeat structure of PCL.	21
Figure 2-4: The condensation of two amino acids forming the peptide linkage (129).	23
Figure 2-5: Extended peptide chain known as β -strand (129).	24
Figure 2-6: Parallel and antiparallel β -sheet, the dotted lines indicate the hydrogen bonds between the chains (129).	25
Figure 2-7: Hierarchical self-assembly model for chiral rod-like units (image adapted from Aggeli et al. (140)).	27
Figure 2-8. Graphs showing the change in state of (A) P ₁₁₋₄ and (B) P ₁₁₋₈ in response to a change in pH of the solution (47).	28
Figure 2-9. Schematic diagram of the needle electrospinning process (image adopted from Ke et al.) (162).	35
Figure 3-1. Examples of SEM micrographs with fibre diameter measurements being made along the yellow lines.	53
Figure 3-2. An acceptable level of L929 cell confluency for cytotoxicity test (image from the current study).	60
Figure 3-3. Apparatus for preparing SBF (198).	67
Figure 3-4. <i>In vitro</i> nucleation tank apparatus.	72
Figure 3-5. Steps 1 to 8 to assemble the samples in the IVN tank.	76
Figure 3-6. Fibrous disk sample embedded in agarose gel.	77
Figure 4-1. SEM micrographs of electrospun webs produced from PCL in HFIP solutions at different PCL combination of concentration, voltage (V) and tip to collector distance (D).	87
Figure 4-2. SEM micrographs of, first row: 100% PCL; second row: PCL/P ₁₁₋₄ and third row: PCL/P ₁₁₋₈ electrospun fibres.	89
Figure 4-3. Fibre diameter distribution of (A) PCL, (B) PCL/P ₁₁₋₄ and (C) PCL/P ₁₁₋₈ webs.	90
Figure 4-4. SEM micrographs of PCL/P ₁₁₋₄ produced with: (first row) negative electrode and (second row) positive electrode. SEM micrographs of PCL/P ₁₁₋₈ produced with: (third row) negative electrode and (fourth row) positive electrode.	91

Figure 4-5. TEM images of PCL/P ₁₁₋₈ with a peptide concentration of 20 mg mL ⁻¹ at 150Kx (top row) and 231Kx (bottom row) magnifications.	92
Figure 4-6. ESEM micrographs of wet and uncoated PCL/P ₁₁₋₈ with peptide concentration of 20 mg mL ⁻¹ , (A) immediately after mounting in microscope and (B) after 25 minutes.....	94
Figure 4-7. ESEM micrographs of vacuum dried but uncoated PCL/P ₁₁₋₈ with peptide concentration of 20 mg mL ⁻¹ , at 30Kx (left) and 60Kx (right) magnifications.	95
Figure 4-8. ESEM (high vacuum mode) micrographs of vacuum dried and coated PCL/P ₁₁₋₈ with peptide concentration of 20 mg mL ⁻¹ , at 30Kx (left) and 60Kx (right) magnifications.	95
Figure 4-9. SEM micrographs of (first row) PCL fibres, (second row) PCL/P ₁₁₋₈ with peptide concentration of 10 mg mL ⁻¹ , (third row) PCL/P ₁₁₋₈ with peptide concentration: 20 mg mL ⁻¹ and (fourth row) PCL/P ₁₁₋₈ with peptide concentration: 40 mg mL ⁻¹	97
Figure 4-10. SEM micrographs of (first row) 100% PCL fibres, (second row) PCL/P ₁₁₋₄ with peptide concentration of 10 mg mL ⁻¹ , (third row) PCL/P ₁₁₋₄ with peptide concentration of 20 mg mL ⁻¹ and (fourth row) PCL/P ₁₁₋₄ with peptide concentration of 40 mg mL ⁻¹	98
Figure 4-11. SEM/EDX analysis of electrospun (A) PCL, (B) PCL/P ₁₁₋₄ and (C) PCL/P ₁₁₋₈ fibres.	99
Figure 4-12. (A) TEM micrograph of PCL/P ₁₁₋₈ and magnified micrographs are showing both submicron fibre and nanofibre. EDX spectroscopy analysis (full scale and magnified scale) are showing the presence of nitrogen element in both of (B) submicron and (C) nanofibre.	101
Figure 4-13. CLSM micrographs of electrospun (A) PCL, (B) PCL/P ₁₁₋₄ and (C) PCL/P ₁₁₋₈ fibres in which peptide samples are fluorescently tagged.	103
Figure 4-14. CD spectra of (A) 20 mg mL ⁻¹ P ₁₁₋₄ solution in 6% w/w PCL/HFIP; (B) 20 mg mL ⁻¹ P ₁₁₋₈ solution in 6% w/w PCL/HFIP (Electrospinning condition), (C) 20 mg mL ⁻¹ P ₁₁₋₄ solution in HFIP and (D) 20 mg mL ⁻¹ P ₁₁₋₈ in HFIP.	105
Figure 4-15. FTIR spectra of PCL and PCL/P ₁₁₋₄ in a HFIP solution at different peptide concentrations.	107
Figure 4-16. FTIR spectra of PCL and PCL/P ₁₁₋₈ in a HFIP solution at different peptide concentrations.	107
Figure 4-17. FTIR spectra of PCL and PCL/P ₁₁₋₄ electrospun fibres at different peptide concentration.	109
Figure 4-18. FTIR spectra of PCL and PCL/P ₁₁₋₈ electrospun fibres at different peptide concentrations.	110
Figure 5-1. Positioning of samples in a 96-well plate for the extract cytotoxicity assay. PCL extract was used as a negative control in row one, PCL/P ₁₁₋₄ extract in row two and PCL/P ₁₁₋₈ extract in row three. Blank DMEM is in row four and the positive control (DMSO) in row five.	115

Figure 5-2. The position of samples in two 24-well plates for direct cytotoxicity assay.	116
Figure 5-3. Self-assembly of peptides from monomers in isotropic fluid to β -sheet tapes, ribbons, fibril and fibres in nematic gel form.	118
Figure 5-4. Transformation from isotropic fluid (monomer) to nematic gel (β -sheet) of (A) P ₁₁₋₄ and (B) P ₁₁₋₈ as a function of pH (47).	118
Figure 5-5. Initial contact angle of a deionised water droplet on electrospun fibre webs (at time = 0 s) on (A) 100% PCL, (B) PCL/P ₁₁₋₄ at a peptide concentration of 10 and (C) 20 mg mL ⁻¹ , (D) PCL/P ₁₁₋₈ at a peptide concentration of 10 and (E) 20 mg mL ⁻¹	122
Figure 5-6. Dynamic contact angle measurements of a droplet of water on (A) PCL, (B) PCL/P ₁₁₋₄ and (C) PCL/P ₁₁₋₈ electrospun fibre webs up to 15 s.	123
Figure 5-7. Initial contact angle of a DMEM liquid droplet on electrospun fibre webs (at time = 0 s) on (A) 100% PCL, (B) PCL/P ₁₁₋₄ at a peptide concentration of 10 and (C) 20 mg mL ⁻¹ , (D) PCL/P ₁₁₋₈ at a peptide concentration of 10 and (E) 20 mg mL ⁻¹	125
Figure 5-8. Dynamic contact angle measurements of a droplet of DMEM on (A) PCL, (B) PCL/P ₁₁₋₄ and (C) PCL/P ₁₁₋₈ electrospun fibre webs up to 15 s.	126
Figure 5-9. Initial contact angle of a droplet of deionised water on (A) PCL and (B) PCL/P ₁₁₋₈ cast films at a peptide concentration of 10 and (C) 20 mg mL ⁻¹ . (D) Dynamic contact angle measurements of a droplet of deionised water on PCL and PCL/P ₁₁₋₈ cast films.	128
Figure 5-10. Optical monochrome digital micrographs of cells treated with the sample extracts; (A) PCL, (B) PCL/P ₁₁₋₄ , (C) PCL/P ₁₁₋₈ , (D) DMEM and (E) DMSO.	130
Figure 5-11. UV absorption of extract samples at 490 nm related to the quantity of formazan produced and the number of living cells.	131
Figure 5-12. Optical monochrome digital micrographs of cells treated with (A) negative sample of PCL, (B) PCL/P ₁₁₋₄ and (C) PCL/P ₁₁₋₈ fibres.	133
Figure 5-13. Optical density absorption of samples at 570-650 nm correlated to the number of living cells.	134
Figure 5-14. Overall percentage (%) of mass loss from electrospun fibres at different pH.	136
Figure 5-15. Mass loss analysis by TGA of (A) PCL/P ₁₁₋₄ fibres after 7 d incubation and 3-times wash in pH 10.5 and (B) PCL/P ₁₁₋₈ fibres after 7 d incubation and 3-times wash in pH 3.5.	139
Figure 5-16 SEM micrographs of 100% PCL fibre webs before and after incubation at pH 3.5 and 10.5 for 1 d and 7 d.	141
Figure 5-17. SEM micrographs of PCL/P ₁₁₋₈ fibre webs before and after incubation at pH 3.5, 7.5 and 10.5 for 1 h and 1 d.	142

Figure 5-18. SEM micrographs of PCL/P11-4 fibre webs after incubation at pH 3.5 and 10.5 for 2 and 7 d.	144
Figure 5-19. SEM micrographs of PCL/P11-8 fibre webs after incubation at pH 3.5 and 10.5 for 2 and 7 d.	145
Figure 5-20. CD spectra of supernatant of fibrous samples dissolved in water for 1d and 7 d at (A) pH 3.5 and (B) pH 10.5.	147
Figure 5-21. CD spectra of the original supernatant and the three step washing process supernatants of electrospun web samples dissolved for 7 d of (A) PCL/P ₁₁₋₄ fibres in pH 10.5 and (B) PCL/P ₁₁₋₈ fibres in pH 3.5.	148
Figure 6-1. Preparation of fibrous electrospun or hydrogel samples for the IVN tank assay (A) positive, negative and PCL fibre control, (B) SAP hydrogel samples and (C) PCL/SAPs fibre samples with their associated SAP concentration.	154
Figure 6-2. Calibration curve of phosphate concentration (μM) using spectrophotometry.	155
Figure 6-3. SEM micrographs of electrospun fibres after 3 d incubation in SBF along with the atomic percentage of element content as determined from EDX analysis (A) PCL fibres, (B) PCL/P ₁₁₋₄ with peptide concentration of 20 mg mL^{-1} and (C) PCL/P ₁₁₋₈ with peptide concentration of 20 mg mL^{-1}	157
Figure 6-4. SEM micrographs of electrospun fibres after 7 d incubation in SBF along with the atomic percentage of element content as determined from EDX analysis (A) PCL fibres, (B) PCL/P ₁₁₋₄ with peptide concentration of 20 mg mL^{-1} and (C) PCL/P ₁₁₋₈ with peptide concentration of 20 mg mL^{-1}	157
Figure 6-5. SEM micrographs of electrospun fibres after two weeks incubation in SBF along with the atomic percentage of element content as determined from EDX analysis (A) PCL fibres, (B) PCL/P ₁₁₋₄ with peptide concentration of 20 mg mL^{-1} and (C) PCL/P ₁₁₋₈ with peptide concentration of 20 mg mL^{-1}	158
Figure 6-6. SEM micrographs of electrospun fibres after one week incubation in SBF.	160
Figure 6-7. SEM micrographs of electrospun fibres after two weeks incubation in SBF.	161
Figure 6-8. SEM micrographs of electrospun fibres after four weeks incubation in SBF.	162
Figure 6-9. Low magnification SEM micrographs of mineralised PCL/P ₁₁₋₄ fibres after (A) 1 week, (B) 2 weeks and (C) 4 weeks incubation in SBF showing the distribution of crystals formed all over the fibres.	163
Figure 6-10. EDX spectra of PCL/P ₁₁₋₄ fibres immersed in SBF for 2 weeks.	164
Figure 6-11. FTIR bands of electrospun PCL fibres before and after incubation in SBF.	167
Figure 6-12. FTIR bands of electrospun (A) PCL/P ₁₁₋₄ and (B) PCL/P ₁₁₋₈ fibres before and after incubation in SBF.	168

Figure 6-13. X-ray diffraction patterns of electrospun PCL fibres (A) before, (B) and (C) after 2 weeks, (D) and (E) after 4 weeks incubation in SBF.	170
Figure 6-14. X-ray diffraction patterns of electrospun PCL/P ₁₁ -4 fibres (A) before, (B) and (C) after 2 weeks, (D) and (E) after 4 weeks incubation in SBF.	171
Figure 6-15. X-ray diffraction patterns of electrospun PCL/P ₁₁ -8 fibres (A) before, (B) and (C) after 2 weeks, (D) and (E) after 4 weeks incubation in SBF.	172
Figure 6-16. IVN assay response of (A) peptide hydrogel samples and (B) electrospun fibrous samples at peptide concentration of 4 mg mL ⁻¹	174
Figure 6-17. IVN assay response of P ₁₁ -4 and P ₁₁ -8 in both hydrogel and electrospun fibrous structure at peptide concentration of 4 mg mL ⁻¹	175
Figure 6-18. IVN assay response of (A) peptide hydrogel samples and (B) electrospun fibrous samples at peptide concentration of 8 mg mL ⁻¹	177
Figure 6-19. IVN assay response of P ₁₁ -4 and P ₁₁ -8 in both hydrogel and electrospun fibrous structure at peptide concentration of 8 mg mL ⁻¹	178
Figure 6-20. IVN assay response of fibrous and hydrogel together versus peptide concentration. (N/S)= p≥0.05, (*) = p≤0.05, (**) = p≤0.01, (***) = p≤0.001, (****) = p≤0.0001.	179

List of Tables

Table 2-1. Diagrams showing the primary structure of P ₁₁₋₄ and P ₁₁₋₈ in physiological conditions (47).	30
Table 3-1. List of peptides used in the experimental work.....	47
Table 3-2. List of chemicals and reagents used in the experimental work.....	48
Table 3-3. Spinning solution compositions (w/w) and associated solute and solvent weights.	49
Table 3-4. Peptide content in each solution of PCL/P ₁₁₋₄	50
Table 3-5. Peptide content in each solution of PCL/P ₁₁₋₈	50
Table 3-6. Ratio (R) of mass of peptide to mass of peptide+PCL in the electrospinning solutions based on different peptide concentrations.....	52
Table 3-7. Ion concentration of SBF and human blood plasma.	66
Table 3-8. Reagents for preparation of SBF in the required order of dissolution.	66
Table 3-9. The reagents required to make 5 L of calcium buffer.....	73
Table 3-10. The reagents required to make 5 L of phosphate buffer.....	73
Table 3-11. The reagents required to make 1 L solution of 2x steady state buffer.....	74
Table 3-12. Negative and positive control samples in IVN tank.	75
Table 4-1. Fibre diameter in PCL, PCL/P ₁₁₋₄ and PCL/P ₁₁₋₈ webs (all data is nm).	90
Table 4-2. Atomic percentages of chemical elements in the electrospun fibres by SEM/EDX.	100
Table 4-3. Atomic percentages of chemical elements in the submicron and nanofiber of the electrospun PCL/P ₁₁₋₈ fibres by TEM/EDX.	102
Table 5-1. Contact angle of a droplet of deionised water on electrospun samples at time = 0 s.	120
Table 5-2. Contact angle of a droplet of DMEM on electrospun samples at time = 0 s.	124
Table 5-3. Overall mass loss (%) of PCL/P ₁₁₋₄ and PCL/P ₁₁₋₈ fibres after degradation at different pH.	137
Table 6-1. Elemental analysis of chemical elements in the PCL/P ₁₁₋₄ fibres immersed in SBF for 2 weeks obtained by SEM/EDX.	164
Table 6-2. Ca:P ratio of the electrospun fibre webs incubated in SBF for up to 4 weeks based on EDX analysis.....	166
Table 6-3. Determination of phosphate concentration (μM) in IVN hydrogel samples, SAP concentration = 4 mg mL^{-1}	173

Table 6-4. Determination of phosphate concentration (μM) in IVN fibrous samples, SAP concentration = 4 mg mL^{-1}	173
Table 6-5. Determination of phosphate concentration (μM) in IVN hydrogel samples, SAP concentration= 8 mg mL^{-1}	176
Table 6-6. Determination of phosphate concentration (μM) in IVN fibrous samples, SAP concentration = 8 mg mL^{-1}	176

CHAPTER 1

Introduction

The loss or failure in tissues or organs is one of the most common human health issues (1). The prevalent approaches for treatment of tissue/organ loss or failure are transplantation or implantation of donor tissue or devices (2). However because of the increasing number of patients in need, compared to the number of donors, in the United States alone, approximately a quarter of patients requiring organ transplants die while waiting for a suitable donor (3). Currently, there is a global population projection of six hundred million people aged sixty five and above (4) and the number of people in this category is expected to double within the following twenty five years (5), due to decreasing birth rates in developed countries. In particular, a substantial number of patients suffer from damaged bones due to trauma, tumours or other bone related disease or incidents. Given the aging population, bone or tooth tissue loss due to pathologies such as osteoporosis or periodontal disease is a major challenge (6). The current therapies for such diseases are bone repair or replacement by either implantation devices, allogeneic transplantation of bone tissue from one person to another, or autologous bone grafts. The latter technique involves using a donor site as bone replacement material from within the patient's own body, which minimises the risk of immune response complexities (7). However, there are number of clinical challenges associated with these therapies, first of which is the need for highly invasive surgery. Moreover, autologous therapy causes additional trauma

in the donor site of the patient and there is a limit to the amount of bone that can be transplanted from donor sites in each person. Owing to the challenges of current therapies, together with the increase in demand, due to the aging global population, the need for alternative bone related therapeutic strategies is growing.

1.1 General Tissue Engineering

Tissue engineering is an emerging field involving the regeneration or repair of living tissue using devices known as scaffolds to guide the process and therefore reduce reliance on donated tissues and organs or permanent implantable devices that replace biological tissues (1). In tissue engineering, by using living cells or stimulation of endogenous cells, the tissue can be formed or regenerated *in vitro* or *in vivo* (8). This field of science has the potential to bring dramatic improvements in medical healthcare for hundreds of thousands of patients annually, and equally dramatic reductions in medical costs as it is an alternative for tissue transplantation and also medical implants.

A central component in tissue engineering is the design of a scaffold into which living cells are supported so that neo-tissue formation can develop. Two main approaches are possible. In the first, a scaffold is seeded with cells and the tissue is cultured *in vitro* before it is implanted in the defect as a prosthesis. Alternatively, the scaffold can be directly implanted into the defect either pre-seeded with a relevant cell type or not, to maintain a space for attraction and stimulation of endogenous cells and eventually tissue formation *in vivo* (9). The scaffold must fulfil several criteria such as biocompatibility and degradability capable of supporting three-dimensional tissue formation. These scaffolds should normally be highly porous with interconnected pores to allow cellular integration and also provide sufficient surface area for cell attachment and cell migration. Bioactive surfaces, which assist in the processes of cell

deposition, proliferation and tissue growth, are of keen interest to tissue engineers since they have the potential to contribute to improved tissue regeneration (1, 10).

One of the most active areas of tissue engineering is mineralised tissue regeneration. Mineralised tissues are biological composite tissues in which minerals are incorporated into soft matrices. The hard tissues consist of mainly collagen type I fibres and the mineral phase of hydroxyapatite (HAP) (11). The scaffold for mineralised tissue/bone regeneration must be of materials that can mimic composition and structure of the extracellular matrix (ECM) of bone tissue. To date, different strategies have been investigated for bone regeneration including cell-based therapies, scaffold-based repair or those involving the use of osteogenic growth factors (12).

1.2 Electrospun Polymer Webs as Tissue Engineering Scaffolds

Fibrous media are commonly used in medical and applied healthcare and hygiene products such as wound dressings, drug delivery, blood filtration and tissue engineering (13). Electrospinning is a simple technique for the production of polymeric nanofibres, the fundamentals of which have been known since the work of Formhals in the 1930s (14). In this method, a high voltage is used to build sufficient electrostatic forces to induce charge repulsion that can overcome the surface tension of polymer solution, and a fibre jet is formed at the tip of a capillary (10, 15). Fibrous nonwoven webs can then be deposited on a collector with fibre diameters ranging from micron down to nanometre-scale (16). Control of fibre diameter and morphological features is readily achieved by varying process parameters (17). Electrospun fibre webs are promising structures for use in tissue engineering because of the structural similarity to natural extra cellular matrix (ECM), and applications in tissue engineering have been extensively studied (10, 14, 18-21). The very small fibre diameters and high surface area to volume ratio are beneficial for cell attachment and the high porosity and pore

interconnectivity are conducive to tissue growth. The electrospinning technique is also very versatile, because it allows spinning of different synthetic and natural polymers or blends, as well as the incorporation of bioactive materials, or inorganic materials to tailor properties to suit different application criteria (22).

In addition to the structural features of electrospun fibres that can mimic the fibrous architecture of the ECM (23), the material composition should be non-toxic and induce the intended response of tissue components *in vivo* or *in vitro* (19). Biocompatible synthetic polymers that have been successfully electrospun include aliphatic linear polyesters such as polyglycolic acid (PGA) (24), polylactic acid (PLA) (25, 26) and polycaprolactone (PCL) (15, 27). Among these, PCL is low-cost, non-toxic and biodegradable and it can be used in FDA approved devices such as for drug delivery and tissue engineering (27, 28).

PCL has been extensively investigated in relation to various biomedical applications, including regenerative bone therapies (29-32) in which it has been shown to support the attachment and growth of different cell types (22, 29, 33-35). However, due to the lack of cell-binding sequences along its polymeric backbone and its hydrophobicity, PCL must be modified by means such as plasma treatment, coating, or blending it with bioactive natural polymers (27, 36, 37).

Several studies have been reported in which electrospun PCL has been enhanced in terms of bioactivity and hydrophilicity, for example by coating with bioactive materials such as self-assembling peptides (SAPs) or by surface modification (36, 37). To avoid post-treatments, biofunctional components can also be blended with PCL to form spinning solutions from which electrospun fibres can be directly manufactured in a one step process (32, 38, 39). The resulting fibres containing peptide not only exhibit higher bioactivity and wettability compared to that of PCL alone, but also improved cell adhesion and proliferation.

1.3 Self-assembling Peptides

Amongst the various materials shown to be biocompatible and hold great promise for tissue regeneration in biological conditions are self-assembling peptides (SAPs). SAPs have been the focus of research in the last two decades due to their ability to spontaneously assemble into ordered nanostructures enabling engineers to manufacture “designer” nanomaterials from the bottom-up. Specifically, they have been the focus of research in light of their potential application in hard and soft tissue repair (40, 41). They have also potential applications in other medical and healthcare devices such as wound dressings, surgical patches, as well as in molecular electronics and numerous other applications (42, 43).

Rationally designed SAPs are composed of amino acidic building blocks that can mimic specific molecular features of ECM found in native tissues, such as the RGD cell-binding peptide sequence (42) and facilitate the enhancement of cell growth on biomaterials (44-46). Designing different primary peptide structures by applying various amino acid side chains and altering peptide sequences, enables the physical and biological properties of peptides to be tuned according to the intended end use (42).

The 11-residue family of peptides (P_{11-X}) consists of negatively or positively charged hydrogelating materials. They self-assemble hierarchically into long β -sheet tapes (a single-molecule thick), ribbons (two stacked tapes), fibrils (multiple stacks of ribbons) and entwined fibrils (referred to by some as fibres), following application of external stimuli (46). Above a critical concentration (C^*), peptide monomers assemble into hydrogen bonded β -sheet tapes, with higher order structures being produced if the concentration is further increased. This class of peptides also undergoes pH (47) and ionic strength-triggered (48) self-assembly which can be relevant for their applicability as drug delivery vehicles. So far, most of the published studies using P_{11-X} peptides have focused on the molecular design of self-supporting gels, whereby

promising properties have been shown with regard to cell growth and specifically hard tissue deposition (42, 44, 46, 49). Once self-assembled, these peptides can produce three-dimensional scaffolds which mimics the ECM of hard tissues and they can induce mineral deposition *in situ* (50).

Furthermore, peptide P₁₁₋₄ (-2 charge) and P₁₁₋₈ (+2 charge) specifically have shown low immunogenicity *in vivo* and no cytotoxic effect to human and murine cells (46, 51, 52) and enhanced bone tissue regeneration (50, 53-55). However, despite their inherent biofunctionality, self-assembled peptide gels frequently suffer from poor mechanical strength and lack of structural stability. This potentially makes their handling and fixation during implantation challenging, particularly in large load-bearing tissue defects. Attaining mechanically competent scaffolds capable of supporting cell growth spatially and temporally until the newly engineered tissue is formed, is one of the major challenges in the design of SAP-based medical devices. Given the practical benefits of electrospun fibres in tissue engineering mentioned in Section 1.2, the incorporation of SAPs within water-stable PCL electrospun fibres is a potential route to address this challenge, and to deliver the SAPs in a structurally reinforced fabric (32, 36, 37).

1.4 Aims and Objectives

The incorporation of self-assembling peptides within polymeric fibres is a potential route to address the challenges associated with mechanical properties of SAPs as well as to enhance the biocompatibility of nonwoven fabrics composed of synthetic polymers such as PCL for applications in bone tissue engineering. Accordingly the aim of this work is to investigate whether a structurally stable fibrous architecture can be accomplished in one-step via electrospinning solutions of two peptides (P₁₁₋₈ and P₁₁₋₄) combined with PCL. This study

focuses on the electrospinning of SAPs within fibres and experimental characterisation of the structure and properties of resulting fibrous assemblies.

The specific objectives of the study are:

- To investigate the feasibility of combining self-assembling peptides (SAPs), P₁₁₋₄ and P₁₁₋₈, with PCL in a one-step manufacturing process and produce electrospun fibre webs.
- To characterise the morphology of resulting fibres and electrospun networks and develop an understanding of how SAP self-assembly is affected by manufacturing conditions during and after electrospinning.
- To investigate the peptide release kinetics and behaviour of PCL/SAP fibre in biological conditions by studying the behaviour of PCL/SAP fibres in aqueous environment.
- To determine the cytocompatibility of PCL/SAP fibres and to evaluate the apatite-formation ability of electrospun PCL/SAPs fibres to understand their potential suitability for hard tissue regeneration.

The outcome of this study will ultimately contribute to the design of an enhanced tissue scaffold device for use in hard tissue regeneration.

CHAPTER 2

Review of Literature

2.1 Introduction

This chapter critically reviews relevant science and technology related to bone tissue engineering and is intended to lay a foundation for the experimental work that follows. Moreover, a brief introduction of the background to bone tissue regeneration is provided including biological apatite, mineral nucleation, biomineralisation and mineralised tissue. This is followed by discussion of the challenges of mineralised tissue repair and tissue engineering as a novel approach, and the required scaffold characteristics relevant to hard tissue. Furthermore, a discussion of taking a biomimetic approach in relation to self-assembling peptides in scaffolds is included. Finally, given the importance to the experimental work, a brief review of electrospun scaffolds is presented.

2.1.1 Principles of Mineral Crystal Nucleation and Secondary Crystal Growth

Crystal nucleation is defined as the initiation of new mineral phase formation (56). According to basic thermodynamic principles, the minerals in a solution, liquid, or vapour can be arranged in a crystalline pattern by which a transition from a high-energy state to a low-energy state occurs. One of the driving forces behind crystal nucleation is supersaturation, when there is more solute in solution than the amount that can be dissolved by the solvent under standard temperature and pressure (56, 57). The nucleation process can occur either

heterogeneously or homogeneously. In the former, an external interface is needed upon which a number of particles (ions, atoms or molecules) will be deposited and arranged to form crystals. The surface can be of any substance such as dust particles, phase boundaries or the wall of a glass container. However, in homogenous nucleation without any pre-existing nuclei, the particles can gather in a correct position while they are moving randomly in the bulk of a medium (58). To create a solid surface, a certain amount of energy is required which is equal to the total surface tension of its area. In nucleation, solid surface formation will be homogenous when a solution with a certain level of internal energy reaches a lower state of energy by deposition of particles and formation of solid surface. Based on the Gibbs free energy concept, the total interfacial energy of the created solid should be lower than the total existing energy of the solution in the first place. Therefore a specific amount of free energy will be released upon the formation of a new phase. Heterogeneous nucleation more readily occurs, since less energy is required to overcome the interfacial energy at the surface of the nucleation sites because their effective surface energy is lower (59).

Once the nucleation has occurred and a crystal is formed, additional particles can be deposited and further crystal growth can take place (58). The processes of nucleation and further growth of mineral crystals are the basis of mineralisation.

2.1.2 Biomineralisation

Biomineralisation is an active or passive procedure during which, a living organism generates and deposits inorganic-based structures (minerals) for its own functional requirements (60). Biomineralisation includes the specific extraction and take-up of minerals from the nearby environment and the interaction of them with extracellular organic molecules, which results in incorporation of them into functional structures (60).

2.1.3 Biological Apatite

The name 'apatite' stands for a family of phosphate minerals that have similar structures but potentially different compositions. It most usually refers to hydroxyapatite (HA), fluorapatite or chlorapatite. In 1926, it has been identified for the first time that calcium and phosphate are the main components of bone and teeth after chemical analysis of enamel, dentin and bone in humans (61). Later on, the similarity in X-ray diffraction (XRD) patterns of these tissues to those of HA, evidenced the fact that the inorganic phase of human mineralised tissues is principally HA with the chemical formula of $\text{Ca}_{10}(\text{PO}_4)_6(\text{OH})_2$ (61, 62). However, there is some complexity in biological HA structure, as there may often be impurities in the mineral composition. For example, it may be calcium deficient and enriched with CO_3^{2-} that replace PO_4^{3-} ions (60). This is known as carbonated apatite, and there are several other calcium phosphate phases in different biological mineralised tissues, with differences in compositional chemistry. For example, the amorphous calcium phosphate phase ($\text{Ca}_8 \text{H}_2 (\text{PO}_4)_6$) is often present in early stage mineralised bone or cartilage. After that, while the mineralisation builds up more and more, the calcium phosphate phase within the tissue can become more crystalline and is readily transformed to HA. Therefore, for most purposes, $\text{Ca}_{10} (\text{PO}_4)_6(\text{OH})_2$ is considered the main calcium phosphate composition of mineralised tissues, and during the course of this study bone minerals are referred to hydroxyapatite (HA) with this compositional chemistry (60).

2.2 Mineralised Tissues

2.2.1 Bone

Bone is one of the hard, mineralised tissues and its function is protection and mechanical support, load bearing, and it contributes towards movement as well. Because bone is continuously engaged in a cycle of mineral growth, dissolution and remodelling (in response

to internal/external signals), it is often known as a 'living mineral'. The architecture of bone is composed of mineralised HA organised within a fibrillary matrix of collagen, glycoproteins (protein with sugar side chain) and other type of proteins. This composite of organic and inorganic elements can provide mechanical strength in bones and increased stiffness in comparison with HA alone (60, 63). The arrangement of collagen fibres together with the amount of mineral content in bone, which controls the level of toughness, can contribute in different types of bone based on their specific functions (63). In immature bone, also known as woven bone, which is formed primarily, collagen fibres are irregularly arranged with a low concentration of mineral deposition. This bone will later be replaced by mature or lamellar bone which itself is classified into two types; compact bone (also called dense or cortical bone) and trabecular bone (also called cancellous or spongy bone). Cortical bone is dense and has a very ordered basic structure whereas cancellous bone is less dense and is often referred to as 'spongy bone' (63). A network of interconnected cells exists within the mineralised structure of the bones as well. There are essentially three major cell types; osteoblasts, osteoclasts and osteocytes that play a role in modelling and remodelling of bone (63). The first two cell types are based at the surface of the bone whereas osteocytes are based in the centre. Osteoblasts contribute to bone modelling, which is the process by which bone is constructed. Osteoclasts then resorb old bone which will be replaced by new bone made by osteoblasts (64). Bone remodelling is defined as the reconstruction of bone during life according to necessity. Osteocytes can sense when a change in mechanical pressure and workload happens and accordingly they can send chemical or electrochemical signals to the surface of the bone. This is to activate osteoblasts or osteoclasts to either begin mineralisation and strengthening of the bone or resorbing and reordering of the bone (63, 65).

2.2.2 Teeth

Teeth are another type of mineralised tissue in body, which like bone, have a structure that is a complex system able to resist different types of mechanical forces. They are essential organs not only for chewing, but also play a role in speech as well. The outer layer of the tooth, which is visible above the gum is called the crown, and it has a coating in the form of a layer of enamel which protects the underlying structure. Enamel is the most highly mineralised and hardest tissue in the human body, composed of 96% (by weight) of highly crystalline HA (60). The remaining proportion is made of organic matrix and water. This large proportion of mineral in enamel contributes not only to its strength but also makes it brittle. The firmly packed rows of calcium phosphate crystals, originally form within a protein matrix structure, after which the fibrillary structure is progressively removed, while the biomineralisation matures and develops (66). Unlike bone, enamel is not a living tissue and it cannot undergo the remodelling process because its extracellular matrix disappears during the maturation stage of enamel formation. Dentine is an elastic mineralised component of the tooth that resides beneath the enamel. It is a softer tissue than enamel (composed of 65% by weight of mineralised HA crystals) and it contains fibrous collagen matrix as well, which contributes to improved energy absorption. The apatite content provides strength and the collagen provides toughness to dentine (67). The structure and composition of dentine is comparable to bone and it is able to remodel itself. Pulp is a soft connective tissue, which is the central component of the tooth and is known as the most vital part of tooth. The primary function of pulp is the formation of dentin. Within the pulp, there is a vascular network to supply nutrients to the tooth together with nerves to provide sensory function e.g. pain or temperature (68, 69). Figure 2-1 displays a schematic diagram of these tissues which form a tooth.

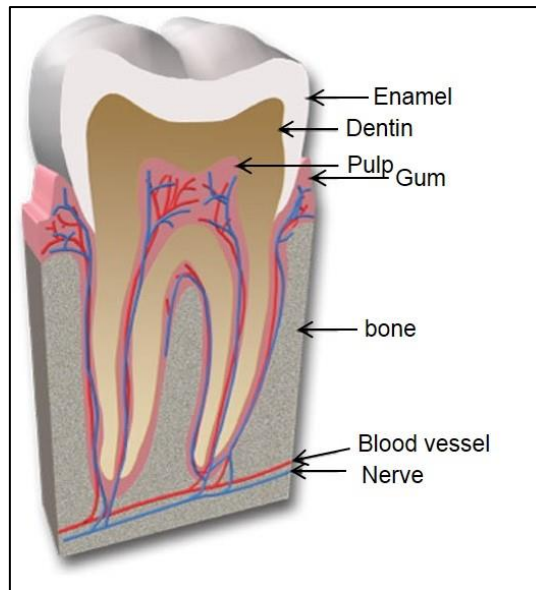


Figure 2-1. Schematic diagram indicating the main tissues of tooth (70).

2.2.3 Clinical Challenges in Mineralised Tissue Repair

There are several diseases associated with mineralised tissues in the human body, which may result in tissue loss, a decrease in bone mineral density or a loss of functionality. There is expected to be a doubling of the incidence in the number of these disorders and conditions by 2020, owing in part to the worldwide ageing population (71, 72). In general these disorders result from diseases or trauma such as traffic accidents, injuries sustained during war, or fighting, primary or secondary tumours related to the bone, chronic joint diseases in older people, crippling diseases and deformities in children, rheumatoid arthritis and spinal disorders. Moreover, there are metabolic disorders such as osteoporosis, in which bone formation and resorption is unbalanced, which may cause severely weakened and fragile bones in patients (72).

Conventionally, the therapy for such disease is the removal of tissue and replacement with either implantable devices (alloplasts) or bone grafts. Bone grafting itself is divided into three categories: (i) autografts (self-donated tissue transplantation); (ii) allografts (tissue donated from another human) or (iii) xenografts (transplantation of a tissue harvested from another

species). Of these options, autografts are considered the ‘Gold Standard’ because of their relative histocompatibility and non-immunogenicity compared to allografts or xenografts, which carry risks of post-operative infection or disease transmission (71, 73). However in autologous implants as well, since the donor tissue has to be taken from another healthy tissue of patient’s own body, there is always a limited supply and it necessitates invasive surgery that can result in increased time for anaesthesia and blood loss (74). In addition to limited availability, immune rejection, pathogen transfer and donor site disruption challenges, there are substantial cost issues associated with these therapies. In the United States alone, bone defect repair cost more than US\$ 2.5 billion per year (72). The drawbacks associated with current bone repair therapies have initiated a search for alternative strategies related to bone tissue engineering over the last two decades, which ideally eliminates many of the existing clinical challenges (71).

2.3 Tissue Engineering

The purposes of tissue engineering are to restore, maintain, or enhance tissue function and it is a rapidly developing field dealing with multiple challenges that are encountered in medical practice (42). Tissue engineering has been an emerging research field for the last few decades and combines biomaterial and biochemical engineering with cell transplantation therapies to reconstruct defects and recover tissues of bio-organisms (75). Any injuries that may cause organ and tissue loss or failure in a body can be a major human health problem. Tissue or organ transplantation and medical implants have been standard therapies to treat such patients, however in terms of transplants, there is a large mismatch between supply and demand of organs and tissues for transplantation. In the United States alone, approximately a quarter of patients die as a result of waiting for a suitable donor (76, 77). Other therapies such as cellular therapy, synthetic prosthesis, medical implants or drug therapy, have their own potential problems. For example prosthesis and medical implants cannot deliver all of the functionalities

of the native organ or tissue (76), and cellular therapy has not been completely successful as full control of cell accumulation and cell-to-cell interaction is not easily achieved without providing any extracellular support for injected cells (78).

In tissue engineering, a suitably engineered 3D scaffold containing appropriate bioactive chemistry, is placed into a tissue defect to guide the regeneration of the tissue or to assist in the restoration of the function of the organ. The scaffold is either seeded with metabolically active cells and cultured *in vitro* before implantation, or it is first implanted into the tissue defect, after which attachment, migration, and differentiation of endogenous cells takes place, and the defected tissue is regenerated *in vivo* (75, 79). Therefore, developing tissue scaffolds capable of being transplanted into a living body to regenerate or restore body tissues with their natural functions, is the fundamental challenge in tissue engineering (80). If successfully achieved, this approach makes transplantation without a donor a reality.

So far, since the first clinical application of tissue engineering as a bio-artificial skin to treat burn injuries in 1990 (81), other applications include regeneration of liver tissue (82), pancreas, intestine, urothelium, esophagus, nerve (83), valve leaflet, cartilage (84), bone (85, 86), ligament, and tendon (76).

2.3.1 Engineering of Mineralised Tissues

One of the promising areas for tissue engineering is hard tissue engineering. Given the challenges involved in the repair of mineralised tissues (Section 2.2.3) and specially treatment of large bone defects, bone tissue engineering can play a major role in providing an alternative approach to speed up healing of bone in all musculoskeletal disorders and injuries. Understanding of bone structure, mechanics and function is crucial to successfully regenerate or repair bone. Moreover, the newly restored bone has to perform the functions of native bone and it has to fully integrate with the neighbouring host bone (71). Currently, there are different

approaches being investigated in bone tissue engineering including cell based and cell free strategies, as well as those using osteogenic growth factors or genetic engineering (12). Cell based strategies are those utilising live and metabolically active cells of different types from the host body (autologous cells) or other donors (exogenous cells), and transplantation of them into a tissue defect. In this method, the cells have to be expanded *in vitro* prior to seeding onto scaffolds and subsequent implantation. The 3D scaffold is used to provide additional mechanical and structural support and direct ingrowth of the tissue both before implantation (*in vitro*) and after that (*in vivo*). Moreover growth factors, which are a family of proteins capable of controlling the activity of tissue-specific cells, specifically bone morphogenetic proteins (BMPs), can be introduced into scaffolds before implantation to enhance the remodelling of bone tissue (87). To improve the success of artificial bone graft substitutes, gene therapy can also be employed by delivering specific genes into cells or tissues (88). This classical tissue engineering approach has faced numerous critical challenges including cell expansion and seeding time which is costly and laborious (89). Figure 2-2 is schematically describing the basic cell-based approach in bone tissue engineering.

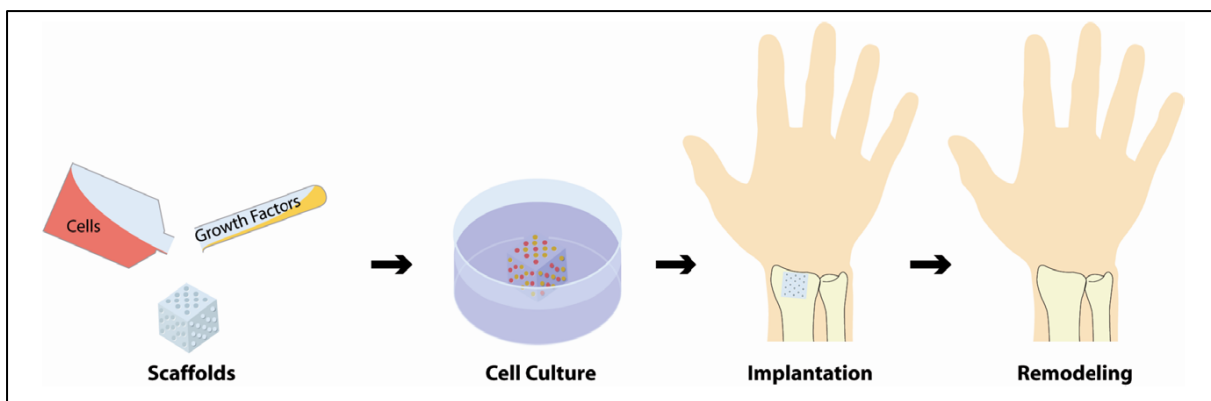


Figure 2-2. Cell based bone tissue engineering, involving the application of metabolically active cells and growth factors using a 3D scaffold for functional bone tissue regeneration (12).

In addition to this approach, cell-free therapies are being investigated as well. This more straight-forward concept also includes applying a 3D scaffold that will be implanted into the tissue defect, but cells are recruited from the body's own resources (resident tissues) to stimulate self-healing mechanisms (90). This method, which is also known as *in situ* tissue regeneration, relies on applying a bioactive scaffold which will home endogenous cells and stimulate local tissues. It has shown great promise in previous tissue regeneration studies such as vascular grafts, nerve as well as hard tissue regeneration (89, 91-94). It can alleviate the risks of using exogenous cells or harvesting cells from the host body, which has similar risks as autografts and allografts (in Section 2.2.3) (90). In both cell-based and cell-free approaches, the scaffold eventually has to undergo cell-mediated degradation and will be replaced with natural extracellular matrix (ECM) of newly formed bone.

2.3.2 Design of Scaffolds for Hard Tissue Engineering

As in general tissue engineering, in hard tissue regeneration, an engineered bone graft substitute, known as scaffold, is needed. *In vivo* each cell benefits from an ECM which provides a microenvironment surrounding it, in order to behave as a functional unit (95). Bone scaffolds must mimic some properties of the original bone ECM, regarding for example its composition, porosity, dimensions and physical properties, and in turn it will guide the formation of new bone (72, 96, 97). The main effort in the design of scaffolds, which serve as temporary matrices for bone regeneration is to try to mimic the microenvironment for cells (78). In the design of an ideal scaffold, selection of the biomaterial and designing appropriate structural and chemical/physical properties are considered to be the main steps (76). Producing a scaffold that meets all the required criteria can be the major challenge in tissue engineering (78). For example, for each application and end use, the scaffold should provide the required support for cells and biochemical signals contributing to the cell behaviour such as cell survival, cell shape development known as morphogenesis, cell populations growth known as

proliferation, and cell evolution known as differentiation (95). Bone ECM is a composite composed of both an organic component (predominantly type-1 collagen) and a mineralised inorganic component (crystalline HA minerals). Therefore, the engineered bone scaffold should be capable of both inducing cellular interactions (attachment, growth, differentiation) and mineralisation within the implant which results in the new bone formation *in vivo* (71).

2.3.2.1 Scaffold Structure

The macro and microstructure of the scaffold play a vital role in bone tissue engineering as they should effectively contribute to form the structure of bone ECM (76). The scaffold that serves as a cell and materials carrier, should be porous and three dimensional to permit cells to grow in three dimensions (98). The external shape of the scaffold should adopt the size and geometry of the bone defect while the internal structure should provide an interconnected permeable framework, which allows capillary ingrowth and the transfer of nutrient and oxygen needed for cell growth (12). The porosity in scaffolds will lead to a better cell accommodation and effective vascularisation. It has also been claimed that having interconnected pores is vital for free migration, attachment, proliferation and differentiation of cells as well as mass transfer in the scaffold and consequently tissue regeneration (43, 99). Moreover the more surface area that is present in scaffolds will provide more places for cell attachment and growth so the cells will properly be held to initiate every cell-to-matrix interaction (100).

Furthermore, it is of pivotal importance that the bone scaffold has sufficient stiffness and strength, particularly because it will be influenced by forces during implantation and upon transplantation, there will also be biomechanical forces and dynamic loads *in vivo*. The mechanical properties of bone scaffolds should be sufficient especially in hard, load-bearing bone tissues, and it should be bio-stable because it will be retained after implantation until the new bone is formed. The strength and elasticity of scaffold, as well as its integration into the

host tissue and chemical stability and degradation profile are therefore important considerations (76).

2.3.2.2 Biomaterials for Scaffolds

In designing tissue engineering scaffolds, another crucial step is selection of a suitable biomaterial, that is both biocompatible and biodegradable (76, 101). Biocompatibility implies an appropriate surface chemistry which can support cell attachment and biodegradability means that the materials can be degraded into non-toxic products, which leave the desired living tissue upon formation (102). Materials used for bone tissue engineering purposes are vary from organic to inorganic biomaterials or a combination of them. The inorganic biomaterials include bio ceramics such as HA and other calcium phosphate-based or calcium sulphate-based ceramics, and bioactive glasses (12, 103). Under the category of organic materials, there are two types of naturally derived polymers (processed allogenic or xenogeneic) and synthetic biodegradable polymers. Naturally occurring polymers include proteins of natural ECM of different tissues, such as collagen, silk fibroin, elastin-mimetic peptide, fibrinogen, casein, lipase enzyme, glycosaminoglycan, alginic acid, chitosan, and even DNA (97). Although use of naturally derived scaffolds can fulfil biocompatibility and biodegradability requirements, they are derived from a foreign biological environment, and therefore still present the risk of pathogen transfer. It is also claimed that these materials can suffer from weak mechanical properties and their processability and manipulation is usually challenging (76, 97).

With regards to mineralised tissues, natural scaffolds from collagen type I, which is the main protein in bone, have shown low immunogenicity and promoted bone formation and stimulated osteoblast cell differentiation (104-106). However since collagen is derived from animals, it still has the limitation of supply problems, and may still carry risk of immunogenicity. Moreover because of a lack of mechanical strength, collagen cannot withstand large forces during load bearing bone formation (107).

Among the organic materials, synthetic polymeric materials have been widely used and they have received increasing attention because of their ease of processing and tuneable biodegradability (97, 108). The most commonly used synthetic polymers for tissue engineering are those approved by the FDA (US food and drug administration) and this includes poly(glycolic acid) (PGA) (24), poly(lactic acid) (PLA) (25, 26), and their copolymer of poly[lactic-co-(glycolic acid)] (PLGA) and poly(ϵ -caprolactone)(PCL) (15, 27, 109). These polymers are biocompatible and they are able to biodegrade in the body over a period of time. Although generally using synthetic materials as tissue scaffold materials has limitations in terms of cell recognition, it can be enhanced by modification of material chemistry and surface treatment before or after scaffold formation. The ability of synthetic materials to be engineered is a major advantage and porosity and physical characteristics can be adjusted to give very promising bone scaffold designs (1).

Poly (ϵ -caprolactone) (PCL):

Among the synthetic biodegradable polymers, PCL has been widely investigated and applied in bone tissue repair (29, 30, 110-114) since it possesses the necessary mechanical properties, structural integrity, controlled pore size and pore interconnectivity suitable for bone tissue engineering (113). PCL is a biodegradable and biocompatible aliphatic polyester with a low melting point of 58–63°C and a glass transition temperature of -60°C. It is low-cost, non-toxic and biodegrades slowly depending on the molecular weight and can be used in FDA approved devices, i.e. for applications in the human body such as drug delivery and tissue engineering (27, 28, 115). The molecular structure of PCL consists of repeating five nonpolar methylene groups and a single relatively polar ester (Figure 2-3) (116). This polymer is regarded as cytocompatible and has been used as a biodegradable structure, in various biomedical applications, including regenerative therapies (22, 33) whilst supporting the attachment and growth of muscle cells, mesenchymal stem cells, and chondrocytes (29-31). The mechanical

properties of bulk PCL ($M_w = 44,000$) has been investigated thoroughly, with a tensile strength of 16 MPa, tensile modulus of 400 MPa, flexural modulus of 500 MPa, elongation at yield of 7%, and elongation at break of 80% (15, 117-120). However, due to the lack of cell-binding sequences along its polymeric backbone, its low degradability and its hydrophobicity, PCL is also modified using various techniques such as plasma treatment and/or coating (32, 34-37).

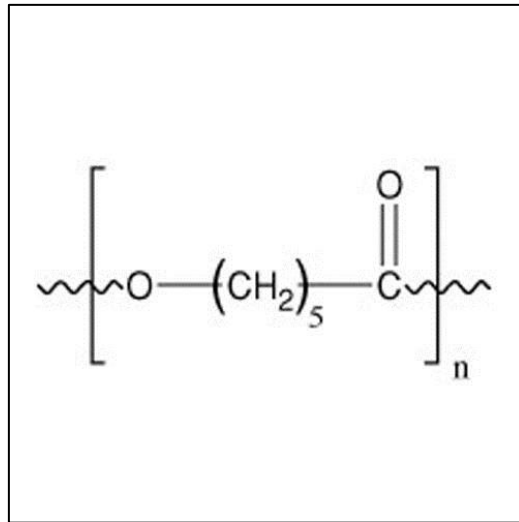


Figure 2-3: Molecular repeat structure of PCL.

As it has been discussed in Section 2.3.2.1, mineralised tissue scaffold should provide a porous structure which can guide cells ingrowth and at the same time it should maintain a sufficient strength to support the structural growth of newly formed bone. With regard to this, it has to be noted that a single material with limited range of properties cannot act entirely as a substitute for a complex composition such as bone. Therefore for bone tissues, it is of interest to develop a composite scaffold that consists of both natural and synthetic polymers, which can combine the appropriate mechanical and physiological properties favourable for bone regeneration (112, 121, 122).

2.3.3 Biomimetic Approach

The term biomimetic is derived from the words ‘bios’ and ‘mimesis’ meaning ‘life’ and ‘to imitate’ respectively (123). In the biomimetic approach, which can take a top-down or a bottom-up perspective, natural structures are analysed in search of architectures or chemistries that can replicate to some extent features of the target tissue. This approach has been adapted by many disciplines e.g. in mineralised tissue regeneration (124, 125), whereby either the architectural or physiochemical aspects of bone tissue have been mimicked.

This study focuses on cell free approach of bone tissue engineering and in particular development of a scaffold and investigation of its performance in the promotion of mineralisation of apatite minerals *in vitro*.

2.4 Self-assembling Peptides

Self-assembling peptides lie between two categories of synthetic and natural materials, as they are not naturally occurring, yet are composed of natural building blocks. Although they are still largely in the research and development phase, they have shown promising results in meeting the criteria of tissue engineering scaffolds (42, 44). Before discussing self-assembling peptides and their application in bone tissue scaffolds, it is worthwhile reviewing peptide structures and self-assembling conformations and triggers.

2.4.1 Peptides and Protein

As discussed in Section 2.3.2, the ECM of mineralised tissues are mainly composed of proteins and the proteins themselves, are composed of amino acids that are linked to each other by peptide bonds. In general, there are 20 natural amino acids that form the building blocks of proteins in the body and that can be combined in different orders to form unique 3D protein structures with specific functions. The distinction between peptides and proteins is that proteins refer to natural well-defined 3D structures made up of hundreds or thousands of amino acids,

but peptides contain significantly shorter sequences of amino acids (between 10 to 100, or even fewer) (126, 127).

Amino acids can be linked via a condensation reaction when a carboxyl group (COOH) (also called C-terminus) from one amino acid reacts with an amine group (NH₃) (also called N-terminus) from another adjacent amino acid via a peptide bond (also called an amide bond), during which one water molecule is released (Figure 2-4). Linkage of a series of amino acids via peptide bonds forms ‘peptide chains’ (also called peptide backbone) and each amino acid unit in a peptide chain is called a ‘residue’. The sequence in which the amino acids are linked in a protein/peptide is termed its ‘primary structure’. This process can be repeated indefinitely to produce longer peptides since the two ends of the resulting peptide are distinct (128).

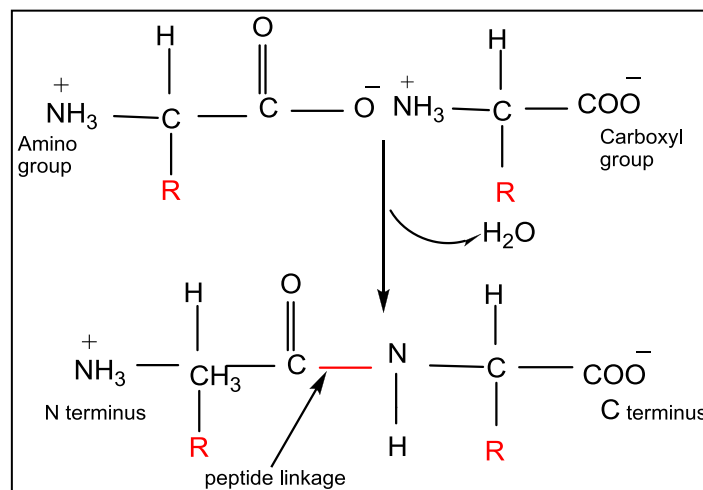


Figure 2-4: The condensation of two amino acids forming the peptide linkage (129).

Designing different primary peptide structures by applying various amino acid side chains and altering peptide sequences, enables the physical and biological properties of peptides to be tuned according to the intended end use (42).

Peptide chains are rich in hydrogen bonding potential because each residue contains a carbonyl group (C=O) and an NH group, which are a good hydrogen-bond acceptor and donor

respectively. The further spontaneous interaction between the NH and C=O groups gives rise to more hydrogen bond formation and leads to peptides being folded into 3D structures. The pattern of these hydrogen bonds and the repetitive conformations in the peptide backbone is termed the 'secondary structure'. The two most common secondary structures for peptides and proteins are α -helix and the β -sheet. Other less common structures, are for example, β -turn and 3-helix (126, 127). The β -sheet secondary structure is constructed from individual extended peptide chains, called β -strands, which are arranged in a zigzag manner (Figure 2-5). The β -sheet tapes are formed by spontaneous association of amino acids to super-molecular fibril-like structures and they are stabilised by hydrogen bonds between C=O groups of amino acids in one β -strand and the N-H groups of the amino acids in another adjacent β -strand (126, 127). Because adjacent strands can have their N- and C- termini oriented in the same or opposite sense, β -Sheet can be observed parallel or anti-parallel (Figure 2-6), the dotted lines indicate the hydrogen bonds between the tapes). Anti-parallel β -sheets have greater stability because the peptide dipoles have a more preferential arrangement and the chains can pack more tightly (130-133).

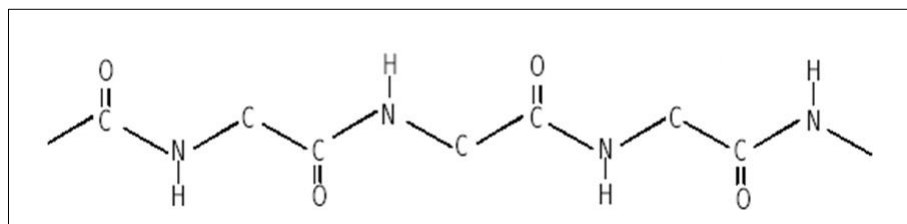


Figure 2-5: Extended peptide chain known as β -strand (129).

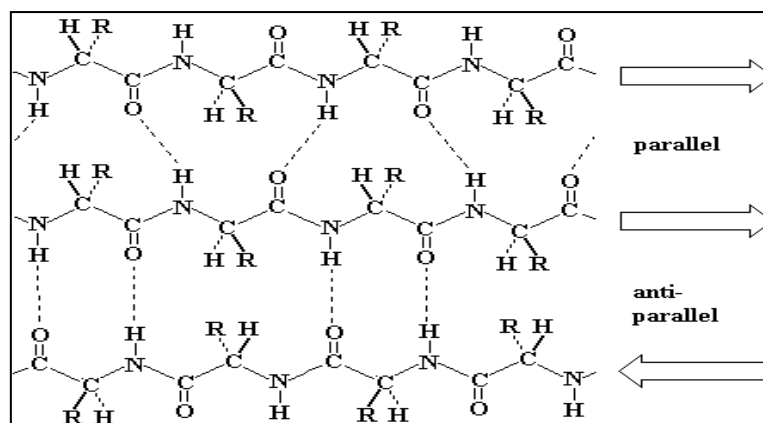


Figure 2-6: Parallel and antiparallel β -sheet, the dotted lines indicate the hydrogen bonds between the chains (129).

2.4.2 Peptide Self-assembly mechanism

Self-assembly is prevalent in nature and is found at both macroscopic and microscopic levels. Molecular self-assembly can be defined as '*the spontaneous association of molecules under equilibrium conditions into stable, structurally well-defined aggregates joined by non-covalent bonds*' (134). Self-assembly of peptides relies on intermolecular forces, which assemble small units into fibrils and fibres with diameters of nanometre scale (135). Particular proteins such as peptides and collagen can undergo spontaneous self-assembly in response to external triggers such as pH, temperature and ion concentration (136). This process also depends on the concentration of the peptide/protein and only above a certain concentration (C^*) does the formation of assembled structures occur. Peptide self-assembly follows a nucleated pathway in which a chemical difference in peptide monomer faces (due to the amino acid side chains), would initiate the assembly process. After this, if all pre-assembly conditions are provided, such as C^* , temperature and pH, the assembly process will begin.

2.4.3 P₁₁ Peptides

The rationally designed 11-residue family of peptides (P₁₁-X) consists of negatively or positively charged peptide chains and self-assemble hierarchically into β -sheet tapes and higher

ordered structures. This transition from isotropic fluid to a self-supporting nematic hydrogel occurs following application of external stimuli (137). Designing different primary peptide structures by applying various amino acid side chains and altering peptide sequences, enables the physical and biological properties of peptides to be tuned according to the intended end use (42).

2.4.3.1 P₁₁ Peptides Background

Aggeli and co-workers first reported the rationally designed, self-assembling P₁₁-2 peptide (Ac-QQRFQWQFEQQ-Am) in 1997 (138). A number of principles were applied by the researchers for a successful design of this β -sheet forming sequence. Side chain interactions are an important factor in driving strand assembly, i.e. dimethylenes and aromatic residues provide hydrophobic side-chain interactions. Aqueous solubility of peptide tapes is promoted through the hydrophilic ends of the side chains of some amino acids. The charges normally present at peptide termini were removed by introducing acetyl functional groups to prevent unwanted interaction between COO⁻ and NH₃⁺. Finally, the positively charged amino acid (arginine acid) and negatively charged one (glutamic acid) residues are positioned such that the complementary charges of arginine and glutamic acid on neighbouring strands are adjacent to each other if the peptide is in an anti-parallel β -sheet configuration (139).

Aggeli et al. have also developed a model describing P₁₁ peptide self-assembly related to its concentration (140). In this model (Figure 2-7), peptide monomers in a β -strand conformation are considered to be chiral rods with chemically distinct faces and complementary donor and acceptor groups aligned on opposite sides. When a random coil monomer changes to a β -strand, there is a free energy loss of configurational entropy. On the formation of a β -sheet tape (a single-molecule thick) from β -strand, there is free energy of intermolecular association for each interacting pair of monomers. Because β -strands have a right-hand twist (viewed down the polypeptide chain), β -sheet tapes have an inherent left-hand twist (viewed down the tape axis)

(141). Tapes contain two distinct faces; one of which interacts more with itself, the other more with the solvent, and this is the reason that tapes adopt a helical form. As one side of the tape is more hydrophilic than the other, tapes pair into twisted ribbons (two stacked tapes) to exclude their less soluble surfaces, in this change there is an associated free energy as well. Fibrils (multiple stacks of ribbons) form when ribbons stack, driven by attraction between their faces, with a free energy per pair of interacting peptides. If the edges of fibrils are mutually attractive, they may stack in pairs and form fibres (or entwined fibrils), with an associated free energy. These free energies determine the critical concentration, C^* , for observing each peptide structure (140).

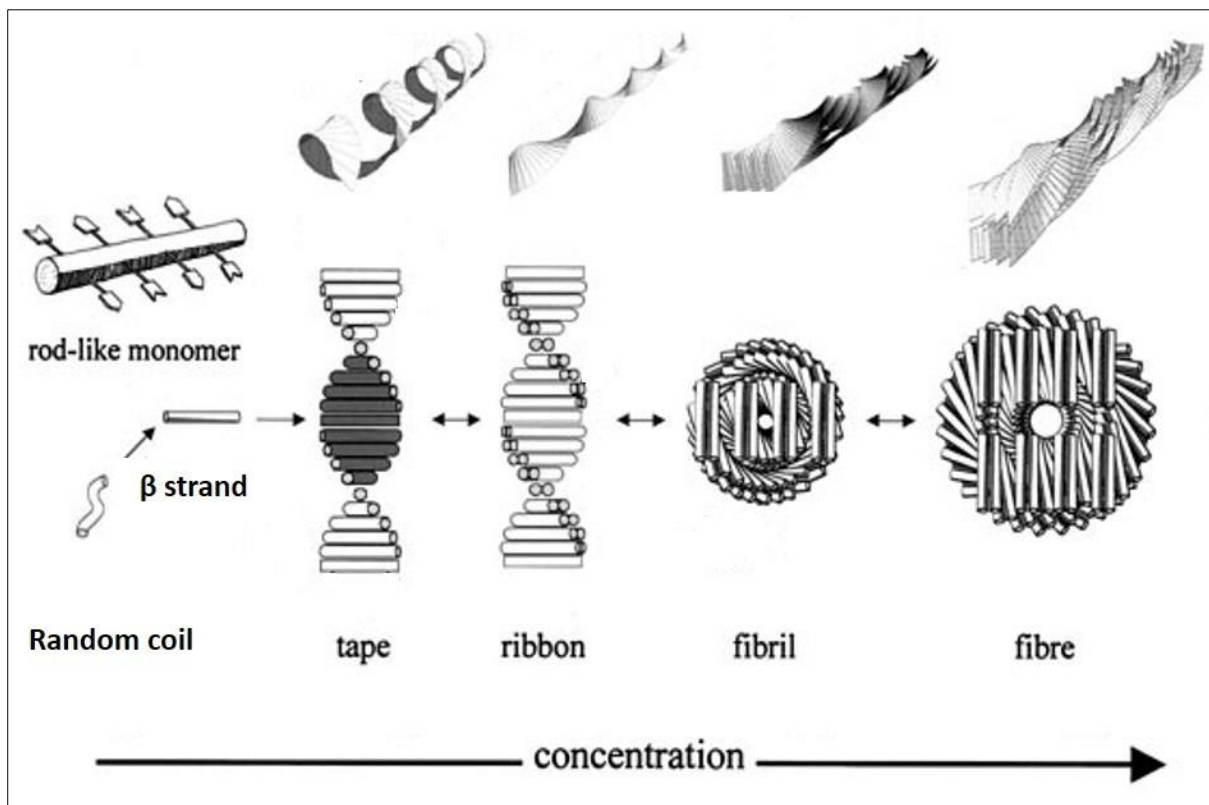


Figure 2-7: Hierarchical self-assembly model for chiral rod-like units (image adapted from Aggeli et al. (140)).

2.4.3.2 Triggers to Peptide Self-assembly

Several mechanisms can trigger the self-assembling of peptides, including internal or external triggers. Internal triggers include combination of complementary pairs of peptides that have opposite net charge (142). The external triggers include pH, temperature and ion concentration of the solutions, light or solvent compositions. The P₁₁ class of peptides has been shown to undergo pH-triggered self-assembly (47) and ionic strength-triggered self-assembly (48).

As an example of the effect of pH, P₁₁-4 (Ac-QQRFWEFEQQ-Am) can be designed to be monomeric in solution at higher pH and to form fibrils at low pH. This allows antiparallel β -sheet assembly by coulombic interactions and switching between low and high pH can be carried out reversibly several times. Conversely, P₁₁-8 (Ac QQRFOWOFEQQ-Am) behaves in the opposite manner. At low pH, it is monomeric, while at pH above 7.8, a fibril-containing gel is obtained (see Figure 2-8).

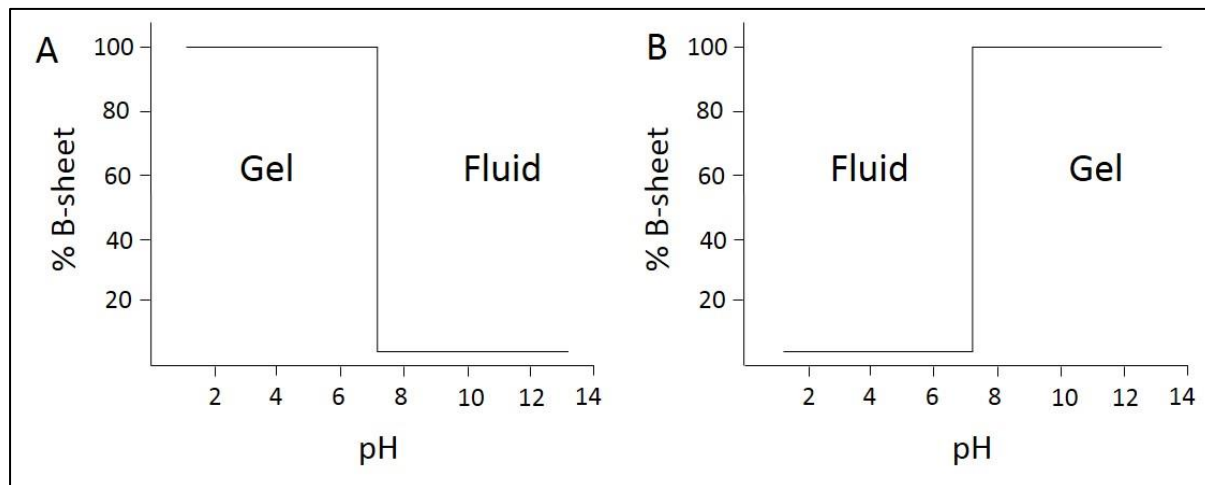


Figure 2-8. Graphs showing the change in state of (A) P₁₁-4 and (B) P₁₁-8 in response to a change in pH of the solution (47).

The physiological ionic strength effect on the self-assembly can be exemplified by examining P₁₁-4 and P₁₁-8 self-assembly with NaCl salt in solution (48). For P₁₁-4 solutions in 130 mM NaCl, the transition from β -sheet to random coil is shifted up from pH 7.8 to pH 12 (more than

4 pD¹ units). This may be the result of a change in side chain acidity by acid-base titration. It was also discovered that the structure of the predominant fibrous structures in gels and the structure of fluids appeared to be unaffected by the presence of salt. Comparable shifts in properties were found when studying P₁₁₋₈ solutions in 130mM NaCl. The β -sheet to random coil transition is decreased by 3 pD units from pH 8 in water to pH 5 in aqueous NaCl solution. These two studies related to pH and ionic strength (47, 48), in particular are significant because they demonstrate that self-assembly of P₁₁ peptides can be adjusted to suit a particular ionic strength and pH, for instance as they are *in vitro* or *in vivo*. Moreover, their triggered self-assembly is reversible and responsive, which makes them potentially useful in applications such as drug delivery.

2.4.4 Self-assembling Peptides Used in This Study

The primary structure of peptide P₁₁₋₄ and P₁₁₋₈ are given in Table 2-1. The amino acid side chains that contain an ionisable acid group are indicated by a negative charge while those that contain ionisable basic group are indicated by a positive charge. It is shown in Table 2-1 that the only difference in the amino acid sequence of these two peptides is ornithine (O) in P₁₁₋₈ which has NH₃⁺, which is replaced by glutamic acid (E) in P₁₁₋₄, which has COO⁻ (48). As it explained in Section 2.4.3.2, self-assembly in both P₁₁₋₄ and P₁₁₋₈ is pH sensitive due to their ionisable groups and they can self-assemble and adopt a hydrogel state in an opposite manner. In physiological conditions, pH 7.4 and a salt concentration of 140 mM, P₁₁₋₄ and P₁₁₋₈ carry a net charge of -2 and +2 respectively and they can form a hydrogel state when the concentration is above 10 mg mL⁻¹.

Among the P₁₁ category of peptides, peptides P₁₁₋₄ and P₁₁₋₈ have been found to be non-cytotoxic after culturing with human and murine cells and they demonstrated acceptable levels

¹ pD is the analogue of pH in deuterated solvents, i.e. $-\log_{10}[D^+]$

of biocompatibility and immunogenicity *in vivo* (143), as well as enhanced bone tissue deposition (44, 52, 53, 55). In biological conditions they can be conveniently self-assembled at the critical concentration and form fibrillary hydrogels (42). This would suggest that they are a promising and novel class of scaffolds for tissue engineering.

Table 2-1. Diagrams showing the primary structure of P₁₁₋₄ and P₁₁₋₈ in physiological conditions (47).

Peptide	Primary structure
P ₁₁₋₄	
P ₁₁₋₈	

2.4.5 Peptides Investigated for Hard Tissue Engineering

A number of self-assembling systems have been previously described and suggested as potential candidate materials for skeletal tissue regeneration. Pioneering work by Stupp's group presented a self-assembling peptide amphiphile (PA) specifically designed to initiate nucleation of hydroxyapatite (144). These molecules were shown to direct the nucleation of hydroxyapatite nanocrystals in a way that resembled the relationship between collagen fibres

and mineral crystals in bone. Later, PAs were combined with porous titanium implants in an attempt to combine the bioactivity of the peptides with the mechanical strength of the metal (145) and were shown to regenerate bone in a rat femoral model. Self-assembling β -hairpin peptides have also been shown to be capable of directing mineralization (146). Several groups have investigated the role of particular motifs derived from or based upon natural peptides or proteins in hydroxyapatite nucleation. Dentine matrix protein 1 (DMP-1) self-assembles in nature and He et al. (147) could nucleate mineral *in vitro* using them, with the acidic domains being central to the nucleation process.

To date, there are several published studies using P₁₁ peptides focusing on their use as self-supporting gels for hard tissue engineering, and these structures have shown promising properties (148). In a study by Kyle et al. (143), P₁₁₋₄ was investigated and shown to form a self-supporting isotropic hydrogel at concentration of 10-30 mg mL⁻¹ while supporting primary human dermal fibroblast cell proliferation in three dimensions (50). Kirkham et al. (50), evaluated P₁₁₋₄ in treating and preventing dental caries which shown to promote deposition and growth of hydroxyapatite. Subsurface caries-like lesions were introduced into extracted human teeth by explosion of the teeth to a demineralising solution (at acidic pH) for several weeks. Treatment was done using either 10 μ l of an aqueous P₁₁₋₄ monomer solution (at pH 8) or a control solution without peptide. The teeth were then exposed to a pH cycling model where the peptide self-assembly into a gel takes place in the caries *in situ* and then they were exposed to mineralising solutions (at neutral pH) at 35° C for 5 days. Phosphorus levels in the solutions were monitored to measure any uptake or loss of mineral and this treatment with peptide resulted in a net mineral gain significantly larger than that of the control (50, 55). Following these promising clinical trial studies, P₁₁₋₄ was patented by University of Leeds and commercialised for dental repairs by the Swiss company Credentis AG (Zurich, Switzerland) (149).

In another study, P₁₁-4 and P₁₁-8 hydrogels were applied to critical size defects in rabbit calvaria and they showed bone regeneration over three months, although the extent to which mineralised tissue ingrowth occurred was greater in the negatively charged P₁₁-4 than positively charged P₁₁-8 (53). It was suggested that this was related to its mirroring of natural ECM proteins in skeletal tissues especially in the presence of negative charged domains on the assembled fibrillar surfaces. The ability of the extracellular matrix (ECM) to influence mineral deposition is key to biomineralisation events (150, 151) and this has stimulated much research in ECM biomimetic materials.

Most of the published studies using P₁₁ peptides have focused on the molecular design of self-supporting gels, however, despite their inherent biofunctionality, self-assembled peptide gels frequently suffer from poor mechanical strength and lack of structural stability. This potentially makes their handling and fixation during implantation *in vivo* challenging, particularly in large load-bearing tissue defects. Attaining mechanically-competent scaffolds capable of supporting cell growth spatially and temporally until the newly engineered tissue is formed, is one of the major challenges in the design of SAP-based medical devices (1). The incorporation of SAPs within water-stable synthetic fibres is a potential route to address this challenge, and to deliver structurally reinforced fabrics. Of the various ways of making fibres, electrospinning is by far the most commonly encountered method for tissue engineering.

2.5 Electrospun Scaffolds

Electrospinning is a simple, inexpensive, and efficient technique to produce fibrous layers. Ma et al. (152) reported that polymeric nanofiber scaffolds produced by electrospinning potentially mimic characteristics of natural extracellular matrix (ECM). As electrospun fibres have a high pore volume and surface area, and can be produced from a wide range of biocompatible polymers, they have been extensively studied in the form of nanofibre scaffolds for tissue

engineering and biotechnology (152). The fact that nanofibres are not tightly bonded together is considered a benefit in tissue engineering scaffolds, since it helps tissue in-growth and cell migration as well as cell distribution in the fibrous structure. However, by producing appropriate layering of fibres in a composite electrospun web, the strength can be improved if needed (153).

For bone tissue engineering applications, a 3D, biodegradable and porous scaffold with interconnected pores and mechanical stability is required. Electrospinning has emerged as a facile method of fabricating bone scaffolds with suitable morphology, porosity and mechanical stability (154).

Typically, synthetic polymers are considerably easier than natural polymers to electrospin, which is reflected by the larger number of synthetic polymers that have been electrospun into nanofibres. Both organic and water soluble biopolymers have been studied. Amongst the most common polymers are poly(ϵ -caprolactone) (PCL), poly(L-lactic acid) (PLA), polyurethane, copolymers of poly(ethylene glycol) (PEG) and PCL, poly(L-lactic acid -co- ϵ -caprolactone) (P(LLA-CL)), and poly (d,l-lactic-co-glycolic acid) (PLGA), poly(ethylene oxide) (PEO) and polyvinyl alcohol (PVA) (24, 155, 156).

In addition to synthetic polymers, the self-assembly of some (poly-) peptides and proteins has been explored using electrospinning, aimed at accomplishing biomimetic scaffolds and unusual architectures. Nuansing et al.(157) attempted to electrospin a short peptide of Fmoc-FG (Fmoc-Phe-Gly) which resulted in rough fibres with diameters of around 300 nm, while Haynie et al. (18) successfully electrospun polypeptides of poly(L-ornithine) (PLO) and poly(L-glutamic acid-co-L-tyrosine) (PLEY) resulting in fibres with diameters ranging from 0.1 μ m to several microns. Tayi et al.(158) also attempted to electrospin peptide amphiphiles (PAs) into micrometre-scale fibres without a polymer carrier. In all of these studies, in addition

to the serious challenges involving the optimisation of the spinning solution as well as electrospinning process parameters, the resulting pure electrospun (poly)- peptides webs were not mechanically robust enough for handling and clinical use. Since the self-assembly is only stabilised by weak non-covalent bonds, resulting architectures can only be partially customised, and electrospinning a classical synthetic polymer containing the bioactive SAPs is a logical solution. Natural polymers are often blended with synthetic polymers or salts to increase the solution viscosity and consistency in electrospinning. For example, to electrospin alginate/chitosan composite fibres, poly (ethylene oxide) (PEO) has been added to increase the chain entanglements and decrease the conductivity of the charged polysaccharide solution (135).

2.5.1 Principles of Electrospinning

A substantial body of research has focused on the manufacture, physical properties, chemical characteristics and biocompatibility of electrospun fibres for medical applications, including bone tissue engineering scaffolds. Electrospinning is an established technology to manufacture continuous fibres with average diameters ranging from tens of microns to tens of nanometres. The fibres can vary in morphology, and have a high aspect ratio and high surface to volume ratio. They are produced from synthetic or natural polymer solutions or synthetic polymer melts, assisted by an electric field (135, 159). Electrospinning is a technique in which there are several adjustable process parameters allowing manipulation of the structure of the matrix and fibre diameter.

The simplest setup for needle electrospinning (Figure 2-9), consists of a high voltage power supply, a spinneret (syringe and needle) and a grounded collector (160). The solution is fed from the syringe at a controlled rate and a sufficient voltage is supplied to the needle. In this process, the polymer is electrically charged. At the tip of the needle, the resulting repulsion of

charges (charge density) overcomes the polymer surface tension and forms a conical shape in the solution called Taylor cone. When the electrical repulsion force is greater than the surface tension of the polymer, jet emission occurs at the tip of the Taylor cone and fibres will be formed. In case of dominance of the surface tension over the repulsion forces, Raleigh instability occurs, and polymer droplets can fall from the needle instead of forming fibres heading to the collector (161).

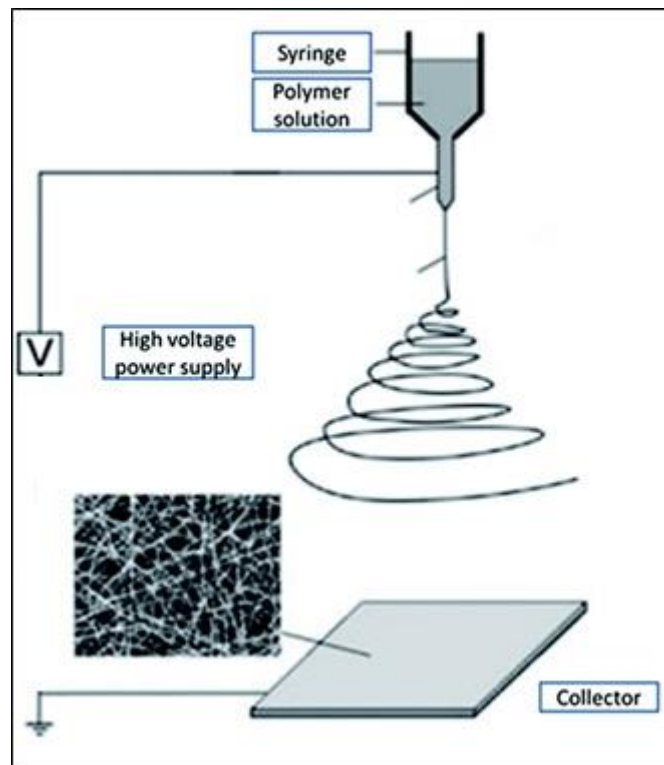


Figure 2-9. Schematic diagram of the needle electrospinning process (image adopted from Ke et al.) (162).

Viscosity and cohesive forces of the polymer play an important role regarding Raleigh instability and continuous fibre forming. As the fibre is electrically charged and travels towards the collector through the electrical field, it interacts with the field and resulting forces make the fibres bend or whip leading to stretching of the jet. This instability and spiral movement is

mainly responsible for attenuation of the jet and for the ultimate fibre diameters deposited on the collector (161).

2.5.2 Electrospinning Parameters

Many parameters influence the ability of the dissolved polymer to be electrospun as well as the properties of resulting fibres. The main parameters include (163):

- Solution properties such as, polymer molecular weight (M_w), concentration, viscosity, elasticity, conductivity, and surface tension.
- System variables which include the flow rate, applied voltage, the polarity of the high voltage power supply, needle diameter, and needle tip to collector distance.
- Environmental conditions such as temperature, humidity, pressure and air velocity.

2.5.2.1 Polymer Solution Parameters

Although research has been reported on thermoplastic polymer melt-electrospinning, most research focuses on electrospinning of polymer solutions. The characteristics of the solution, directly affect fibre formation characteristics and consequently influence diameter and the morphology of the produced fibres (164). Among the various parameters, M_w and polymer concentration have the most direct effect on the viscosity of the polymer and the quality and fibres in terms of morphological consistency and freedom from defects (163).

In practice, polymer concentration usually has an upper and lower limit, if the polymer concentration or M_w is too low, there is insufficient chain-entanglement for the formation of filaments and there will be bead formation or electro-spraying instead of electrospinning. At very high polymer concentrations or M_w it is impossible to electrospin as the flow of the polymer solution to the needle tip is interrupted due to the viscosity and needle blockage may occur (163).

There is a relationship between the fibre diameter and polymer solution concentration known as the Berry number ($[\eta]c$), and this has been reported for polymers such as PVA (165).

Equation 2-1 shows the relationship between Berry number and fibre diameter (D):

Equation 2-1

$$D \text{ (nm)} = 18.6 ([\eta] C)^{1.11}$$

Where;

$[\eta]$ is the intrinsic viscosity of the polymer solution, (mL g^{-1})

C is the concentration of the polymer solution, (g mL^{-1})

Equation 2-1 shows the fibre diameter directly depends on the molecular conformation of the polymer in the solution (concentration and viscosity). In constant electrospinning conditions, the diameters of fibres obtained from solutions of lower concentration have smaller fibre diameters than those obtained from those of higher concentration. In another study, it was shown that, at very low concentrations, droplets are formed instead of fibres, and when the concentration increases, the fibre diameter increases (166).

The choice of solvent plays an important role in electrospinning because of the effect on resulting fibre properties (164). The rate of solvent evaporation is critical in fibre formation, and is affected by the environmental conditions and type of solvent. A study using different solvents for electrospinning of polystyrene suggested that the rate of solvent evaporation along with jet stretching due to electrical forces, are responsible for the diameter, structure, and properties of the deposited nanofibres (164). The rate of solvent evaporation is also likely to influence the cross-sectional shape and morphology of fibres collected during electrospinning, and whether they are approximately cylindrical or flat, ribbon-like or porous (159).

One important physical aspect of electrospun fibres, which can affect fibre shape and diameter, is the dryness of the fibres as they are collected. In a study by Wannatong et al. (164), it was found that the dryness of electrospun fibres increases if the density and the boiling point of the solvent decreases. In addition to the solvent type, the morphologies of electrospun fibres are strongly dependent on electrospinning conditions. Therefore, dryness can also be increased by increasing the applied voltage and collection distance (164).

The electrospinning process can only occur when a solution has sufficient charges so that the repulsive forces within the solution can overcome the surface tension. The ability for a solution to incur stretching and drawing also depends on how well the solution can carry charges (167). There are a number of studies reporting that high solution conductivity can cause fibre formation free from beads (168-170). Another study has shown that addition of salts to the electrospinning solution, can lead to a higher charge density on the jet surface resulting in an increase in the elongation and formation of finer fibres free from beads (171).

2.5.2.2 Processing Parameters

Understanding electrospinning process parameters is fundamental to controlling web characteristics and the structural features of the collected webs.

Voltage

A sufficiently high voltage is essential to initiate jet formation. Voltage firstly induces the required electrical charges on the polymer solution and secondly it creates the electric field in which the jet emerges from the needle tip and is elongated as it travels towards the collector. As the voltage increases, the jet is accelerated and the polymer is stretched due to the increase in electrical charge (171), which usually leads to smaller diameter fibres. However, when the voltage is too high, the acceleration is so fast that the solvent does not have enough time to be evaporated and wet fibres may be formed on the collector (172-174).

The effect however, is not consistent between polymers. In study by Wannatong et al. (164), in which polystyrene fibres were electrospun at different voltage, it was found that by increasing applied voltage, bead formation and fibre diameter decreased. There was a slight decrease in fibre diameter with increasing applied voltage (from 10kV to 25kV), but with a further increase in voltage to 30 kV, the fibre diameter increased. Moreover, the distribution of the fibre diameters changed according to voltage. It was very broad at low voltage, narrowed as voltage increased, but broadened again at the highest voltages of 25 and 30 kV.

In order to explain the effect of applied voltage on the fibre diameter, one must refer to the relationship of three major forces, coulombic, viscoelastic and surface tension all of which operate during the electrospinning process (164). Coulombic force is mainly responsible for the stretching of the jet between the spinneret and the collector, as it tries to push apart adjacent charged carriers. The viscoelastic force opposes stretching of the charged jet, as does the surface tension.

When the applied voltage is low (164), the coulombic force is not high enough compared to the surface tension, resulting in fibres with large diameters and the presence of beads within the collected web. When a moderate voltage is applied, all three forces are well balanced, resulting in a narrow distribution of fibre diameters and a decrease in fibre diameter. Further increases in voltage, lead to coulombic forces being much greater than that of the viscoelastic force, resulting in breakage of filaments due to over-stretching of the charged jet between the needle and the collector. The coulombic force causes both longitudinal and transverse stretching, the latter of which increases the fibre diameter. Moreover, at higher voltage, the jet flies to the collector much quicker, and the solvent does not have sufficient time to evaporate, leading to formation of merging and thicker fibres in the resulting web (164).

By considering the effect of applied voltage in electrospinning, it is recognised that in low-viscosity (low concentration) solutions, the higher applied voltage causes an increase in fibre diameter, because at the constant strain rate, the mass flow rate increases. However, in high-viscosity (high concentration) solutions, if the applied voltage increases, fibre diameter decreases, because in this situation frictional forces between the solution molecules are high, and it limits the mass flow rate, while the strain rate increases, and therefore there is a decrease in fibre diameter (166). Some other studies have reported that changing the applied voltage while keeping the distance between the electrodes constant, does not significantly change the fibre diameter (166).

Distance

It is known that by increasing the distance between the needle tip and the collector, the polymer solution has more time to travel and be stretched, therefore a smaller fibre diameter can be achieved (167). When the distance is too low, it may result in collection of wet fibres that are merged and form junctions in the resulting web (173).

In a study by Cengiz et al. (166), it was found that polymer solution concentration, the distance between the needle and the collector, and applied voltage can significantly control the fibre diameter. In the mentioned research (166), polyacrylonitrile (PAN) polymer was dissolved in pure dimethyl sulfoxide (DMSO) with concentrations ranging from 10, 13, 15 to 17 w %. Moreover different voltage values of 10, 15, 20, 22.5, 30, 35, 40 kV were applied and various tip to collector distances of 5, 10, 15, 20 and 25 cm were explored. In terms of the effects of applied voltage and the distance between the spinneret and the collector on fibre diameter, the fibre diameter increased with increasing voltage and distance. These results were obtained in experiments using low solution concentration values (13% w, 15% w). However, at higher concentration values such as 17 w%, the opposite behaviour was observed (166). It may be

concluded that for each characteristic of polymer solution, the effects of voltage and distance on fibre diameter can vary.

Flow rate

Typically the polymer solution is ejected from the needle assisted by hydrostatic pressure, using a syringe pump. If the electrospinning setup is vertically oriented, gravitational force can also affect on the polymer flow rate (175). Finding an appropriate polymer flow rate depends on factors such as polymer viscosity and the needle orifice or spinneret diameter. If the flow rate is very low, the solution may solidify in the needle and will not be able to form a Taylor cone. If the Taylor cone does form the diameter of produced fibres can be very small. In contrast, when the flow rate is high, due to the larger volume of solution being discharged, at a set distance, the resulting fibres will be thicker (171).

Polarity of High Voltage Power Supplier

Electrospinning uses electrical force to draw and stretch a polymer jet instead of mechanical forces (like in melt and wet spinning). In electrospinning, the syringe is usually charged by a power supply and the collector plate is grounded, although this can be reversed. Kilic et al. (176) investigated the reverse setup and discovered that fibre production efficiency in terms of collection of small diameter fibres was inferior to that associated with the conventional setup of a charged syringe and grounded collector. In the reverse setup, the columbic force is not high enough to stretch the polymer jet (176). Moreover in conventional electrospinning setups the power supply is connected to positive polarity electrode, but alternatively, it can be connected to negative polarity. Supaphol et al. (177) studied the change in the polarity of charge of the syringe needle in electrospinning of polyamide-6 dissolved in formic acid. Their result showed that negatively charged jets led to larger fibre diameters than those that were positively charged. They claimed that PA-6 cations and PA-6 anions are injected in positively and negatively charged needle respectively, and as the cations are larger and bulkier than PA-6

anions, more columbic force acts in the negatively charged needle which leads to greater polymer flow rate and consequently larger fibre diameters in negatively charged conditions (177).

2.5.2.3 Ambient Condition Parameters

As previously mentioned, environmental parameters such as humidity and temperature can affect the electrospinning process and the resulting webs (175).

Humidity

According to the type of the solvent, humidity can affect the properties of the polymer solution. Aqueous solutions are obviously more affected, since the humidity is a function of vapour pressure, can influence the solvent evaporation rate. In non-aqueous solutions, humidity can be influential in several ways. For example the solution can absorb water during flight of the polymer jet (178), and reduce solvent evaporation and consequently increase fibre diameter and create pores in the fibre surface. If the water vapour pressure is too high the evaporation rate decreases as a result of the saturation effect.

Temperature

Increasing the temperature has two main effects on fibre formation in electrospinning, which are an increase in the solvent evaporation rate and a decrease in the viscosity of the solution (167). At high temperatures, the polymer solution dries quicker and there is less time for elongation of the jet during its flight toward the collector. In contrast, high temperature can lead to a decrease in viscosity, which means there is reduced flow resistance in the polymer solution, allowing the fibre to elongate more readily during its flight (175).

2.5.3 Production of Electrospun Scaffolds Containing Self-assembling Peptides

As indicated in Section 2.4.5, self-assembling peptides have utility as tissue engineering materials, particularly if they can be delivered in a form that lends them greater strength and stability when formed in to a scaffold.

A nano-structured scaffold of PCL fibres coated with self-assembling peptide amphiphile (PA) nanofibres, was reported by Tambralli et al. (179). TEM images verified successful PA self-assembly into nanofibres (diameters of 8 – 10 nm) using a solvent evaporation method. This evaporation coating method was used to successfully coat PAs onto PCL nanofibres (diameters of 300 – 400 nm), to develop a hybrid bioactive scaffold. SEM characterisation showed not only that the PA coatings did not interfere with the porous PCL nanofibre network, but there was also greater attachment and spreading of human mesenchymal stem cells (hMSCs), which were seeded onto the scaffolds to evaluate their bioactivity. This novel strategy seems to be a new solution to overcome the current bioactivity challenges of electrospun scaffolds and combines the unique characteristics of PCL fibres and self-assembling PAs, for various biomedical applications (179).

Andukuri et al.(36) coated electrospun PCL fibres with peptide amphiphiles (PAs) for cardiovascular implants, whereby PAs were self-assembled at the surface of the nanofibres by a solvent evaporation technique. These peptides are capable of carrying enzyme-mediated degradable sites and cell-adhesive ligands to biomimic the native endothelium environment. Significant improvement was observed in adhesion and proliferation of human umbilical vein endothelial cells (HUVECs), however there were limitations in smooth muscle cell proliferation and adhesion of platelet cells (36). In another study, electrospun PCL scaffolds were covalently modified by perlecan domain IV peptide, and this approach led to significantly enhanced cell adherence and infiltration in a 3-D pharmacokinetic cancer model (37).

To avoid such post coating treatments, peptides components can also be directly blended with polymer in solutions to fabricate commixed electrospun fibres in one step. Single step electrospinning of a mixture of poly(lactic-co-glycolic acid) (PLGA) and peptide (CGGRGDS) was demonstrated by Gentsch et al. (38), which resulted in fibre surface enrichment with peptide. In other approaches, PCL/peptide conjugates were electrospun to specifically and non-covalently guide the spatial arrangement of biomolecules such as glycosaminoglycans (GAGs) within the scaffold, so that biological gradients found in native tissues could be successfully mimicked. (39) Furthermore, a variety of self-assembling peptides (EAK, DAK, EAbuK, EYK, RGD-EAK, and RGD-EAKsc) have been added into PCL solutions prior to electrospinning (32). The resulting fibres containing peptide not only exhibited higher surface wettability and amorphous phase compared to that of PCL, but there was also an improvement in h-osteoblast cell adhesion.

A few drug delivery applications using a combination of polycaprolactone and self-assembling peptides via electrospinning have also been reported, the result of which suggests that encapsulated PCL/SAP electrospun matrices may impact the drug controlled release technology area in the future (180, 181).

2.6 Summary

Bone tissue engineering has potential to transform medical care for hundreds of thousands of patients annually, with the possibility of dramatic reductions in medical costs, since it provides an alternative to bone transplantation. The required characteristics of a bone tissue engineering scaffold are: 3D structure, highly permeable and porous, interconnected pore network, biocompatible and biodegradable material composition, suitable surface chemistry and sufficient mechanical properties similar to those of healthy surrounding tissues.

For effective bone tissue engineering, which is a complex and dynamic process, osteoprogenitor cells (preosteoblast cells) need to migrate, proliferate and differentiate such that eventually, bone tissue matrix will be formed. Beside this, remodelling of the bone by nucleation and growth of bone minerals needs to occur throughout the bone tissue scaffold, which should provide mechanical support during the process of repair and regeneration of damaged or diseased bone (182).

Whilst biomaterials in the form of synthetic polymers have good mechanical and physical properties and can support tissue growth, they may lack cell recognition signals. Unfortunately, natural biomaterials that are biocompatible may promote cell adhesion and proliferation, but they usually have poor physical stability.

Self-assembling peptides are one class of biomaterial that have undergone rapid development in the last two decades, and they show promise as scaffold biomaterials. Specifically, peptides P₁₁₋₄ and P₁₁₋₈ have been found to be non-cytotoxic to human and murine cells and they demonstrated acceptable levels of biocompatibility and immunogenicity for tissue engineering. There is substantial evidence to support the suggestion that rationally designed P₁₁₋₄ and P₁₁₋₈ SAPs are capable of inducing *de novo* mineral nucleation and supporting mineral growth for hard tissue regeneration (53). However, despite their inherent biofunctionality, self-assembled peptide gels suffer from poor mechanical strength and lack of structural stability. This potentially makes their handling and fixation during implantation *in vivo* challenging, particularly in large load-bearing tissue defects. Attaining mechanically-competent scaffolds capable of supporting cell growth spatially and temporally until the newly engineered tissue is formed, is one of the major challenges in the design of SAP-based medical devices (1). The incorporation of SAPs within water-stable synthetic fibres is a potential route to address this challenge, and to deliver structurally reinforced fabrics.

Among the possible manufacturing processes to produce scaffolds containing SAPs, electrospinning benefits from simplicity and is an inexpensive setup with the ability to control many key factors, such as the fibre diameter, morphology and composition. Electrospun webs have the advantage of small fibre diameter and large surface area, which is beneficial for cell attachment, and bioactive factors such as SAPs aimed at improving mineralisation can potentially be incorporated.

Therefore, as indicated in Chapter 1, Section 1.4, the aim of this work was to investigate the feasibility of producing a functional and structurally stable fibrous scaffold in one-step electrospinning of P₁₁₋₄/P₁₁₋₈ SAP and PCL.

CHAPTER 3

Materials and Methods

This chapter details the raw materials and chemicals used in the research as well as the experimental setups, methodologies and characterisation techniques used for the experimental work.

3.1 Materials

The peptides and other polymers and reagents used in this study for the experimental work together with the suppliers are listed in Table 3-1 and Table 3-2 respectively.

Table 3-1. List of peptides used in the experimental work.

Peptides	Supplier
Peptide P ₁₁ -4 (CH ₃ CO-Q-Q-R-F-E-W-E-F-E-Q-Q-NH ₂) (1,595 Mw)	Neosystems SNPE, France. Credentis, Switzerland.
Peptide P ₁₁ -8 (CH ₃ CO-Q-Q-R-F-O-W-O-F-E-Q-Q-NH ₂) (1,565 Mw)	Neosystems SNPE, France. C.S. Bio, USA.
Fluorescein- β -Ala – P ₁₁ -4 (Fluorescein- β -Ala-Gln-Gln-Arg-Phe-Glu-Trp-Glu-Phe-Glu-Gln-Gln-NH ₂ (HPLC purity 95.1%).	Polypeptide Group, France.
Fluorescein- β -Ala – P ₁₁ -8 (Fluorescein- β -Ala-Gln-Gln-Arg-Phe-Orn-Trp-Orn-Phe-Glu-Gln-Gln-NH ₂ (HPLC purity 95.1%).	Polypeptide Group, France.

Table 3-2. List of chemicals and reagents used in the experimental work.

Chemicals	Supplier
Poly(ϵ -caprolactone) (PCL) (80,000 Mw)	Sigma Aldrich, UK.
Hexafluoro-2-propanol (HFIP), purity \geq 99.0%	Sigma Aldrich, UK.
Dulbecco's modified eagle's medium (DMEM)	Sigma Aldrich, UK.
Dimethyl sulfoxide (DMSO), purity \geq 99.0%	Sigma Aldrich, UK.
4-(2-hydroxyethyl)-1-piperazineethanesulfonic acid (HEPES)	Sigma Aldrich, UK.
Sodium phosphate dibasic dihydrate ($\text{Na}_2\text{HPO}_4 \cdot 2\text{H}_2\text{O}$)	Sigma Aldrich, UK.
Calcium nitrate ($\text{Ca}(\text{NO}_3)_2$)	Sigma Aldrich, UK.
Sodium chloride (NaCl)	Sigma Aldrich, UK.
Hydrochloric acid (HCl), 37%	Sigma Aldrich, UK.
Sodium hydroxide (NaOH), \geq 98.0%	Sigma Aldrich, UK.
Foetal bovine serum (FBS)	Sigma Aldrich, UK.
Penicillin/streptomycin (P/S)	Sigma Aldrich, UK.
Methylthiazolyldiphenyl-tetrazolium bromide (MTT)	Sigma Aldrich, UK.
CellTiter 96® AQueous One Solution (MTS)	Promega, USA.
Sodium hydrogen carbonate (NaHCO_3)	Sigma Aldrich, UK.
Potassium chloride (KCl)	Sigma Aldrich, UK.
Di-potassium hydrogen phosphate trihydrate ($\text{K}_2\text{HPO}_4 \cdot 3\text{H}_2\text{O}$)	Sigma Aldrich, UK.
Magnesium chloride hexahydrate ($\text{MgCl}_2 \cdot 6\text{H}_2\text{O}$)	Sigma Aldrich, UK.
Calcium chloride (CaCl_2)	Sigma Aldrich, UK.
Sodium sulphate (Na_2SO_4)	Sigma Aldrich, UK.
Tris- hydroxymethyl aminomethane ($(\text{HOCH}_2)_3\text{CNH}_2$)	Sigma Aldrich, UK.
Agarose	Sigma Aldrich, UK.
Poly-L-glutamic acid sodium	Sigma Aldrich, UK.
Nitric acid (HNO_3), \geq 90.0%	Sigma Aldrich, UK.
Acetone, 99.5%	Sigma Aldrich, UK.
Distilled water	Distilled in house.

3.2 Experimental methods

3.2.1 Electrospinning Solution Preparation

To determine the best conditions for electrospinning PCL/Peptide solutions to produce a suitable web, initial experiments were carried out by first making solutions of 100% PCL in hexafluoro-2-propanol (HFIP) at concentrations of 6% (w/w), 8% (w/w), 10% (w/w) and 12% (w/w) (Table 3-3). Solutions were prepared by adding PCL material into 10 mL of solvent while being stirred with a stirrer bar on a UC151 Stuart stirrer. Each solution was continuously stirred at room temperature for 24 h to obtain a clear solution. After stirring, the solutions were stored at room temperature under a fume cupboard for 24 h in order to liberate any air bubbles.

Table 3-3. Spinning solution compositions (w/w) and associated solute and solvent weights.

Sample	Solvent HFIP (volume)	Solvent HFIP (weight)	PCL (weight)	Concentration (w/w) %
1	10 mL	15.9 g	0.95 g	6%
2	10 mL	15.9 g	1.27 g	8%
3	10 mL	15.9 g	1.59 g	10%
4	10 mL	15.9 g	1.90 g	12%

Next, to prepare the commixed PCL and peptide solutions, all solutions were prepared by dissolving PCL in HFIP at a concentration of 6% (w/w) according to the method described at the beginning of the current section (Section 3.2.1). The 6% PCL concentration was chosen based on the optimum concentration of PCL found in the preliminary results which will be described in Section 4.2.1. Then different peptides were added to make two separate spinning solutions. The first was P₁₁₋₄ with a peptide sequence of CH₃CO-Gln-Gln-Arg-Phe-Glu-Trp-Glu-Phe-Glu-Gln-Gln-NH₂ (M_w =1,595, a peptide content ~ 94.9% and a HPLC purity of 95.0%). The second was P₁₁₋₈ with peptide sequence of CH₃CO-Gln-Gln-Arg-Phe-Orn-Trp-Orn-Phe-Glu-Gln-Gln-NH₂ (M_w =1,565, peptide content ~ 77.8% and a HPLC purity of 96%). The peptides were added to the solutions individually at concentrations of 10, 20 and

40 mg mL⁻¹. Then, the solutions were left for 24 h until clear mixtures were obtained. The peptide contents for P₁₁-4 and P₁₁-8 in each solution are given in Table 3-4 and Table 3-5.

Table 3-4. Peptide content in each solution of PCL/P₁₁-4.

P₁₁-4 in the solution of (6% w/w) PCL in HFIP	Peptide concentration mg mL⁻¹	Peptide content mg mL⁻¹
1	10	9.49
2	20	18.98
3	40	37.96

Table 3-5. Peptide content in each solution of PCL/P₁₁-8.

P₁₁-8 in the solution of (6% w/w) PCL in HFIP	Peptide concentration mg mL⁻¹	Peptide content mg mL⁻¹
1	10	7.78
2	20	15.56
3	40	31.12

3.2.2 Needle Electrospinning

The schematic of conventional needle electrospinning setup used in this study was previously shown in Figure 2-9. The electrospinning solutions were poured in to a 5 mL or a 10 mL syringe fitted with a 21 gauge blunt tipped needle. The syringe was connected to a dual head syringe pump (Kd Scientific Model 200 Series) and the solution was evacuated with a feed rate of 1 mL h⁻¹. The voltage was supplied to the needle at its base (Glassman Inc.) via a copper electrode. Voltages of 20 kV to 25 kV and a tip to collector distance between 160 mm to 200 mm was used. The power supply was connected to a positive polarity electrode unless otherwise stated. An aluminium foil collector (150 mm × 150 mm) was placed on a non-conducting board and was grounded by connecting to a ground cable. The electrospinning procedure was conducted in a fume cupboard with continuous suction to evacuate the solvent vapour. An ambient temperature of 21°C ± 2°C and a humidity of 43% ± 2% were consistently recorded in the spinning chamber. After deposition, fibre webs were transferred into a

Gallenkamp OVL570 010J vacuum oven to be dried at room temperature under 10×10^3 Pa vacuum for 7 days to ensure all solvent residues were evaporated, unless otherwise stated.

To determine the approximate concentration of peptides within the as-spun fibres, the weight of the spun webs was recorded after drying. Since in needle electrospinning there is always deposition of a small amount of fibre outside the collection zone, this calculation is approximate. The mass of SAP in the spun webs was calculated assuming a homogeneous distribution of peptide within the spun fibres, and based on the initial mass of PCL and SAPs in the spinning solution, as in Equation 3-1 and Equation 3-2:

Equation 3-1

$$\text{Mass of SAPs in electrospun fibres} = M_s \times R$$

Equation 3-2

$$R = M_{\text{SAP}} / (M_{\text{SAP}} + M_{\text{PCL}})$$

Where;

M_s is mass of electrospun fibre sample.

M_{SAP} is mass of SAPs in each mL of electrospinning solution.

M_{PCL} is mass of PCL in each mL of electrospinning solution.

Since the mass of PCL in each mL of the PCL/SAPs electrospinning solutions (at a concentration of 6% (w/w)) was always 95 mg, and based on the pure peptide contents at each concentrations (Table 3-4 and Table 3-5), the R for each peptide-concentration was determined in Table 3-6.

Table 3-6. Ratio (R) of mass of peptide to mass of peptide+PCL in the electrospinning solutions based on different peptide concentrations.

Peptide	Concentration of SAP (mg) in 1 mL ES solutions	R
P ₁₁₋₄	10	0.090
	20	0.166
	40	0.285
P ₁₁₋₈	10	0.075
	20	0.140
	40	0.246

3.2.3 Scanning Electron Microscopy (SEM)

To elucidate details of the morphology of the electrospun webs as well as the degree of bead formation, fibre diameter and fibre orientation, electrospun samples were imaged using a scanning electron microscope. A LEO 1530 Gemini field emission scanning electron microscope (FESEM) (manufacturer: Zeiss) or a SU8230 high performance cold field emission (CFE) microscope (manufacture: Hitachi) were used during the course of this study according to the availability of machines. An accelerating voltage between 2 kV and 15 kV were used in order to record morphological features of individual fibres. SEM has the advantage of producing images with an increased depth of field and greater resolution compared to optical microscopes. In the SEM a beam of electrons is focused onto a specimen and the radiation emitted from the specimen is detected, which forms the image (183). In order to overcome build-up of electrical charge on the surface of the fibres, which have low conductivity, and to obtain high resolution images, samples were first coated with a thin layer of conducting material such as gold or platinum (184). Prior to imaging, all samples were cut and mounted onto 25 mm aluminium stubs and were sputter coated with platinum /palladium in vacuum for 3-4 min to a thickness of 7 nm using an Agar AGB7234 high resolution sputter coater machine.

3.2.4 Fibre Diameter Measurements

Fibre diameter measurements of PCL and PCL/SAP fibres were obtained based on SEM images using Image Pro Plus 6.2.1 software (Media Cybernetics). In this study, at least 100 fibre diameter measurements per sample were obtained to determine mean, maximum and minimum fibre diameters, and the associated frequency distributions. In order to ensure random selection of fibres, for diameter measurements, two diagonal lines were drawn from top right to bottom left and top left to bottom right of the image and the diameter of every fibre crossing the two lines were recorded (185). Two examples of the fibre diameter measurement procedure are shown in Figure 3-1. Diameters were measured based on multiple SEM images and at different magnifications (20Kx - 120Kx).

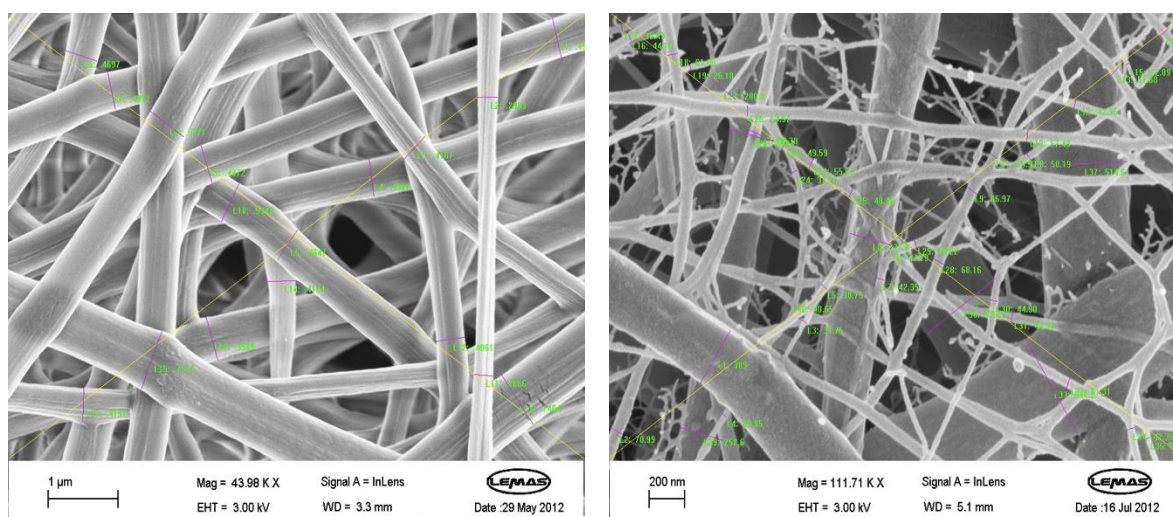


Figure 3-1. Examples of SEM micrographs with fibre diameter measurements being made along the yellow lines.

3.2.5 Transmission Electron Microscopy (TEM)

To more extensively investigate the nano- and submicron architecture of the fibres, transmission electron microscopy (TEM) was employed as it has the advantage of achieving up to fifty million times magnification. TEM is based on transmitted electrons wherein electrons are passed through an ultra-thin specimen and as they interact with the atoms of the

specimen, the image is formed (186). TEM round copper grids coated with carbon (3.05 mm OD) were mounted on the electrospinning collector (aluminium foil) using double sided tape and a thin layer of the fibres was directly electrospun onto the collector and consequently onto the TEM grids. In this study, TEM analysis was performed using a FEI Tecnai TF20 and carbon coated copper grids were purchased from Agar Scientific.

3.2.6 Environmental Scanning Electron Microscopy (ESEM)

ESEM is a scanning electron microscopy technique which is able to image specimens in a wet or uncoated state by allowing a gaseous environment in the specimen chamber and operating in a low vacuum mode. In order to elucidate the effect of drying procedures and solvent evaporation on the as-spun fibre and fibril morphology, ESEM was employed. This was conducted to understand if air or vacuum drying (immediately after electrospinning) or vacuum drying (during the coating preparation of samples, as well as within the vacuumed chamber of the normal SEM) have any effects on the structure of fibres. ESEM uses a specialised electron detector different from a normal SEM and also employs a differential vacuum pumping system (187). However, ESEM has limitations in terms of the resolution of images due to its reliance on a gaseous environment, and use of uncoated, electrically low conductive samples creates difficulties during imaging due to the lack of surface conductivity. In this research, a FEI Quanta 200F FEG ESEM was used in both low vacuum and high vacuum modes. To study as-spun fibres with the ESEM whilst minimising opportunities for them to fully dry on the collector, after a short electrospinning time of 3 min, samples were transferred in liquid nitrogen immediately and imaged in low vacuum mode (60 Pa) of ESEM. To determine if subsequent drying of as-spun fibres to remove residual solvent had any influence on their morphology, the same samples were vacuum dried under the conditions explained in Section 3.2.2 and inspected in the ESEM at 30Kx magnification in the uncoated state under high vacuum mode (0.0006 Pascal). After that, to understand the effects of coating the vacuum dried

samples were coated (according to the coating procedure explained in Section 3.2.3) and they were imaged under high vacuum mode (0.0006 Pascal).

3.2.7 Confocal Laser Scanning Microscopy (CLSM)

The blank (100% PCL samples) and peptide-loaded samples were observed using a confocal laser scanning microscopy (Zeiss LSM510) at 3K-5K magnifications. Confocal laser scanning microscopy (CLSM) is a technique for obtaining high-resolution optical images that can be taken at defined depth of field levels at a time, and therefore the depth of focus can be controlled. CLSM is a conventional microscope equipped with a laser light source, a laser scanning head, an automatic focusing stage. It can be operated in reflected light or in fluorescence mode. In CLSM biological features can be detected if they are first labelled with fluorescent dyes (188). In this study, to investigate the peptide distribution throughout the fibres, both SAPs in the spinning solution were fluorescently labelled with the oppositely charged SAPs functionalized by a fluorescent dye (flouro-SAPs), to aid viewing by confocal microscopy. To do this, fluorescein-labelled SAPs, Fluorescein- β -Ala – P₁₁-4 and Fluorescein- β -Ala – P₁₁-8 were purchased from Polypeptide, France. Each of the SAPs prior to adding into the electrospinning solution were doped with its oppositely charged SAPs functionalised by a fluorescein moiety at the ratio of 1:60 (flouro-P₁₁-4:P₁₁-8 = 1:60 and flouro-P₁₁-8:P₁₁-4 = 1:60). The SAPs were labelled with their opposite functionalised SAPs to produce a polyelectrolyte- β -sheet complex. Mixing an anionic and cationic peptide is an alternative way to induce self-assembly (137) which in this case was the preferred method to ensure full mixing of the flouro-tagged peptides with peptides in solution. A large fluorescein moiety will have a high degree of steric hindrance which would, in an anionic-anionic or cationic-cationic system phase separate and exclude itself from the bulk of the β -sheet structures formed (137).

3.2.8 Energy-Dispersive X-Ray Spectroscopy (EDX)

Energy-dispersive X-ray spectroscopy (EDX) is an analytical technique for elemental analysis of SEM specimens. In this technique, atoms of the elements in the sample are targeted and excited by a high energy beam of electrons, protons, or X-rays and as a result of disturbance in the energy of atoms in their own shell, they emit X rays. By analysing and measuring emitted radiation by means of energy-dispersive spectrometers, and since each element has specific radiation characteristics, chemical analysis of the material can be performed (189). In this research, to characterise the electrospun samples chemically and to detect Nitrogen within the fibres, solely attributable to the peptide component, EDX was employed. An Oxford Instruments (HAADF detector), INCA 350 EDX system was used in combination with the TEM and an AZtecEnergy EDX system was used in combination with SEM analysis at an accelerating voltage of 15 kV to generate sufficient X-rays to allow reliable identification of peaks.

3.2.9 X-Ray Diffraction Crystallography (XRD)

X-ray diffraction crystallography is an analytical technique to determine atomic and molecular structure of crystalline materials. In this method, a beam of incident X-ray is directed towards a sample, and the interaction of the incident rays and the crystalline atoms within the sample diffracts the beam into different specific directions. This allows identification of different minerals because each mineral has a set of unique diffraction peaks (190). In this study to identify any hydroxyapatite crystals formed during biological evaluation of the fibrous samples, an XRD instrument of PANalytical X'Pert MPD fitted with an X'pert Highscore Plus software was employed. Fibre samples were ground to a fine powder and data collection was performed by the 2θ scan method using Cu $K\alpha$ radiation. Spectra were collected between 5° and 70° with a step size of 0.05° .

3.2.10 Fourier Transform Infra-Red Spectroscopy (FTIR)

Fourier transform infrared spectroscopy (FTIR) is a technique used to identify materials by means of qualitative analysis. The analysis is performed by means of transmission of the IR radiation through an interferometer and onto the sample. The sample absorbs all the different wavelengths characteristics of its spectrum and this subtracts specific wavelengths from the interferogram. The atoms and bonds inside the molecule vibrate at different frequencies depending on the type of bond. A detector in the machine records the variation in energy versus time for all wavelengths simultaneously. Fourier transform analysis allows the conversion of the intensity vs. time spectrum into an intensity vs. frequency spectrum. According to the sample components, resulted spectrum shows molecular IR radiation absorption and transmission. The spectrum consists of absorption/transmission picks which represent frequencies of vibrations between the bonds of the atoms (191).

FTIR is also a powerful instrument to determine protein morphology or secondary conformations by analysis of amide region vibrations (192, 193). It probes the amide bonds in peptide molecules and displays distinct spectra for each conformation. To detect the secondary structure of peptides within the fibres in this study, infrared absorption spectrometry was performed with a FTIR Perkin Elmer Spectrum BX spotlight spectroscope attached to a diamond ATR. Measurements were taken in the range between $4000 - 400 \text{ cm}^{-1}$ with a resolution of 4 cm^{-1} and interval scanning of 2 cm^{-1} . 64 scans were averaged for each spectrum. To analyse the peptide status in each spinning solution a Nicolet 6700 FTIR was used to record FTIR spectra and the samples were held onto Calcium Fluoride (CaF_2) windows. 32 scans were averaged for each spectrum and the HFIP solvent spectrum (blank) was subtracted from the spinning solution spectra.

3.2.11 Circular Dichroism Spectroscopy (CD)

To analyse the secondary structure of the peptide in solution, circular dichroism was also utilised. CD spectroscopy is a technique in which the difference in the absorption of left-handed circularly polarised light (L-CPL) and right-handed circularly polarised light (R-CPL) is measured over a range of wavelength. The far-UV CD spectroscopy is frequently used to reflect secondary structure content of proteins (194).

In this study CD spectra were recorded using a Chirascan CD spectrometer and the solutions were analysed in 1 mm path-length cuvettes at 22°C (spinning condition). The data were acquired in the step resolution of 1 nm and at a scan speed of 60 nm min⁻¹. A bandwidth of 4.3 nm was used to have smoother spectra. Far-UV spectra were recorded in wavelength range of 190 to 240 nm. Each spectrum is the average of two scans. The spectrum of HFIP as blank solvent has been subtracted from the spectra of the spinning solutions. The data then were converted to mean residue ellipticity (deg cm² dmol⁻¹) and finally a seventh order polynomial fitting operation was performed ($R^2 \geq 0.95$).

3.2.12 Contact Angle Measurement

Contact angle measurement was employed to characterise the wettability of the webs. Normally, this method is used to analyse solid surfaces. Note that in the analysis of electrospun webs, the contact angle between the wetting liquid and the wetted surface is the result of surface energy interactions between the solid-liquid-air phases (rough surface).

In this study an FTA4000 Microdrop goniometer was used to measure the contact angle. The main components are a camera, dosing syringe, and a lighting system. The size of the droplet, needle to table distance and the image settings are controllable by the goniometer software. The test kit and the test procedure are designed based on the EN 828:2013 standard for wettability determination by measurement of contact angle. For this test the software was set up to start

taking images immediately after the liquid droplet is deposited. For each image the contact angles for both right and left sides of the droplet were measured and averaged. A drop of either deionised water (Milli-Q) or Dulbecco's Modified Eagle's medium (DMEM) with a volume of 1.5 μL was deposited and contact angles over 15 s were measured. Three replicates per sample were examined. In order to account for the porosity of electrospun webs, and determine its influence on wettability properties, films also were prepared out of the same spinning solutions to investigate the surface wettability in the absence of void space. PCL (6% w/w) and PCL/SAPs solutions in HFIP (with SAP contents reported in Table 3-4 and Table 3-5) were cast on glass slides and films were prepared by drying in a Gallenkamp OVL570 010J vacuum oven at room temperature under 10×10^3 Pa vacuum for 48 h. Contact angle measurements were carried out with deionised water and measurements were carried out in the same manner as described for fibrous samples (at the beginning of the current section).

3.2.13 BS EN ISO 10993:2009 Biological Evaluation of Medical Devices

(Cytotoxicity)

The ISO 10993 standard describes methods to assess *in vitro* cytotoxicity of medical devices. These methods specify the incubation of cultured cells in contact with a device and/or extracts of a device either directly or through diffusion. This allows both qualitative and quantitative assessment of cytotoxicity. In this research, both extract cytotoxicity and direct cytotoxicity, methods were employed to study the electrospun materials (195, 196) (195, 196).

3.2.13.1 Extract Cytotoxicity Method

To prepare for extract toxicity testing, 300 mg of electrospun fibres, PCL, PCL/P₁₁₋₄ and PCL/P₁₁₋₈ (both with a peptide concentration of 20 mg mL⁻¹), were prepared according to the method explained in Sections 3.2.1 and 3.2.2. The samples were sent to an external company to be sterilised under gamma irradiation. Samples were then incubated (80 r min⁻¹) in Dulbecco's

Modified Eagle's medium (DMEM) supplemented with 10% foetal bovine serum (FBS) and 1% penicillin/streptomycin (P/S). The amount of fibres soaked in the medium was 100 mg mL⁻¹ and they were incubated for 72 h at 37 °C in 5% (v/v) CO₂ in air (pH 7.4). The fibres were then removed and 100 µl of the leftover medium was collected as the extract of the samples.

For primary cell culture needed to perform the cytotoxicity tests, L929 mouse fibroblast cells were cultured in DMEM using an available cell line (provided in house), with 10% foetal bovine serum (FBS) and 1% penicillin/streptomycin (P/S) at 37 °C in 5% (v/v) CO₂ in air until confluence (usually for 48 h until cell confluency is confirmed). An example image for an acceptable cell confluency level for L929 cells is shown in Figure 3-2.

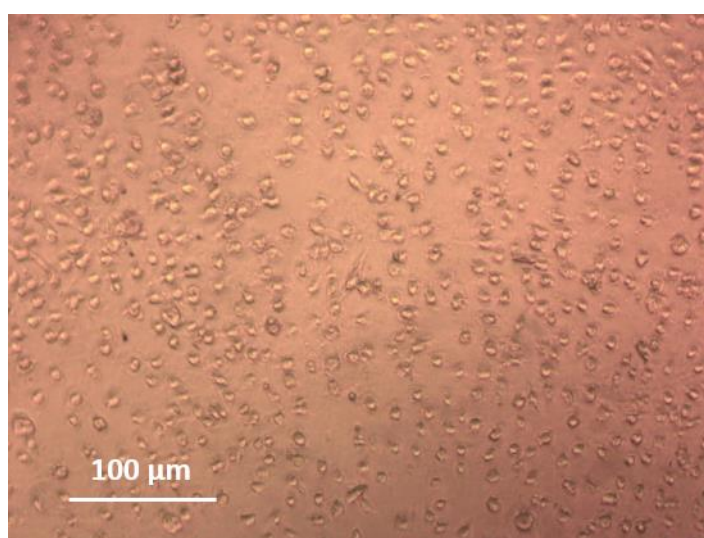


Figure 3-2. An acceptable level of L929 cell confluency for cytotoxicity test (image from the current study).

The cell density was adjusted to 10⁵ cells mL⁻¹ by manually counting the cells. A counting chamber (haemocytometer) which is a microscope slide was used and a drop of cell culture was placed in its sink. The area of the sink is marked with a grid and by looking at the sample under an optical microscope, the number of cells in a given area can be counted. In this study, an Improved Neubauer haemocytometer was used, and based on the predefined depth of the sink,

the volume of the counted culture can be calculated. After measuring the cell density based on that, the required dilution took place to reach the density of 10^5 cells mL^{-1} .

For the cytotoxicity experiment, a 96-well plate (Corning® Carbo-BIND) was used and 100 μL cell suspension with the density of 10^5 cells mL^{-1} was placed into each well plate. After 24 h the cell culture medium was carefully removed and replaced with 100 μL of PCL (negative control), PCL/P₁₁₋₄ and PCL/P₁₁₋₈ samples' extracts, whilst the last two rows were fed with DMEM (blank control) and positive control of DMSO (Dimethyl Sulfoxide, purity ≥ 99.9). Eight replicates were used for each samples and the controls as well. The well plates containing cells and extract of the samples were incubated at 37°C in 5% (v/v) CO₂ in air for 48 h to allow the extracts react with the cells.

Optical Cell Confluency Assessment

After incubation, the well plates were optically examined under Leica DFC365 FX monochrome digital microscope and images were recorded at 200x magnifications to see the morphology of the cells.

MTS Assay

MTS assay is a colorimetric method to quantify viable cells in proliferation and cytotoxicity assay. In this method, MTS tetrazolium compound is reduced by viable cells to generate a coloured formazan product which is soluble in cell culture media. The formazan dye produced by viable cells can be quantified by measuring the absorbance at 490 nm. MTS reagent contains a novel tetrazolium compound [3-(4, 5-dimethylthiazol-2-yl)-5-(3-carboxymethoxyphenyl)-2-(4-sulfophenyl)-2H-tetrazolium, inner salt; MTS] and an electron coupling reagent (phenazine ethosulfate; PES) (197).

In this study after incubating cells and samples for 48 h and optical analysis, the samples were exposed to 20 μL MTS reagent of 'CellTiter 96® Aqueous One' solution directly and incubated

for 4 h at 37°C. The 96-well plate was then placed in Varioskan Flash Reader and the absorbance was recorded at 490 nm. The quantity of formazan product as measured by UV absorption at 490 nm is directly proportional to the number of living cells in culture.

3.2.13.2 Direct Cytotoxicity Method

A brief summary of the method of test performed for direct cytotoxicity is given below.

To prepare for direct toxicity testing, electrospun samples of PCL, PCL/P₁₁₋₄ and PCL/P₁₁₋₈ (both at a peptide concentration of 20 mg mL⁻¹), were prepared according to method explained in Sections 3.2.1 and 3.2.2 and they were sterilised under gamma irradiation in an external company. Samples were cut into 10×10 mm squares. Electrospun PCL was used as negative control as its non-cytotoxicity response is well documented in the literature (27, 31).

For primary cell culture needed to perform the cytotoxicity tests, L929 mouse fibroblast cells were cultured in DMEM (Dulbecco's modified Eagle's medium) using available cell line (provided in house), with 10% foetal bovine serum and 1% Penicillin/Streptomycin (P/S) at 37°C in 5% (v/v) CO₂ in air till confluence (usually for 48 h).

The cell density was adjusted to 10⁵ cells mL⁻¹ by manually counting the cells. A counting chamber (hemocytometer), which is a microscope slide, was used and a drop of cell culture was placed in its sink. The area of the sink is marked with a grid and by looking at the sample under an optical microscope the number of cells can be counted in a given area. In this study, an Improved Neubauer hemocytometer was used, and based on the predefined depth of the sink, the volume of the counted culture can be calculated. After measuring the cell density based on this, the required dilution took place to reach the density of 10⁵ cells mL⁻¹.

For the direct cytotoxicity experiment, two 24-well plates (Corning® Costar) were utilised and 400 µL of either cell suspension (cells +DMEM) with the density of 10⁵ cells mL⁻¹ or DMEM

only was placed into each row of 24-well plate (6 replicates for each sample). The plates were incubated at 37°C for 24 h and the sub-confluency of cells were verified with a microscope. After that the culture medium were removed from each plates and 500 µL of fresh DMEM were placed into the wells. The electrospun samples were firstly soaked with culture medium for 2 h to prevent additional adsorption of DMEM in the test and then each sample was carefully placed in the cell layer in the centre of wells. The blank row was left with DMEM only and in the positive control wells, 250 µL of DMSO (Dimethyl Sulfoxide, purity ≥ 99.9) and 250 µL of DMEM was added. Plates were incubated for 48 h at 37°C in 5% (v/v) CO₂ in air.

Optical Cell Confluency Assessment

After incubation, the well plates were optically examined under a phase-contrast monochrome digital microscope of Leica DFC365 FX to see the morphology of the cells at the edges of fabrics in contact with the cells, and images at 200x magnifications were recorded.

MTT Assay

To quantify the viability of cells in direct contact with eletrospun samples, MTT assay was employed. MTT assay is colorimetric assay to assess viability of cells via cell metabolic activity. Yellow water soluble MTT compound (3-(4, 5-dimethylthiazol-2-yl)-2, 5-diphenyltetrazoliumbromid) is metabolically reduced in viable cells to a blue-violet insoluble formazan. A solubilisation solution (usually either dimethyl sulfoxide, an acidified ethanol solution, or a solution of the detergent sodium dodecyl sulphate in diluted hydrochloric acid) is added to dissolve the insoluble purple formazan product into a coloured solution. After dissolving the formazan, the colour intensity was determined by optical density readings of photometric measurements at 570 nm and 650 nm.

In this study, after the incubation and optical assessment, the culture medium was aspirated from each of the wells and the wells were washed using 200 µL of PBS (Phosphate buffered saline).

Then 200 μL of a filtered sterilised MTT solution ($1 \text{ mg}\cdot\text{ml}^{-1}$ of (3-(4, 5-dimethylthiazol-2-yl)-2, 5-diphenyltetrazoliumbromid) was added to each well and the plates were incubated at 37°C for 2 h. The MTT solution was removed from every well and replaced with 400 μL isopropanol to dissolve the generated blue-violet insoluble formazan. After swaying the plates they were placed in a micro-plate reader and readings were obtained at 570 nm and 650 nm. The quantity of formazan product measured as OD_T (Equation 3-3 and Equation 3-4) is correlated to the number of living cells in each culture.

Equation 3-3

$$\text{OD} = (\text{OD}_{570} - \text{OD}_{650})$$

Equation 3-4

$$\text{OD}_T = \text{OD} - \text{OD}_B$$

Where;

OD_{570} is the mean value of the measured optical density of each sample at 570 nm.

OD_{650} is the mean value of the measured optical density of each sample at 650 nm.

OD_B is the measured optical density of the blank sample.

OD_T is the overall optical density of the test sample.

3.2.14 BS ISO 23317:2014 *In Vitro* Evaluation for Apatite-Forming Ability of

Materials Using Simulated Body Fluid (SBF)

Different kind of materials can bond to living bone through a layer of apatite and this apatite can be reproduced on the surface of the materials in an acellular and protein-free Simulated Body Fluid (SBF). Ion concentrations in SBF is nearly equal to those of human blood plasma and therefore composition and structure of apatite which is formed in SBF is similar to bone mineral (198). A brief summary of the method of test performed in SBF is described below.

3.2.14.1 Preparation of Test Specimens

According to the international standard any configuration and size of the specimens can be used in this test. In the first run, electrospun samples were cut into $10\pm 2 \times 10\pm 2$ mm rectangular shapes (regardless of the weight). In the second run, samples were prepared with regard to their weight and content of peptide in them. However as in needle electrospinning there is always waste of fibres and/or polymer solutions, the calculation would be approximate. The aim was to prepare samples in which there is approximately 40 mg of peptides. Therefore, electrospinning solutions for PCL/SAPs (at peptide concentration of 20 mg mL^{-1}), were electrospun and the fibrous webs (size $\sim 150 \text{ mm} \times 150 \text{ mm}$) were folded twice to make them thicker and with higher concentration of peptide in unit area. Then based on Equation 3-1 and Table 3-6, 240 mg fibres of PCL/P₁₁₋₄ and 285 mg fibres of PCL/P₁₁₋₈ were cut and weighed out. The samples were in rectangular shape ($70\pm 10 \text{ mm} \times 70\pm 10 \text{ mm}$) and with approximate 40 mg of peptide. A control sample of 100% PCL with 250 mg weight was also prepared.

3.2.14.2 Preparation of Simulated Body Fluid (SBF)

The concentration of ions in SBF was defined based on the standard and with this SBF a correlation between *in vivo* bone ingrowth and *in vitro* apatite-forming ability has been observed (198).

SBF Ion Concentration

The ion concentration in SBF and blood plasma is defined in Table 3-7.

Table 3-7. Ion concentration of SBF and human blood plasma.

Ion	Concentration (10^{-3} mol) in	
	SBF (pH 7.4)	Blood plasma (pH 7.2 to 7.4)
Na ⁺	142.0	142.0
K ⁺	5.0	5.0
Mg ⁺	1.5	1.5
Ca ⁺	2.5	2.5
Cl ⁻	147.8	103.0
HCO ₃ ⁻	4.2	27.0
HPO ₄ ²⁻	1.0	1.0
SO ₄ ²⁻	0.5	0.5

Reagents Used in SBF

To prepare SBF, ion-exchanged and distilled water in accordance with ISO 3696:1987 (provided in house) and the following amount of recognised analytical grade chemicals (Table 3-8) were used.

Table 3-8. Reagents for preparation of SBF in the required order of dissolution.

Order	Reagent	Amount	Purity	Formula weight (g/mol)
1	Sodium chloride (NaCl)	8.03 g	99.5 %	58.44
2	Sodium hydrogen carbonate (NaHCO ₃)	0.35 g	99.5 %	84.00
3	Potassium chloride (KCl)	0.25 g	99.5 %	74.55
4	Di-potassium hydrogen phosphate trihydrate (K ₂ HPO ₄ · 3H ₂ O)	0.23 g	99.0 %	228.22
5	Magnesium chloride hexahydrate (MgCl ₂ · 6H ₂ O)	0.31 g	98.0 %	203.30
6	Hydrochloric acid solution (HCl) = 1 mol/L	39 mL	-	-
7	Calcium chloride (CaCl ₂)	0.29 g	95.0 %	110.98
8	Sodium sulphate (Na ₂ SO ₄)	0.07 g	99.0 %	142.04
9	Tris- hydroxymethyl aminomethane ((HOCH ₂) ₃ CNH ₂)	6.11 g	99.0 %	121.13

SBF Preparation Procedure

An inappropriate preparation method could lead to precipitation of apatite in solution since SBF is supersaturated with respect to apatite. Therefore during the preparation, additional care must be taken and the solution must remain colourless, transparent and without any deposit on the surface of glass. 700 mL water was put in a 1 litre plastic beaker with a stirrer bar and covered with a watch glass and they were set in a water bath on top of the stirrer. The water was heated to 36.5 ± 1.5 °C while stirring. Figure 3-3 shows an example of the apparatus for preparing SBF.

After that, the required reagents were dissolved in the order given in Table 3-8 in distilled water at the set temperature. The reagents were dissolved one by one only after the preceding one was completely dissolved. This was more sensitive in the case of TRIS, and therefore by careful note of the pH and temperature change, it was added little by little taking only when pH was stable and temperature was at 36.5 ± 0.5 °C. This is because addition of large amount of TRIS can radically increase the local pH of solution which could lead to precipitation of apatite. Increase in solution temperature can decrease the pH so the pH was kept below 7.4 by the addition of HCl solution. After dissolving all of TRIS, the pH of solution was adjusted to 7.4 ± 0.1 at 36.5 ± 0.2 °C using HCl solution. Then the solution was transferred into a 1 litre volumetric flask and after cooling down to 20°C, a 1 L the solution was prepared by adding required amount of distilled water.

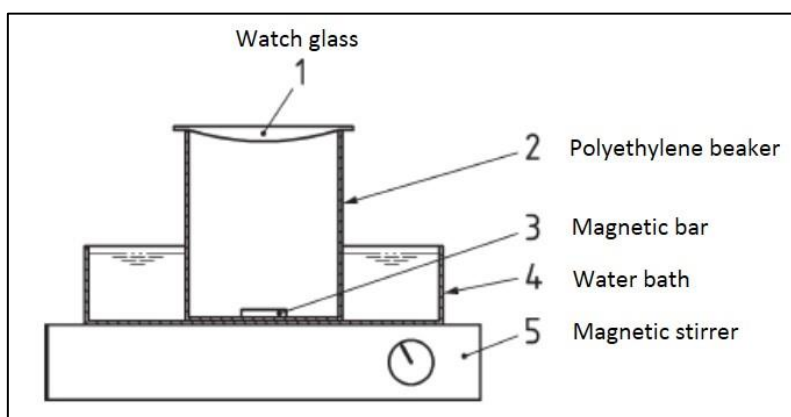


Figure 3-3. Apparatus for preparing SBF (198).

3.2.14.3 Calculation of Volume of SBF

In this study and in the first run, where the specimens were prepared according to their area, the required volume of SBF for each specimen was calculated based on Equation 3-5:

Equation 3-5

$$V_s = 100\text{mm} \times S_a$$

Where;

V_s is the volume of SBF in mm^3 .

S_a is the apparent surface area of the specimen in mm^2 .

In this equation, based on the international standard (198), if the material is porous volume of SBF should be greater than the calculated V_s . Therefore for a $10 \pm 2 \text{ mm} \times 10 \pm 2 \text{ mm}$ rectangular electrospun sample, the consumed SBF was greater than 20 mL and in this study 25 mL was used for each sample.

In the second run, where the samples were prepared based on their weight, a sample to SBF ratio of 0.5 mg mL^{-1} was chosen with inspiration from the work done by Poologasundarampillai et al. (199). Therefore for each 250 mg fibrous sample, 500 ml SBF was used.

The calculated amount of SBF (in each run) was poured in a plastic bottle with a cap. After SBF was heated up to 36.5°C , the samples were placed in each bottle and they were put in an incubator at 36.5°C . In the first run samples were soaked in SBF for three time points of 3 d, 1 week and 2 weeks and in the second run three time points of 1 week, 2 weeks and 4 weeks were applied.

After incubation for different periods within four weeks, the specimens were taken out from SBF and some of them were gently rinsed with distilled water and some were kept unwashed to see

the effect of the washing process. Then the samples were dried in a desiccator at room temperature.

After all the above procedures, to detect any apatite crystals formed on the surface of fabrics they were examined using SEM/EDX, FTIR and XRD analysis.

3.2.15 Peptide Release from Electrospun PCL/SAPs Fibres in Water

The main purpose of this experiment was to see the release behaviour of SAPs from PCL/SAP fibres in aqueous solution at different pH. Self-assembly of the peptides used in this study are pH-sensitive and they can form amphiphilic tapes in water (and further assembly to ribbons and fibrils) depending on pH of the solution and their concentration in solution (200). In principle, all of the transformation from monomeric random coil to fibrils are reversible (47). Therefore based on this behaviour, PCL/SAPs fibres with peptide concentration of 40 mg mL^{-1} were dissolved in aqueous solution at different pH to find out the kinetics of peptide disassembly and release and therefore to estimate the stability of peptides within the fibres in biological conditions. Fibres were first weighed out at their dry state and then they were dissolved in deionised water at pH 3.5, 7.5 and 10.5. The ratio of fibre to deionised water was 1 mg in 3 mL and the pH of deionised water was titrated with 1 μL additions of HCl (1 M) or NaOH (1 M). The samples were incubated at 120 rpm in an orbital shaker incubator of ES-20 model from Grant Bio and the temperature was set at 37°C . After the time points of 30 min, 1 h, 24 h, 48 h and 1 week the samples were taken out of the solution. In some of the time points, the samples were washed three times in the same pH solution to make sure all the peptide residues are washed off. Then the samples were air-dried and weighed out to measure the weight loss. After that the dried samples were subjected to SEM to study any possible morphological changes during the degradation. To confirm the release of peptides into the solution, the supernatant fluid was subject to CD analysis according to the method described in Section 3.2.11. In order to determine

that the overall weight loss in the samples is exactly related to which component (PCL or SAP), the samples were analysed via TGA.

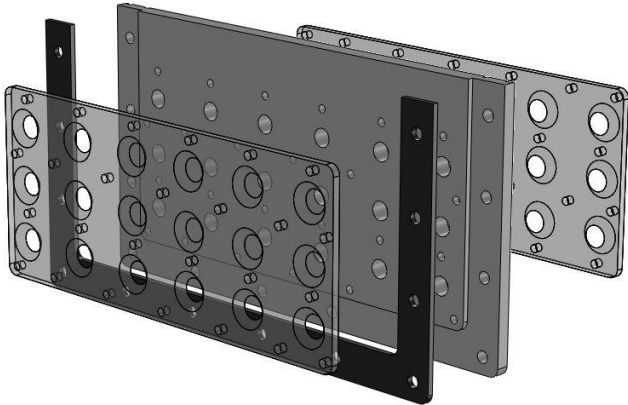
3.2.15.1 Thermogravimetric Analysis (TGA)

The degradation rate of PCL/peptides in aqueous solutions was measured by determining the weight loss of a sample by linearly increasing the temperature in a conventional TGA machine. The thermogravimetric analyses were performed on a TGA Q50 model from TA Instruments, using nitrogen as purge gas. Inert gas flow was 40 mL min⁻¹ for balance purge flow and 60 mL min⁻¹ for sample purge flow. The heating rate used was 10°C per minute and temperature range was 25°C through to 800°C.

3.2.16 IVN Tank Apparatus

The ability of fibres to nucleate hydroxyapatite mineral and support mineral growth *in vitro* was determined using a steady state agarose gel system, based on the method originally described by Hunter and Goldberg (201, 202). Briefly, there are 18 individual cells in a single 10 mm thick sheet of PTFE (sample holder) and each cell was filled with 1 mL of a solution and was allowed to gel. Squares of dialysis membrane (SpectraPor-3 dialysis membrane) large enough to cover a single sample cell were cut and placed on both sides of the gels. The samples were then fixed and screwed using two other plastic cover plates (with perforated holes related to the cells) on either side of the dialysis membranes, and the whole sample holder was placed in the middle of a tank vertically and it was screwed using a u-shaped protector. The inner component of the cells have been coated by dichlorodimethylsilane treatment for several seconds, which creates a hydrophobic surface to minimise any unwanted nucleation point which can result in false positives. Two reservoir buffers (calcium- and phosphate-containing solutions) were prepared and poured on either side of the sample holder and therefore the buffers would perfused through the cells. The entire apparatus was incubated at 37°C for 5 d. Figure 3-4 is showing the schematics of the tank apparatus and its components and how it is set up step by step (part 1 to 5).

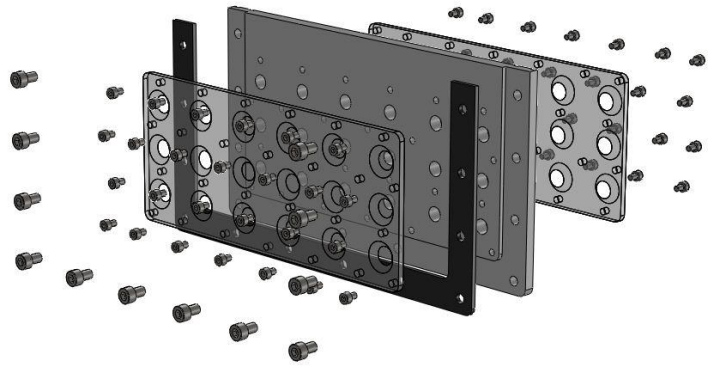
1



2



3



4



5

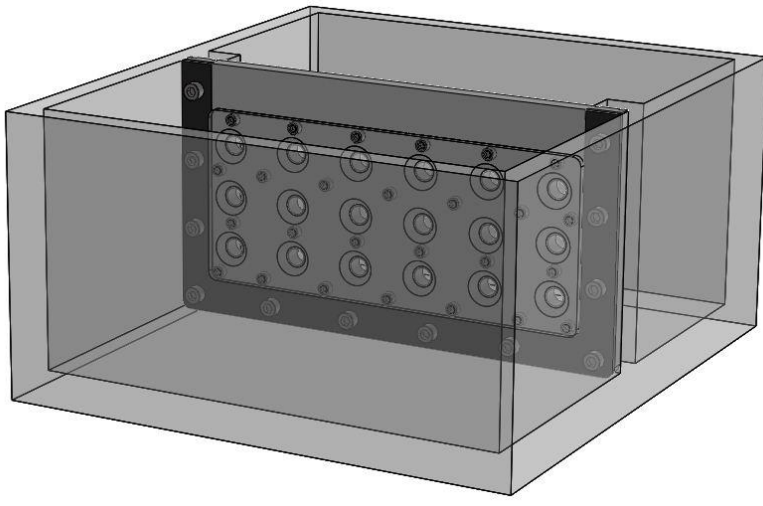


Figure 3-4. *In vitro* nucleation tank apparatus.

3.2.16.1 Preparation of Calcium and Phosphate Buffers

The masses of reagents required for calcium and phosphate buffers are shown in the Table 3-9 and Table 3-10 respectively. To make the solutions, first all the reagents were added into a 5 L volumetric flask and then they were volumised using distilled water. Stirrer and stirrer bar were used to dissolve all reagents (until clear solutions were obtained). Buffers were then pH adjusted to 7.4 through the use of concentrated NaOH (5M) immediately before final volume correction. At the end, the solutions were filtered using a vacuum pump and a 22 μ m filter.

Table 3-9. The reagents required to make 5 L of calcium buffer.

Calcium Buffer 5L	Concentration required	Mass required
Calcium nitrate	6.5mM	7.67g
HEPES	20mM	23.83g
NaCl	150mM	43.84g

Table 3-10. The reagents required to make 5 L of phosphate buffer.

Phosphate Buffer 5L	Concentration required	Mass required
Sodium phosphate dibasic dihydrate	3.9mM	3.41g
HEPES	20mM	23.83g
NaCl	150mM	43.84g

3.2.16.2 Preparation of Negative and Positive Control Samples

In each run of the tank, there were normally negative and positive sample gels in triplicate. To prepare the samples the following steps were followed;

- 1) A solution of 2x steady state buffer was prepared according to Table 3-11. It was then filtered using 50 mL syringe fitted with a 22 μm filter tip.

Table 3-11. The reagents required to make 1 L solution of 2x steady state buffer.

2x Steady State Buffer 1L	Concentration Required	Mass required for 1L
HEPES	40mM	23.81g
NaCl	300mM	43.83g

- 2) 0.8 g of agarose was dissolved in 40 ml of filtered distilled water (filtered with 50ml syringe fitted with a 22 μm filter tip) to produce a 2% solution. The mixture was heated in a microwave until it begins to bubble and it was mixed in vortex to make a homogeneous mixture, it was then placed into a 60°C water bath.
- 3) A 2 mg mL⁻¹ high molecular weight (83 kDa) poly-L-glutamic acid (PGA) solution was prepared by adding 1 mg PGA into 0.5 mL filtered distilled water (filtered with 22 μm filter) and it was mixed until homogenous solution was obtained. Poly(l-glutamic acid) is a known nucleator of hydroxyapatite in this system (203).
- 4) 20 mL of 2x steady state was added to a 50 ml falcon tube and it was labelled as negative.
- 5) 19.8 mL of 2x steady state and 0.2 mL of the 2 mg mL⁻¹ PGA solution were added to a 50 ml falcon tube and it was labelled as positive. This produced a 20 μg mL⁻¹ PGA/2x steady state solution.
- 6) 20 mL of the agarose sample was added into each of the negative (prepared in step 4) and the positive (prepared in step 5) solutions and they were used as the final negative

control and positive control respectively. In brief the negative and positive samples are indicated in Table 3-12.

- 7) The control samples were then sonicated to remove any air bubble using a heated sonicator (60°C water bath).

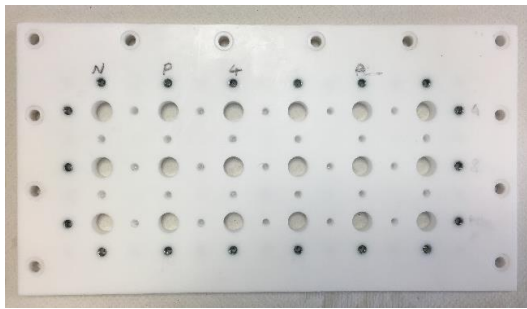
Table 3-12. Negative and positive control samples in IVN tank.

Negative control	1% agarose prepared in 150 mM NaCl, 20 mM HEPES, pH 7.4.
Positive control	10 µg/mL poly-L-glutamic acid in 1 % agarose solution as above.

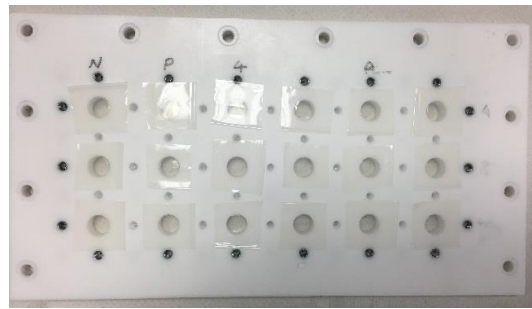
3.2.16.3 Assembling the Samples and the Controls for Testing

To set up the experiment, first of all the tank components were soaked in 0.1 M HCl overnight and then were thoroughly brushed using Decon® and rinsed with distilled water to remove any contamination. To prepare the sample holder a dialysis membrane square was paced over each cell on one side (Figure 3-5, step 1 and 2) and clamped in place using the Perspex® clamping plate and all the small bolts were screwed (Figure 3-5, step 3). Sample holder was then turned around and sample holes were filled with either samples (self-assembled peptide gels) or controls until each cell was full (approx. 1 mL) (Figure 3-5, step 4). Samples were then left to set (approximately 20 min) and a square of dialysis tubing was then placed over each sample and the second the second Perspex® clamping plate were screwed into place (Figure 3-5, step 5 and 6). After that the outside of the sample holder was greased and was placed into the tank. Lastly the system was sealed by adding the U-shaped protector on the top and the sample holder was screwed with the large screws (Figure 3-5, step 7). The seal was further supported by applying a high viscosity grease on the inner surface of U-shape protector prior to assembly. The tank was then placed onto two stirrers (in each side) with a stirrer bar in each reservoir, then the two buffers were poured in each side and the lid was placed on the tank and wrapped with para film (Figure 3-5, step 8). The whole setup was incubated at 37°C for 5 d. After 5 d, the samples were

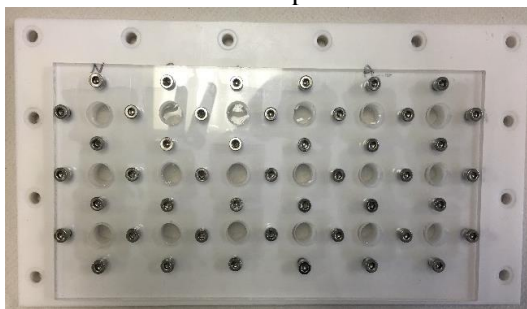
removed from the sample wells and phosphate assay were done to determine the phosphorous content spectrophotometrically (204).



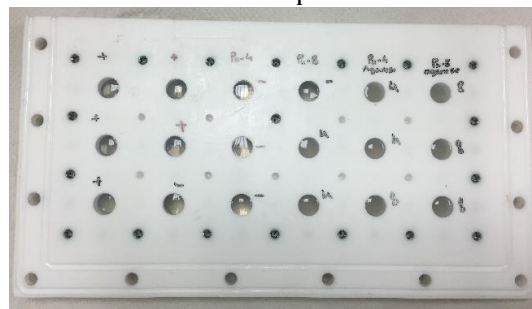
Step 1



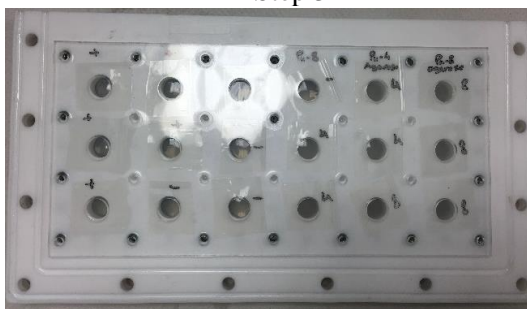
Step 2



Step 3



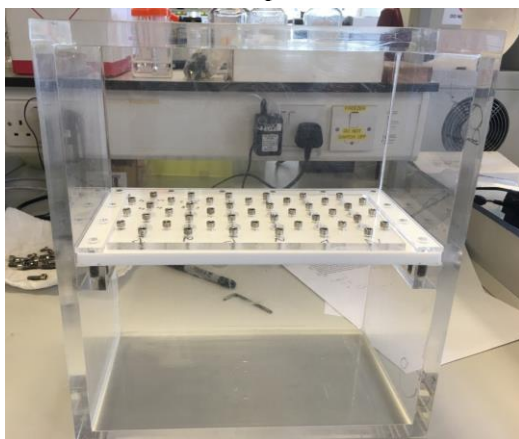
Step 4



Step 5



Step 6



Step 7



Step 8

Figure 3-5. Steps 1 to 8 to assemble the samples in the IVN tank.

Conventionally in this method the samples are self-assembled peptide gels, however in this study it was intended to study the ability of fibrous samples to nucleate hydroxyapatite mineral. To prepare fibrous samples, the electrospun PCL/SAPs (at peptide concentration of 40 mg mL^{-1}) were spun according to method described in Section 3.2.2 until a very thick layer is deposited (spinning time: 4 h). The fibre mats were then folded twice to obtain approximately 4 mm thick layer and after that the mats were cut into disks of 10 mm dimension (same as inner diameter of cells in the sample holder) using a punch cutter. The fibrous sample weights were $13 \pm 1 \text{ mg}$ and based on Equation 3-1 each disk contains approximately 4 mg peptide. The aim was to embed the fibrous disks within two layers of agarose negative sample (with neutral effect on nucleation) on both sides of the fibrous disks. In order to do this, first approximately 0.4 mL aliquots of agarose solutions were pipetted into each cell, then the fibrous disk was carefully placed on top of it, and at last another aliquot of agarose solution was poured on the top of the fibres for the sample cell to be sealed. The samples were then left to gel (for approximately 20 min) and then steps 5 and 6 was followed as above. Figure 3-6 shows the schematic and a picture of embedded fibrous disk in agarose gel.

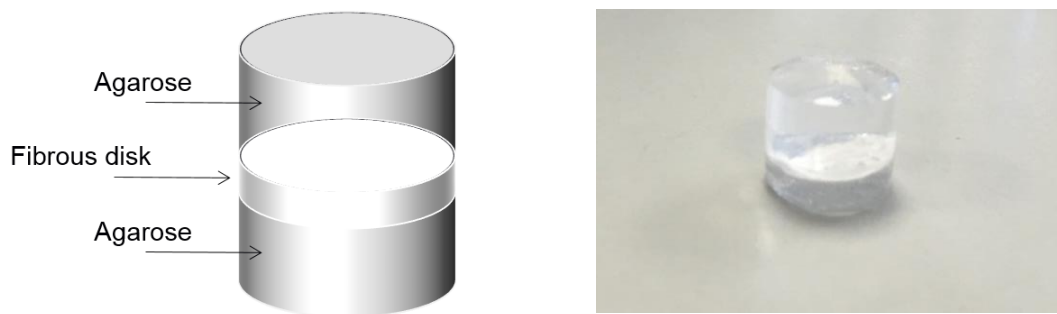


Figure 3-6. Fibrous disk sample embedded in agarose gel.

3.2.16.4 Phosphate Assay

After removing the samples from the tank, each sample was transferred to a single labelled glass vial. 2 mL of concentrated nitric acid was added to each sample and they were boiled on a hotplate at 80°C until a volume of ≤ 1 mL was achieved. 3 replicates of blank sample (2 mL nitric acid) also underwent this process as was required during the analysis. After boiling, each sample (approx. 1 mL) was made up to 10 mL using distilled water and then each sample was diluted another 10 times (30 μ L of sample to 270 μ L of distilled water). This 100-time dilution is to bring the phosphate content in to the range of the plotted calibration curve.

Stock solution of AB was made of one part (A) of 10% ascorbic acid (0.5 g in 5 mL distilled water) and six parts (B) of 0.42% ammonium molybdate. $4\text{H}_2\text{O}$ in H_2SO_4 (4.2 g ammonium molybdate. $4\text{H}_2\text{O}$, 27.8 mL H_2SO_4 and 972.2 mL H_2O). By adding 700 μ L of AB solution to each 300 μ L of sample solutions, the final samples were produced from which 300 μ L was pipetted in triplicate into a 96 well plate and was incubated for 1.5 h at 37°C. The 96-well plate was then placed in Varioskan Flash Reader and the absorbance was recorded at 820 nm.

A calibration standard for the assay was also prepared by dissolving 0 – 100 μ M of Na_2HPO_4 (phosphate standard solution 1000 ppm) in distilled water. The standard solution dilution (with AB) was then followed in the same way as the sample dilution expressed above. The standard solution was then analysed by reading their absorbance at 820 nm and the resulting standard curve is corresponding to the expected phosphorous content of the gels.

3.2.16.5 Statistical Analysis of Data

Statistical analysis was carried in order to determine if the positive and negative controls significantly differ in each run to assure the success of the assay. Moreover each data set was subjected to a Kolmogorov-Smirnov test to ascertain if the data were normally distributed. After that, a t-test was carried out comparing each data set with its corresponding controls data set.

CHAPTER 4

Characterisation of Electrospun PCL/SAPs Fibres

4.1 Introduction

As reported in Section 2.5.3, electrospinning of PCL with peptide is an area of interest in tissue engineering and drug delivery applications. Electrospun PCL/peptide webs have shown significant improvement in biological properties compared to 100% scaffolds in terms of wettability, adhesion, and proliferation of different cell models (32, 36, 37, 45). Accordingly, the aim of this chapter was to investigate the feasibility of combining specific self-assembling peptides (SAPs), P₁₁₋₄ and P₁₁₋₈, with PCL in a one-step manufacturing process to produce electrospun fibres. It was also of interest to verify the incorporation and presence of the SAPs in the electrospun fibres as well as to determine how the secondary conformation of the SAPs changes before and after spinning.

4.2 Experimental Details

4.2.1 100% PCL Electrospun Fibres

Different concentrations of PCL solution in HFIP were prepared to investigate suitable spinning conditions to produce fibres free from defects. The majority of previous studies have reported electrospinning of PCL with a molecular weight of 80,000 resulting in fibres free from beads (27). Initial experiments were carried out to check the spinning ability of PCL with a molecular weight of 80,000 in HFIP solution. With regards to the previous works reported in the literature

using different solvents (27), different PCL concentrations ranging from 6% (w/w) to 12% (w/w) at 2%-increment interval were prepared. The solutions were prepared according to the method explained in Section 3.2.1. The prepared PCL solutions were electrospun to determine spinning ability of each solutions using the needle electrospinning method described in Section 3.2.2. Based on previous literature (36), a flow rate of 1 mL h⁻¹, voltages of 20 kV or 25 kV and tip to collector distances of 160 - 200 mm were employed.

4.2.2 PCL/SAPs Electrospun Fibres

Based on preliminary experiments involving spinning of 100% PCL solutions at 6% (w/w), 8% (w/w), 10% (w/w), and 12% (w/w) it was found that a 6% (w/w) concentration of PCL in HFIP was the most favourable for producing fine and smooth fibres free from defects. The smallest mean fibre diameter of 520 nm (standard deviation: 107 nm) was achieved with a 1 mL h⁻¹ flow rate, a voltage of 20 kV and a spinning distance of 180 mm on an aluminium foil collector (results are presented in Section 4.3.1). According to the literature (43, 46, 47), both P₁₁₋₄ and P₁₁₋₈ can self-assemble and form nematic gels at a minimum concentration (critical chain entanglement concentration: C*) of 10-20 mg mL⁻¹ (depending on the pH, temperature and ionic strength of the solution). Therefore, 20 mg mL⁻¹ of each the SAPs (P₁₁₋₄ and P₁₁₋₈) was added to the prepared PCL solution. Over the course of this study, the concentration of peptides used in electrospinning solutions was fixed at 20 mg mL⁻¹ unless otherwise stated. HFIP was selected as electrospinning solvent in light of its fast evaporation and ability to break down hydrophobic interactions and hydrogen bonds even at 20 mg mL⁻¹ SAP concentration (205) so that clear solutions of PCL and SAPs random coils could be obtained prior to spinning. The method of peptide solution preparation was extensively explained in Section 3.2.1. After 24 h, clear solutions were obtained and the solutions were ready for spinning. Electrospinning for all of the solutions was conducted according to the method explained in Section 3.2.2. The flow rate was set at 1 mL h⁻¹, with a tip to collector distance of 180 mm and a voltage of 20 kV. These were

found to be the optimum spinning conditions in the preliminary experiments dealing with 100% PCL solutions (Section 4.3.1). The samples were subjected to SEM analysis and the fibre diameters were analysed according to the methods explained in Sections 3.2.4. In order to further understand the fibre morphology and formation of the nanofibres, TEM and ESEM analysis were performed using the methods detailed in Sections 3.2.5 and 3.2.6.

4.2.3 Influence of the Polarity of the High Voltage Power Supply during Electrospinning on Fibre Morphology

As discussed in Section 2.5.2.2, the polarity of the high voltage power supply during electrospinning can potentially affect fibre formation. In a conventional electrospinning setup, the power supply is connected to a positive polarity electrode and this arrangement was also used in the present experiments, unless otherwise stated. In order to investigate the effect of a change in the polarity on the fibre morphology in PCL/SAP webs, PCL/P₁₁₋₄ and PCL/P₁₁₋₈ solutions with a SAP concentration of 20 mg mL⁻¹ were electrospun at constant spinning conditions explained in Section 4.2.2, with either negative or positive polarity electrodes. The resulting electrospun samples were subjected to SEM analysis to critically analyse any changes in fibre morphology.

4.2.4 Effect of Concentrations of SAP in PCL/SAPs Electrospun Fibres

To investigate the effect of peptide concentration in the electrospinning solution on fibre morphology, solutions of 10 mg mL⁻¹, 20 mg mL⁻¹ and 40 mg mL⁻¹ of P₁₁₋₄ and P₁₁₋₈ were prepared according to the method in Section 3.2.1. These solutions were electrospun at room temperature at a flow rate of 1 mL h⁻¹, a voltage of 20 kV and a spinning distance of 180 mm. The samples were subjected to SEM analysis to critically analyse any changes in fibre morphology.

4.2.5 Peptide Presence in Fibres; Energy-Dispersive X-Ray Spectroscopy

Energy-dispersive X-ray spectroscopy analysis was employed to detect nitrogen, which is indicative of the presence of peptide within the as-spun PCL/SAP fibres, as described in Section 3.2.8. Dry electrospun samples produced from PCL/P₁₁₋₄ and PCL/P₁₁₋₈ solutions at a peptide concentration of 20 mg mL⁻¹ were sputter coated with platinum with a thickness of 8 nm. Electrospun fibres were subjected EDX spectroscopy (Oxford Instruments, AztecEnergy) and the electron beam was focused with the help of a field emission gun scanning electron microscope (LEO1530 Gemini) under high vacuum. An accelerating voltage of 15 kV was applied and three random spots per sample were tested across each sample.

EDX was also applied to samples of PCL/P₁₁₋₈ with a peptide concentration of 20 mg mL⁻¹ in conjunction with TEM to be able to achieve higher magnification. The FEI Tecnai TF20 TEM microscope was fitted with an EDX system (Oxford Instruments INCA 350). As EDX is mainly considered a qualitative analysis in which some elements may be missed or falsely identified, a control sample of electrospun PCL fibres was also analysed to validate data. Three random spots per sample was tested using both SEM/EDX and TEM/EDX, and the results are expressed as mean ± standard deviation.

4.2.6 Peptide Distribution in Fibres; Florescent Microscopy

In order to visually observe the peptide distribution throughout the fibres, the peptides in the spinning solution were fluorescently labelled with oppositely charged functionalised peptides by a fluorescein moiety [ratio of flour-P₁₁₋₄:P₁₁₋₈ = 1:60 and ratio of flour-P₁₁₋₈:P₁₁₋₄ = 1:60] to aid viewing by confocal microscopy. The method is extensively explained in Section 3.2.7. Opposite charged functionalised peptide was used in this case to produce a polyelectrolyte β -sheet complex. Mixing an anionic and cationic peptide is an alternative way to induce self-assembly (206), which in this case was the preferred method to ensure full mixing of the fluoro-

tagged peptides with peptides in solution. Electrospun fibres produced from PCL/P₁₁₋₄ and PCL/P₁₁₋₈ solutions at a peptide concentration of 20 mg mL⁻¹ (doped with oppositely charged fluoro-SAPs) along with a blank sample of PCL were observed by confocal laser scanning microscopy (Zeiss LSM510).

4.2.7 Peptide Secondary Structures in Solution and in As-Spun Fibres

Both Fourier Transform Infra-Red spectroscopy (FTIR) and Circular Dichroism spectroscopy (CD) were employed to determine the secondary structure of the peptides in solution (before electrospinning) and in the fibre state. The methods are detailed in Sections 3.2.10 and 3.2.11.

4.2.7.1 Peptides Secondary Structure in Spinning Solution

The secondary state of peptides within the solutions prior to spinning were investigated using FTIR and CD methods.

FTIR and CD on PCL/SAPs Solutions

Spinning solutions of PCL/P₁₁₋₄ and PCL/P₁₁₋₈ at different peptide concentrations were prepared in a same manner to that used for electrospinning and they were assessed for both CD and FTIR analysis. A control sample of PCL in HFIP (6% w/w) was analysed by FTIR and the spectrum of HFIP was subtracted from the solutions spectra in both the CD and FTIR results.

CD spectroscopy is a fast photometric technique that can determine the secondary structure of peptides/proteins in the "far-UV" spectral region (190-250 nm). At these wavelengths, the chromophore is the peptide bond and the signal arises when it is located in a regular, folded environment. α -helix, β -sheet and random coil structures each give rise to a characteristic CD spectrum. The CD software gives the output in ellipticity (symbol θ), and its unit is millidegrees (mdeg). However to be able to compare the results with those of others, the ellipticity θ is usually converted to the molar ellipticity (symbol $[\theta]$) with the unit of deg cm² dmol⁻¹ (Equation 4-1).

Equation 4-1

$$[\theta] = \theta / (10 \times c \times l)$$

$$c = (1000 \times n \times cg) / Mr$$

Where;

c is the molar concentration of the sample (mole L⁻¹).

l is the pathlength in cm.

cg is the macromolecule concentration in g ml⁻¹.

Mr is the molecular weight of the species.

Alternatively, for far UV CD measurements, the data can be reported in mean residue molar ellipticity (symbol $[\theta]$ MRW) with the unit of deg cm² dmol⁻¹, and it can be calculated by Equation 4-2 and Equation 4-3;

Equation 4-2

$$[\theta] \text{ MRW} = \theta / (10 \times c_r \times l)$$

Equation 4-3

$$c_r = n \times c$$

Where;

c_r is the mean residue molar concentration.

n is the number of peptide bonds in the protein or peptide (207-210).

The CD data herein were converted to mean residue ellipticity (deg cm² dmol⁻¹) and each spectrum is the average of two scans. The spectrum of HFIP as a blank solvent was subtracted from all the spectra and finally a seventh order fitting operation was performed using OriginPro software (0.95 < R² < 0.99).

4.2.7.2 Peptides Secondary Structure in As-Spun Fibres

The secondary state of SAPs within the fibres after spinning and vacuum drying procedures were evaluated using ATR-FTIR method.

ATR-FTIR on PCL/SAPs Fibre Webs

Infrared spectra of PCL, PCL/P₁₁-4 and PCL/P₁₁-8 fibres (at different peptide concentrations) deposited on the aluminium foil were obtained using a Perkin Elmer FTIR with diamond Attenuated Total Reflectance (ATR) attachment system. A total of 64 scans were averaged for each spectrum in the range between 4000 and 400 cm⁻¹ with a resolution of 4 cm⁻¹ and interval scanning of 2 cm⁻¹.

4.3 Results and Discussion

4.3.1 Fibre Morphological Results of 100% PCL Electrospinning

A summary of the needle electrospinning behaviour of PCL solutions at different concentrations and by applying different electrospinning parameters is given in Figure 4-1. This reports visual observations during electrospinning as well as SEM micrographs of samples produced using successful spinning conditions. SEM micrographs were taken at a magnification of 800-3Kx to provide an initial examination of morphological characteristics of the as-spun PCL fibres. At the highest PCL concentration of 12% (w/w) regardless of spinning parameters used in this study, spinning was not possible. This can be attributed to the relatively high viscosity of PCL polymer solutions at 12% (w/w) and the insufficient electrostatic force that could be generated to overcome the surface tension. At 10% (w/w) PCL concentration, the polymer solution dried at the needle tip. Particularly, when a higher voltage (25 kV) was applied, an electrospinning jet was formed but it produced very thick merged fibres similar to a film. At a reduced solution concentration of 8% (w/w), regardless of the spinning conditions employed in this study, wet and thick fibres were formed and merged fibres could be observed at their junctions. Again, it appeared that the applied electrostatic charges (20-25 kV) were not able to stretch the viscoelastic solution and form elongated and defect free fibres. Electrospinning was found to be possible at 6% (w/w), although not at voltages as high as 25 kV. When a lower voltage of 20 kV was applied, fibres could be formed when the spinning distances were between 160 – 180 mm. However, when the distance was increased to 200 mm, the polymer solution dried at the tip of the needle and no fibres were produced. A spinning distance of 160 mm produced fibres that were very thick (average: 4.3 μm), which could be attributed to insufficient time for the polymer solution to elongate. When the spinning distance was 180 mm, there was sufficient time to allow the applied electrostatic charges to elongate the jet and create fibres free from defects in a submicron diameter range from 400-600 nm.

V (kV)	D (mm)	Concentration (w/w)		
		6%	8%	10%
20	160			Unspinnable
20	180			Unspinnable
20	200	Polymer dried at the needle tip		Unspinnable
25	160	Unspinnable		Polymer dried at the needle tip
25	180	Unspinnable		
25	200	Unspinnable		

Figure 4-1. SEM micrographs of electrospun webs produced from PCL in HFIP solutions at different PCL combination of concentration, voltage (V) and tip to collector distance (D).

4.3.2 Fibre Morphological Results of PCL/SAPs Electrospinning

Electrospun webs of PCL and SAPs were successfully produced and the nano- and submicron scale structures were studied to elucidate fibre morphology and fibre diameter. In this section, electrospun fibres made of 100% PCL (control sample), PCL/P₁₁₋₄ and PCL/P₁₁₋₈ solutions at a peptide concentration of 20 mg mL⁻¹ were studied; spinning parameters are given in Section 4.2.2 (1 mL h⁻¹ flow rate, a voltage of 20 kV and a spinning distance of 180 mm on an aluminium foil collector) and were not varied for these experiments.

4.3.2.1 SEM of As-Spun Fibre Webs

Spinning conditions that produced good coverage of fibres on the collector were analysed by SEM imaging using the method explained in Section 3.2.3. Figure 4-2 shows micrographs taken from low (12Kx) to high magnifications (102Kx) for 100% PCL, PCL/P₁₁₋₄ and PCL/P₁₁₋₈ electrospun fibres. It can be seen from Figure 4-2 that electrospinning of the commixed PCL and SAPs induced detectable changes in the fibre morphology as compared to 100% PCL. PCL fibres were uniformly distributed in terms of their shape and diameter. In contrast, the PCL webs containing P₁₁₋₄ or P₁₁₋₈ peptide consisted of two superimposed fibre networks. The first network consisted of submicron fibres and the second was a nanofibre network in which the constituent fibres were substantially smaller in diameter than the first. There was a marked difference between the PCL/P₁₁₋₄ and the PCL/P₁₁₋₈ fibre webs in terms of this biphasic fibre diameter. In the PCL/P₁₁₋₈ webs, two distinct networks were evident, consisting of both submicron and nanofibre phases. Micrographs of the PCL/P₁₁₋₄ fibre webs revealed relatively fewer nanofibres, which were distributed locally rather than uniformly across the submicron fibre network.

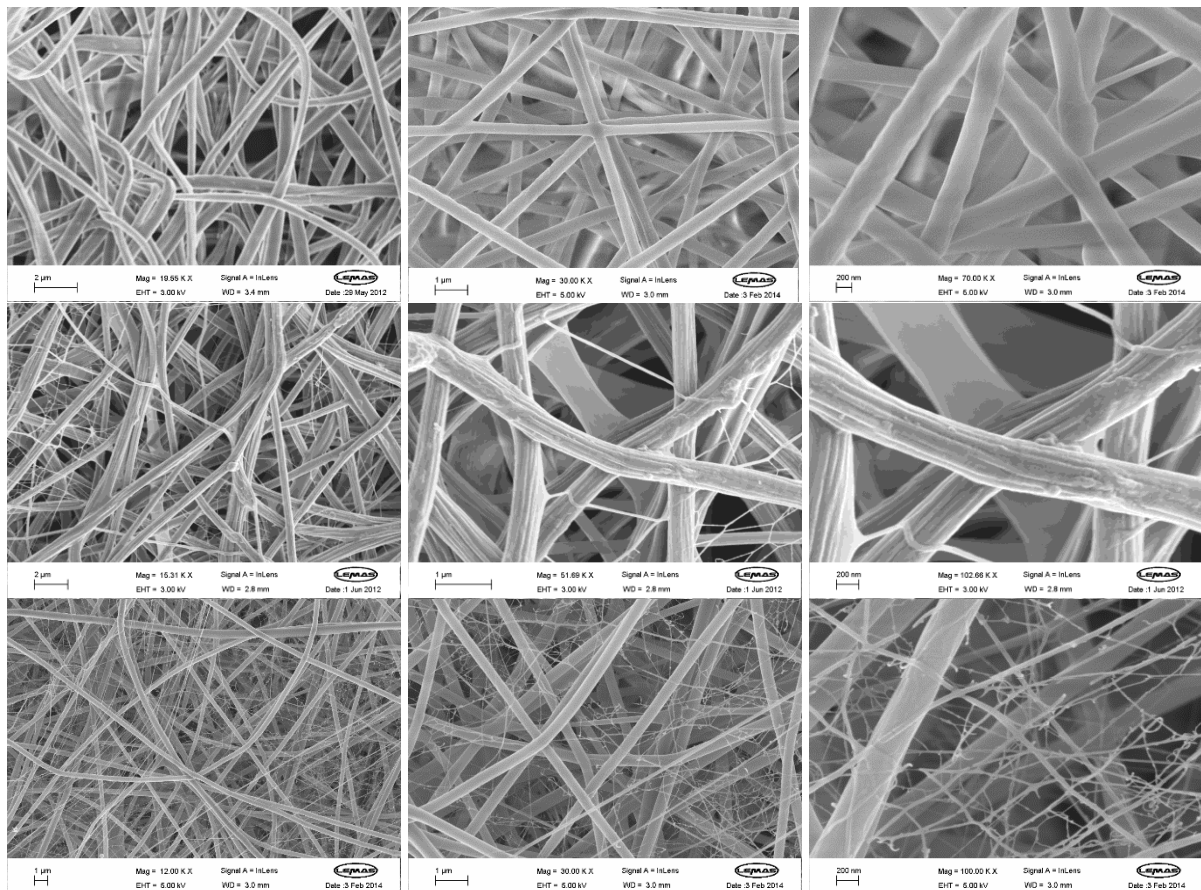


Figure 4-2. SEM micrographs of, first row: 100% PCL; second row: PCL/P₁₁-4 and third row: PCL/P₁₁-8 electrospun fibres.

4.3.2.2 Fibre Diameter in the PCL/SAPs Electrospun Webs

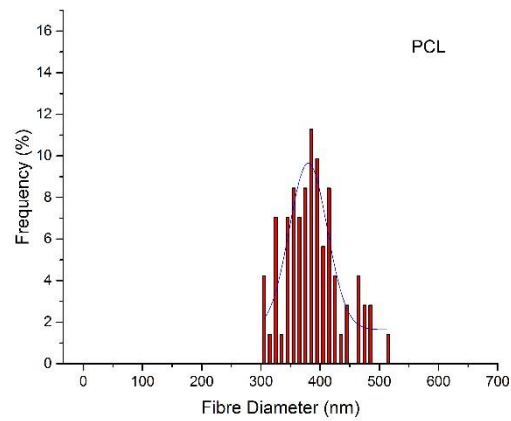
Fibre diameter was measured according to the method described in Section 3.2.4 and data is reported in Figure 4-3. Figure 4-3 reveal that the 100% PCL fibres were quite uniformly distributed with diameters ranging between 300 nm and 500 nm. The peptide enriched samples however revealed a bimodal fibre diameter distribution attributable to the regions of submicron- (100-1000 nm) and nano-scale (below 100 nm). The nanofibres had a mean fibre diameter of around 30 nm and the submicron fibre diameter was typically between 100 nm and 700 nm. The mean, standard deviation (SD), and the minimum and maximum values of fibre diameters are summarised in Table 4-1. In order to take the bimodal distribution into account, the measurements were obtained by treating the biphasic data as two independent distributions,

the first containing fibres with a diameter below 100 nm and the second with fibres above 100 nm.

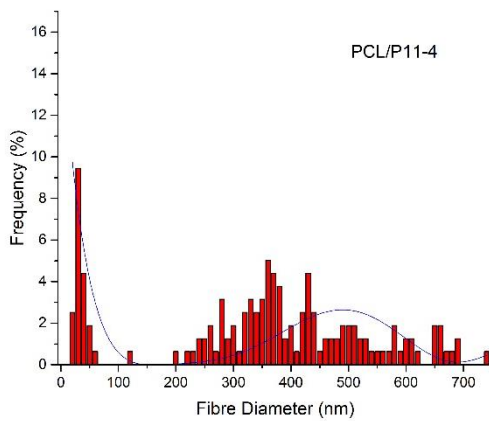
Table 4-1. Fibre diameter in PCL, PCL/P₁₁₋₄ and PCL/P₁₁₋₈ webs (all data is nm).

Sample	Distribution for fibres <100 nm				Distribution for fibres >100 nm			
	Mean	SD	Min	Max	Mean	SD	Min	Max
PCL					386.9	47.7	302	514
PCL/P₁₁₋₄	28.5	8.9	15.3	51.2	418.7	125.2	112.9	734.2
PCL/P₁₁₋₈	36.9	20.1	10.1	95.9	326.9	113.2	106.5	700

A



B



C

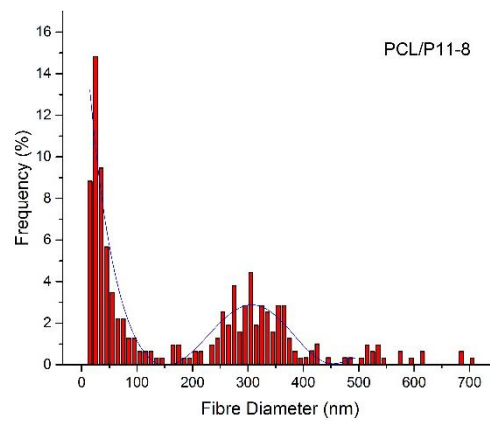


Figure 4-3. Fibre diameter distribution of (A) PCL, (B) PCL/P₁₁₋₄ and (C) PCL/P₁₁₋₈ webs.

4.3.2.3 SEM Of Fibres Produced with Different Electrode Polarities in the Electrospinning Setup

As discussed in Section 4.2.3, electrospinning was conducted with negative and positive polarity electrodes. This resulted in successful production of four samples of PCL/P₁₁-4 and PCL/P₁₁-8 (Figure 4-4). In Figure 4-4 no marked observable difference was seen in the nanofibres extent and morphology of PCL/P₁₁-4 and PCL/P₁₁-8 (6% w/w PCL at 20 mg mL⁻¹ SAP concentration) fibre webs related to polarity which was in contrary to the literature (177).

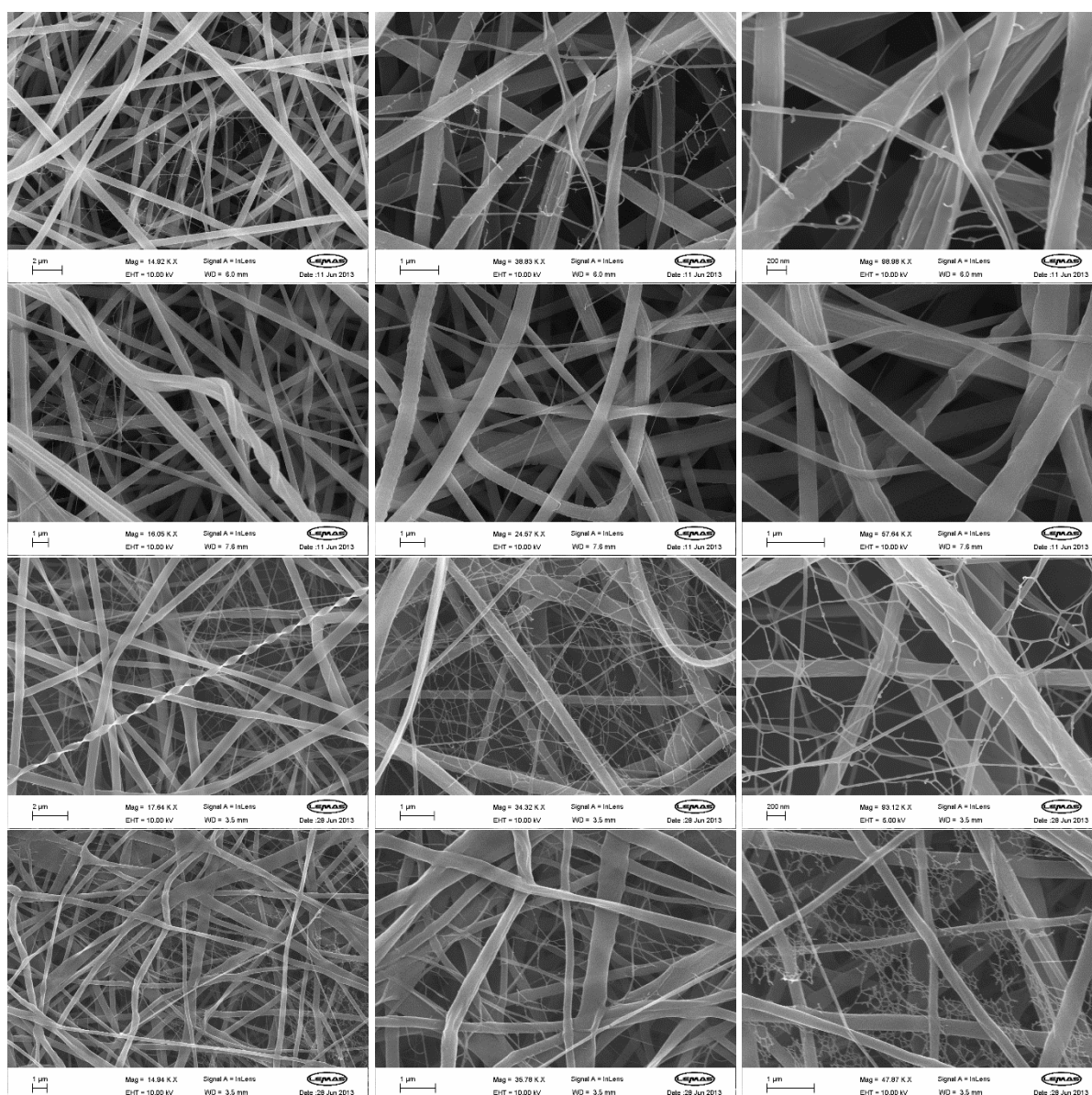


Figure 4-4. SEM micrographs of PCL/P₁₁-4 produced with: (first row) negative electrode and (second row) positive electrode. SEM micrographs of PCL/P₁₁-8 produced with: (third row) negative electrode and (fourth row) positive electrode.

4.3.2.4 TEM of As-Spun Electrospun Fibre Webs

To investigate the nano-scale architecture of the PCL/SAP electrospun webs, PCL/P₁₁₋₈ (6% w/w) solutions containing 20 mg mL⁻¹ peptide concentrations were directly electrospun onto TEM grids (mounted on aluminium foil). Only a thin layer of the fibres were collected (3 min spinning time) and TEM analysis was performed subsequently using a FEI Tecnai TF20. Figure 4-5 shows TEM micrographs of PCL/P₁₁₋₈ webs deposited on the TEM grids at low (top row) and high magnification (bottom row) of 150Kx and 231Kx respectively. In these images, the overlaid nano- (<100 nm) and submicron (>100 nm) diameter fibres are clearly visible.

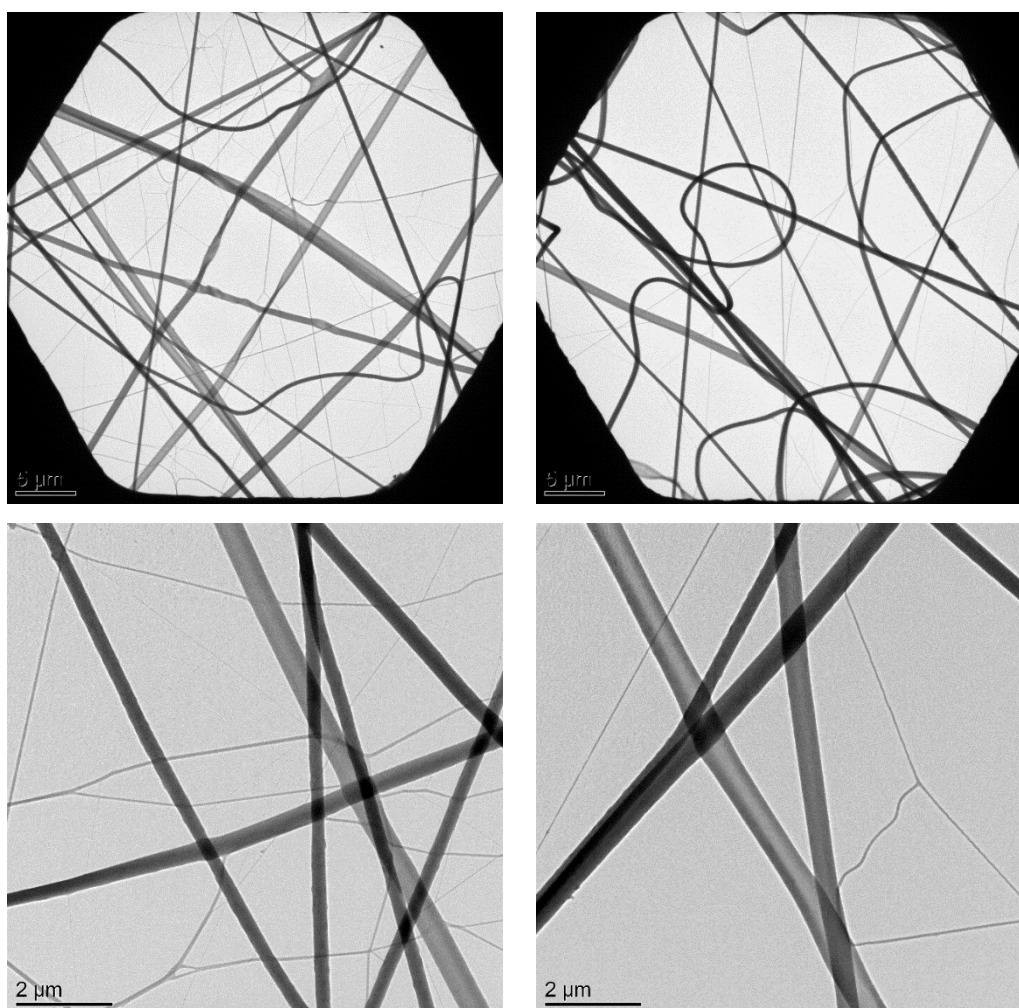


Figure 4-5. TEM images of PCL/P₁₁₋₈ with a peptide concentration of 20 mg mL⁻¹ at 150Kx (top row) and 231Kx (bottom row) magnifications.

It is apparent from Figure 4-5 that the micro and nano-scale fibres are in contact at certain intersections, but in many locations the nanofibres appear to overlay the larger submicron fibres without merging.

4.3.2.5 ESEM of PCL/SAPs Multi-Scale Fibrous Structure

In solution electrospinning, the solvent is predominantly evaporated during the flight of the polymer jet from the tip of needle to the collector. However, it is conceivable that some residual solvent can be left in the fibres of the web and that evaporation can continue to some extent after deposition. The self-assembly of peptides here, is thought to be driven by solvent evaporation due to the critical peptide concentration (C^*) being reached (43, 46, 47). Therefore, the evaporation rate of the solvent can be hypothesised to be connected with the formation of peptide beta-sheets, which could resemble a nanofibre network. When P₁₁₋₈ are self-assembled into β sheets, they form fibres of 20–30 nm in dimensions (48) and it therefore may be partly responsible for the bimodal fibre diameter distributions observed in PCL/SAP networks. It was reasoned that by gradually drying the as-spun fibres, it might be possible to track the formation of fibrils post spinning, especially when it was known that residual solvent was left on board the fibres. The ESEM was used to track the effect of the drying procedure and solvent evaporation on the fibre and fibril morphology according to the procedure explained in Section 3.2.6. A 6% (w/w) PCL solution with 20 mg mL⁻¹ P₁₁₋₈ peptide concentration was electrospun for up to 3 min under the conditions described in Section 3.2.2, and the as-spun fibres were then immediately transferred into liquid nitrogen to minimise the solvent evaporation. In order to eliminate the effects of vacuum pressure in coating and in the SEM chamber, the samples were first imaged in the uncoated state. From liquid nitrogen, the wet fibres were then immediately mounted on SEM stubs and transferred into the low vacuum mode of the ESEM. The results are shown in Figure 4-6, both immediately after mounting (A) and after 25 min (B). It can be observed that in Figure 4-6 (A), the nanofibres are not visible, whereas in image (B)

one or two nanofibres might be seen which can be contributed to the solvent being gradually evaporated but not fully, because the samples are still in low vacuum environment.

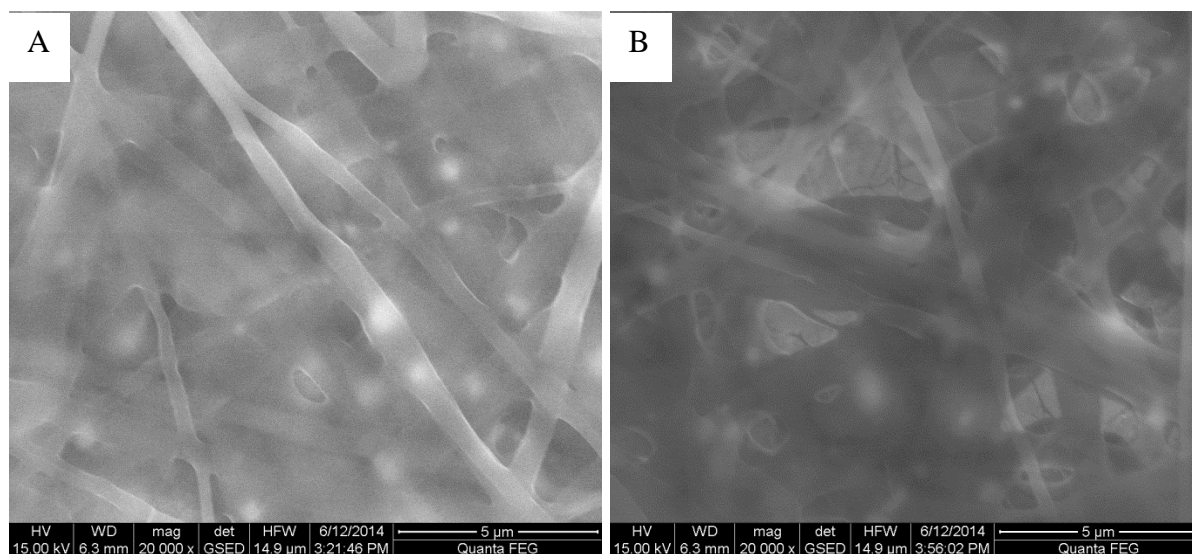


Figure 4-6. ESEM micrographs of wet and uncoated PCL/P₁₁-8 with peptide concentration of 20 mg mL⁻¹, (A) immediately after mounting in microscope and (B) after 25 minutes.

In the next step, the same sample was left to be dried completely in vacuum for 24 h under the vacuum conditions explained in Section 3.2.2 and then subjected to ESEM in uncoated state to see any changes followed by complete solvent residue evaporation. The images are shown in Figure 4-7 at 30Kx (left) and 60Kx (right) magnifications and it can clearly be seen that some nanofibres are formed and appeared following the drying procedure. However, compared with PCL/P₁₁-8 images in Figure 4-2 and Figure 4-4, the nanofibres here (in Figure 4-7) may be less visible which can be due to the low resolution of images and lack of surface conductivity on the fibres, which is because of lack of coating. Therefore the same sample were subjected to Pd/Pt coating (procedure explained in Section 3.2.3) and it was imaged under high vacuum mode (normal SEM conditions). The result is shown in Figure 4-8 (at different magnifications of 30K-60K x) and the presence of extensive nanofibre networks are evident in this image (similar to Figure 4-2).

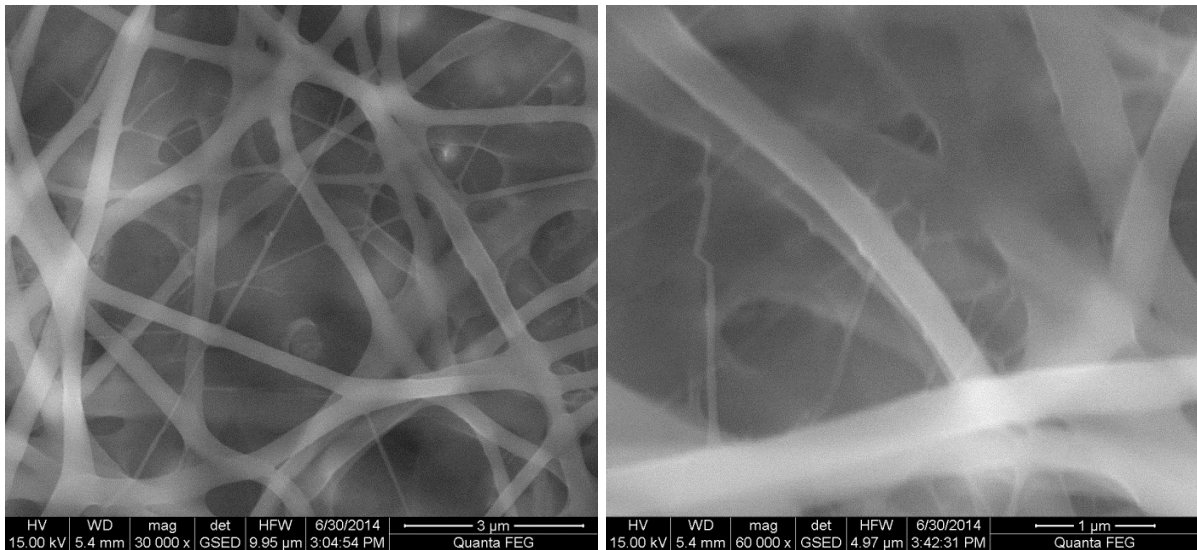


Figure 4-7. ESEM micrographs of vacuum dried but uncoated PCL/P₁₁₋₈ with peptide concentration of 20 mg mL⁻¹, at 30Kx (left) and 60Kx (right) magnifications.

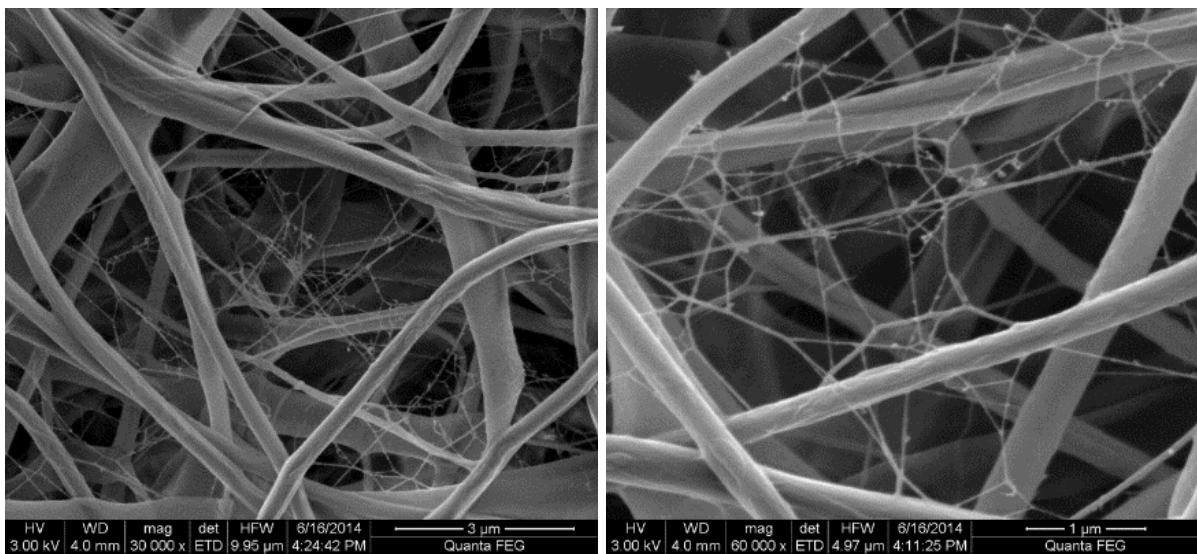


Figure 4-8. ESEM (high vacuum mode) micrographs of vacuum dried and coated PCL/P₁₁₋₈ with peptide concentration of 20 mg mL⁻¹, at 30Kx (left) and 60Kx (right) magnifications.

By investigation of these results, it can be suggested that as the as-spun fibres are gradually dried, the nanofibres network may be more formed even after spinning. This can be due to the residual solvents being evaporated and consequently the concentration of SAPs being increased. However due to the nature of fibrous samples, it is not favourable to use ESEM

technique to image uncoated and wet samples which may result in low resolution images, and false conclusions.

4.3.3 Effect of Peptide Concentration on Fibre Morphology and Diameter

In order to investigate the effect of SAP concentration on fibre morphology, solutions of PCL/P₁₁₋₄ and PCL/P₁₁₋₈ with peptide concentrations of 10 mg mL⁻¹, 20 mg mL⁻¹ and 40 mg mL⁻¹ were prepared and electrospun according to the method explained in Section 3.2.1 and 3.2.2. A control sample of 100% PCL was prepared as well. The fibres were then critically analysed using SEM imaging. Electrospinning parameters were set at 1 mL h⁻¹ flow rate, a voltage of 20 kV and a spinning distance of 180 mm.

4.3.3.1 Effect of P₁₁₋₈ Concentration on PCL/P₁₁₋₈ Fibre Morphology

Figure 4-9 shows SEM micrographs at two different magnifications, 12Kx (left column) and 60Kx (right column) of webs containing PCL and varying concentrations of P₁₁₋₈ peptide (0-40 mg mL⁻¹). It can clearly be seen that increasing the concentration of P₁₁₋₈ results in an increase in the extent of nanofibrous network formation.

4.3.3.2 Effect of P₁₁₋₄ Concentration on PCL/P₁₁₋₄ Fibre Morphology

Figure 4-10 shows SEM micrographs at three different magnifications (5Kx, 12Kx, and 25Kx from left to right) of webs containing PCL and varying concentrations of P₁₁₋₄ peptide (0-40 mg mL⁻¹). It could be seen from the SEM images that the addition of P₁₁₋₄ into pure PCL solution results in network of nanofibres being introduced to the structure. However as explained before (Section 4.3.2.1), with P₁₁₋₄ (in contrast with P₁₁₋₈) the nanofibre network are not dominantly distributed and they are locally formed. By increasing P₁₁₋₄ concentration from 10 mg mL⁻¹ to 20 mg mL⁻¹, the extent of the nanofibrous network increased. Any further addition of P₁₁₋₄ from 20 to 40 mg mL⁻¹ does not create any observable difference in the web.

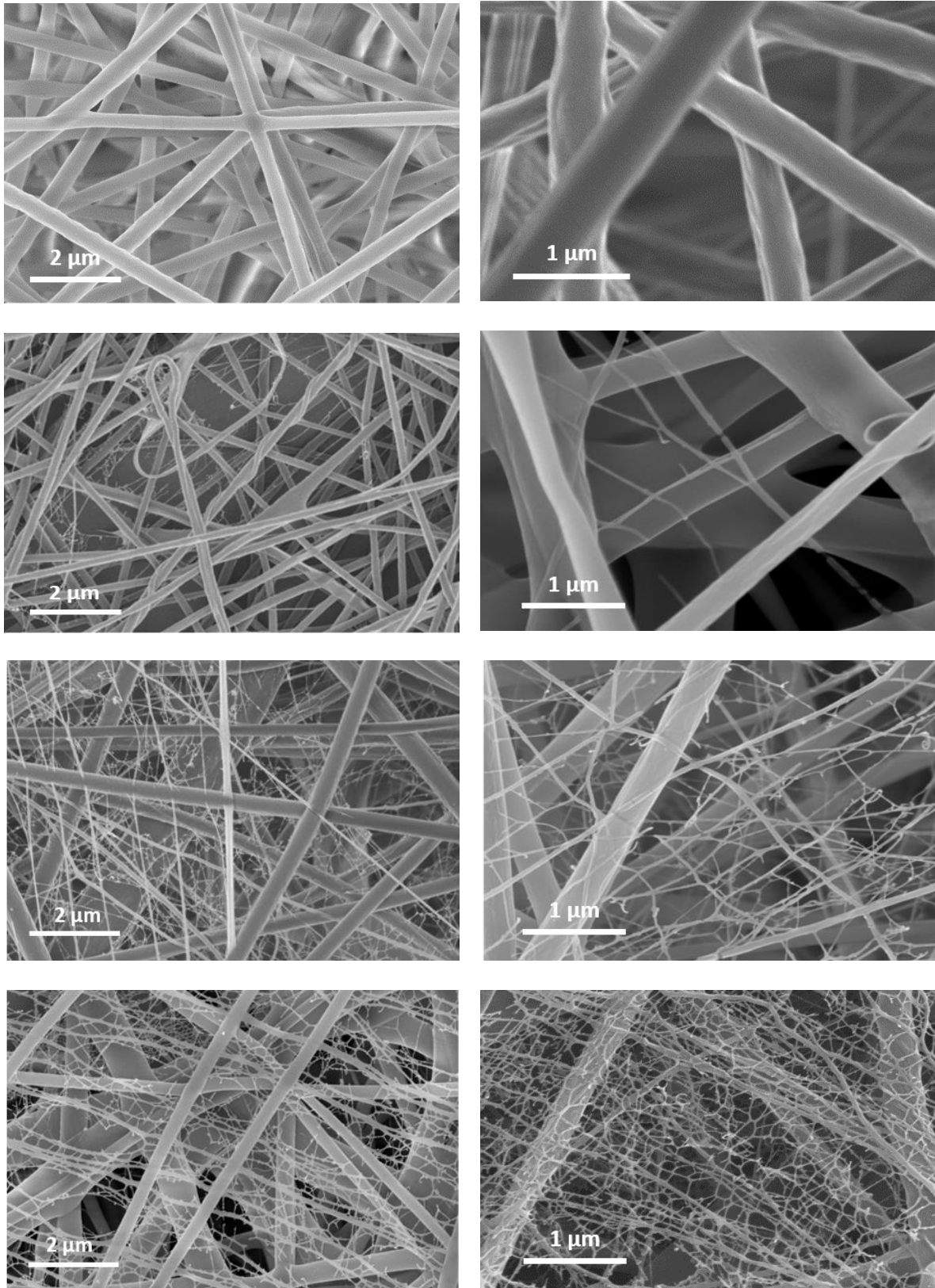


Figure 4-9. SEM micrographs of (first row) PCL fibres, (second row) PCL/P₁₁₋₈ with peptide concentration of 10 mg mL⁻¹, (third row) PCL/P₁₁₋₈ with peptide concentration: 20 mg mL⁻¹ and (fourth row) PCL/P₁₁₋₈ with peptide concentration: 40 mg mL⁻¹.

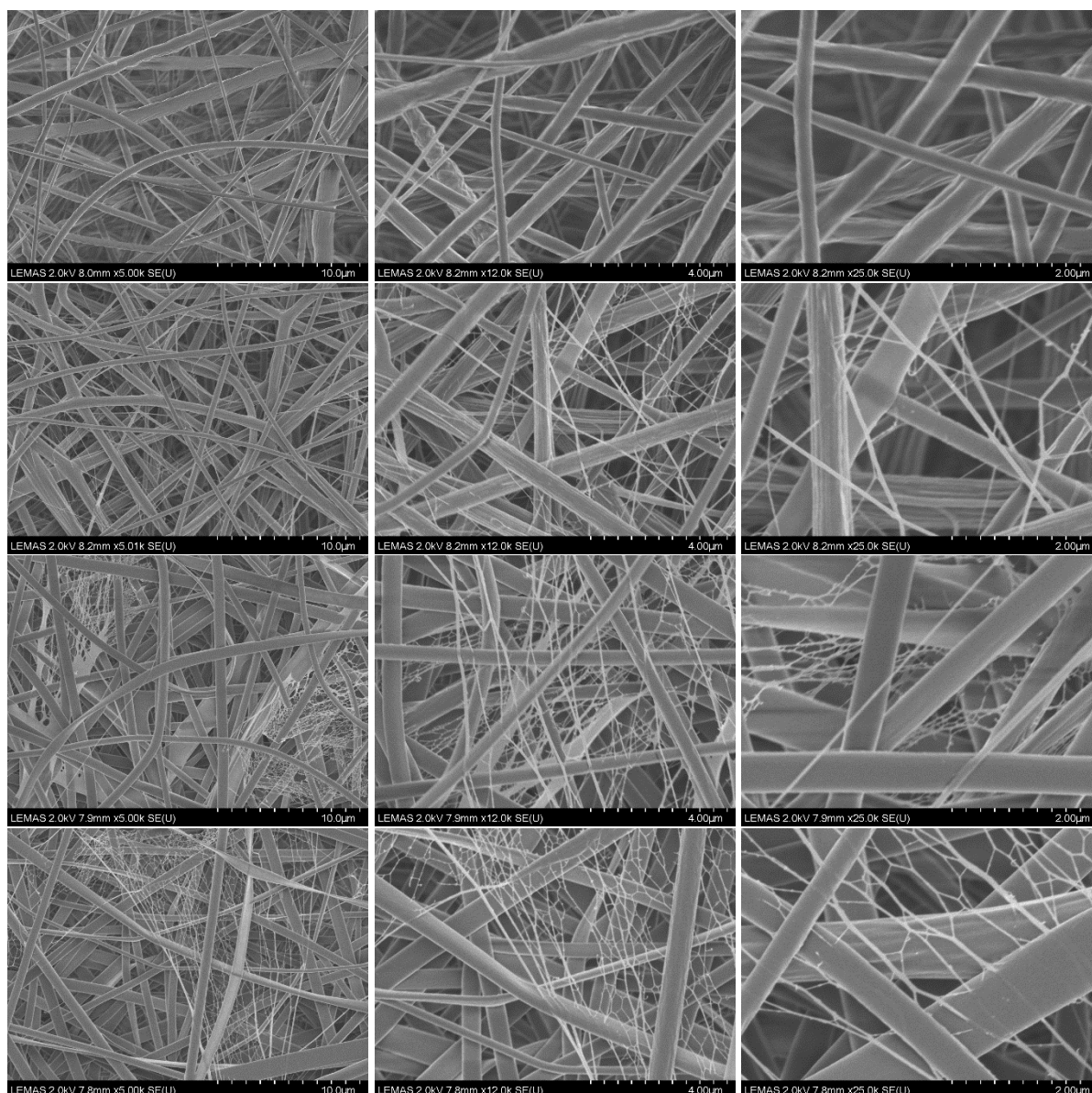


Figure 4-10. SEM micrographs of (first row) 100% PCL fibres, (second row) PCL/P₁₁₋₄ with peptide concentration of 10 mg mL⁻¹, (third row) PCL/P₁₁₋₄ with peptide concentration of 20 mg mL⁻¹ and (fourth row) PCL/P₁₁₋₄ with peptide concentration of 40 mg mL⁻¹.

4.3.4 Peptide Presence and Distribution in Fibres

4.3.4.1 Elemental Analysis on PCL/SAPs Fibre Webs by SEM-EDX

The SEM-EDX spectra of the PCL control, PCL/P₁₁-4 and PCL/P₁₁-8 fibres at a peptide concentration of 20 mg mL⁻¹ are shown in Figure 4-11. The presence of nitrogen peaks are observed in PCL/P₁₁-8 and PCL/P₁₁-4 spectra. The nitrogen peak in the EDX spectra is attributed to the peptide molecules which indicate the successful incorporation of peptides in the PCL/P₁₁-8 and PCL/P₁₁-4 fibres. As expected, nitrogen peak is not present in the PCL control spectrum.

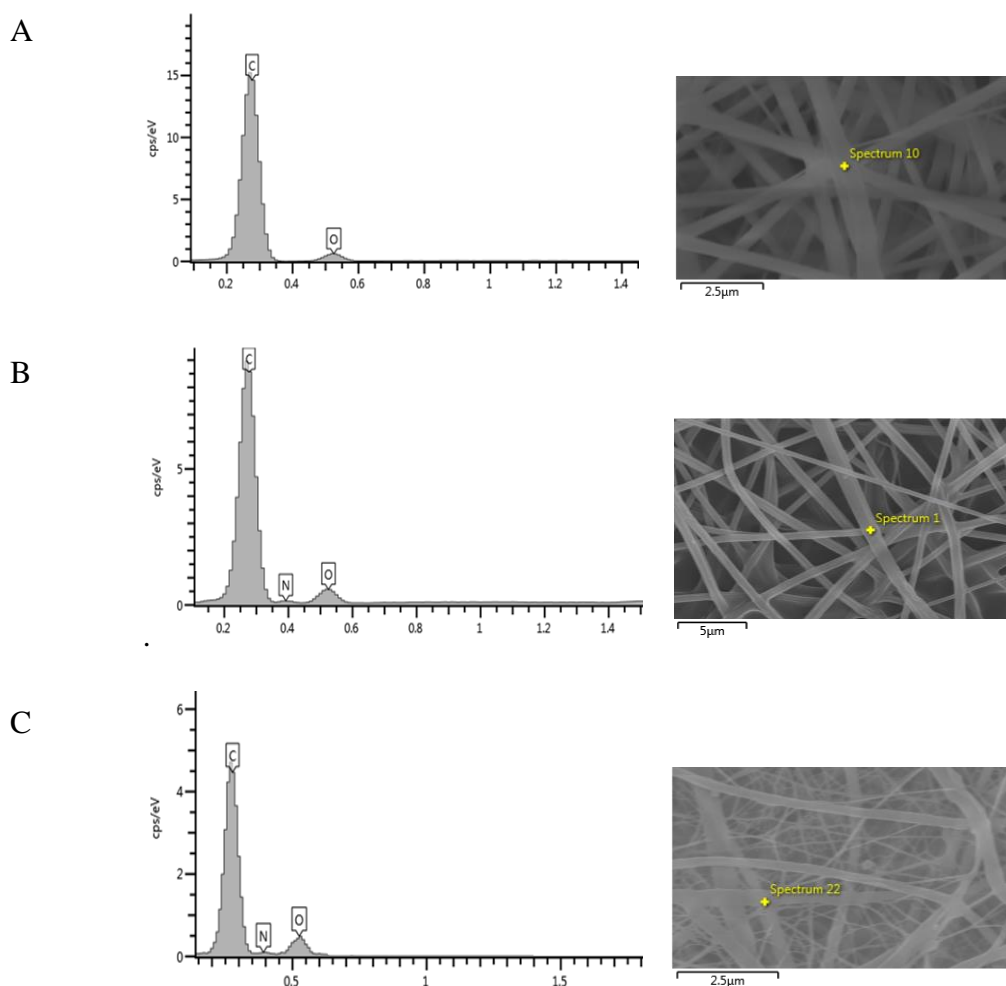


Figure 4-11. SEM/EDX analysis of electrospun (A) PCL, (B) PCL/P₁₁-4 and (C) PCL/P₁₁-8 fibres.

Table 4-2 summarises the average \pm standard deviation of atomic percentage results of the chemical elements in each samples.

Table 4-2. Atomic percentages of chemical elements in the elctrospun fibres by SEM/EDX.

Sample	C%	N%	O%
PCL	91.8 \pm 3.6	0.0	8.2 \pm 3.7
PCL/P₁₁-8	80.4 \pm 13.1	7.3 \pm 2.9	12.3 \pm 6.6
PCL/P₁₁-4	81.5 \pm 13.7	5.4 \pm 3.9	13.1 \pm 4.2

4.3.4.2 Elemental Analysis on PCL/P₁₁-8 Fibre Webs by TEM-EDX

In addition to SEM-EDX, EDX spectrometry was applied to high resolution TEM images of the nano- and submicron scale fibres in the PCL/P₁₁-8 web (samples which were analysed in Section 4.3.2.4). Figure 4-12 shows one example of typical submicron fibre (diameter around 300 nm) and a single connected nanofibre (diameter less than 50 nm). EDX spectrometry was applied to each of these fibres and an average nitrogen content of $6.5 \pm 1.4\%$ in the submicron fibres and $4.1 \pm 1.3\%$ in the nanofibers were confirmed. There is a large peak in the TEM spectra attributed to copper, which is related to the TEM grids. Table 4-3 summarises the average \pm standard deviation of atomic percentage results of the chemical elements in each of the two types of fibres. The fact that TEM-EDX was carried out in 100% vacuum mode excludes the possibility of detecting environmental nitrogen residue. These observations are indicative of the presence of peptide within both the larger submicron (100-700 nm) and nanofibre architecture (10-100 nm), providing evidence of the absence of phase separation between PCL and the peptide during electrospinning.

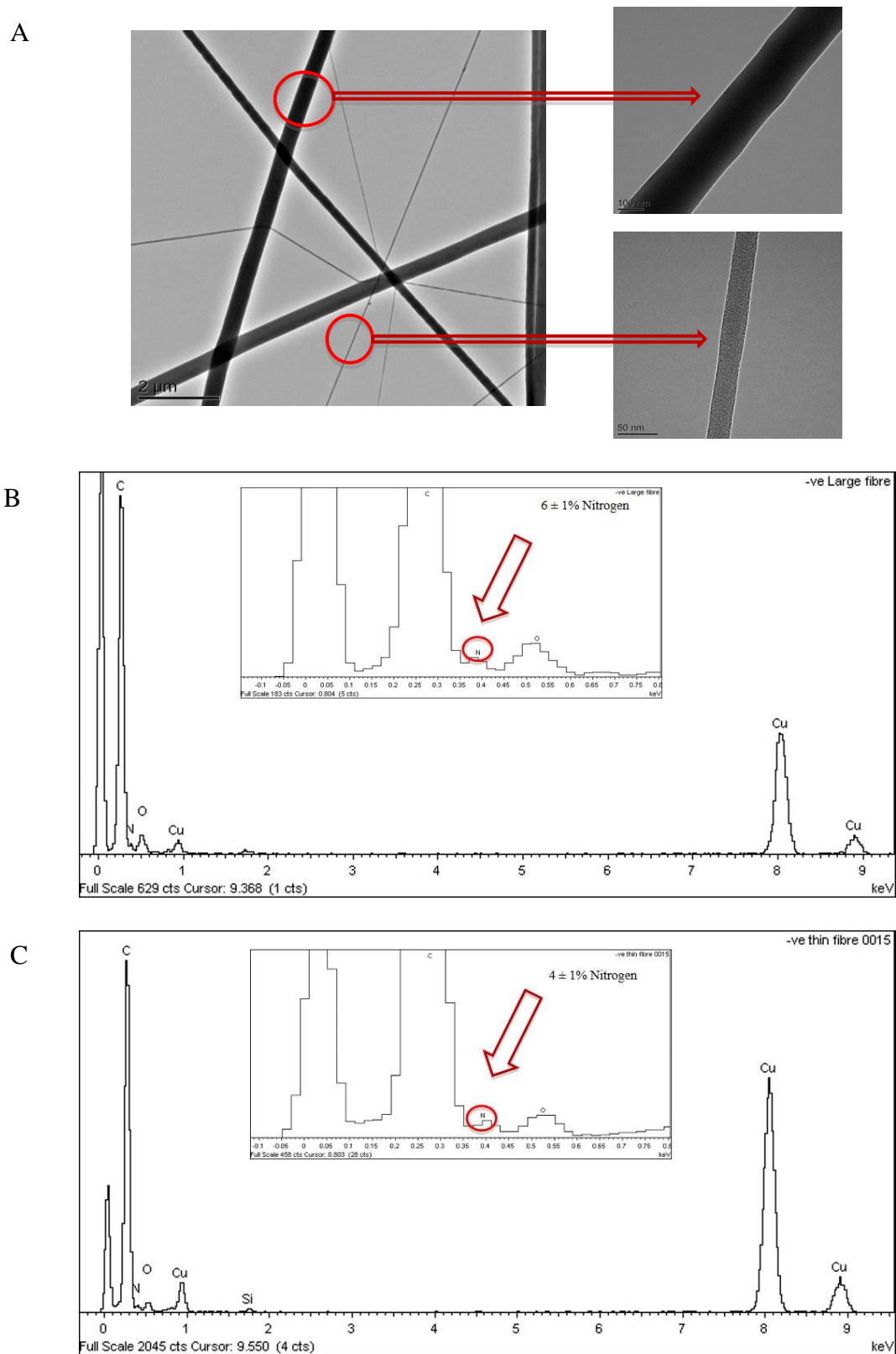


Figure 4-12. (A) TEM micrograph of PCL/P₁₁₋₈ and magnified micrographs are showing both submicron fibre and nanofibre. EDX spectroscopy analysis (full scale and magnified scale) are showing the presence of nitrogen element in both of (B) submicron and (C) nanofibre.

Table 4-3. Atomic percentages of chemical elements in the submicron and nanofiber of the electrospun PCL/P₁₁-8 fibres by TEM/EDX.

EDX spot	C%	N%	O%
Submicron fibre	86.3 ± 3.2	6.5 ± 1.4	7.2 ± 2.8
Nanofibre	91.1 ± 1.9	4.1 ± 1.3	4.8 ± 2.1

4.3.4.3 SAPs distribution analysis on PCL/SAPs fibre webs by CLSM

Micrographs of electrospun PCL/P₁₁-4 and PCL/P₁₁-8 webs containing fluorescently tagged peptides as well as PCL control sample are shown in Figure 4-13. No fluorescence background was detected in the PCL control. In contrast, the PCL/P₁₁-4 and PCL/P₁₁-8 samples clearly show individual fibres (green fluorescence). This confirms homogenous incorporation of peptides throughout the entire fibrous structure and the results are in agreement with the SEM/EDX and TEM/EDX elemental analysis.

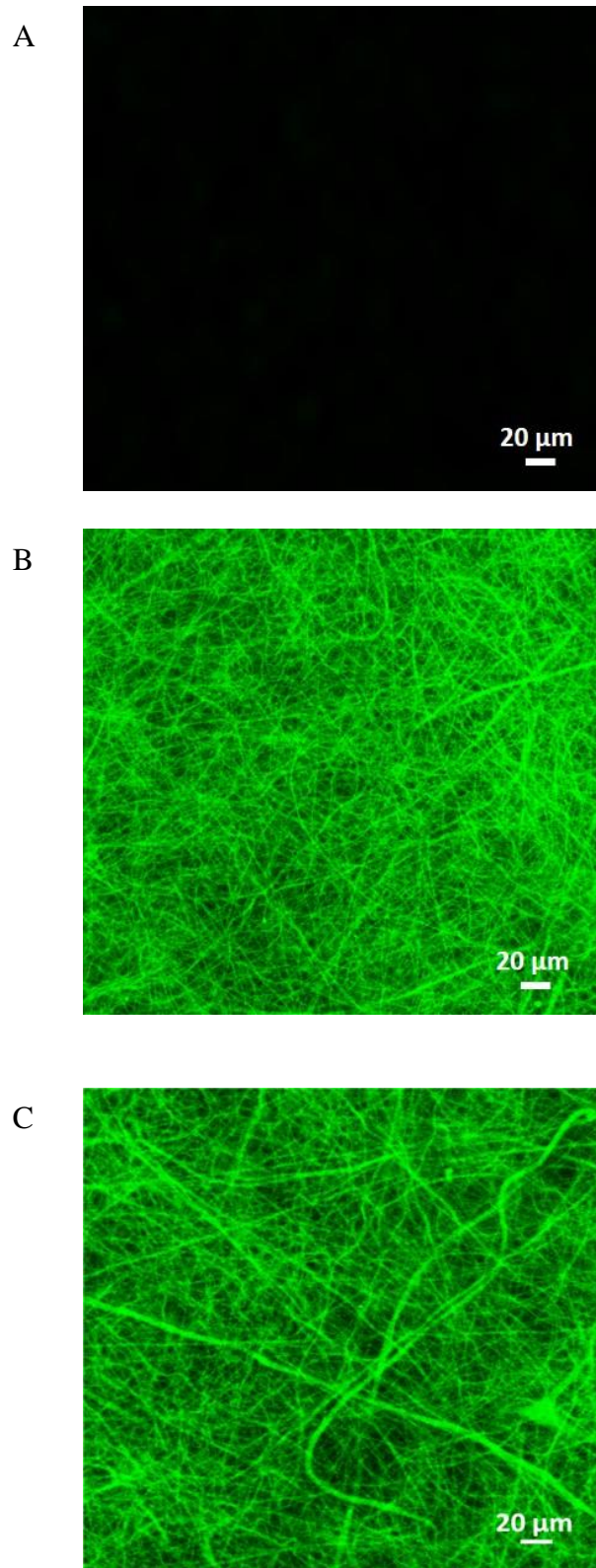


Figure 4-13. CLSM micrographs of electrospun (A) PCL, (B) PCL/P₁₁₋₄ and (C) PCL/P₁₁₋₈ fibres in which peptide samples are fluorescently tagged.

4.3.5 Peptide Secondary State in PCL/SAPs Solutions

The secondary state of peptides within the solutions prior to spinning were investigated using FTIR and CD methods and the results are presented in this section.

4.3.5.1 Peptide Secondary Structure in PCL/SAPs Solutions by CD Analysis

P₁₁₋₄ and P₁₁₋₈ solutions were prepared by dissolving 20 mg of the peptides in 1 mL of PCL solution (6% w/w in HFIP) same as the method based of which, solutions for electrospinning were prepared (explained in Section 3.2.1). In addition, solutions of only peptides (P₁₁₋₄ and P₁₁₋₈) in HFIP at a concentration of 20 mg mL⁻¹ were prepared and left for 24 h to obtain clear solutions, to compare with the electrospinning solutions. CD spectra were recorded according to the method described in Section 4.2.7.

The CD spectra of the P₁₁₋₄ and P₁₁₋₈ spinning solutions (in PCL/HFIP) display a negative minimum at around 190-200 nm and a positive maximum at around 210-215 nm (Figure 4-14 A-B), which is consistent with the random coil peptide conformation in the solution (211). This explanation is supported by the lack of a negative band at 218 nm and a strong positive maximum at lower wavelengths (198 nm), which would be characteristic of a β -sheet conformation (43, 46). This behaviour was also observed in the peptide solutions without PCL (Figure 4-14 C-D) with a small difference in the intensities. Generally a slight shift in wavelengths and slight shift in intensity of the peptide bands herein was observed when comparing the obtained spectra with previously reported CD plots (43, 46). This effect is likely to be related to much higher concentration of peptide used in this study (20 mg mL⁻¹) compared to the average concentrations previously analysed during CD spectroscopy of P_{11-X} peptides (0.15 mg mL⁻¹) (43, 46). The random coil conformation showed herein, is due to the HFIP-triggered breakdown of hydrogen bonds along the peptide molecules within the solutions. HFIP is a strong and volatile solvent and it was selected as electrospinning solvent in this study. In

the light of its fast evaporation and ability to break down hydrophobic interactions and hydrogen bonds, clear solutions of PCL and peptide random coils were obtained prior to spinning (205).

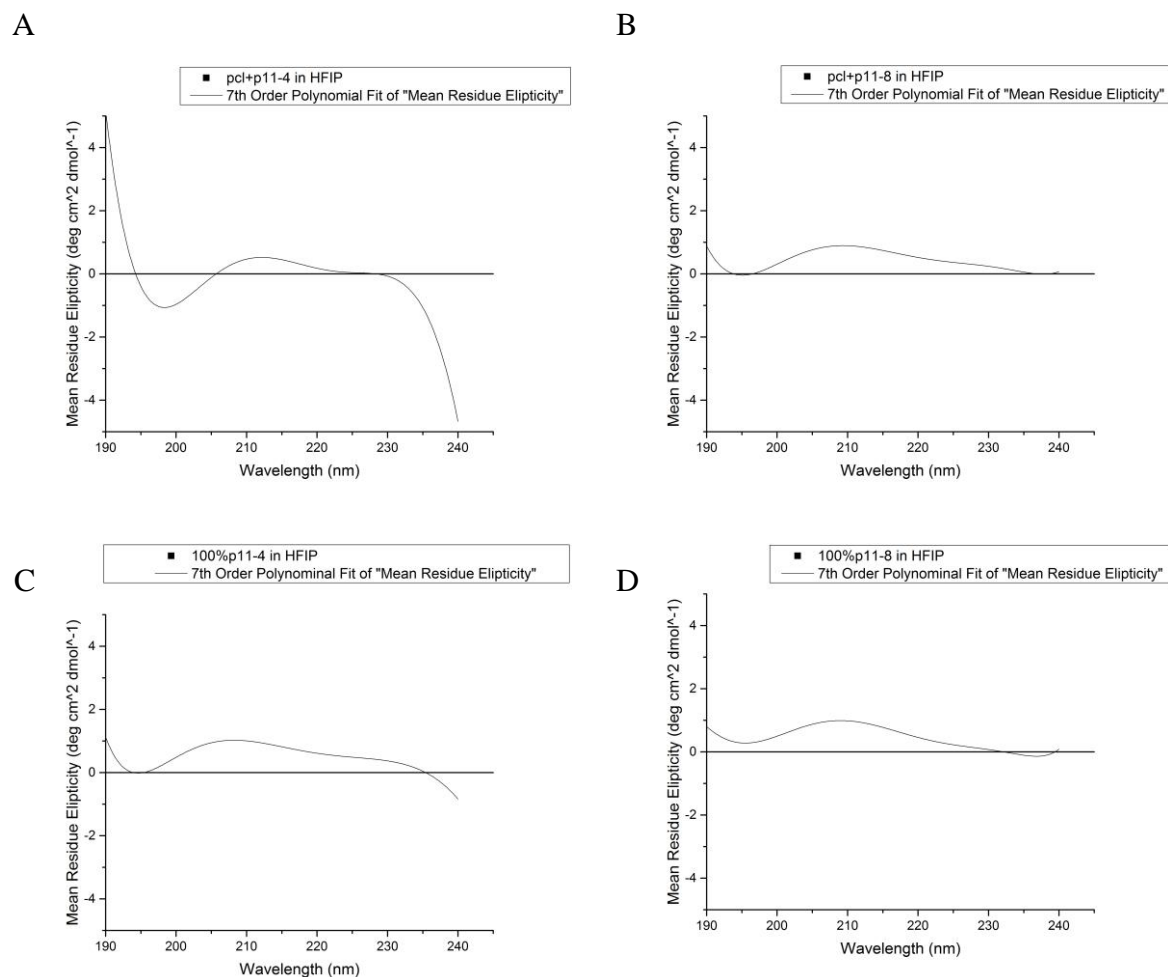


Figure 4-14. CD spectra of (A) 20 mg mL⁻¹ P₁₁₋₄ solution in 6% w/w PCL/HFIP; (B) 20 mg mL⁻¹ P₁₁₋₈ solution in 6% w/w PCL/HFIP (Electrospinning condition), (C) 20 mg mL⁻¹ P₁₁₋₄ solution in HFIP and (D) 20 mg mL⁻¹ P₁₁₋₈ in HFIP.

4.3.5.2 Peptide Secondary Structure in PCL/SAPs Solutions by FTIR Analysis

Figure 4-15 and Figure 4-16 display FTIR spectra obtained for PCL/P₁₁₋₄ and PCL/P₁₁₋₈ solutions respectively at different peptide concentrations (0, 10, 20 and 40 mg mL⁻¹). As reported in literature (212), PCL has a distinct carbonyl stretching band at around 1720 cm⁻¹. In all of the spectra, the strong peak at around 1710 cm⁻¹ can be attributed to the C=O stretching vibration in carbonyl group of PCL, however this peak might slightly be shifted in solutions, which can be because of a possible peptide/PCL/HFIP secondary interaction. By looking at these spectra in the amide I' region (1600-1700 cm⁻¹), a broad peak was observed at around 1650 cm⁻¹ in both peptide (P₁₁₋₄ and P₁₁₋₈) containing solutions, confirming a random coil configuration (43). This is due to the HFIP-triggered breakdown of hydrogen bonds along the peptide molecules in solution (26). Moreover, in the amide II' region (1500-1600 cm⁻¹), there is a band at 1550 cm⁻¹ in SAPs containing solutions, which corresponds to COO⁻ group at the peptides' backbone (48).

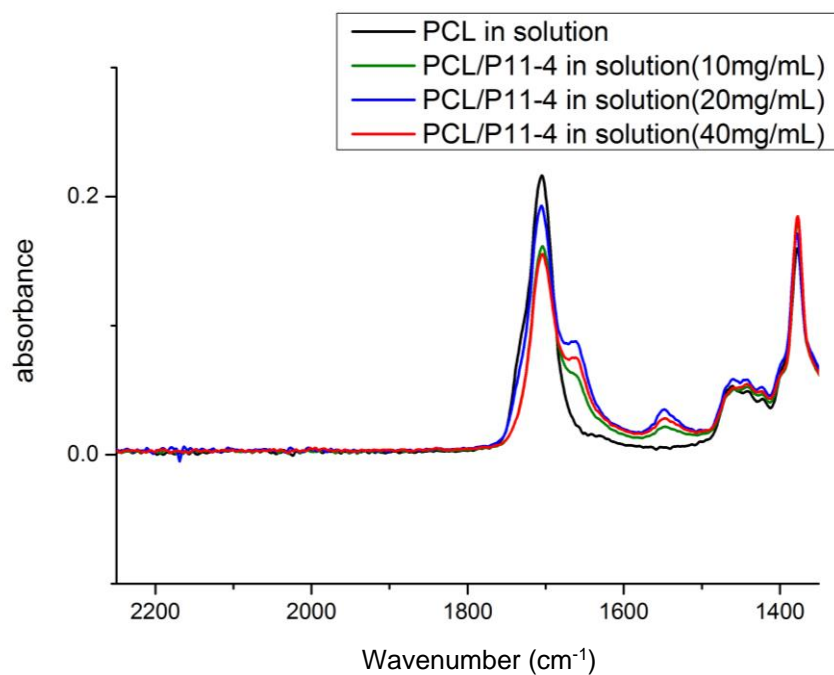


Figure 4-15. FTIR spectra of PCL and PCL/P₁₁₋₄ in a HFIP solution at different peptide concentrations.

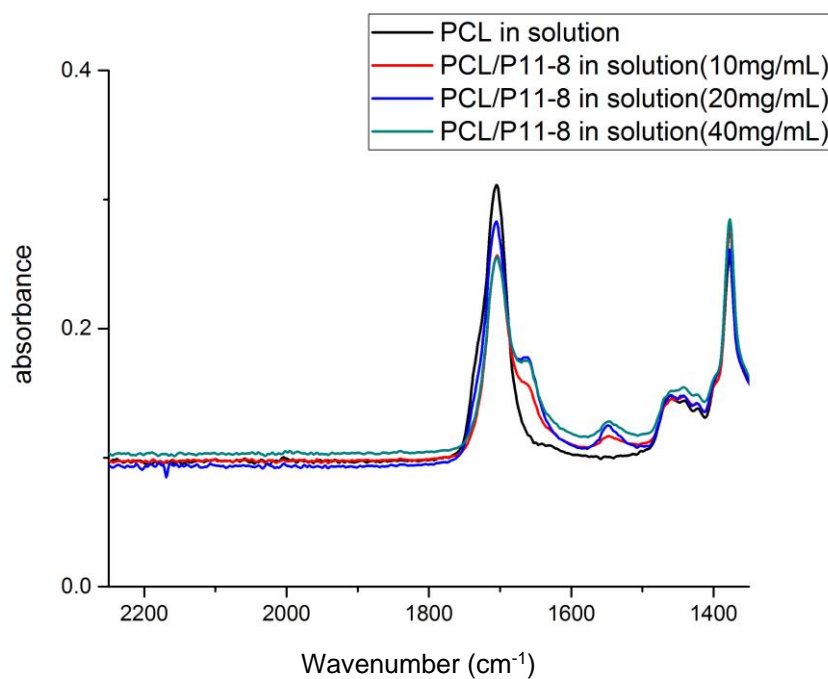


Figure 4-16. FTIR spectra of PCL and PCL/P₁₁₋₈ in a HFIP solution at different peptide concentrations.

4.3.6 Peptide Secondary State in PCL/SAPs As-Spun Fibres

The secondary state of SAPs within the fibres after spinning and vacuum drying procedures were evaluated using ATR-FTIR method and the results are presented in this section.

4.3.6.1 Peptide Secondary Structure in PCL/SAPs Fibre Webs by ATR-FTIR Analysis

Figure 4-17 displays the ATR-FTIR results obtained for electrospun PCL and PCL/P₁₁₋₄ fibres at different peptide concentrations (10, 20 and 40 mg mL⁻¹). Beside the strong peak at 1727 cm⁻¹ representing the carbonyl stretching of PCL in all of the spectra (212), the broad band at around 1650 cm⁻¹ in peptide samples can be the result of random coil/non-assembled state of P₁₁₋₄ peptide within the fibres. This peak at 1654 cm⁻¹ can also be attributed to the glutamine amino acid side chain of P₁₁₋₄ (213). However, by precisely looking at the spectra in amide I' region, a weak absorbance at around 1630 cm⁻¹ can be observed as well. This peak at 1630 cm⁻¹ coincides with β -sheet characteristic peak. Therefore, it can be assumed in PCL/P₁₁₋₄ fibre, the conformation of peptide is dominantly in a non-assembled/random coil state, however an evidence of β -sheet conformation is found as well. Moreover, in the amide II' region, it can be seen that by the increase in peptide concentration from 10 to 40 mg mL⁻¹ in solutions, the band at 1550 cm⁻¹ is intensified, which corresponds to COO⁻ group at the peptides' backbone (48).

Figure 4-18 displays the ATR-FTIR results obtained for electrospun PCL and PCL/P₁₁₋₈ fibres at different peptide concentrations (10, 20 and 40 mg mL⁻¹). As reported previously in Section 4.3.5.2, PCL has a distinct FTIR peak at 1727 cm⁻¹ attributed to its carbonyl group and this characteristic peak is observed in all spectra of PCL/P₁₁₋₈ fibres. In the amide I' region, peaks at 1630 cm⁻¹ and 1690 cm⁻¹ give supporting evidence of the predominant anti parallel β -sheet conformation of peptide in the PCL/P₁₁₋₈ fibres (in comparison with PCL/P₁₁₋₄), the intensity of which increases with the increase in P₁₁₋₈ concentration. Thus, the random coiled P₁₁₋₈ present in the PCL spinning solutions (Section 4.3.5) are likely to self-assemble during

electrospinning to yield predominant β -sheet conformation in the collected fibres. This can be the result of the critical peptide concentration (C^*) being reached during electrospinning due to solvent evaporation. Moreover, in the amide II' region, the band at 1550 cm^{-1} can be assigned to COO^- group at the peptides' backbone (48).

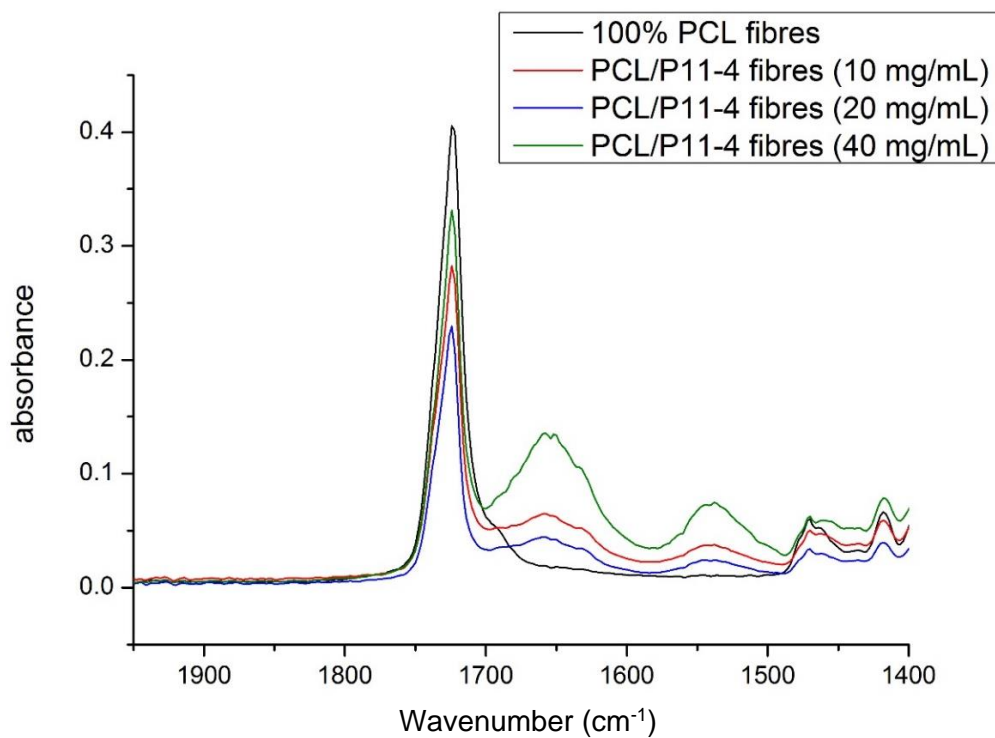


Figure 4-17. FTIR spectra of PCL and PCL/P₁₁₋₄ electrospun fibres at different peptide concentration.

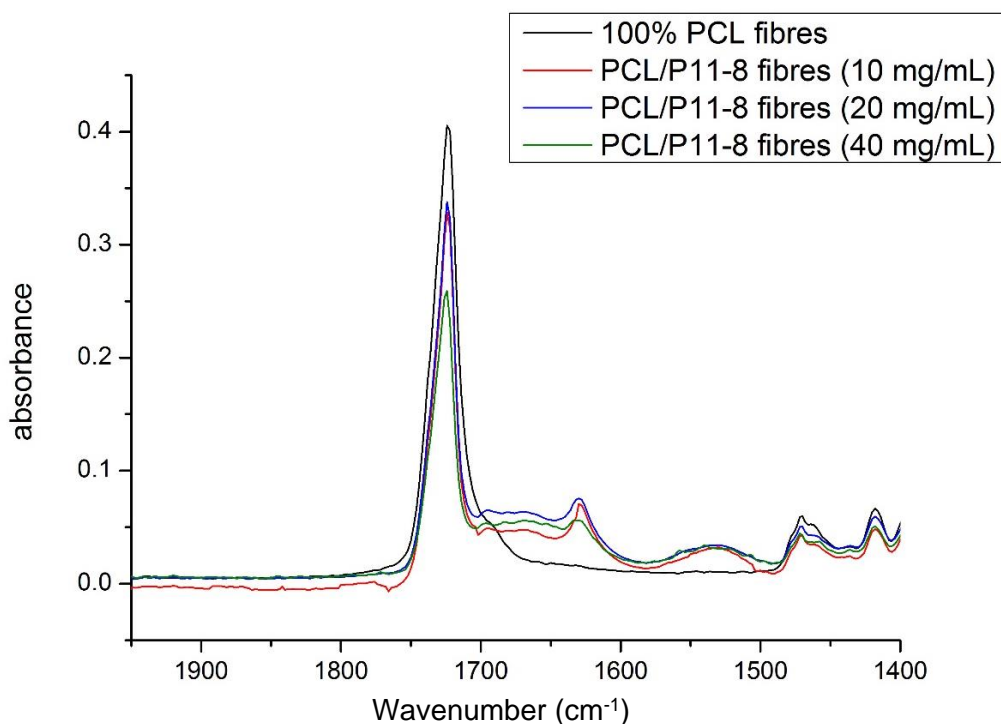


Figure 4-18. FTIR spectra of PCL and PCL/P₁₁₋₈ electrospun fibres at different peptide concentrations.

4.4 Summary

It was established that PCL at 6% (w/w) concentration in HFIP solution, can be electrospun using a single spinneret setup and produce smooth fibres that are free from defects. The smallest mean fibre diameter was achieved with a 1 mL h⁻¹ flow rate, a voltage of 20 kV and a spinning distance of 180 mm on an aluminium foil collector. Then the successful encapsulation of self-assembling P₁₁₋₄ and P₁₁₋₈ peptides within PCL fibres through a one-step electrospinning process was demonstrated. This resulted in a multiscale fibrous network containing both submicron (below 1 micron) and nano (below 100 nm) fibres; in contrast, the PCL control web was in submicron scale only. Polarity of the power supply does not create any observable difference in the morphologies of nanofiber in PCL/P₁₁₋₄ and PCL/P₁₁₋₈ fibres. Adjusting the peptide concentration in the electrospinning solution was found to be the main parameter in formation of the nanofibrous network; the nanofibrous network occurrence generally increased

by increasing the peptide concentration in the spinning solution. This was more obvious in the case of PCL/P₁₁₋₈ webs. This further can be a useful means of systematically customising the internal nanoscale structure of the webs which provides a convenient way of controlling nonwoven architecture at a nanoscale. SEM/EDX confirmed the presence of peptides within the bulk of electrospun fibres. TEM/EDX revealed both the superimposed nano- and submicron scale fibres contain peptides, providing evidence of the absence of phase separation between PCL and the peptides during electrospinning. The homogenous distribution of peptides within the fibres was further confirmed by CLSM analysis. Peptide secondary conformation analysis of the spinning solution and as-spun fibres by CD and FTIR revealed a switch from monomeric to β -sheet peptide conformation and this was more apparent in PCL/P₁₁₋₈ fibres compared to PCL/P₁₁₋₄ fibres. This can confirm that electrospinning process of PCL/SAPs was able to trigger the molecular self-assembly mechanism and induce nanofibre formation. The hydrogen bonding mediated self-assembly of peptides during electrospinning is most likely related to the rapid solvent evaporation (above C*). Within the constraint of using ESEM method for uncoated fibrous samples, it is still reasonable to assume that some of the solvent evaporation-driven self-assembly and the consequent nanofibre formation occurs after fibre deposition during the vacuum drying procedure. Although, most of the solvent is evaporated via the solvent jet from the nozzle tip to the collector, it is also possible that changes in peptide conformation continue if residual solvent is present in the deposited fibres.

CHAPTER 5

Biological Properties of Electrospun PCL/SAPs Fibre Webs

5.1 Introduction

In Chapter 4, the production of PCL/SAPs fibres was successfully carried out via needle electrospinning resulting in a multiscale (submicron and nano-) diameter fibrous scaffold. Moreover, it was shown that the peptides were thoroughly incorporated into the fibrous network and electrospinning was able to trigger self-assembly and therefore resulting fibres contained β -sheet structure, though to varying extents. The aim of this chapter is to evaluate characteristics of the produced fibres when placed in a biological environment relevant to tissue repair and regeneration. Specifically, as key factors affecting the suitability of a scaffold for biological implantation, the wettability, cytotoxicity and degradation of the new materials were investigated.

5.2 Experimental Details

5.2.1 Wettability of PCL/SAPs Fibre Webs

In the present study, by commixing PCL with SAPs, one of the intentions was to enhance and expand the potential applicability of PCL in tissue engineering by altering its hydrophilicity as well as its biofunctionality. Wettability can be characterised by contact angle measurements,

specifically the angle between the wetting liquid and the wetted surface, which is the result of the surface energy interactions between the solid-liquid-air phases. Given that water represents most of the weight fraction of the extracellular matrix of biological tissues, wetting is important and the contact angle of electrospun webs made of PCL and PCL/SAP were measured via application of deionized water and DMEM (Dulbecco's Modified Eagle's medium), to simulate biological medium. Since the surface of electrospun webs comprises solid fibres and pores such that the resulting discontinuities can potentially influence wetting behaviour, films were also prepared using the same polymer solutions as electrospinning solutions, to investigate the surface wettability of the non-porous material.

The goniometer (explained in Section 3.2.12) was used to measure the contact angles of pristine PCL controls and samples containing the peptide. Electrospun samples of 100% PCL, PCL/P₁₁₋₄, and PCL/P₁₁₋₈ (both at peptide concentrations of 10, 20 and 40 mg mL⁻¹) prepared as described in Section 3.2.1 and 3.2.2, were cut out into 10×10 mm squares. A 1.5 μL drop of either deionised water (Milli-Q) or DMEM was deposited on the surface and the contact angles were recorded for 15 s. Three replicates per sample were examined. For each image the contact angles for both the right and left sides of the droplet boundary were measured and the mean angle calculated. In some PCL/SAP samples, the duration of the test was substantially less than 15 s because of substantially improved wetting behaviour compared to 100% PCL.

Contact angle can be useful in the evaluation the hydrophilicity in electrospun webs, however in porous media such as this, the value also depends on the surface porosity and surface roughness based on Wenzel theory (214). In contact angle measurements of fibrous webs, only a fraction of the liquid is directly supported by contact with the fibres because of the large void volume. Therefore, to be able to verify the effects of SAPs content on the observed contact angle, two samples of identical material compositions as used to make the electrospun webs i.e. PCL and PCL/P₁₁₋₈ at peptide concentrations of 10 and 20 mg mL⁻¹ were also prepared as

films. 1 mL of PCL and PCL/P₁₁₋₈ in HFIP were poured on to glass slides and films were cast by drying the solution under vacuum for 48 h in a Gallenkamp OVL570 010J vacuum oven at room temperature under 10×10^3 Pa vacuum. Contact angle measurements were then carried out with deionised water as described in the previous paragraph.

5.2.2 Cytotoxicity Evaluation of PCL/SAPs Fibre Webs

In this research, PCL/SAPs electrospun materials were analysed by both extract cytotoxicity and direct cytotoxicity methods as below.

5.2.2.1 Extract Cytotoxicity Method

Extract cytotoxicity assays are used to analyse the reaction of cells in contact with the material extracted from samples. The method employed in this study is explained in Section 3.2.13.1. Extracts of PCL/P₁₁₋₄ and PCL/P₁₁₋₈ electrospun web samples at a medium peptide concentration of 20 mg mL^{-1} were obtained. The extract of 100% PCL fibres was also taken as negative control because of its non-cytotoxicity (27, 31) and DMSO was used as positive control due to its strong cytotoxicity effect on cells and DMEM (cell culture medium) was used as blank control. After culturing the prepared cells in suspension for 24 h, the culture medium was replaced with these extract samples or with control solutions. The position of each sample (with 8 replicates) in a 96-well plate is shown in Figure 5-1.

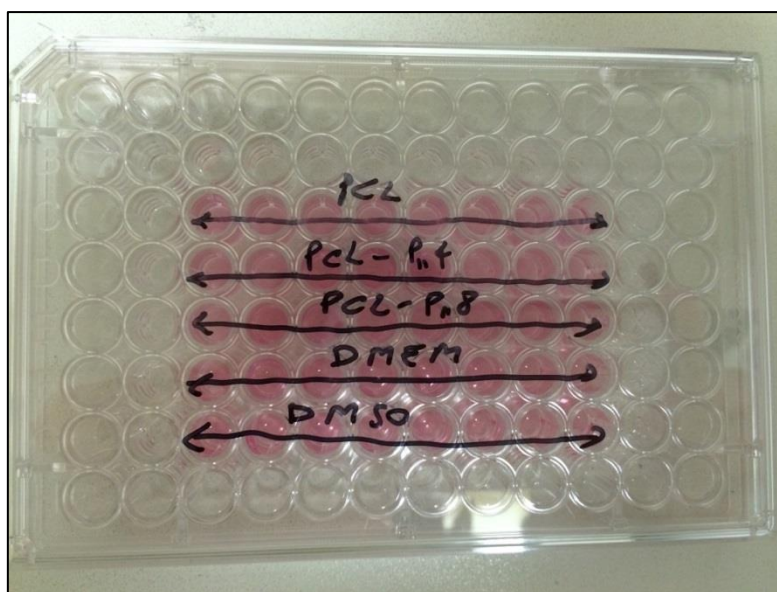


Figure 5-1. Positioning of samples in a 96-well plate for the extract cytotoxicity assay. PCL extract was used as a negative control in row one, PCL/P₁₁₋₄ extract in row two and PCL/P₁₁₋₈ extract in row three. Blank DMEM is in row four and the positive control (DMSO) in row five.

The well plates containing cells and extracts from each of the samples (or controls) were incubated at 37°C in 5% (v/v) CO₂ in air for 48 h to allow the extracts to react with the cells. After that the well plates were optically examined under a Leica DFC365 FX monochrome digital microscope to observe the cell morphology. To quantify cell viabilities after exposure to the sample extracts, the samples were directly exposed to 20 µl of CellTiter 96® AQueous One Solution reagent and incubated for 4 h as described in Section 3.2.13.1. This reagent can be bio-reduced by cells into a coloured formazan product that is soluble in DMEM. The 96-well plate was then placed in a Varioskan Flash Reader and the absorbance was recorded at 490 nm. The quantity of formazan product as measured by the absorbance at 490 nm is directly proportional to the number of living cells in culture. Additional work reported in the next section (5.2.2.2) was carried out to address the response of cells cultured directly on to the surface of the nonwoven samples.

5.2.2.2 Direct Cytotoxicity Method

A direct cytotoxicity assay was used to assess *in vitro* cytotoxicity of electrospun PCL/P₁₁-4 and PCL/P₁₁-8 fibres in direct contact with cultured L929 mouse fibroblasts. The method employed in this experiment was extensively explained in Section 3.2.13.2. PCL fibres were used as a negative control and DMSO as a positive control. After culturing the prepared cells in suspension for 24 h, the culture medium was replaced with fresh DMEM. In the case of the positive control wells, DMEM was replaced with 250 µg of fresh DMEM and 250 µg of DMSO. Then the pre-soaked fibrous scaffolds (in DMEM) were placed in each sample well. A blank row was also left with DMEM only. The position of each sample (with 6 replicates) in two 24-well plates is shown in Figure 5-2.

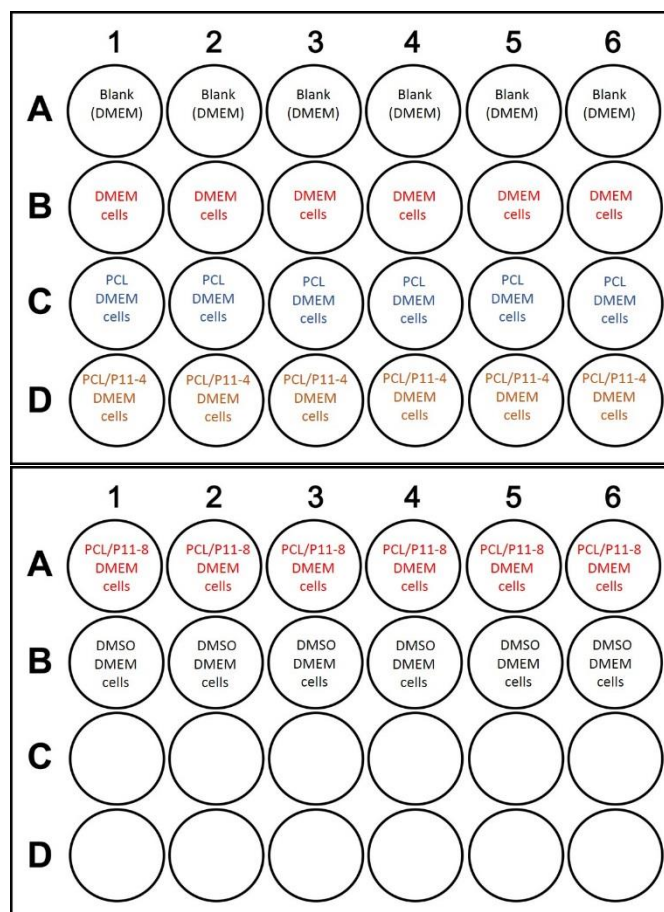


Figure 5-2. The position of samples in two 24-well plates for direct cytotoxicity assay.

The well plates containing cells and the electrospun scaffold samples (or controls) were incubated for 48 h at 37 °C in 5% (v/v) CO₂ in air to allow the samples to interact with the cells. After incubation, the cell morphologies were analysed under a phase-contrast microscope at 200x magnification. To quantify the viability of cells in direct contact with electrospun samples, a MTT assay was used as described in Section 3.2.13.2. MTT is metabolically reduced in viable cells to a blue-violet insoluble formazan. The quantity of formazan product as measured by the absorbance at 570-650 nm (Equation 3-3 and Equation 3-4), is directly proportional to the number of living cells in culture.

5.2.3 Peptide Release Behaviour of PCL/SAPs Fibre Webs into Aqueous

Solution

Additionally, in this chapter the SAP release behaviour from the PCL/SAP fibre webs was explored in a simulated biological environment. For biomedical applications, it is of major importance to know the degradation or release kinetics of polymeric material components as it plays a major role in determining functional performance *in situ*. It is known that PCL is biodegradable through hydrolysis as reported in several studies depending on its molecular weight (27). However, the degree to which the SAPs are stable and remain within a PCL fibrous structure is currently unknown and it was therefore of interest to study the release of this material due to hydrolytic or diffusion effects.

The release of SAP in an aqueous environment is to be anticipated because of its water solubility. Moreover because of the reversible transient self-assembly properties of P₁₁ SAPs (47), such peptides structures are readily diffused in water-based media (upon a change in the environment i.e. pH or decrease in the concentration) even at the self-assembled state. Therefore, there is a risk they will migrate away from where they are needed to remain in a biological environment. Figure 5-3 shows self-assembly of P₁₁ peptides from monomeric

random coil into hierarchical structures of fibrils and fibres and in principle, all of these transformations are reversible (47).

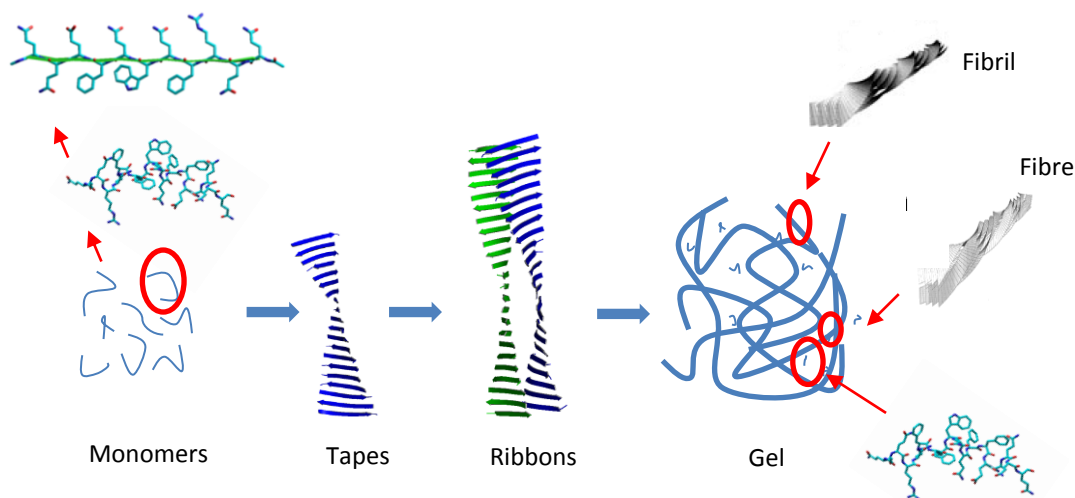


Figure 5-3. Self-assembly of peptides from monomers in isotropic fluid to β -sheet tapes, ribbons, fibril and fibres in nematic gel form.

Moreover it is known that peptide self-assembly into hierarchical structures in the case of P₁₁₋₄ and P₁₁₋₈ is a pH dependant phenomena with the opposite phase behaviour (Figure 5-4) (200). Therefore, based on this behaviour, fibres containing peptides were incubated in aqueous solution at different pH to find out the kinetics of peptide disassembly and release and therefore to estimate the stability of peptides within the fibres in biological conditions.

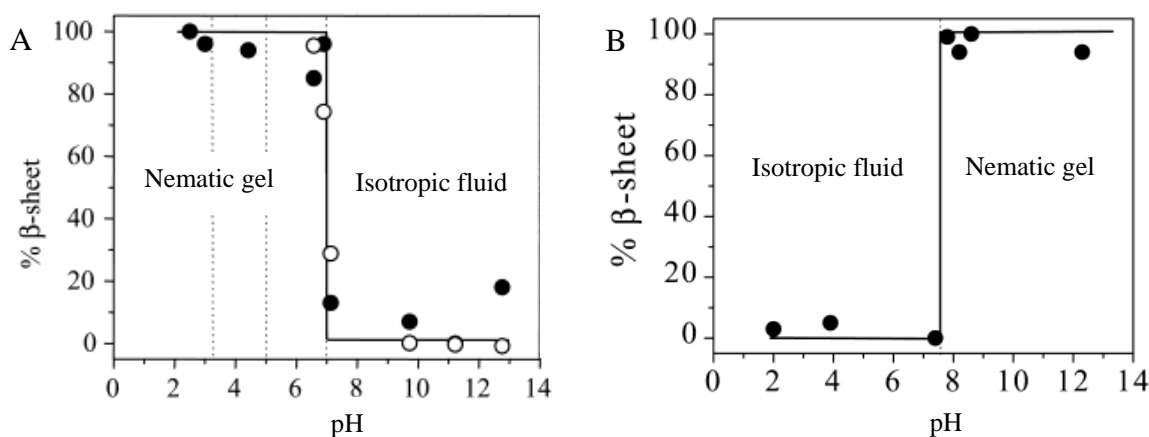


Figure 5-4. Transformation from isotropic fluid (monomer) to nematic gel (β -sheet) of (A) P₁₁₋₄ and (B) P₁₁₋₈ as a function of pH (47).

The incubation method is described in Section 3.2.15. In brief, fibres were incubated in deionised water at pH 3.5, 7.5 and 10.5 at a stirring rate of 120 r min⁻¹ and temperature of 37 °C for 1 h, 24 h, 48 h and 7 d. After the incubation, the fibrous samples were analysed based on mass loss (TGA) and fibre morphology (SEM), and the peptide release in the supernatant of solutions was analysed through UV-CD.

5.3 Results and Discussion

5.3.1 Wettability Behaviour of Electrospun PCL/SAPs Fibre Webs

The wetting behaviour of electrospun webs composed of PCL and PCL/SAPs has not been previously studied and revealed remarkable differences in behaviour, as detailed in the following sections.

5.3.1.1 Contact Angle of Water on PCL/SAPs Electrospun Fibres

Figure 5-5 shows examples of a droplet of deionised water on the surface of the electrospun webs at time = 0 s. Contact angles greater than 90° were observed on electrospun PCL, whilst decreased contact angle values were measured in PCL/SAPs samples. Furthermore it can be seen that as the P₁₁₋₄ and P₁₁₋₈ concentration (0-20 mg mL⁻¹) increased, the contact angle values decreased. The contact angles on both PCL/P₁₁₋₄ and PCL/P₁₁₋₈ at a peptide concentration of 40 mg mL⁻¹ could not be imaged and measured because of the rapid penetration of the droplet into the web structure due to its super hydrophilicity. Table 5-1 summarises the average of three replicates for initial contact angles ± standard error.

Table 5-1. Contact angle of a droplet of deionised water on electrospun samples at time = 0 s.

Sample	100% PCL	PCL/ P ₁₁₋₄ (10 mg mL ⁻¹)	PCL/ P ₁₁₋₄ (20 mg mL ⁻¹)	PCL/ P ₁₁₋₈ (10 mg mL ⁻¹)	PCL/ P ₁₁₋₈ (20 mg mL ⁻¹)
Contact angle (°)	130 ± 0.5	70.3 ± 0.8	57.6 ± 1.1	78.8 ± 0.6	23.9 ± 1.2

To improve the characterisation of wettability in these porous samples, the time factor was taken into the account and the rate of wetting was determined over 15 s using goniometry wherein several contact angles were measured at 1 s time interval. Figure 5-6 shows the dynamic contact angles of the liquid on the surfaces of each electrospun sample. Wetting was found to progressively increase by addition of only 10 mg peptide in each mL of the electrospinning spinning solution. However interestingly, when the concentration of both of

the peptides is at 20 mg mL^{-1} , the rate of wetting was very quick, such that after 2-3 s the droplet completely penetrated the web surface. The contact angle could not be satisfactorily measured when the peptide concentration was increased to 40 mg mL^{-1} because of the rapid penetration of the droplet into the web structure due to its increased wettability.

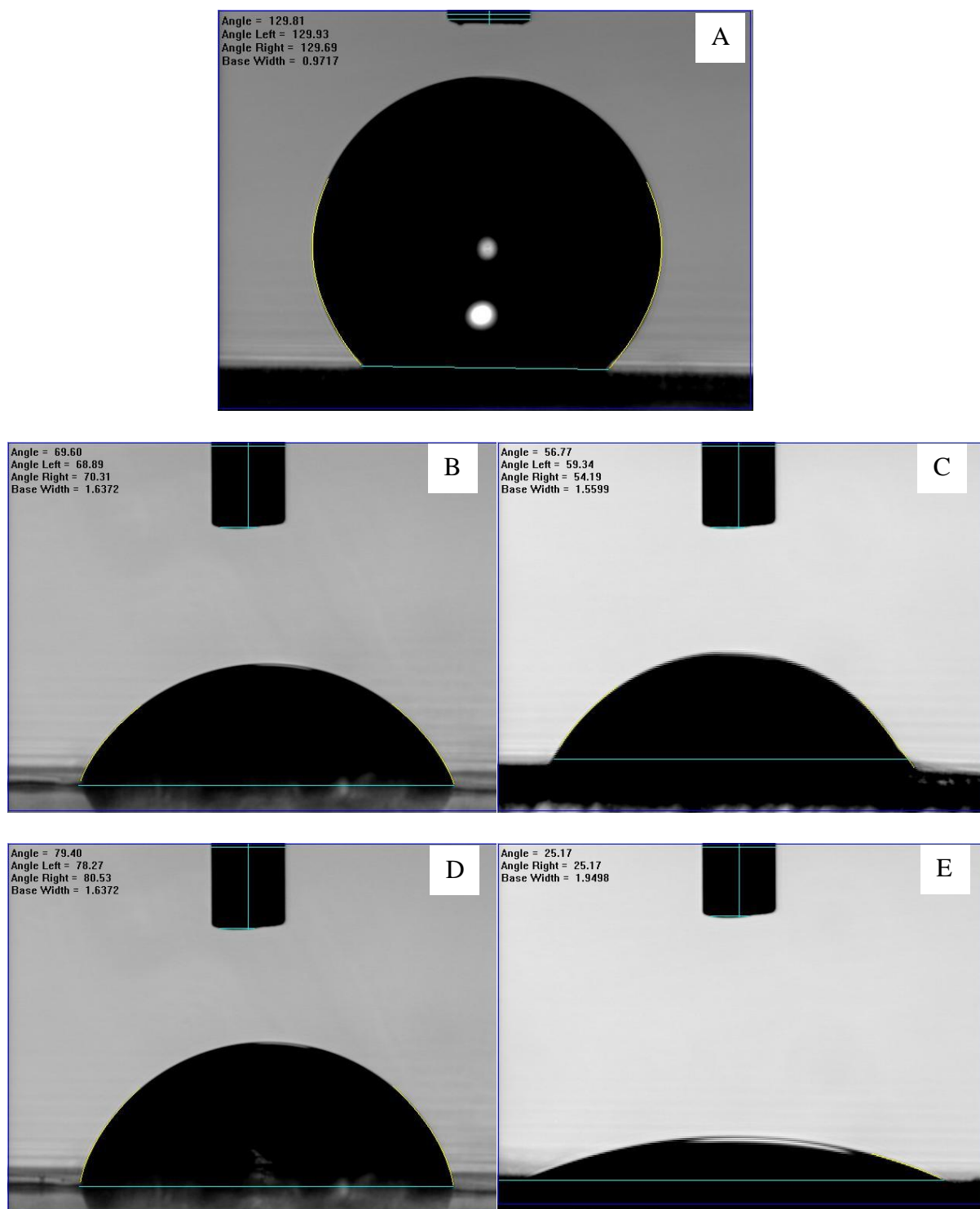
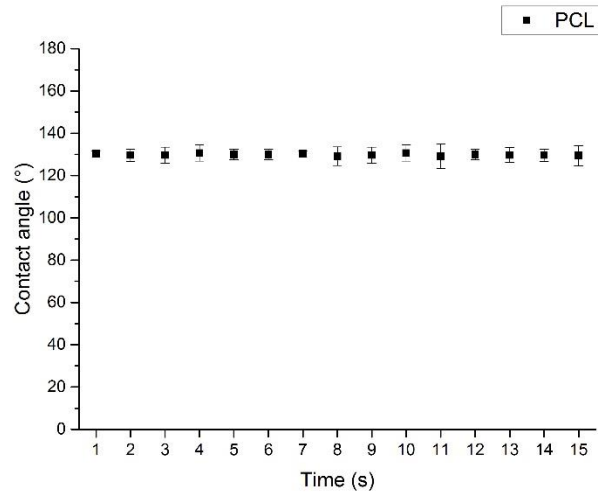
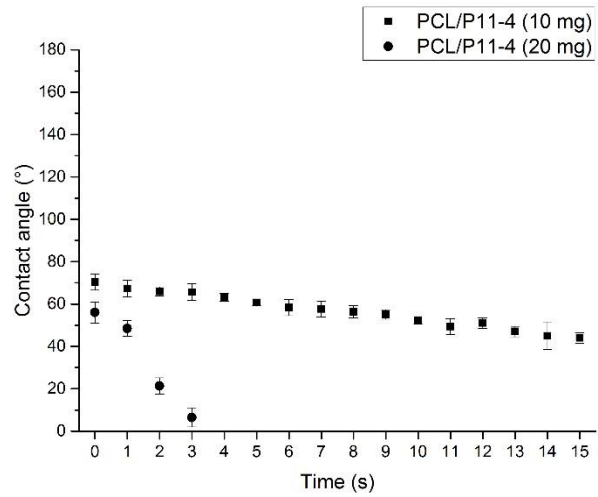


Figure 5-5. Initial contact angle of a deionised water droplet on electrospun fibre webs (at time = 0 s) on (A) 100% PCL, (B) PCL/P₁₁-4 at a peptide concentration of 10 and (C) 20 mg mL⁻¹, (D) PCL/P₁₁-8 at a peptide concentration of 10 and (E) 20 mg mL⁻¹.

A



B



C

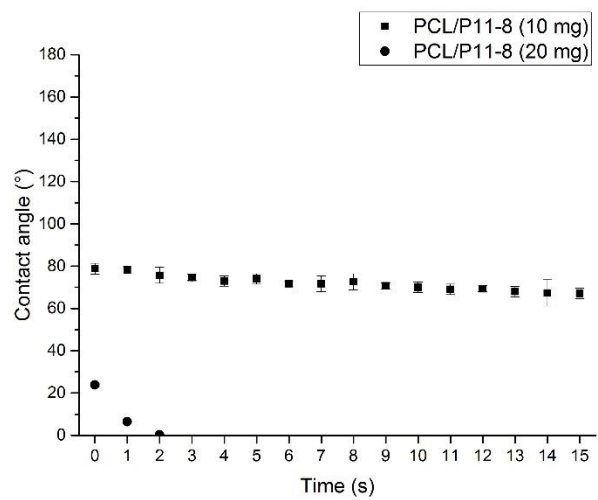


Figure 5-6. Dynamic contact angle measurements of a droplet of water on (A) PCL, (B) PCL/P₁₁₋₄ and (C) PCL/P₁₁₋₈ electrospun fibre webs up to 15 s.

5.3.1.2 Contact Angle of DMEM on PCL/SAPs Electrospun Fibres

Figure 5-7 shows representative examples of the behaviour of droplets of DMEM on the surface of electrospun webs at time = 0 s. Contact angles greater than 90° were also observed herein on electrospun PCL, whilst decreased contact angle values were measured for the PCL/SAPs samples. Furthermore, it can be seen that as the P₁₁₋₄ and P₁₁₋₈ concentration (0-20 mg mL⁻¹) increased, the contact angle values decreased. From a biological perspective, this effect can be expected to be beneficial because it is likely to promote cell adhesion and proliferation in PCL-based materials (215). Table 5-2 reports the average of three replicates' initial contact angles ± their standard errors.

Table 5-2. Contact angle of a droplet of DMEM on electrospun samples at time = 0 s.

Sample	100% PCL	PCL/ P ₁₁₋₄ (10 mg mL ⁻¹)	PCL/ P ₁₁₋₄ (20 mg mL ⁻¹)	PCL/ P ₁₁₋₈ (10 mg mL ⁻¹)	PCL/ P ₁₁₋₈ (20 mg mL ⁻¹)
Contact angle (°)	125 ± 0.8	65.9 ± 2.2	46.5 ± 1.0	56.8 ± 0.7	50.6 ± 0.3

The wetting rate of DMEM on electrospun samples was also determined over 15 s (Figure 5-8). It was observed here that by increasing the concentration of peptide from 0 to 20 mg mL⁻¹ wetting increased similar to the case of deionised water. When the concentration of peptide in the electrospinning solution was 40 mg mL⁻¹, the initial contact angle of DMEM on fibres could not be measured above 0° due to the very high wettability.

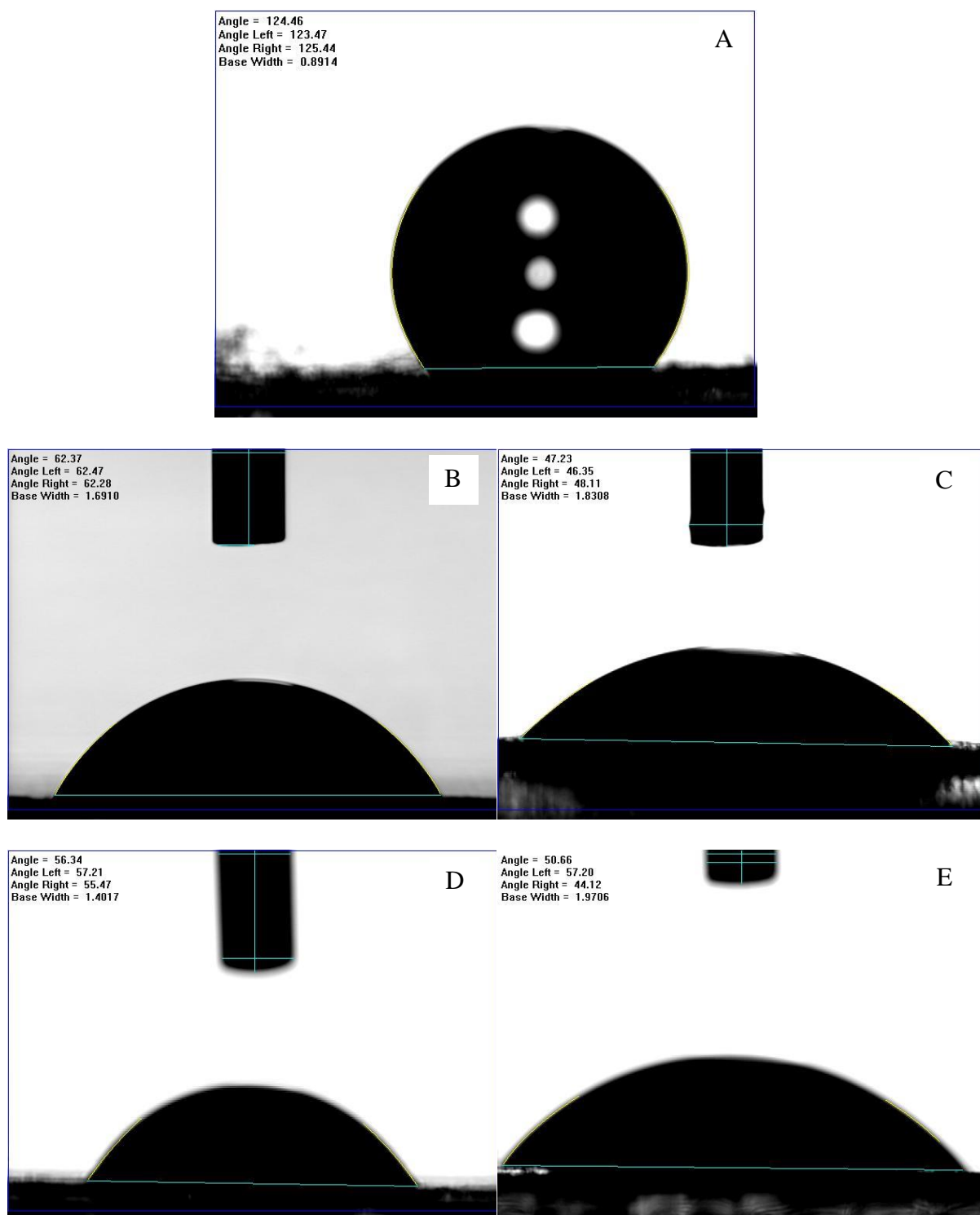
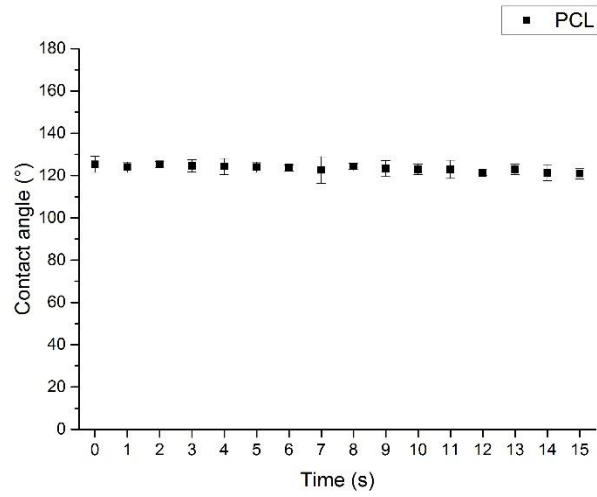
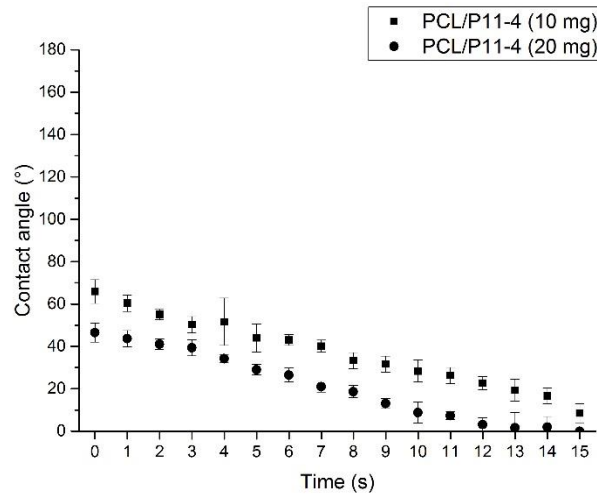


Figure 5-7. Initial contact angle of a DMEM liquid droplet on electrospun fibre webs (at time = 0 s) on (A) 100% PCL, (B) PCL/P₁₁₋₄ at a peptide concentration of 10 and (C) 20 mg mL⁻¹, (D) PCL/P₁₁₋₈ at a peptide concentration of 10 and (E) 20 mg mL⁻¹.

A



B



C

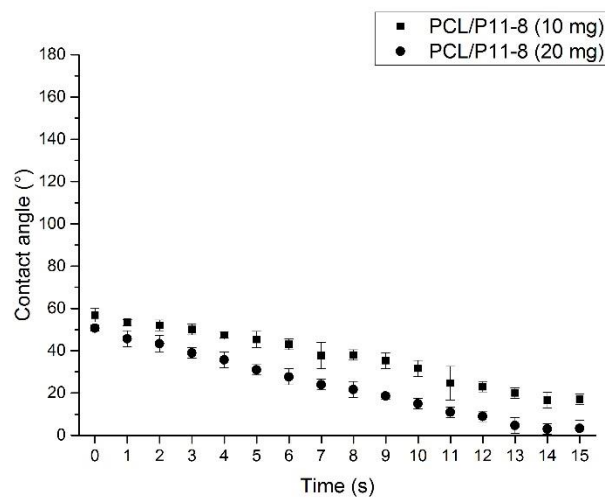


Figure 5-8. Dynamic contact angle measurements of a droplet of DMEM on (A) PCL, (B) PCL/P₁₁₋₄ and (C) PCL/P₁₁₋₈ electrospun fibre webs up to 15 s.

5.3.1.3 Contact Angle of Water on PCL/SAP Films

Three electrospinning solutions of PCL and PCL/P₁₁₋₈ at peptide concentrations of 10 and 20 mg mL⁻¹ were selected to make continuous cast films to eliminate the effect of porosity on contact angle measurements. The contact angles of droplets of deionised water on the surface of the cast films are shown in Figure 5-9 (A-C). Similar to the trend observed with the electrospun fibre webs, the hydrophilicity increased with increasing peptide concentration from 0 up to 20 mg mL⁻¹. This corresponded to contact angles ranging from $79 \pm 3^\circ$ for 100% PCL film, $59 \pm 2^\circ$ for PCL/P₁₁₋₈ at a peptide concentration of 10 mg mL⁻¹ and $18 \pm 3^\circ$ for PCL/P₁₁₋₈ at peptide concentration of 20 mg mL⁻¹. Figure 5-9 (D) shows the wetting rate of deionised water on cast films over a 15 s period of time, which also increased at the higher peptide concentration. The contact angles on films were found to follow the same trend as the electrospun samples, which verifies the primary influence of peptide content on wettability, although the range of contact angles for the films was lower. This difference in wetting may be attributed to the surface roughness effects of electrospun samples at the nano- and submicron scales, which has previously been reported in the literature (216). Based on Wenzel theory this lower contact angle is related to the higher specific surface area in films and based on the Cassie and Baxter theory, it can be attributed to the trapped air in the cavities of a rough surface in fabrics (214).

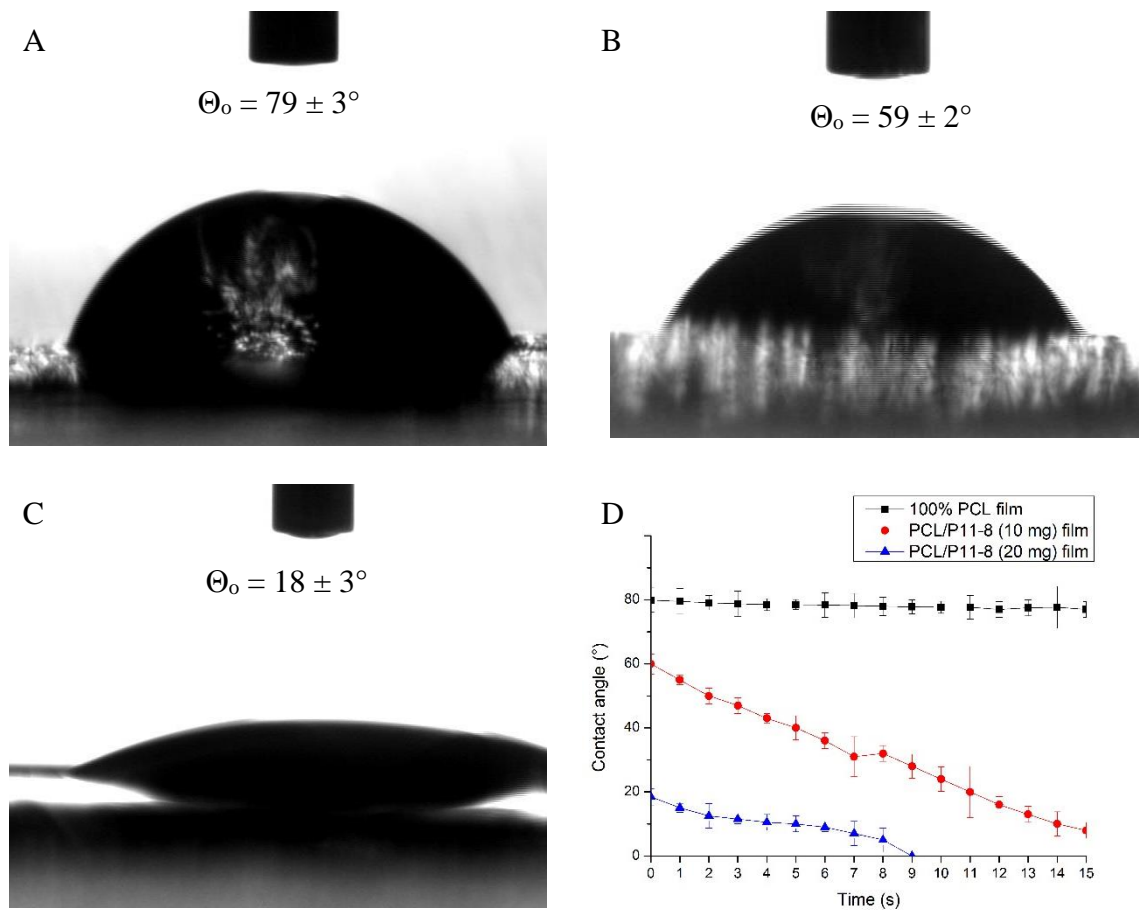


Figure 5-9. Initial contact angle of a droplet of deionised water on (A) PCL and (B) PCL/P₁₁₋₈ cast films at a peptide concentration of 10 and (C) 20 mg mL⁻¹. (D) Dynamic contact angle measurements of a droplet of deionised water on PCL and PCL/P₁₁₋₈ cast films.

5.3.2 Cytotoxicity Assessment of PCL/SAPs Electrospun Fibres

Extract and contact cytotoxicity results for the samples were of interest because of the lack of existing data on the cytotoxic response of PCL/SAP fibres. This assessment was crucial to understand the degree to which the materials would be suitable for practical use as biomaterials in a biological environment.

5.3.2.1 Result of Extract Cytotoxicity assessment of PCL/SAPs Fibres

Cell Morphology

Figure 5-10 shows the morphology of cells exposed to the sample extract after incubation. Microscopic examination revealed that mouse fibroblasts are still able to proliferate in contact with the extract of all of PCL/P₁₁-4 and PCL/P₁₁-8 samples and the cellular morphologies were healthy with no evidence of cytotoxicity, comparable with that of negative control (PCL). The blank sample (DMEM) exhibited slightly lower cell proliferation while the positive control (DMSO) exhibited the lowest number of cells being elongated and proliferated.

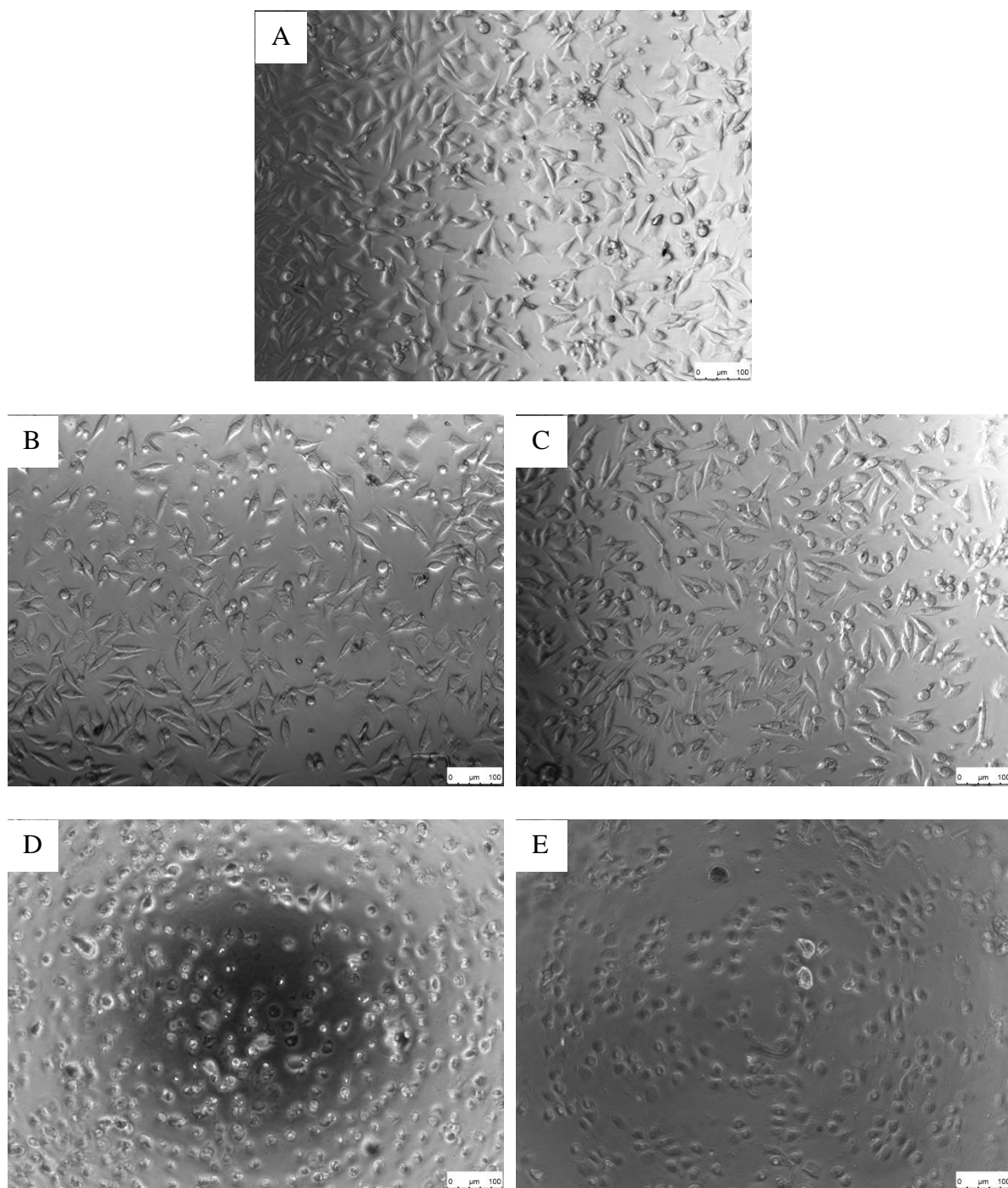


Figure 5-10. Optical monochrome digital micrographs of cells treated with the sample extracts; (A) PCL, (B) PCL/P₁₁₋₄, (C) PCL/P₁₁₋₈, (D) DMEM and (E) DMSO.

MTS Assay

The cell response in terms of metabolic activity quantified by MTS assay is shown in Figure 5-11, which relates to the average absorbance values (mean \pm standard error).

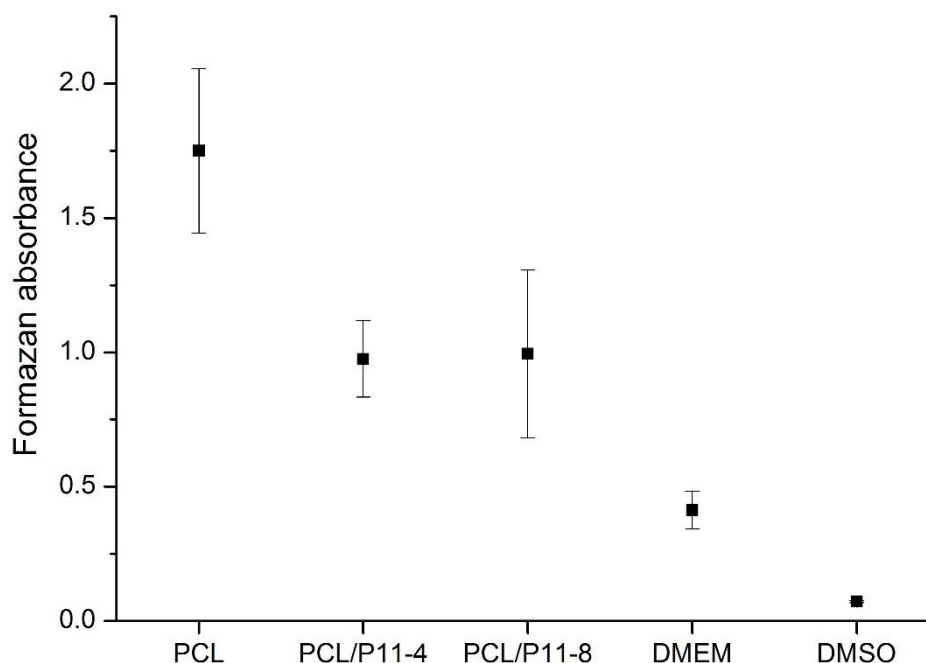


Figure 5-11. UV absorption of extract samples at 490 nm related to the quantity of formazan produced and the number of living cells.

The quantitative results indicated that all of the fibrous webs exhibited significantly greater average absorbance ($p \leq 0.05$) compared to the DMSO positive control sample. The results for the fibrous webs were also significantly better in terms of absorbance than the DMEM blank control sample. Evidently, the PCL (negative control) fibrous scaffold exhibited the greatest average absorbance value ($p \leq 0.05$) followed by PCL/P₁₁-8 and PCL/P₁₁-4 fibrous scaffolds, which had comparable average absorbance values ($p \geq 0.05$). The quantity of formazan is directly proportional to the number of living cells and the higher absorbance values observed for the PCL and PCL/SAPs samples is indicative of greater cell viability on these samples, as compared to the DMEM and DMSO controls. Therefore all the results suggest that electrospun webs of PCL as well as PCL/SAP fibres were nontoxic to L929 cells and may be considered

good candidates for evaluation as tissue scaffolds. The lower formazan absorbance of PCL/P₁₁-4 and PCL/P₁₁-8 compared with the PCL control extracts may indicate that some peptide release occurred during the extract preparation (72 h incubation at 37°C). This is possible as peptides can be diffused into monomeric form when in a water-based medium, which may have slightly affected the metabolic activity of L929 mouse fibroblasts, despite the cell affinity to peptides when they are in self-assembled form (27).

5.3.2.2 Results of Direct Cytotoxicity assessment of PCL/SAPs Fibres

Further to the extract cytotoxicity data, direct cytotoxicity was explored to understand the response of cell morphology and the MTT assay.

Cell Morphology

The PCL, PCL/P₁₁-4 and PCL/P₁₁-8 fibres in contact with cells were examined under a phase-contrast microscope and the digital micrographs of cells exposed to the fibrous samples at 200x magnification are shown in Figure 5-12. Based on the microscopic examination, L929 mouse fibroblasts were clearly observed to proliferate in contact with the PCL/P₁₁-4 and PCL/P₁₁-8 samples as well as the PCL control sample. The cells grew with healthy cellular morphologies towards the edges (dark areas) of both the negative control and peptide samples with no evidence of cytotoxicity. It is also obvious from Figure 5-12 that PCL/P₁₁-8 fabric is more promoting the cell growth compared with PCL/P₁₁-4 fabric.

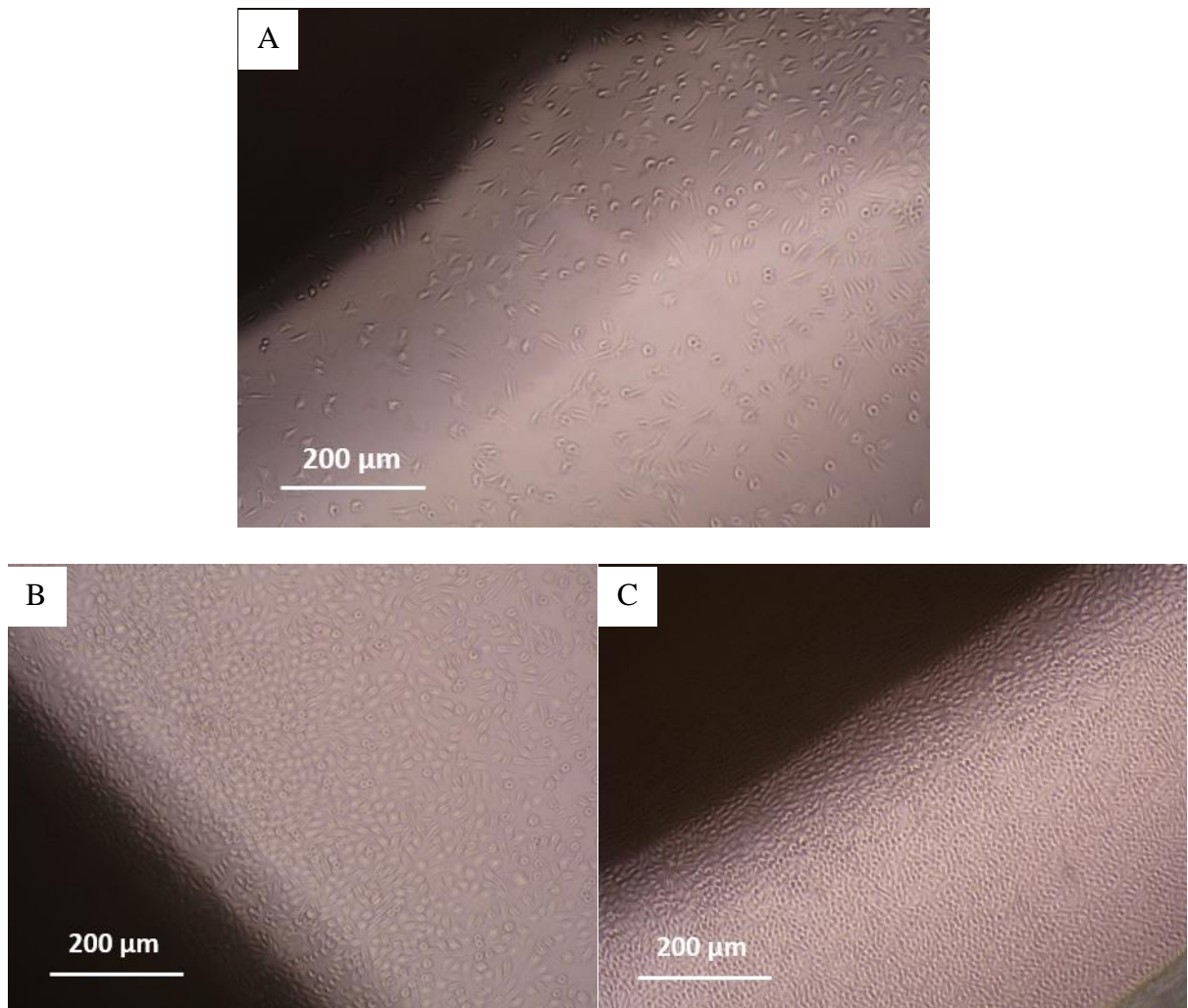


Figure 5-12. Optical monochrome digital micrographs of cells treated with (A) negative sample of PCL, (B) PCL/P₁₁-4 and (C) PCL/P₁₁-8 fibres.

MTT Assay

Figure 5-13 shows the average absorbance obtained from the MTT assay of the cells cultured with the fibrous web samples as well as the blank and positive controls (mean \pm standard error).

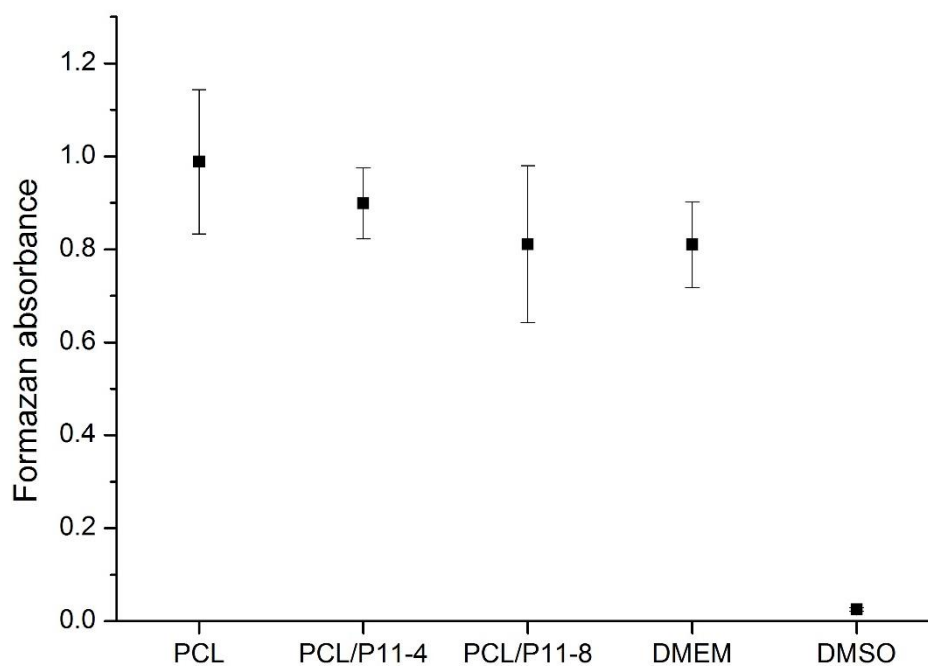


Figure 5-13. Optical density absorption of samples at 570-650 nm correlated to the number of living cells.

The quantitative results from the direct cytotoxicity assay also revealed that the number of living cells in the PCL/P₁₁₋₄ and PCL/P₁₁₋₈ samples were comparable to that of the PCL negative control sample ($p \geq 0.05$) and the DMEM blank control. This is to be expected due to the non-cytotoxic nature of PCL and self-assembled SAPs during the 24 h cell culture incubation. Generally, it was observed that the electrospun webs containing PCL/SAPs fibres were nontoxic to L929 cells, which is consistent with their potential application as tissue scaffolds.

5.3.3 Peptide Release Behaviour of PCL/SAPs Fibres

According to an unpublished *in vivo* study by Burke et al. (53), P₁₁-4 and P₁₁-8 hydrogels injected into full thickness calvarial defects in rabbits have shown to be capable of partially supporting bone repair (53). Although there was evidence of peptide hydrogel release/diffusion within the cavity by day 7, which could have contributed to the defect not being fully repaired, there was evidence of healing from the defect margins with differences in healing patterns according to the type of SAP used. Based on these results, the degradation study in the present work was carried out until day 7 to investigate the stability of SAPs combined with fibres as a function of time.

5.3.3.1 Mass Loss of Electrospun Fibres after Dissolution

Fibres were first weighed in their dry state and after incubation samples were taken out of the solution and were air-dried and weighed out to measure mass loss. Figure 5-14 shows that the mass loss of fibres increased over a period of 7 d. However, the PCL control fibres were not degraded over the same period of time since no mass loss could be observed in the PCL only control fibres regardless of the pH of the solutions. Therefore, the overall mass loss in the PCL/SAPs fibres can be reliably attributed to the release of SAPs from the fibres into solution. Table 5-3 summarises the mass loss (%) of PCL/P₁₁-4 and PCL/P₁₁-8 fibres after degradation at different pH and different time points.

As expected, the highest mass loss in PCL/P₁₁-4 fibres took place after 7 d of incubation at pH 10.5 (up to 9.3%) and for PCL/P₁₁-8, after 7 d of incubation at pH 3.5 (up to 14.5%). Note that these are the pH values at which each of the peptides can be expected to transform from self-assembled β -sheet to isotropic fluid (monomer) (200). Based on Equation 3-1, Equation 3-2 and Table 3-6 in Chapter 3, the initial concentration of peptides prior to degradation in the PCL/P₁₁-4 and PCL/P₁₁-8 fibres (both at peptide concentration of 40 mg mL⁻¹) is 28% and 24% respectively. Therefore, since the maximum mass losses in both PCL/SAPs fibres does not reach

the estimated on-board peptide content after 7 d, it can be posited that some SAPs remains combined with the fibres. Based on this analysis, it is apparent that in the PCL/P₁₁-4 fibres, up to only 33% (9.3% out of 28%) of the on-board SAP was released. For the PCL/P₁₁-8 fibres, up to 60% (14.5% out of 24%) of the available SAP was released over the same seven-day period. These are the maximum mass losses taking place at the least favourable pH for each of the SAPs. At pH 7.5 however, which is the closest pH to biological conditions (pH 7.4), 75% of the P₁₁-4 and 45% of the P₁₁-8 still remained within the electrospun fibres which is a promising result, bearing in mind how much SAPs appears to have been lost when they are presented only in hydrogel form as reported in the work *in-vivo* of Burke et al. (53).

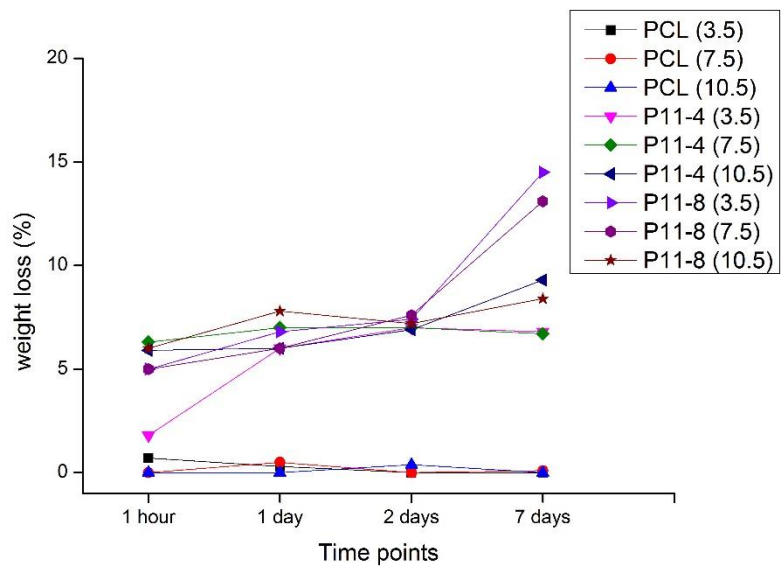


Figure 5-14. Overall percentage (%) of mass loss from electrospun fibres at different pH.

Table 5-3. Overall mass loss (%) of PCL/P₁₁₋₄ and PCL/P₁₁₋₈ fibres after degradation at different pH.

	PCL/P ₁₁₋₄			PCL/P ₁₁₋₈		
	pH 3.5	pH 7.5	pH 10.5	pH 3.5	pH 7.5	pH 10.5
1 h	1.8	6.3	5.9	5.0	5.0	6.0
1 d	6.0	7.0	6.0	6.8	6.0	7.8
2 d	7.0	7.0	6.9	7.4	7.6	7.2
7 d	6.8	6.7	9.3	14.5	13.1	8.4

To ensure that any residual peptide was washed off after taking the samples out of the solution, samples were washed three times in a fresh solution with the same pH. However, by weighing out the air-dried samples after this three step washing process, it was found that there were no marked changes in the mass loss percentages of the fibre webs.

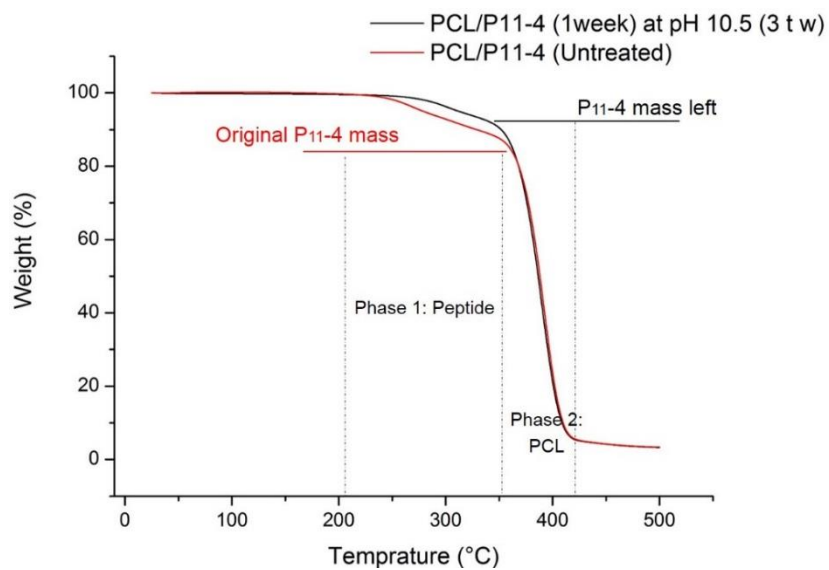
Mass Loss Analysis of PCL/SAPs Fibres by TGA

The overall mass loss related to the PCL or SAP content in each sample was analysed via TGA as well. Measurements were made on the PCL/P₁₁₋₄ fibres after 7 d of incubation at pH 10.5 after three washes and on the PCL/P₁₁₋₈ fibres after 7 d of incubation at pH 3.5 after three washes. Figure 5-15 shows the TGA results of PCL/SAPs fibres at their maximum mass loss condition versus the TGA of the untreated PCL/SAPs fibres before incubation. Two major mass loss phases were observed. The first, between 200-350 °C corresponds to the peptide component and the second, between 350-420 °C corresponds to the PCL component (M_w = 80,000) (217, 218). Note that the only difference between the untreated and dissolved samples in both the PCL/SAP fibres is in the temperature range of the peptide component and there is no mass decrease in the PCL phase after incubation. This confirms that the overall mass loss reported in Section 5.3.3.1, is solely related to the peptide component. Secondly, it is clear that even after incubation, in both samples there are two mass loss phases, which confirms that even after 7 d

peptide is still left in fibres. Moreover, from the TGA results, it is apparent that the peptide component mass loss was between 40-60% of the original peptide mass, and this is in agreement with the mass loss percentages reported at the beginning of Section 5.3.3.1. This further confirms the stability afforded by combining the peptide with the PCL polymer in fibres, wherein nearly 40% of the SAPs within the electrospun fibres remains after 7 d of degradation, despite the unfavourable pH and aqueous solution.

The practical and clinical significance of this is that it could provide a means of retaining peptide within the site of a tissue defect for longer than it can currently be achieved when the peptide is applied in the form of a hydrogel.

A



B

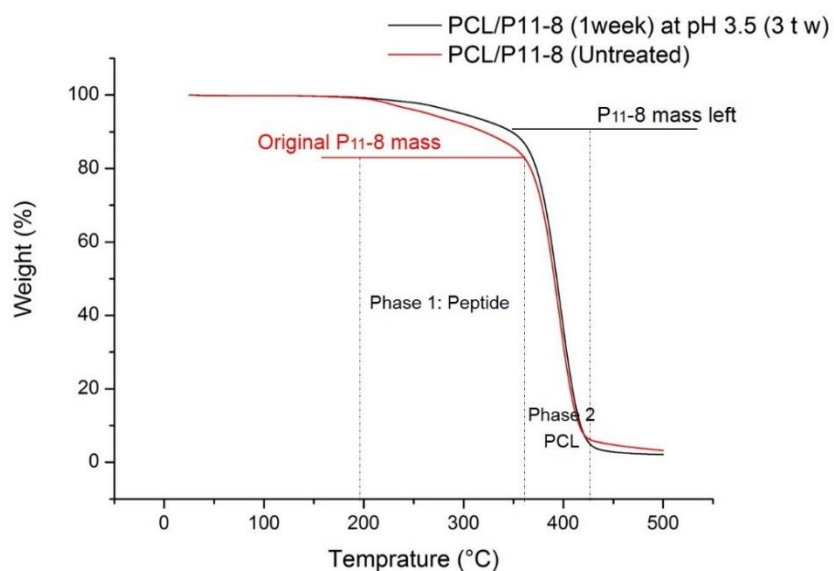


Figure 5-15. Mass loss analysis by TGA of (A) PCL/P₁₁₋₄ fibres after 7 d incubation and 3-times wash in pH 10.5 and (B) PCL/P₁₁₋₈ fibres after 7 d incubation and 3-times wash in pH 3.5.

5.3.3.2 Effect of Peptide Release on the Morphology of PCL/SAPs Fibres

To detect any changes in the morphology of the electrospun fibre web, SEM micrographs of PCL, PCL/P₁₁₋₄ and PCL/P₁₁₋₈ fibres before and after incubation in water at different pH were studied. Figure 5-16 shows SEM micrographs of the untreated PCL control sample before and after 24 h and 7 d of incubation at the lowest pH (3.5) and highest pH (10.5). No major change in the PCL fibre morphology was observed after incubation apart from minor swelling. The mean fibre diameter of 100% PCL fibres after 7 d increased from 390 nm to 490 nm, which may be attributed to a small degree of water absorption.

As-spun PCL/P₁₁₋₈ electrospun fibres with their distinctive two-phase nanofibre network were incubated at pH 3.5, 7.5 and 10.5 for 1 h and 24 h and then studied to detect any morphological changes. It was hypothesised that if the very small nanofibrous phase mainly contained peptide, this would not be visible after incubation. Figure 5-17 shows the SEM micrographs of the PCL/P₁₁₋₈ electrospun fibres before and after incubation at pH 3.5, 7.5 and 10.5. It can be observed that fibres started to swell in water regardless of the pH and some fissures and holes can be detected especially in the surface of the larger submicron fibres in the network. This may be explained by the possible release of peptides incorporated within the surface of the submicron fibres. What is also apparent is that the second nanofibrous phase remains intact after incubation suggesting that these fibres are not entirely formed from peptides. It is possible that peptide is also released from these nanofibres, which are known to contain peptide (see Section 4.3.4.2).

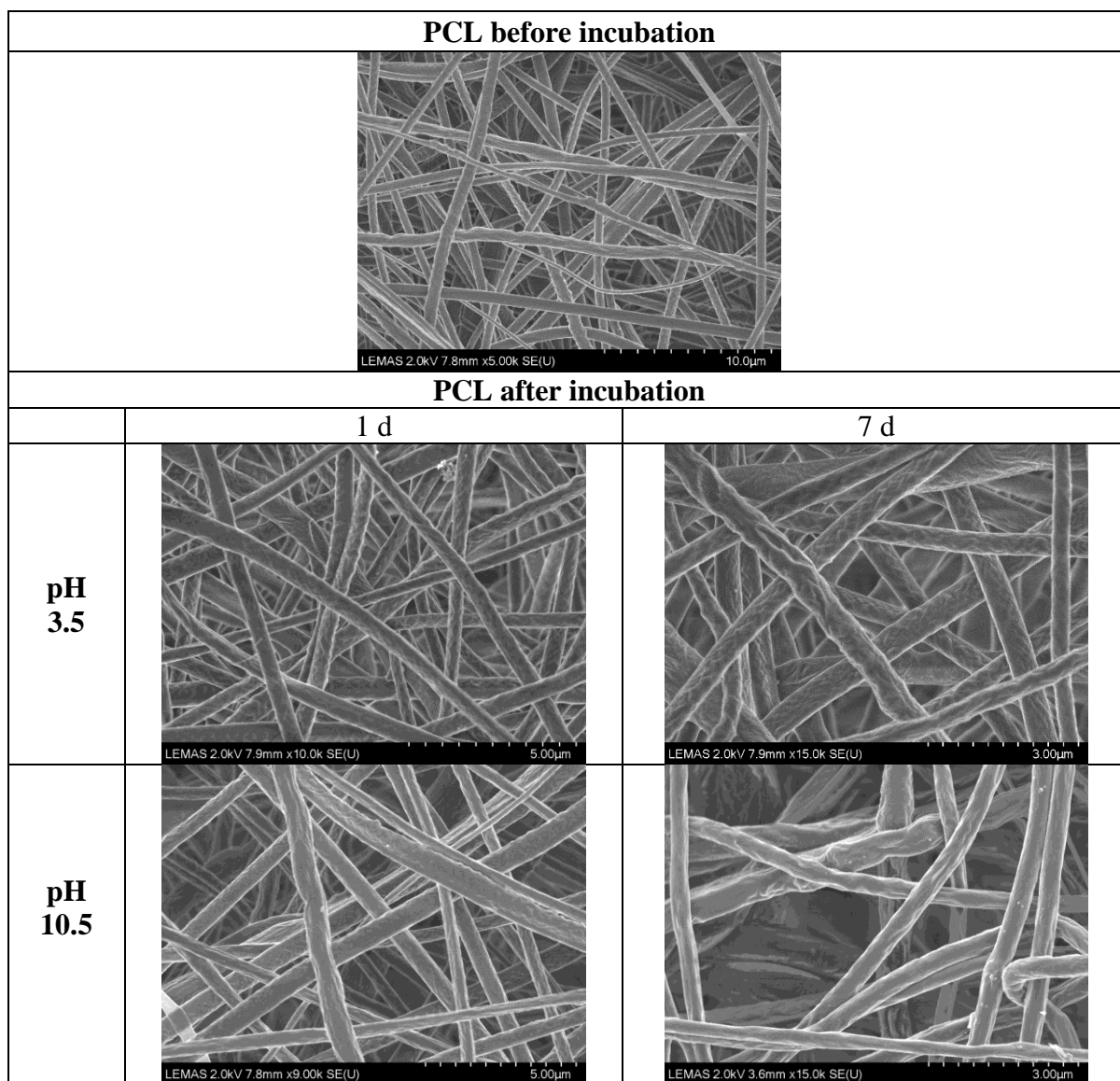


Figure 5-16 SEM micrographs of 100% PCL fibre webs before and after incubation at pH 3.5 and 10.5 for 1 d and 7 d.

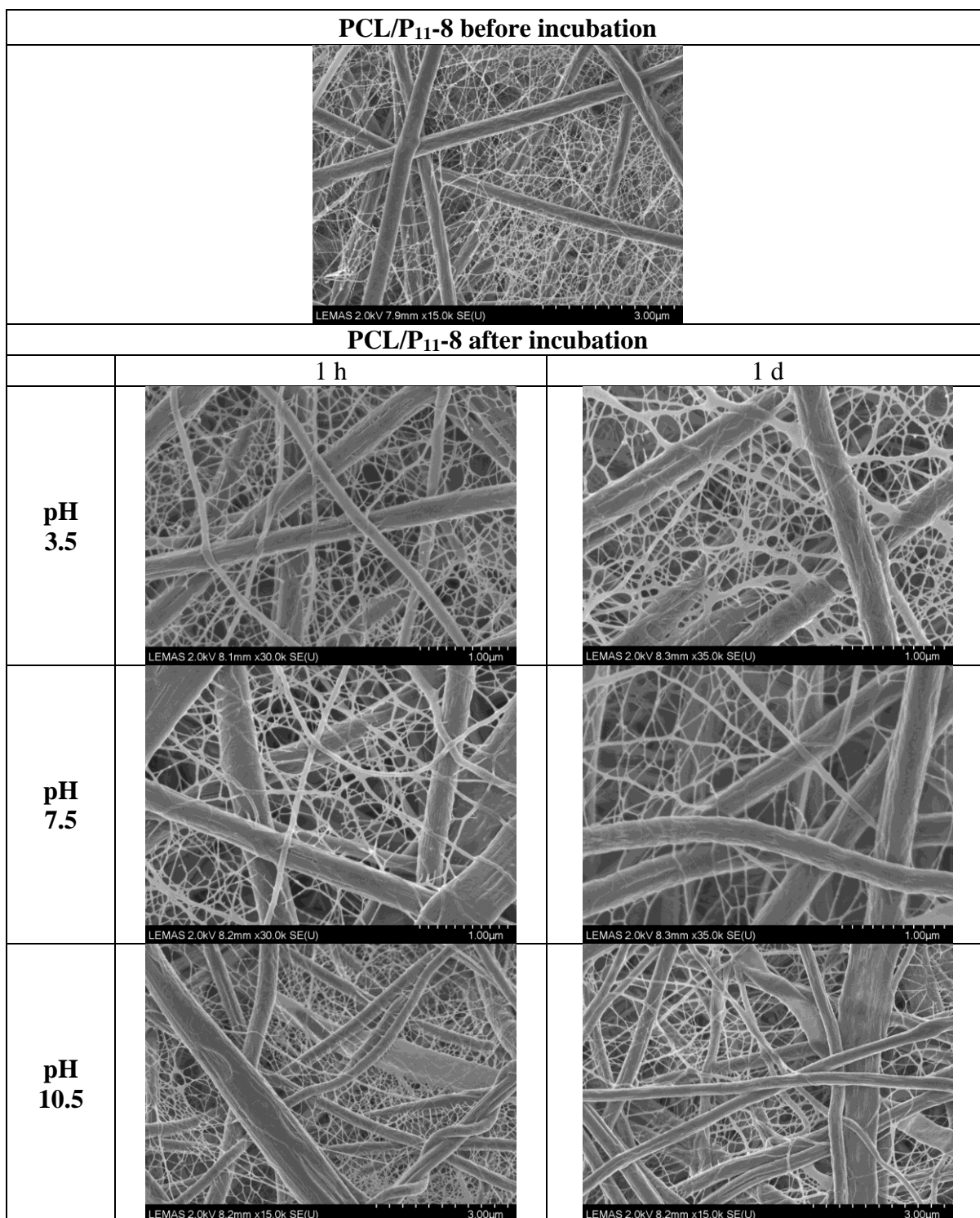


Figure 5-17. SEM micrographs of PCL/P₁₁-8 fibre webs before and after incubation at pH 3.5, 7.5 and 10.5 for 1 h and 1 d.

Subsequently, both PCL/P₁₁₋₄ and PCL/P₁₁₋₈ samples incubated for up to 2 d and 7 d were studied by SEM. Figure 5-18 and Figure 5-19 show SEM micrographs of incubated PCL/P₁₁₋₄ and PCL/P₁₁₋₈ fibres respectively incubated in the lowest and highest pH conditions (pH 3.5 and pH 10.5 respectively). In all the SEM micrographs shown, fibres were washed three times using solutions of the same pH. It is evident in Figure 5-18 and Figure 5-19 that there is no major morphological change or fibre degradation in either PCL/P₁₁₋₄ or PCL/P₁₁₋₈ fibres even after 7 d of incubation apart from fibres becoming flattened and swollen. The mean fibre diameter after 7 d in the PCL/P₁₁₋₄ sample increased from 420 nm to 800 nm and in the PCL/P₁₁₋₈ sample, from 330 nm to 710 nm, most probably due to water uptake in the hydrolytic conditions. Specifically in these incubated samples, the nanofibrous network is still present, with an apparent fusing together of fibres at their intersections. Nanofibres can be observed locally in the PCL/P₁₁₋₄ webs and all around the fibrous network in the PCL/P₁₁₋₈ web, which is similar to the findings reported in Section 4.3.3, where the nanofibres in PCL/P₁₁₋₄ (unlike PCL/P₁₁₋₈) webs were distributed locally and not across the entire fibrous web. In the samples washed three times, the appearance of merged fibre intersections may be related to peptide residues on the surface of the fibres being washed out by the washing process resulting in morphological changes.

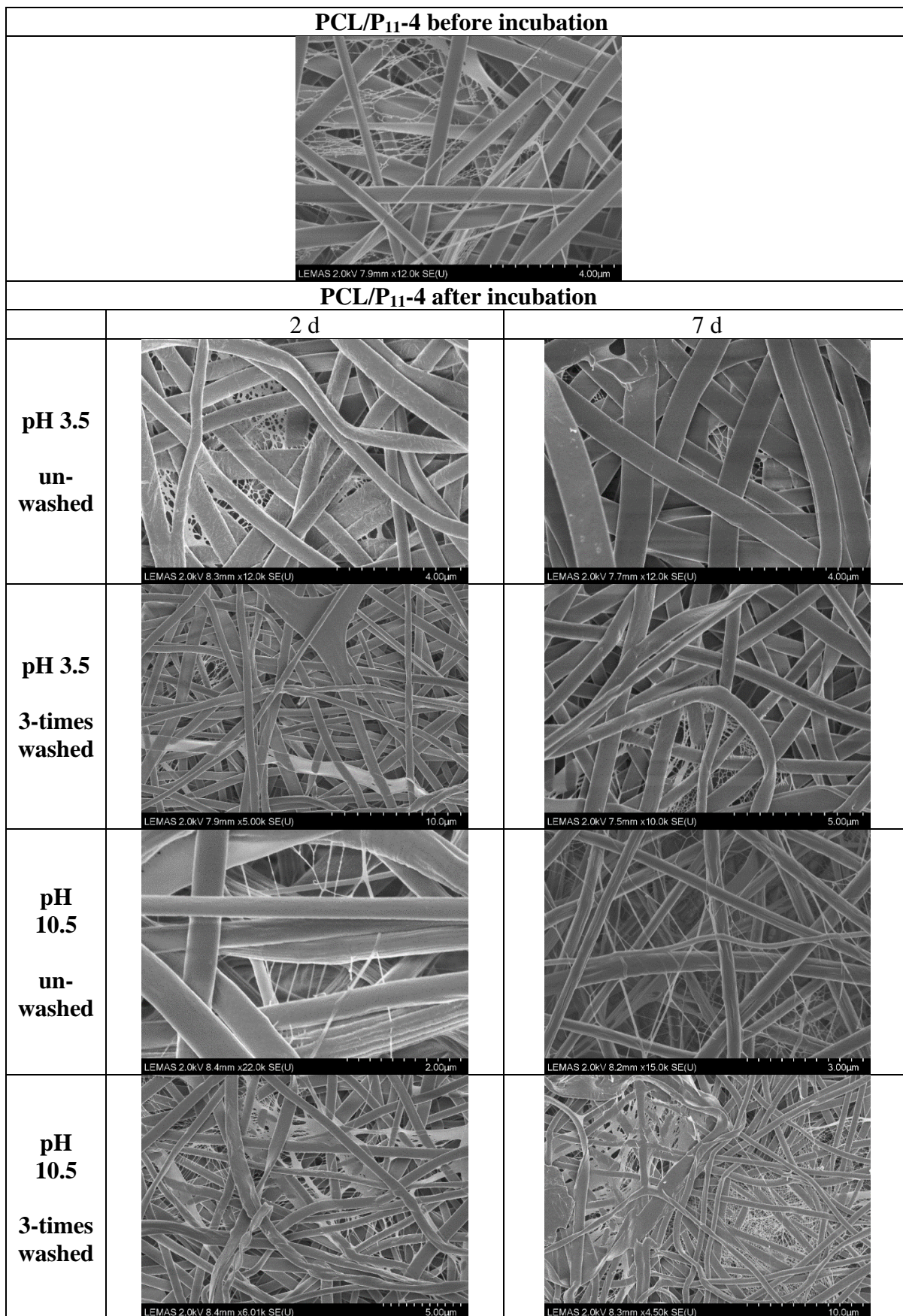


Figure 5-18. SEM micrographs of PCL/P₁₁-4 fibre webs after incubation at pH 3.5 and 10.5 for 2 and 7 d.

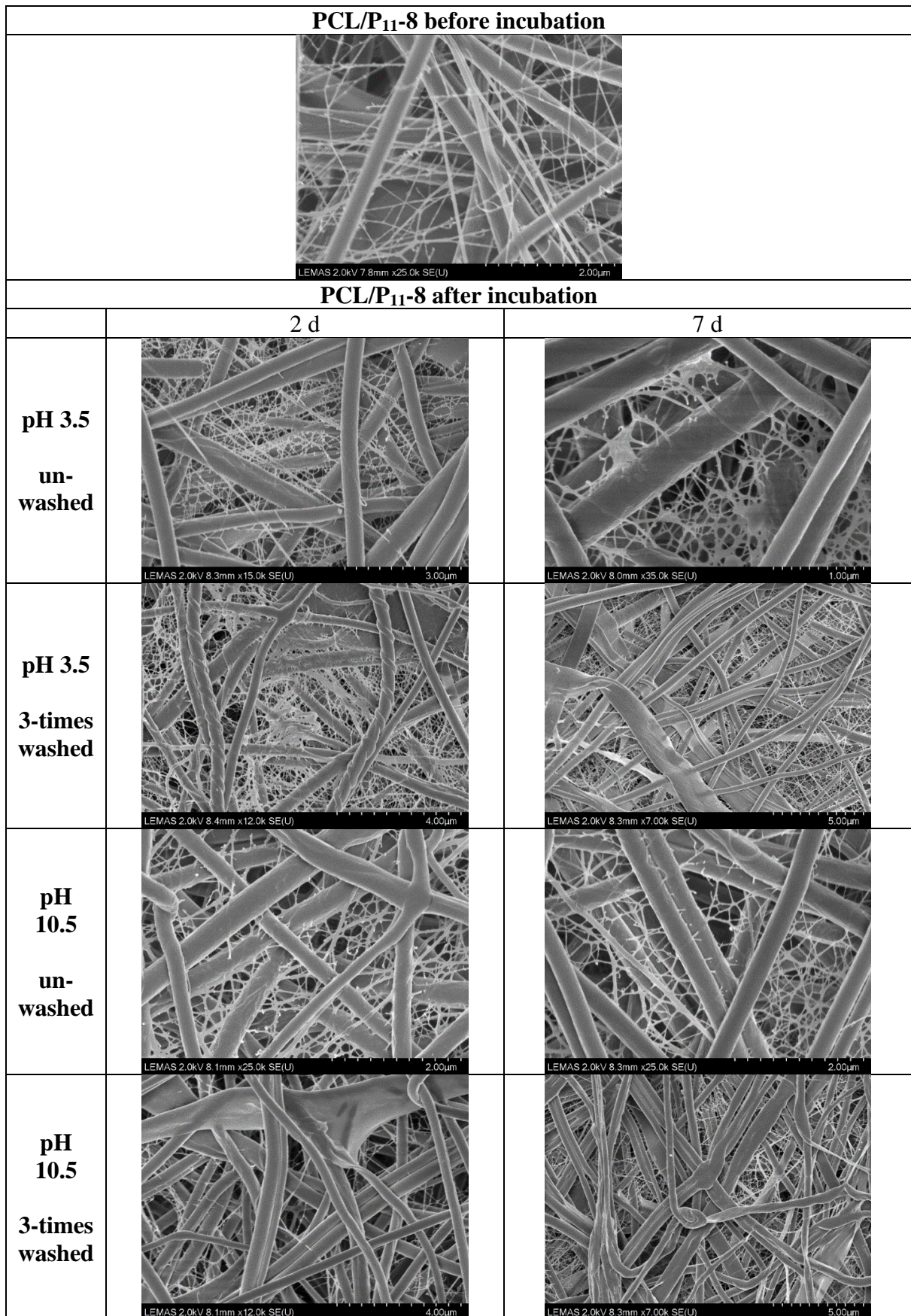


Figure 5-19. SEM micrographs of PCL/P₁₁₋₈ fibre webs after incubation at pH 3.5 and 10.5 for 2 and 7 d.

5.3.3.3 Peptide Release into Solution by CD analysis

To confirm release of peptides into the solution, the supernatant fluid was subject to CD analysis according to the method described in Section 3.2.11. The supernatant of PCL, PCL/P₁₁₋₄ and PCL/P₁₁₋₈ webs incubated at the lowest (pH 3.5) and highest (pH 10.5) pH for 1 d and 7 d periods of time, were analysed via CD and the results are shown in Figure 5-20. The spectra of each relevant blank solution, which is water at the pH 3.5 or 10.5, has been subtracted from these spectra.

As is evident from Figure 5-20, all the CD spectra for the PCL/P₁₁₋₄ and PCL/P₁₁₋₈ supernatants exhibit a negative minimum centred at 195-200 nm and a slightly positive band at around 220 nm, which is consistent with the random coil peptide conformation in the solution (46, 211). This explanation is supported by the lack of a negative band at 218 nm and a strong positive maximum at lower wavelengths (198 nm), which would be characteristic of a β -sheet conformation (43, 46). By comparing these results with the results of the PCL fibre supernatant, which exhibits no peaks in the far-UV spectral region (190-250 nm), it can be confirmed that peptides have been disassembled into solution over time.

Moreover, by observing peak intensities in the CD spectra, the results of the mass loss experiments (Section 5.3.3.1) can be verified, in which the highest mass losses obtained for the PCL/P₁₁₋₄ and PCL/P₁₁₋₈ webs after 7 d of degradation were at pH 10.5 and pH 3.5 respectively.

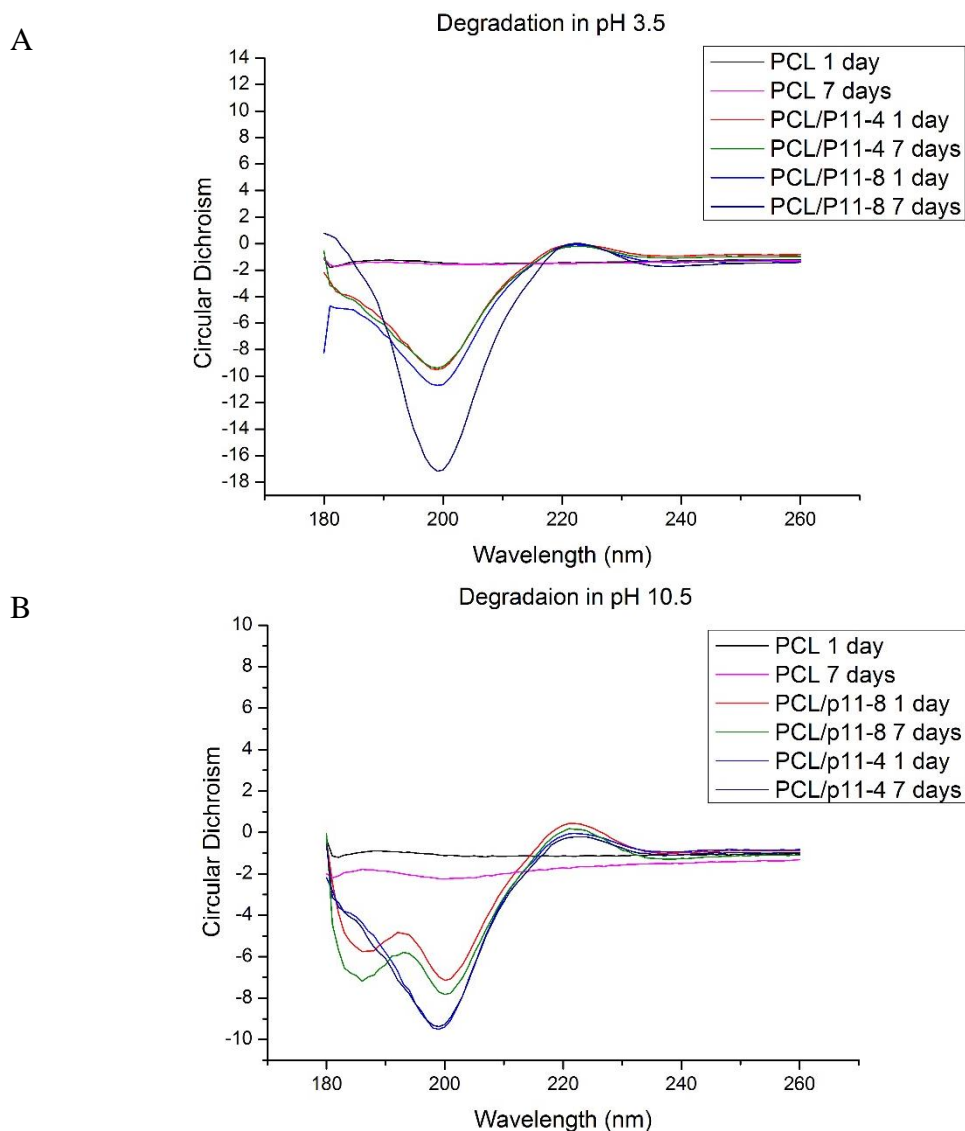


Figure 5-20. CD spectra of supernatant of fibrous samples dissolved in water for 1d and 7 d at (A) pH 3.5 and (B) pH 10.5.

Even though it has been shown that a three-step washing procedure did not have a major effect on the mass loss of peptide, and had only a slight effect on fibre morphology, the supernatants from the washing process were also analysed via CD.

The CD spectra of the original supernatants and the three-step washing procedure supernatants obtained for the PCL/P₁₁-4 and PCL/P₁₁-8 fibres dissolved for 7 d at pH 10.5 and pH 3.5 respectively, are shown in Figure 5-21. Note that only in the original supernatant did peptide

release occur, and after each of the three step washes, no marked peptide release could be observed.

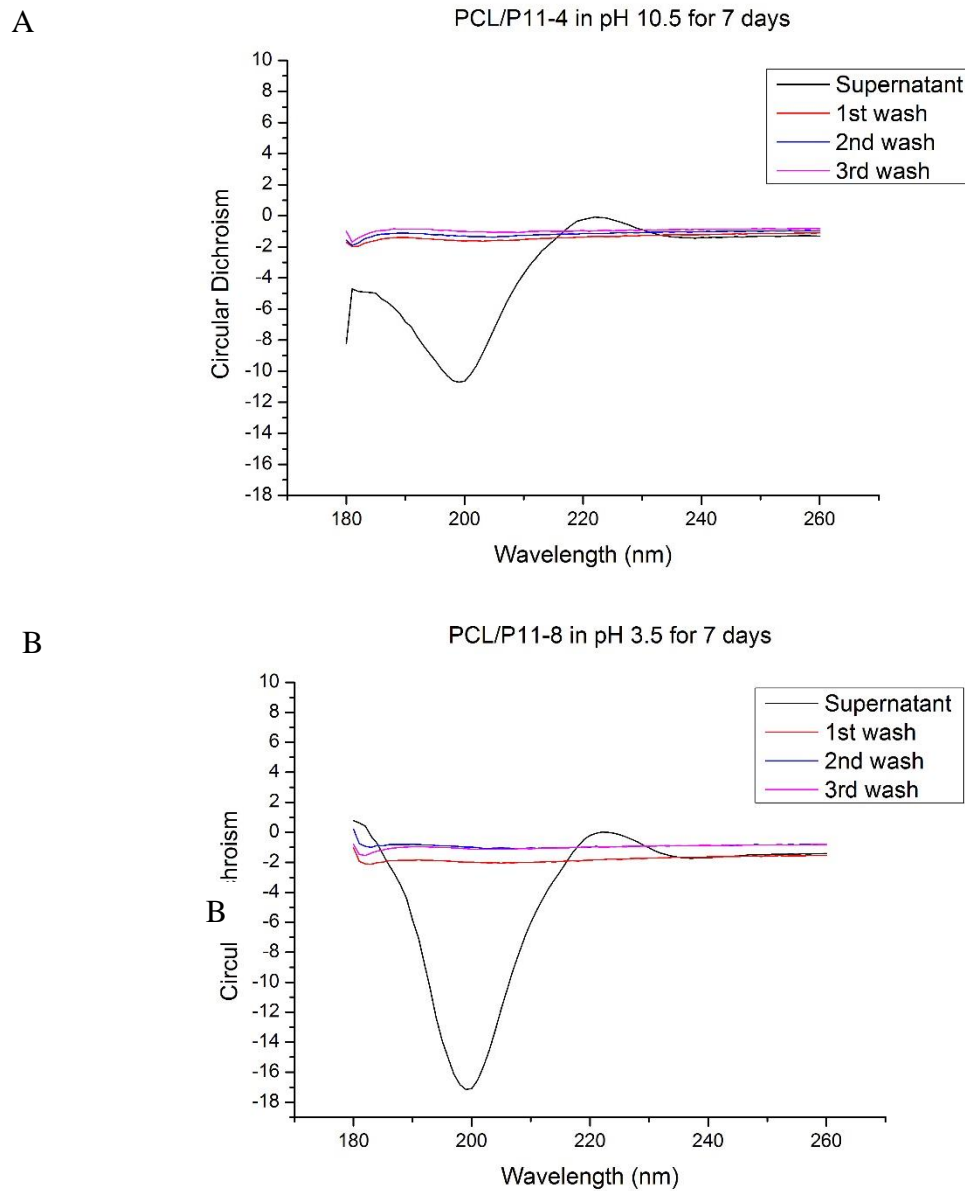


Figure 5-21. CD spectra of the original supernatant and the three step washing process supernatants of electrospun web samples dissolved for 7 d of (A) PCL/P₁₁-4 fibres in pH 10.5 and (B) PCL/P₁₁-8 fibres in pH 3.5.

5.4 Summary

The contact angle studies of deionised water and DMEM on electrospun webs have shown that the hydrophilicity and wetting characteristics of PCL electrospun fibre webs are considerably improved by incorporation of peptides in the fibres. This was evidenced by a decrease in the contact angle from above 90° (hydrophobic) to 0° when the peptide concentration in the electrospinning solution was increased from 0 to 40 mg mL⁻¹. The importance of the peptide content on wetting was confirmed by studying contact angles on continuous cast films made of exactly the same material compositions.

Extract cytotoxicity assays were used to assess the cytocompatibility of PCL/P₁₁₋₄ and PCL/P₁₁₋₈ fibres with L929 mouse fibroblasts. This preliminary experiment showed no toxic response in cells cultured with PCL/SAP sample extracts, although the cell viability in PCL/SAP extract was slightly reduced, compared with the PCL control sample. This could be due to peptide disassembly in the aqueous solution during extraction, which could affect the metabolic activity of L929 mouse fibroblasts. Therefore, a direct cytotoxicity assay was conducted in which L929 mouse fibroblasts were cultured in contact with electrospun peptide loaded samples. The PCL/SAPs fibres proved to be well tolerated by mouse fibroblast cells and nearly no cytotoxic response (<90% cell viability) was observed, providing additional confirmation that the PCL/SAPs fibres are good candidates to be used as tissue scaffolds.

Furthermore, a 7-day mass loss degradation study in aqueous medium demonstrated that at least 40% of SAPs in the PCL fibres is still available even in conditions of unfavourable pH where their transformation to monomers can be expected to take place. The peptide release into the solution was further confirmed via CD analysis. At pH 7.5, which is close to biological pH, at least 75% of the P₁₁₋₄ and 45 % of the P₁₁₋₈ were found still to be present within the fibres. The

considerably greater release of P₁₁₋₈ compared to P₁₁₋₄ can be explained by the morphological characteristics of the PCL/P₁₁₋₄ and PCL/P₁₁₋₈ electrospun fibres.

The PCL/P₁₁₋₈ fibres form a biphasic web structure in which fibre diameters are distributed widely, with some below 100 nm and others above 100 nm. The nanofibrous network (<100 nm) was confirmed to contain P₁₁₋₈, and by having smaller diameters and therefore higher surface areas can contribute to faster release of peptide in solution. By comparison, in the PCL/P₁₁₋₄ fibres, where the fibres were mostly of submicron scale, with fewer in the nanofibre scale range, P₁₁₋₄ peptide incorporated into the fibres will be less freely available for diffusion in to solution because of the larger diffusion boundary. In terms of fibre morphological changes during degradation, it was found that regardless of the pH of the solution, the PCL/SAPs fibres do not change markedly apart from small regions in which fibres appear to become slightly flattened giving the appearance of being fused at their intersections. The morphological stability of fibres was maintained even after 7 d of degradation, and it was shown that the nanofibrous network is also stable.

The conclusions in Section 4.3.4.2, were that both the nanofibre and submicron fibre phases in the web contained peptides, however it could not be concluded that the nanofibre phase also contained PCL. However, the results in the present chapter clearly suggest that the nanofibre phase in both the PCL/P₁₁₋₄ and PCL/P₁₁₋₈ electrospun webs contain both PCL and peptide components, as during 7 d of hydrolytic incubation the nanofibers were still stable. Furthermore, combining peptide with PCL appears to improve its stability in terms of the rate at which it is solubilised and removed from the simulated biological environment. When combined with fibres, a large proportion of the original peptide loading is still present even after 7 d incubation in conditions that are unfavourable to peptide stability (aqueous medium and wide variations in pH).

CHAPTER 6

***In Vitro* Evaluations for Apatite Forming Ability of PCL/SAPs Fibre Webs**

6.1 Introduction

In Chapter 5, it was shown that electrospun PCL/SAPs fibres were non-cytotoxic when cultured with L929 cells and therefore biocompatible to be used as hard tissue regeneration scaffolds. Moreover, it was shown that at least 40% of the SAPs content is still present within fibres webs even in the most unfavourable aqueous conditions for at least seven days. As reported previously in Section 2.4.5, P₁₁₋₄ and P₁₁₋₈ SAPs have demonstrated their ability to nucleate hydroxyapatite *de novo* (50) and they have shown to be able to repair early enamel caries (“decay”) lesions by restoring mineral in clinical trials (55). Accordingly, the purpose of this chapter is to evaluate the apatite-formation ability of electrospun fibres enriched with SAPs. To the author’s knowledge, no such study has ever previously been performed. The fibres were assessed for their capacity to promote mineral crystal nucleation and to support their subsequent growth. In this study, two methods were employed based on the BS ISO 23317:2014 standard method and the IVN tank method, details of which were outlined in Sections 3.2.14 and 3.2.16 respectively.

6.2 Experimental Details

6.2.1 Nucleation of Apatite in Simulated Body Fluid (SBF)

The ability of fibres to nucleate apatite was firstly evaluated using the BS ISO 23317:2014 standard method, which was extensively explained in Section 3.2.14. The electrospun fibre webs were exposed to simulated body fluid (SBF) solution to determine their ability to nucleate Ca-P crystallisation using a method previously used to evaluate textile materials (199, 219-221). In summary, electrospun samples of PCL, PCL/P₁₁-4 and PCL/P₁₁-8 (both at a medium concentration of peptide, 20 mg mL⁻¹) were prepared and cut into 10±2 × 10±2 mm (first run) or 70±10 × 70±10 mm (second run) squares. The SBF was prepared according to the standard method (Section 3.2.14.2) and the samples were immersed in SBF for different lengths of time (3 d, 7 d and 14 d) in the first experiment. Then, the fibres were dried in a desiccator and examined under SEM and EDX spectroscopy for the purpose of detecting the formation of any apatite crystals on the fibres, and to determine the Ca:P ratio of the crystals based on the EDX method.

Following the initial evaluation, in the second experiment samples were prepared according to the mass and content of peptide within them, and then incubated in SBF for an extended period, up to four weeks. Thus, electrospinning solutions for PCL/SAP (at peptide concentration of 20 mg mL⁻¹), were electrospun and the fibrous webs (size ~ 150 mm × 150 mm) were folded twice to make them thicker and to increase the effective concentration of peptide per unit area. Then, based on Equation 3-1 and Table 3-6, 240 mg fibres of PCL/P₁₁-4 and 285 mg fibres of PCL/P₁₁-8 were cut and weighed out. The samples were prepared as rectangles (70±10 mm × 70±10 mm) containing 40 mg peptide. A control sample of 100% PCL with a weight of 250 mg and size of 70±10 mm × 70±10 mm was also prepared. The specimen to SBF weight to volume ratio was 0.5 mg mL⁻¹. Incubation was carried out at 37 °C for up to 4 weeks. Moreover, to ensure no

extraneous material was present on the samples following incubation, in the second experiment, half of the samples were washed with deionised water to remove superficial deposition of magnesium, sodium and chlorine ions and then samples were dried in the desiccator.

In addition to SEM/EDX, samples were examined under XRD to identify the configuration of any nucleated crystals, and FTIR was used to determine the degree of SAP dissolution/stability during the assay, as well as the persistency of self-assembled structures within the fibres.

6.2.2 Nucleation of Apatite in the *In Vitro* Nucleation (IVN) Tank

To evaluate the ability of PCL/SAP fibres to nucleate mineralisation and support mineral growth *in vitro*, the IVN tank method, described in Section 3.2.16 was followed as well. In this method electrospun PCL/P₁₁₋₄ and PCL/P₁₁₋₈ fibres were tested against P₁₁₋₄ and P₁₁₋₈ hydrogel samples respectively, with regard to the concentration of peptide in each cell of the sample holder in both fibrous and hydrogel samples. As a positive control specimen, 10 µg mL⁻¹ poly-L-glutamic acid in 1 % agarose hydrogel and as negative control only 1% agarose hydrogel and 100% PCL electrospun fibres were used. As indicated in Section 3.2.16.3, all the fibrous electrospun samples were embedded within two layers of 1 % agarose hydrogel. The fibrous or hydrogel samples prepared for this experiment and the peptide concentration in each of them (for both P₁₁₋₄ and P₁₁₋₈) are shown in Figure 6-1.

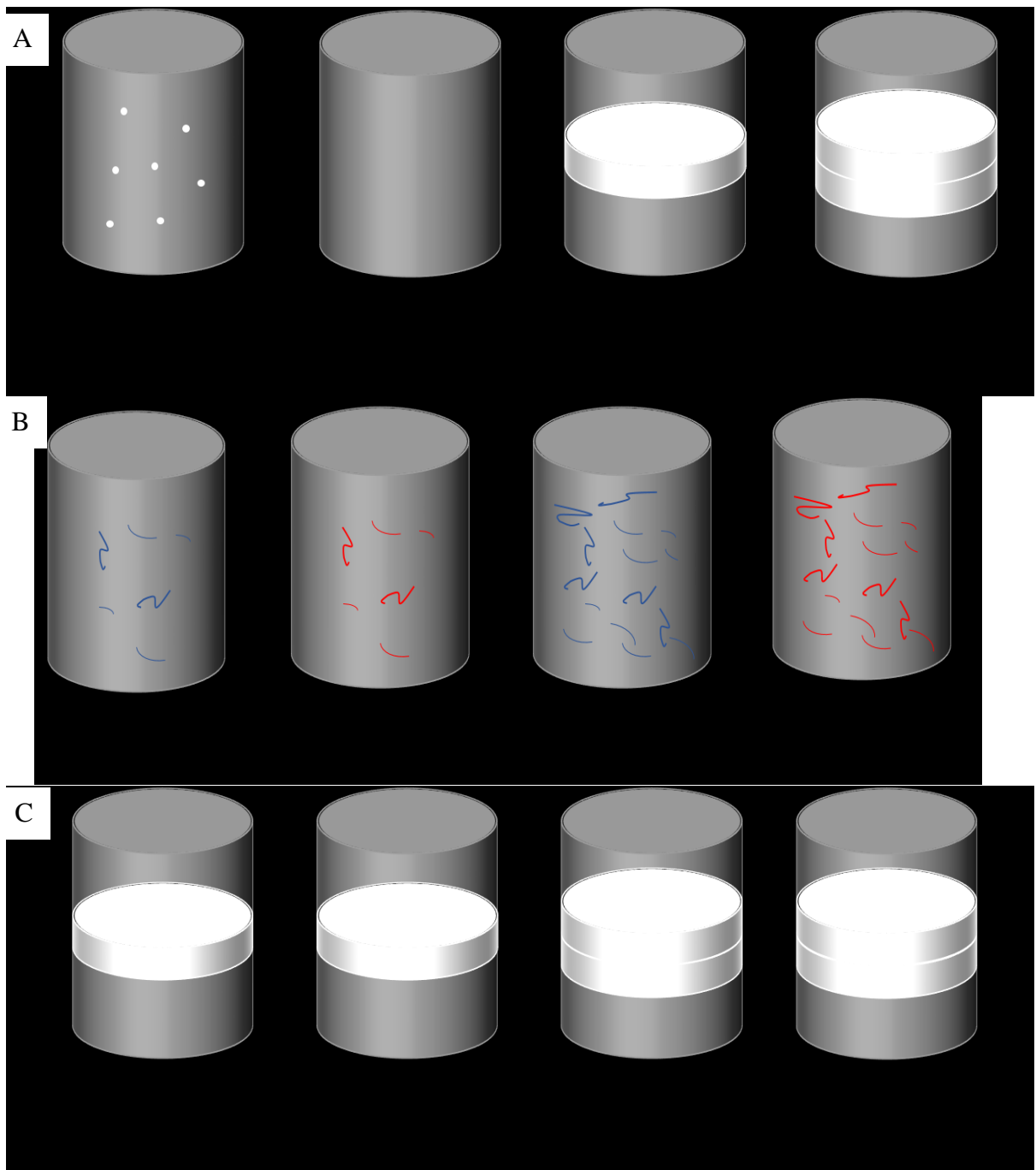


Figure 6-1. Preparation of fibrous electrospun or hydrogel samples for the IVN tank assay (A) positive, negative and PCL fibre control, (B) SAP hydrogel samples and (C) PCL/SAPs fibre samples with their associated SAP concentration.

At the end of each experiment, after five days incubation, samples were analysed using a phosphate assay and the PO_4^{3-} content was determined spectrophotometrically using a standard calibration curve. Figure 6-2 shows the calibration curve obtained by dissolving different concentrations (0-100 μM) of phosphorus standard solution of 1000 ppm (Na_2HPO_4), in deionised water and analysing the absorbance at 820 nm. The calibration curve shows a linear relationship between light absorption at 820 nm and $\mu\text{g mL}^{-1}$ of phosphate (PO_4^{3-}).

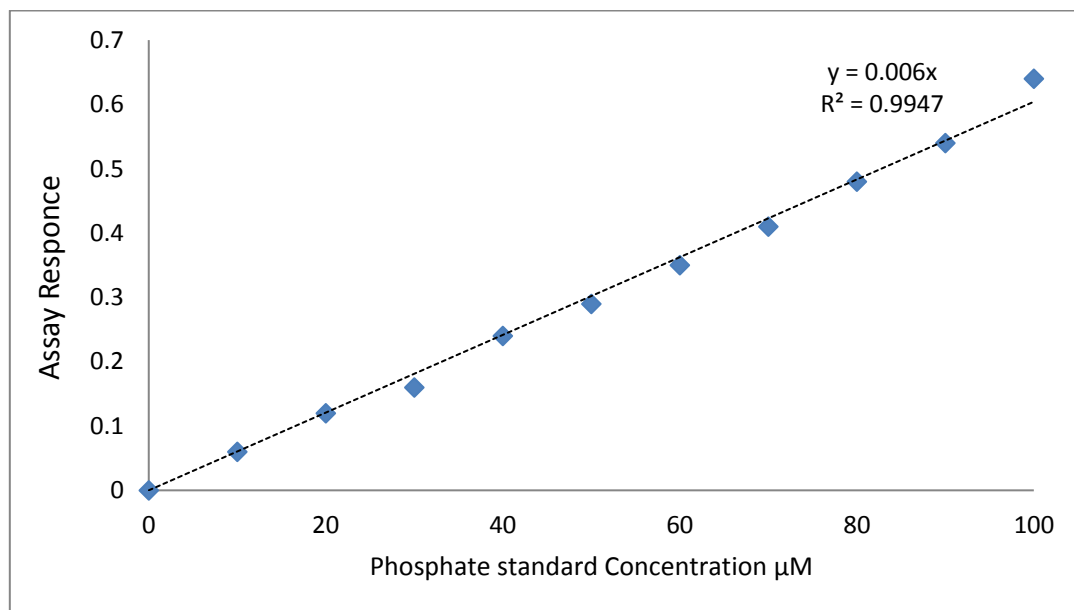


Figure 6-2. Calibration curve of phosphate concentration (μM) using spectrophotometry.

6.3 Results and Discussion

6.3.1 Apatite Forming Ability of PCL/SAPs Fibres in SBF

Results of two SBF studies of PCL/SAPs along with PCL control fibres are presented in this section.

6.3.1.1 SBF Method - First Experiment

Figure 6-3, Figure 6-4 and Figure 6-5 show SEM micrographs of each sample and the associated deposited mineral elements with their atomic percentage for each samples after three days, seven days and fourteen days of incubation respectively. As it can be observed, no Ca-P crystal deposition could be observed on these samples apart from some small particles that can be attributed to the precipitation of salts during incubation in the SBF. In the elemental analysis results, no substantial mineral deposition of calcium or phosphorus was found to be deposited on the fibres and the small amounts of mainly chlorine or sodium can be attributed to the precipitation of these minerals on the samples while in SBF. Among these results PCL sample, as control, and PCL/SAPs samples look similar to each other with no substantial mineral deposition.

The lack of mineral deposition observed in the first experiment can be attributed to the very small amount of SAP present in each of the $10\pm 2 \times 10\pm 2$ mm samples. During the preparation of a 150×150 mm sample in electrospinning, 2.5 mL of electrospinning solution was used with a 20 mg mL^{-1} concentration of peptide in solution. This means that only 50 mg of SAP in total will be distributed throughout a 150×150 mm sample. Therefore, assuming all of the SAPs in the solution are contained within the spun fibres and that there is a uniform distribution, only 0.22 mg of SAP will be present in each square centimetre of fibrous web. This was considered in the design of the second experiment, such that more SAP would be available in the samples.

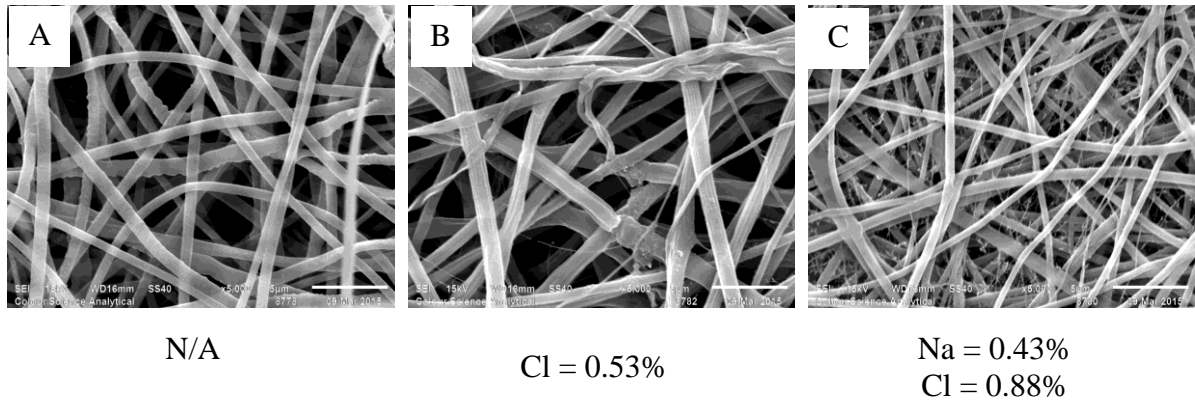


Figure 6-3. SEM micrographs of electrospun fibres after 3 d incubation in SBF along with the atomic percentage of element content as determined from EDX analysis (A) PCL fibres, (B) PCL/P₁₁₋₄ with peptide concentration of 20 mg mL⁻¹ and (C) PCL/P₁₁₋₈ with peptide concentration of 20 mg mL⁻¹.

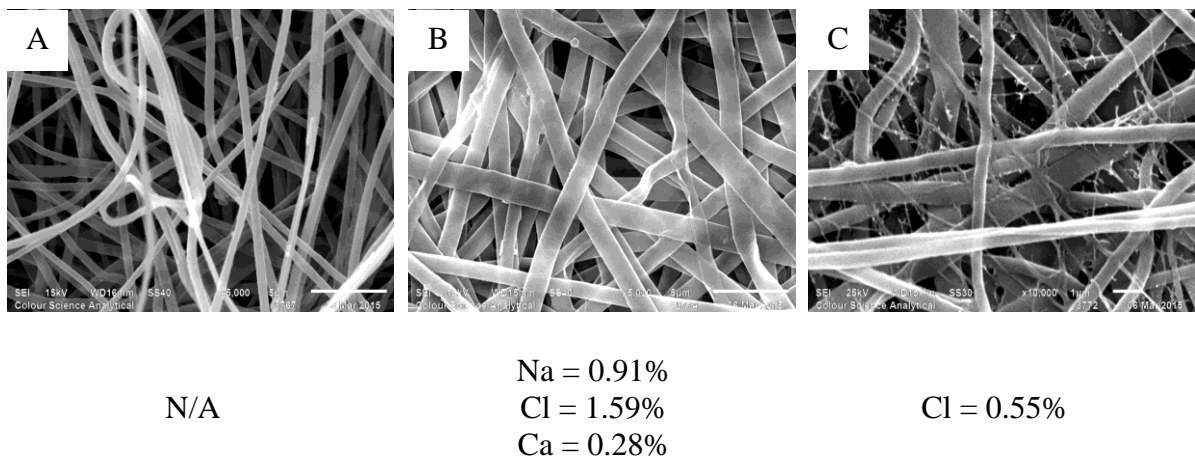
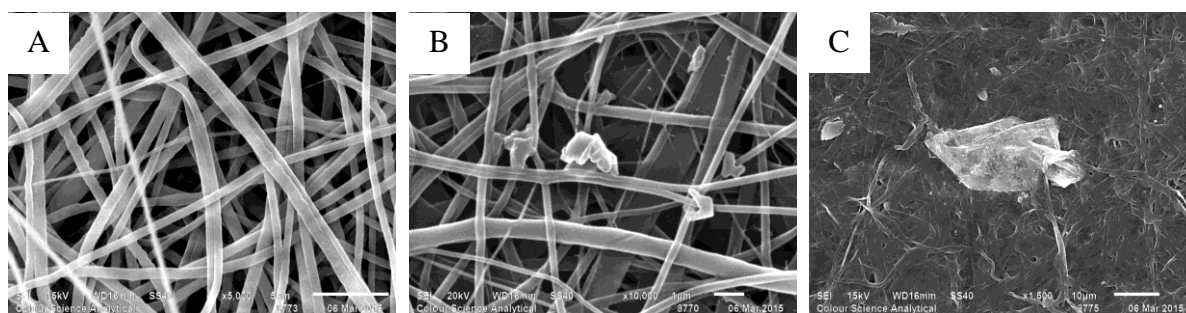


Figure 6-4. SEM micrographs of electrospun fibres after 7 d incubation in SBF along with the atomic percentage of element content as determined from EDX analysis (A) PCL fibres, (B) PCL/P₁₁₋₄ with peptide concentration of 20 mg mL⁻¹ and (C) PCL/P₁₁₋₈ with peptide concentration of 20 mg mL⁻¹.



Cl = 0.35%

Na = 1.22%

Cl = 2.08%

Ca = 0.18%

K = 0.10%

Na = 1.51%

Cl = 3.27%

Figure 6-5. SEM micrographs of electrospun fibres after two weeks incubation in SBF along with the atomic percentage of element content as determined from EDX analysis (A) PCL fibres, (B) PCL/P₁₁₋₄ with peptide concentration of 20 mg mL⁻¹ and (C) PCL/P₁₁₋₈ with peptide concentration of 20 mg mL⁻¹.

6.3.1.2 SBF method - Second Experiment

Based on the results obtained from the first study, further experiments were carried out with the intention of providing more peptides in each sample, and by increasing the incubation time in SBF. SEM micrographs of electrospun fibres incubated in SBF for one, two and four weeks are shown in Figure 6-6 and Figure 6-7 and Figure 6-8 respectively. In this experiment, half of the samples were washed with deionised water after incubation to remove superficial precipitations, and SEM micrographs of washed fibres were obtained as well. It was reasoned that nucleation of apatite was more likely to occur after incubation times beyond one week, so washing was performed after two and four weeks to determine residual apatite content.

As expected, in Figure 6-6, after one week incubation in SBF, the control PCL and PCL/P₁₁₋₈ samples showed no mineral crystals and only in the PCL/P₁₁₋₄ fibres was a small amount of mineral crystallisation observed. However, after longer incubation times in SBF, as shown in Figure 6-7 (2 weeks) and Figure 6-8 (4 weeks), crystal growth on the surface and in between electrospun fibres was clearly observed. It was established from all the SEM evidence, that PCL control fibres containing no SAP, even after 4 weeks are not capable of supporting crystal

formation. This is to be expected, given that no SAP was present. Moreover it can be observed in Figure 6-7 and Figure 6-8 that the washing process does affect the morphology of the fibres at the surface and therefore it is possible that some of the crystals may be removed during the process if present in the exterior surface. However, crystals were still visible in between the fibres after washing. The higher magnification images, Figure 6-7 (unwashed PCL/P₁₁-4 and PCL/P₁₁-8), revealed that deposited minerals formed on the surface and in between the fibres and their structures appear as a globular cauliflower shape, resembling the crystal morphology of hydroxyapatite (199). Moreover, from the SEMs of unwashed PCL/SAPs fibres in Figure 6-7 and Figure 6-8, it can be observed that a primary layer of calcium phosphate at the surface of the fibres is formed over which further growth of spheroidal clusters proceeds.

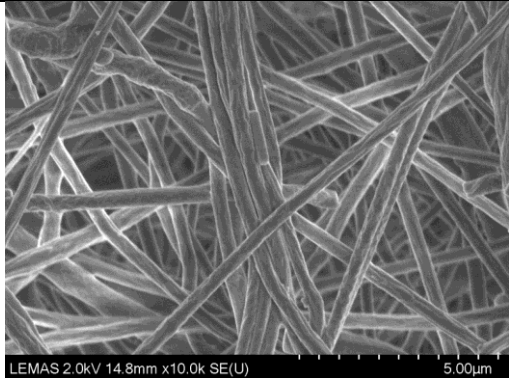
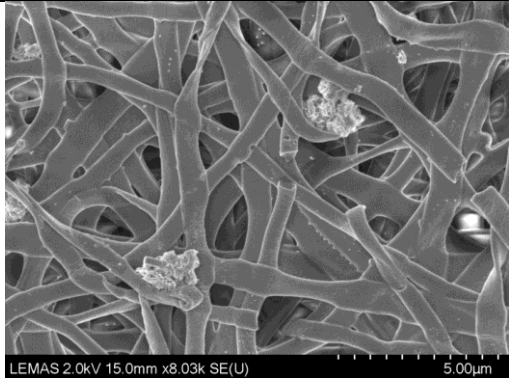

Sample	Incubation time	
	1 week	
	washed	unwashed
PCL	N/A	
PCL/P ₁₁ -4	N/A	
PCL/P ₁₁ -8	N/A	

Figure 6-6. SEM micrographs of electrospun fibres after one week incubation in SBF.

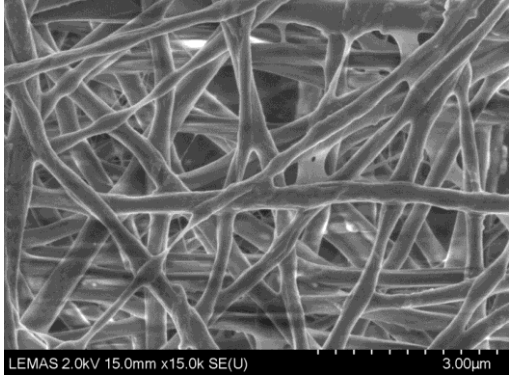
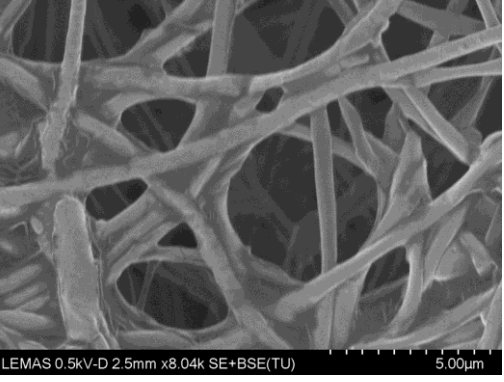
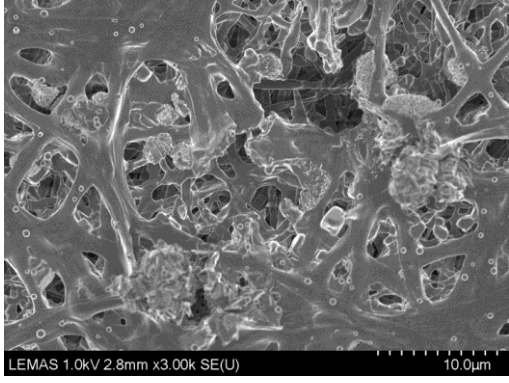
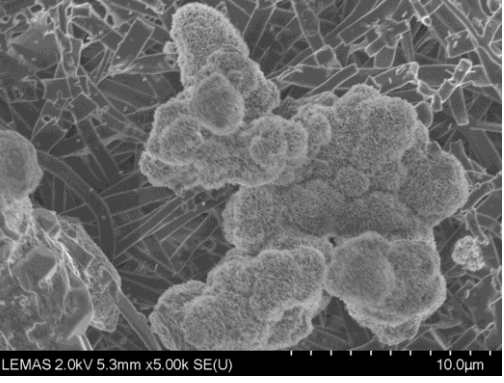
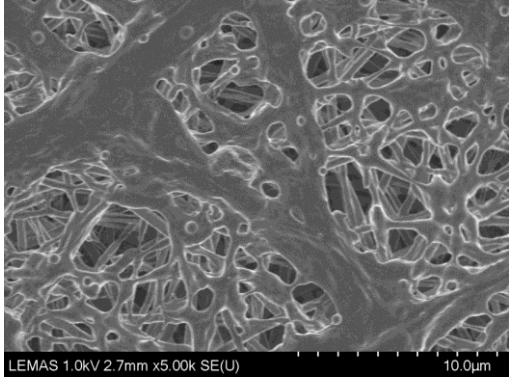
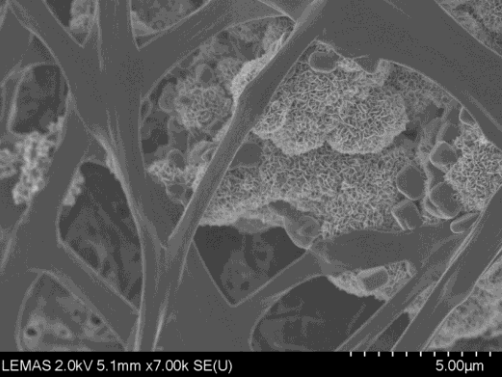
Sample	Incubation time	
	2 weeks	
	washed	unwashed
PCL		
PCL/P ₁₁ -4		
PCL/P ₁₁ -8		

Figure 6-7. SEM micrographs of electrospun fibres after two weeks incubation in SBF.

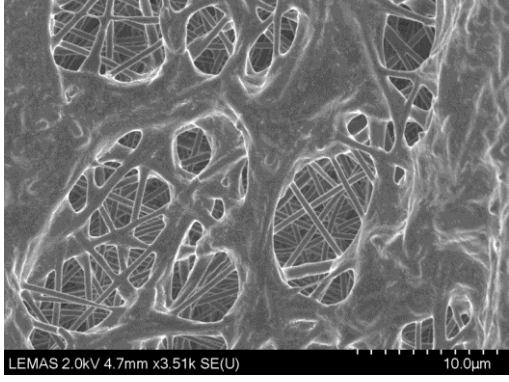
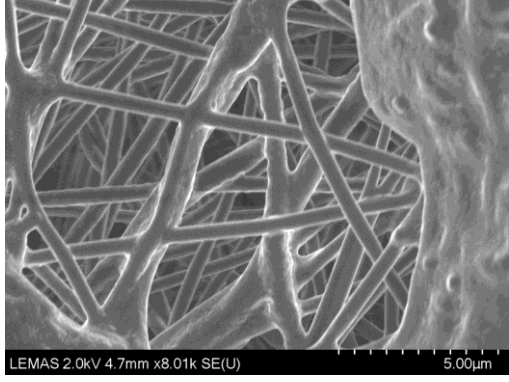
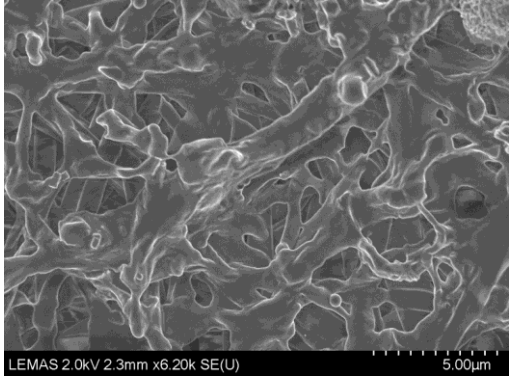
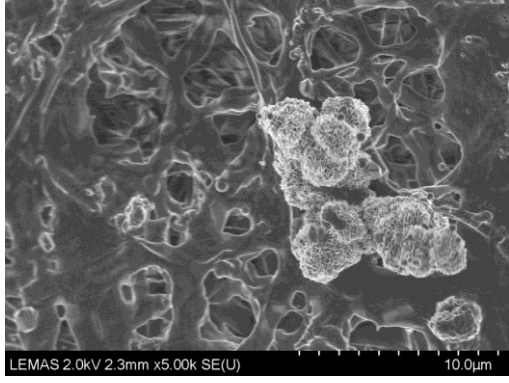
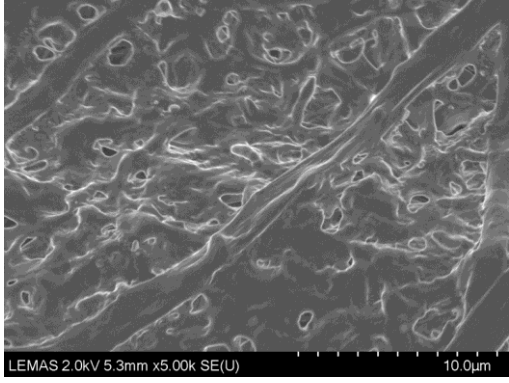
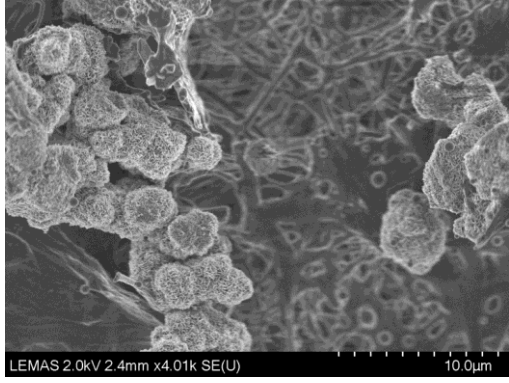
Sample	Incubation time	
	4 weeks	
	washed	unwashed
PCL		
PCL/P ₁₁ -4		
PCL/P ₁₁ -8		

Figure 6-8. SEM micrographs of electrospun fibres after four weeks incubation in SBF.

In Figure 6-9, the low magnification (1-3 Kx) SEM micrographs of PCL/P₁₁₋₄ fibres after 1, 2 and 4 weeks incubation in SBF, show the distribution of mineralised crystals all around the fibrous structure. It was observed that by increasing the incubation time in SBF, the prevalence of formed crystals within the fibrous structure increases. Thus, it was established that PCL/SAPs fibres are capable of nucleating apatite crystals, as well as providing a structural support for the crystals as they grow. Furthermore, they could be substantially retained on the electrospun webs even after washing.

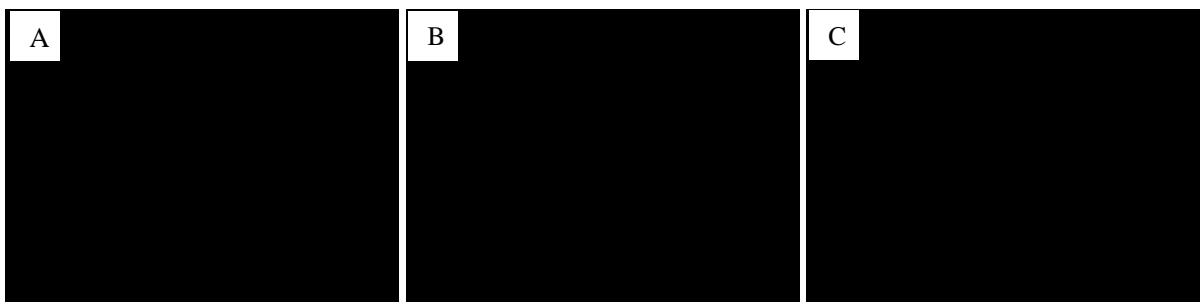


Figure 6-9. Low magnification SEM micrographs of mineralised PCL/P₁₁₋₄ fibres after (A) 1 week, (B) 2 weeks and (C) 4 weeks incubation in SBF showing the distribution of crystals formed all over the fibres.

The EDX data was also collected for all the PCL and PCL/SAPs fibres immersed in SBF for different period of times. A representative exemplar is given in Table 6-1, which summarises the atomic percentages of chemical elements in the washed PCL/P₁₁₋₄ fibres immersed in SBF for 2 weeks. The calcium to phosphorous ratio in this particular PCL/P₁₁₋₄ sample was 1.72, and the accompanying EDX pattern is shown in Figure 6-10.

Table 6-1. Elemental analysis of chemical elements in the PCL/P₁₁-4 fibres immersed in SBF for 2 weeks obtained by SEM/EDX.

Element	Atomic Content (%)
C	37.07
O	40.54
Na	1.40
Mg	0.44
P	6.85
Cl	1.61
K	0.09
Ca	11.80
Cu	0.02
Ir	0.19
Total:	100.00

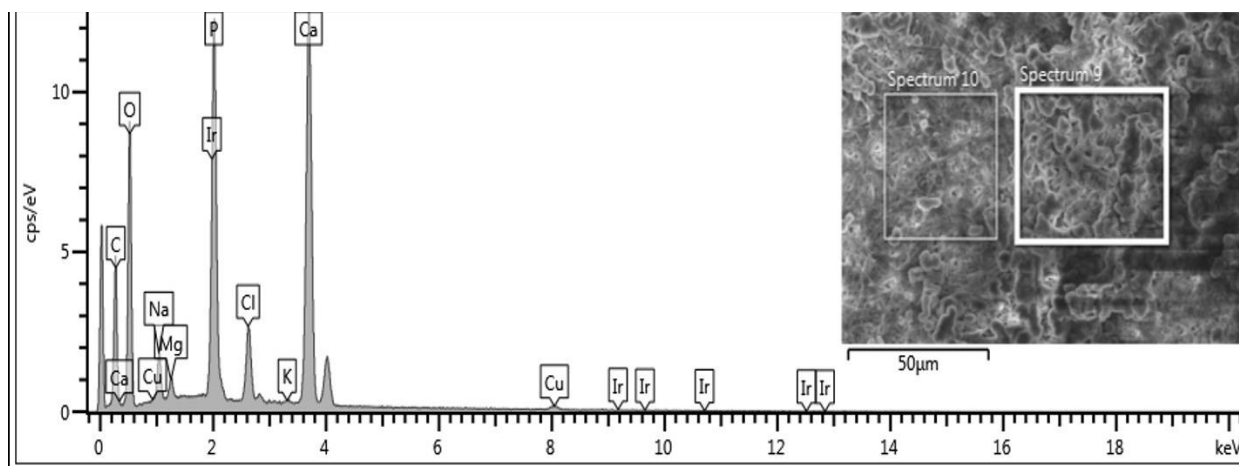


Figure 6-10. EDX spectra of PCL/P₁₁-4 fibres immersed in SBF for 2 weeks.

Similar to this example of the EDX results, in most of the EDX data for the incubated PCL and PCL/SAPs fibres, peaks corresponding to C and O together with some minor peaks, e.g. Na, Cl, K and Mg related to ion precipitation were visible. While in the mineralised scaffolds containing PCL/SAPs fibres, a characteristic peak corresponding to phosphorous at 2.01 eV and one corresponding to calcium at 3.69 eV was also observed. The Ca:P ratio obtained from EDX measurements of minerals deposited on all samples before and after washing are summarised in Table 6-2. The EDX analysis was carried out on specific points on individual mineralised particles, to make the results comparable. Three random spots per sample were tested and the mean of each Ca:P ratio together with the standard deviation are expressed.

In the PCL control sample no calcium-phosphorous mineral deposition was observed, which is in agreement with the visual observations in the SEM images. The Ca:P ratios obtained from the EDX analysis also show that in the PCL/P₁₁₋₄ samples from week 1, regardless of the washing process, the Ca:P ratio was very close to 1.67, which is that of hydroxyapatite (199). In PCL/P₁₁₋₈ fibres however, the ratio increases with time of exposure to the SBF and reaches 1.65 after 4 weeks. The ratios reported herein also express that the washing process does not affect remarkably the Ca-P mineral deposition on PCL/P₁₁₋₄ fibres, despite its marked effect on the Ca:P ratio of minerals deposited on PCL/P₁₁₋₈ fibres. This can be attributed to differences in the morphology of the PCL/P₁₁₋₄ fibres compared to the PCL/P₁₁₋₈ fibres. Since PCL/P₁₁₋₈ fibres comprised a larger number of peptide-enriched nanofibres, which fill the pores between the submicron fibres at the surface, these nanofibres may be dissolved faster due to their higher surface area and fragility. The diffusion lengths of SAPs to the surface of these fibres will also be shorter than in coarser fibres, making the peptides together with crystals more readily removable during washing. In contrast, in the PCL/P₁₁₋₄ fibres, where most of peptides are incorporated within larger submicron fibres, any minerals attached to the nucleating site of the SAP, will also be attached to a more stable substructure, less likely to be removed by washing.

Moreover, the superficial washing out of peptide at the surface of these fibres, will be replenished as more of the functional material diffuses towards the surface to support crystal growth.

Table 6-2. Ca:P ratio of the electrospun fibre webs incubated in SBF for up to 4 weeks based on EDX analysis.

Sample	Incubation time					
	Ca:P (1 week)		Ca:P (2 weeks)		Ca:P (4 weeks)	
	washed	unwashed	washed	unwashed	washed	unwashed
PCL	N/A	0	0	0	0	0
PCL/P₁₁₋₄	N/A	1.77 (SD=0.03)	1.72 (SD=0.09)	1.64 (SD=0.42)	1.76 (SD=0.30)	1.82 (SD=0.27)
PCL/P₁₁₋₈	N/A	0.31 (SD=1.8)	0.50 (SD=0.7)	1.50 (SD=0.1)	0.21 (SD=0.33)	1.65 (SD=0.39)

The spheroidal growth of the calcium phosphate crystals on the SAP enriched fibres may arise from the chemistry and structure of the nucleating site in SAPs and their affinity for mineral ions. Moreover, the molecular organisational structure of the peptides in to fibrils and presentation of charge domains at the fibrillar surface can effect on the ability of the assembled peptides to nucleate and support crystal growth *in vitro*. Moreover, it is known that the persistence of the assembled fibrils during the experimental period will contribute as a driver for mineral deposition and growth. To determine this, FTIR was performed on the incubated fibres in SBF after 1, 2 and 4 weeks to analyse the secondary structure of peptides within them and the spectra are shown in Figure 6-12.

As can be observed from the spectra, and as reported previously in Chapter 4, Section 4.3.6, as-spun PCL/P₁₁₋₄ fibres initially exhibited a combination of β -sheet and random coil states and PCL/P₁₁₋₈ fibres exhibited a predominant β -sheet state. It can be noted that after incubation for up to 2 weeks in highly ion concentrated SBF, there was still evidence of β -sheet in the both of the PCL/SAPs fibre web samples, even though there was some transition from β -sheet to a

random coil state during this time. However, after 4 weeks of incubation there was a marked decrease in the β -sheet peptide content and in turn some of the SAPs appears to have diffused into the solution or transformed into monomer at the surface of the fibres. This is evidenced by the decrease in the density of the peak at 1630 cm^{-1} and also in some samples, there was decrease in the peak density of COO^- at 1550 cm^{-1} in week 4, which reflects a decrease in the overall concentration of peptide regardless of its secondary conformation. The FTIR spectra of PCL-only samples are shown in Figure 6-11 for reference.

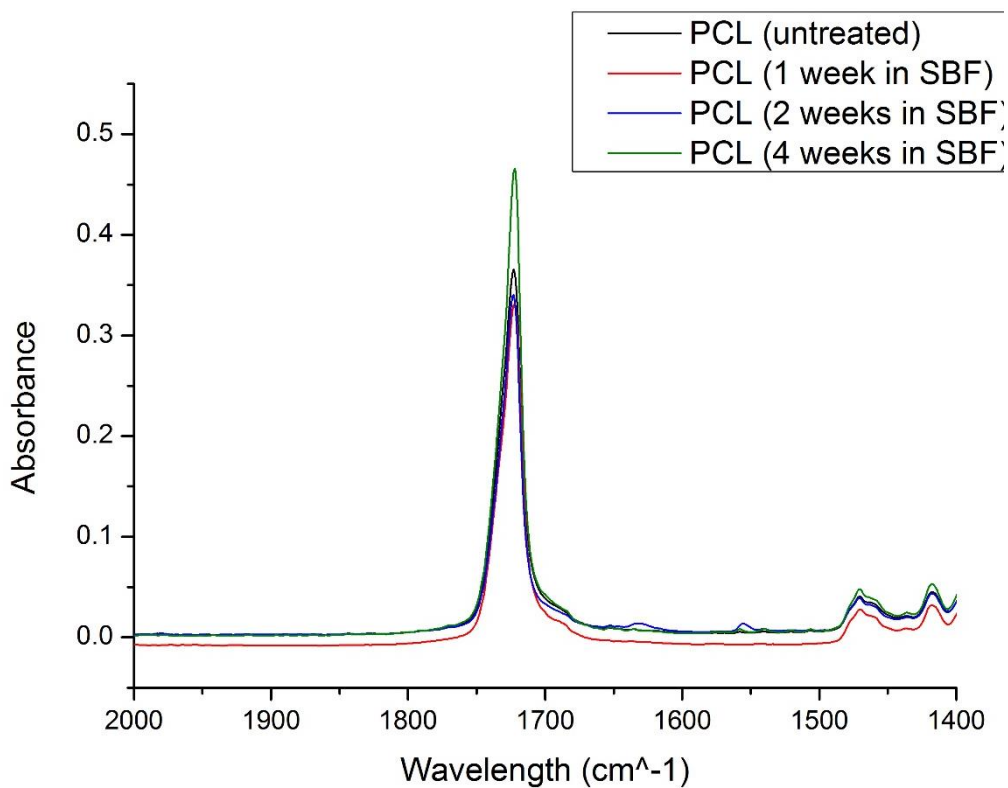
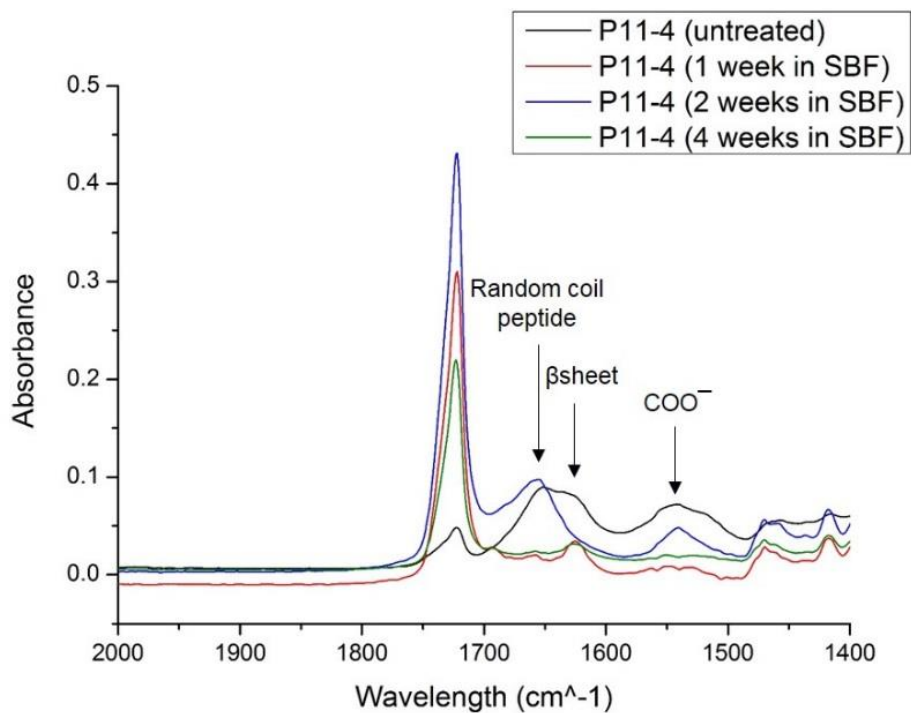


Figure 6-11. FTIR bands of electrospun PCL fibres before and after incubation in SBF.

A



B

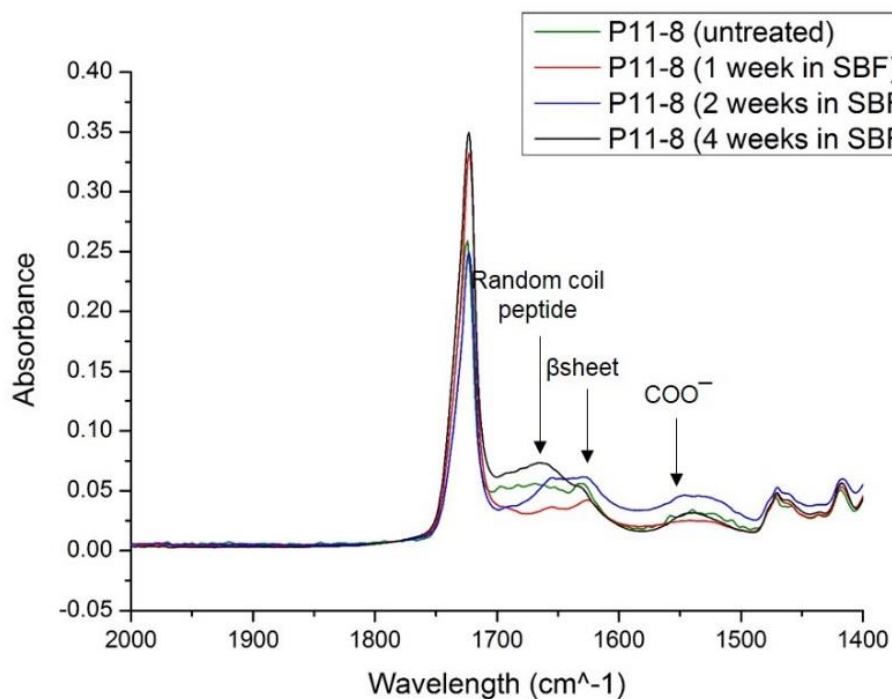


Figure 6-12. FTIR bands of electrospun (A) PCL/P₁₁₋₄ and (B) PCL/P₁₁₋₈ fibres before and after incubation in SBF.

X-ray diffraction patterns were also recorded to understand the chemical structure of the mineralized crystals on the electrospun PCL, PCL/P₁₁-4 and PCL/P₁₁-8 fibres after two and four weeks and are reported in Figure 6-13, Figure 6-14 and Figure 6-15 respectively. Two distinct diffraction peaks are observable for all samples at $2\theta = 21.5^\circ$ and $2\theta = 23.8^\circ$ which were indexed to crystalline structure of PCL (222, 223). As it can be observed from the PCL patterns (Figure 6-13), there were no additional peaks after incubation in SBF in all PCL samples. However after the incubation of PCL/SAPs fibres in SBF (Figure 6-14 and Figure 6-15), additional X-ray diffraction peaks were observed.

The peak at $2\theta = 31.8$ and an isolated peak at $2\theta = 46.6$, in PCL/P₁₁-4 and PCL/P₁₁-8 fibres after incubation is indicative of the presence of hydroxyapatite (HAP) (220). The patterns related to HAP in the PCL/SAPs fibres are sharper when the fibres are unwashed indicating that the crystallinity of HAP or the concentration of crystals is decreased after the washing process. However, the XRD patterns of both mineralised PCL/SAPs fibres after two weeks are substantially equivalent to those of after four weeks, which may indicate that there was no significant increase in nucleation or growth of minerals after two weeks.

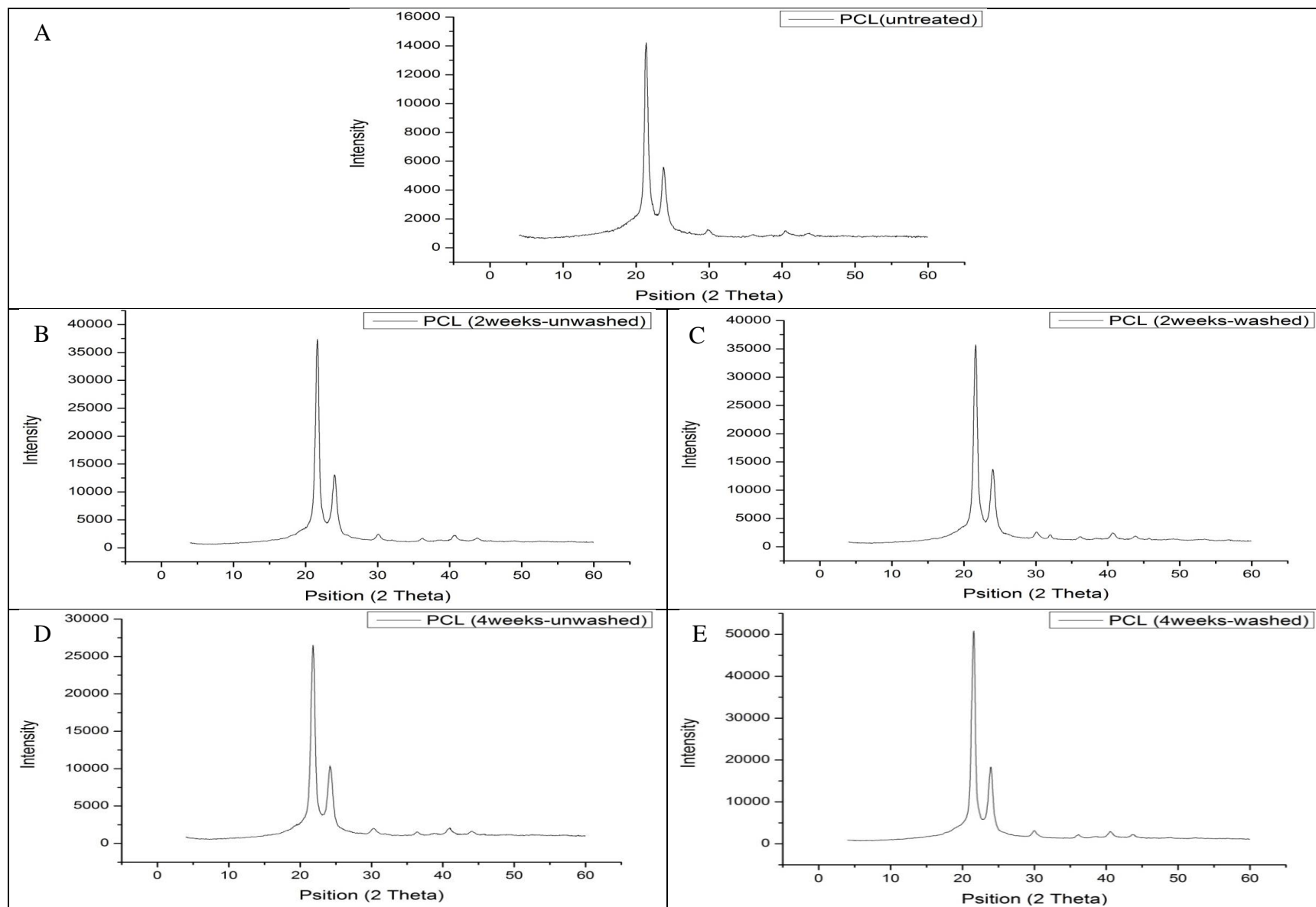


Figure 6-13. X-ray diffraction patterns of electrospun PCL fibres (A) before, (B) and (C) after 2 weeks, (D) and (E) after 4 weeks incubation in SBF.

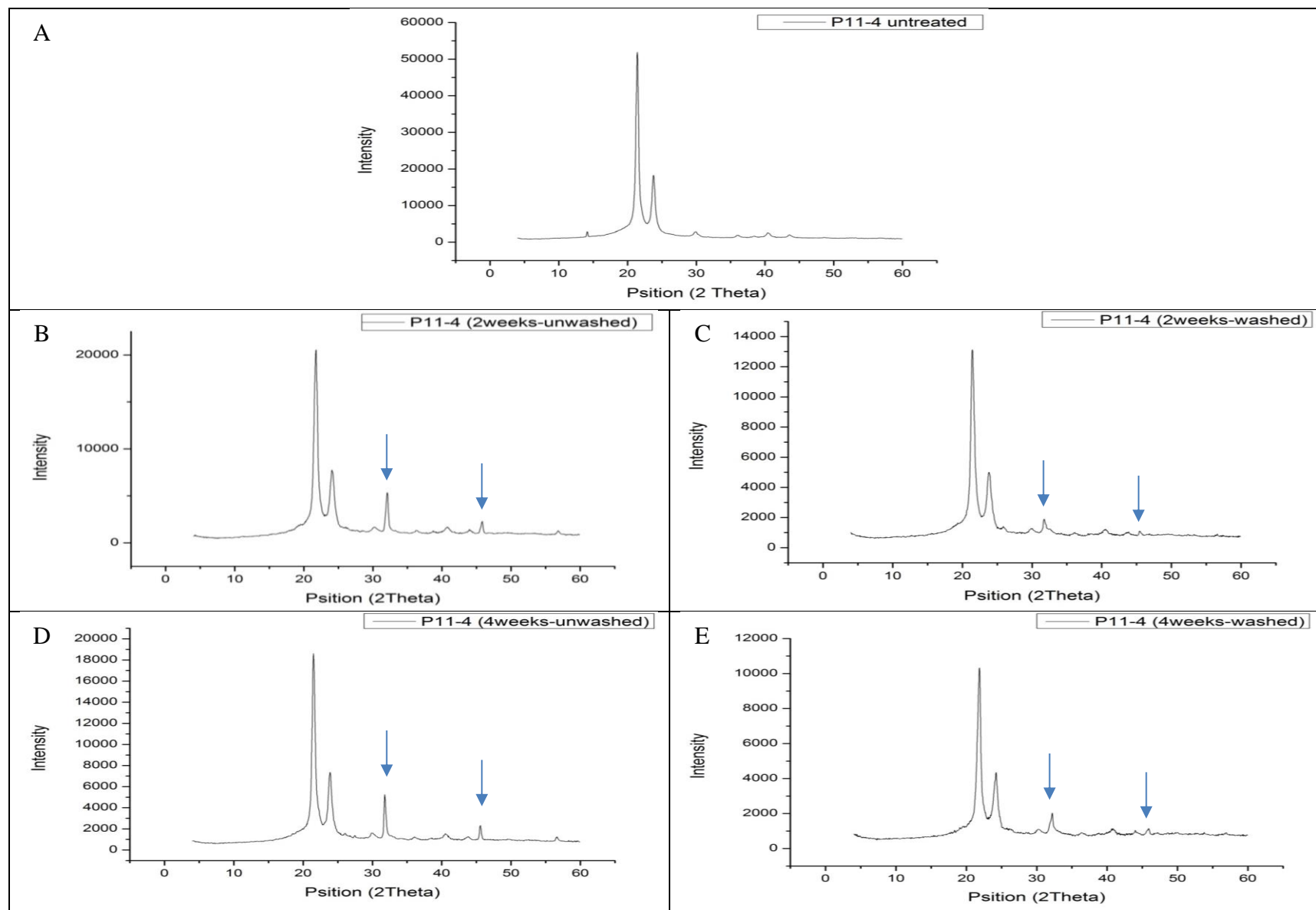


Figure 6-14. X-ray diffraction patterns of electrospun PCL/P₁₁₋₄ fibres (A) before, (B) and (C) after 2 weeks, (D) and (E) after 4 weeks incubation in SBF.

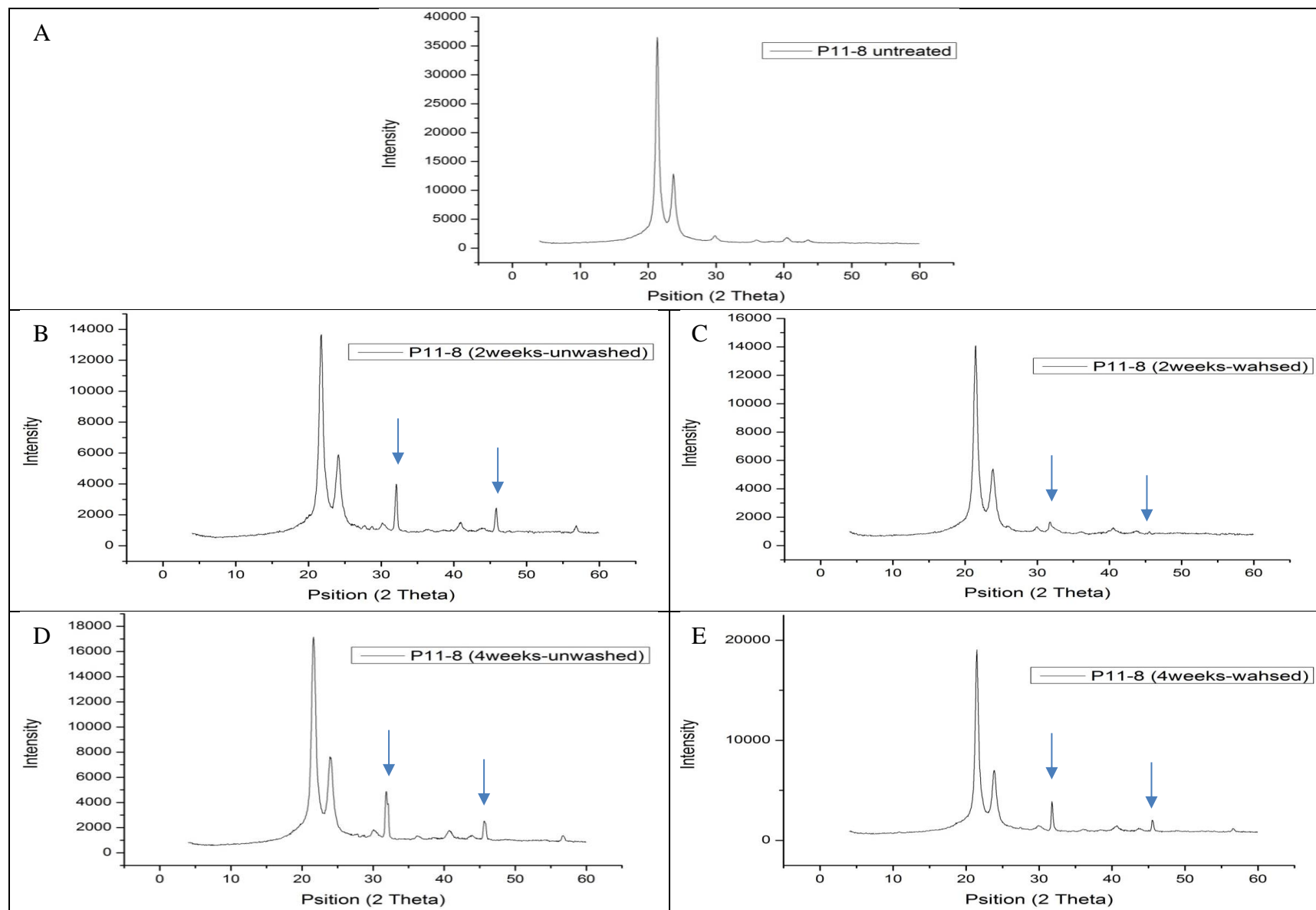


Figure 6-15. X-ray diffraction patterns of electrospun PCL/P₁₁₋₈ fibres (A) before, (B) and (C) after 2 weeks, (D) and (E) after 4 weeks incubation in SBF.

6.3.2 IVN Tank Results

The test samples, consisting of either electrospun fibres or hydrogel enriched SAPs, were incubated for 5 d, in *in vitro* IVN assay (described in Section 3.2.16). Subsequently, the samples were ashed (phosphate assay) and their PO_4^{3-} content was quantified spectrophotometrically. Table 6-3 and Table 6-4 shows the average absorbance at 820 nm and the phosphate content of the SAPs hydrogels and PCL/SAPs fibres respectively, when only 4 mg of peptide is present in each well. The concentration of PO_4^{3-} in μM was determined according to the standard curve obtained in Section 6.2.2.

Table 6-3. Determination of phosphate concentration (μM) in IVN hydrogel samples, SAP concentration = 4 mg mL^{-1} .

Sample	Absorbance average	Phosphate (μM)
Positive	0.57	95.5
P ₁₁ -8 gel	0.36	61.0
P ₁₁ -4 gel	0.23	39.6
Negative	0.18	31.5

Table 6-4. Determination of phosphate concentration (μM) in IVN fibrous samples, SAP concentration = 4 mg mL^{-1} .

Sample	Absorbance average	Phosphate (μM)
positive	0.58	97.5
P ₁₁ -8 fibre	0.31	53.0
P ₁₁ -4 fibre	0.32	54.3
PCL fibre	0.22	38.0
Negative	0.18	30.4

The relative ability of the PCL/SAP fibres and SAPs in agarose hydrogel to nucleate mineral *de novo*, when there was only 4 mg peptide in each well together with positive and negative controls is shown in Figure 6-16. Figure 6-16 shows that positive control (poly-L-glutamic acid) performed significantly ($p \leq 0.001$) better than all fibrous or hydrogel samples and also all the samples performed significantly ($p \leq 0.05$) better than negative control (agarose only), which confirms that the experiment was successful. The statistical analysis comparing means of the hydrogel samples indicates that P₁₁₋₈ performed significantly ($p \leq 0.01$) better than P₁₁₋₄. This is while when P₁₁₋₄ and P₁₁₋₈ were incorporated into the fibres, there were no significant difference ($p \geq 0.05$) in their performance. Moreover, the assay confirmed that fibres with SAPs (both PCL/P₁₁₋₄ and PCL/P₁₁₋₈ fibres), performed significantly ($p \leq 0.05$) better than PCL-only fibres. This confirms the ability of SAP enriched fibres to nucleate hydroxyapatite and supporting the crystal growth. This is the first time that PCL/P₁₁₋₄ and PCL/P₁₁₋₈ fibres electrospun fibres have been shown to nucleate apatite in the IVN tank, and for the first time fibrous samples, rather than hydrogels have been studied in this way.

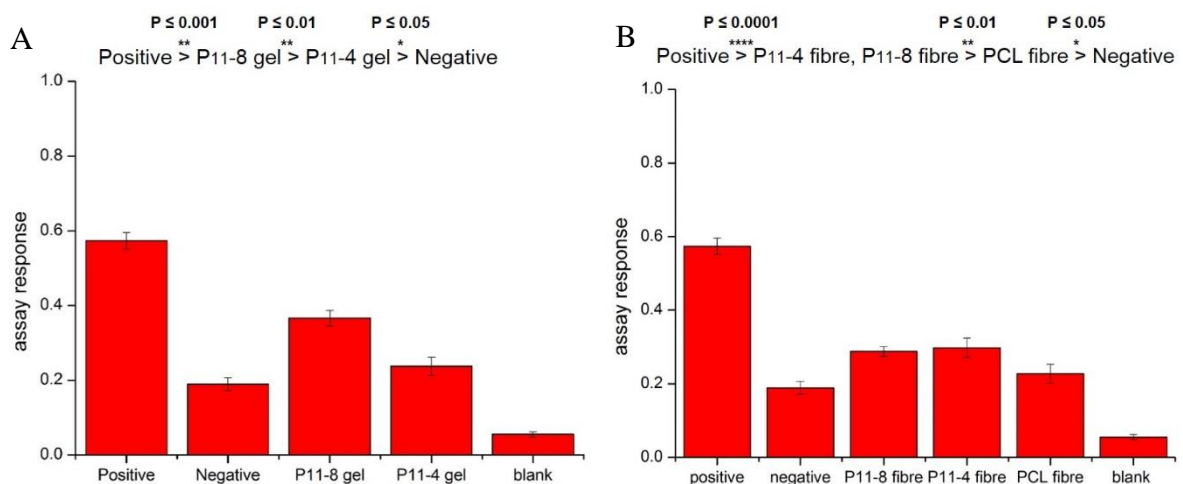


Figure 6-16. IVN assay response of (A) peptide hydrogel samples and (B) electrospun fibrous samples at peptide concentration of 4 mg mL⁻¹.

Figure 6-17 compares the percentage (%) of minerals nucleated on fibre and hydrogel structure performance relevant to their own positive control in each assay, when the peptide concentration is 4 mg mL⁻¹. It can be observed that in general, performance of SAPs in hydrogel form and in fibre form (at 4 mg mL⁻¹) concentration were comparable. However, by statistically analysing the result, it was found that P₁₁₋₈ in the gel form performed significantly ($p \leq 0.01$) better than in the fibre form, while P₁₁₋₄ peptide exhibited opposite behaviour. Based on these results, further experiments were carried out by doubling the concentration of peptide in each cell of the sample holder.

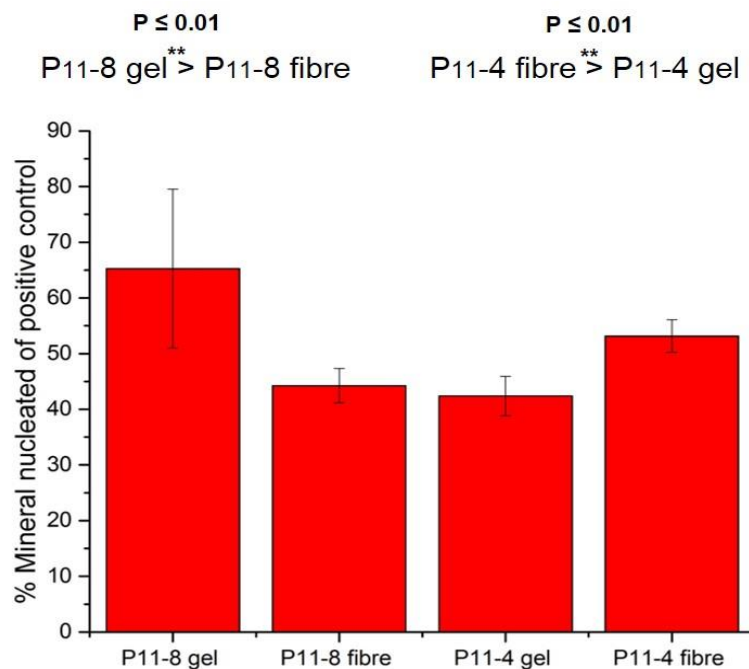


Figure 6-17. IVN assay response of P₁₁₋₄ and P₁₁₋₈ in both hydrogel and electrospun fibrous structure at peptide concentration of 4 mg mL⁻¹.

Table 6-5 and Table 6-6 give the average absorbance at 820 nm and the phosphate content of SAP hydrogels and PCL/SAP fibre web samples respectively, when the concentration of SAPs is increased to 8 mg in each well. The concentration of PO_4^{3-} in μM is determined according to the standard curve obtained in Section 6.2.2.

Table 6-5. Determination of phosphate concentration (μM) in IVN hydrogel samples, SAP concentration=8 mg mL^{-1} .

Sample	Absorbance average	Phosphate (μM)
Positive	0.55	92.7
P ₁₁ -8 gel	0.75	125.9
P ₁₁ -4 gel	0.65	108.6
Negative	0.18	30.3

Table 6-6. Determination of phosphate concentration (μM) in IVN fibrous samples, SAP concentration = 8 mg mL^{-1} .

Sample	Absorbance average	Phosphate (μM)
Positive	0.62	104.2
P ₁₁ -8 fibre	0.30	50.5
P ₁₁ -4 fibre	0.37	62.6
PCL fibre	0.28	46.6
Negative	0.21	35.4

Figure 6-18 shows the plotted assay response of the PCL/SAP fibre webs or SAP hydrogels, which reflects their ability to nucleate mineral *de novo*, when there is 8 mg peptide in each well. Statistical analysis was performed on the results, and this indicated a highly statistically significant difference ($p \leq 0.0001$) between the positive control and the negative control of each experiment, which confirms that the experiment was successful. As it can be observed in Figure 6-18 (A), both P₁₁₋₄ and P₁₁₋₈ peptides in the hydrogel form were more highly capable of nucleating hydroxyapatite and supporting significant crystal growth compared to the positive control, though to varying extents. However, when SAPs are incorporated in PCL fibres, even by doubling the concentration in the assay, they still did not perform better than their positive control. This was evidenced by a highly statistically significant difference indicated by a T-test ($p \leq 0.001$).

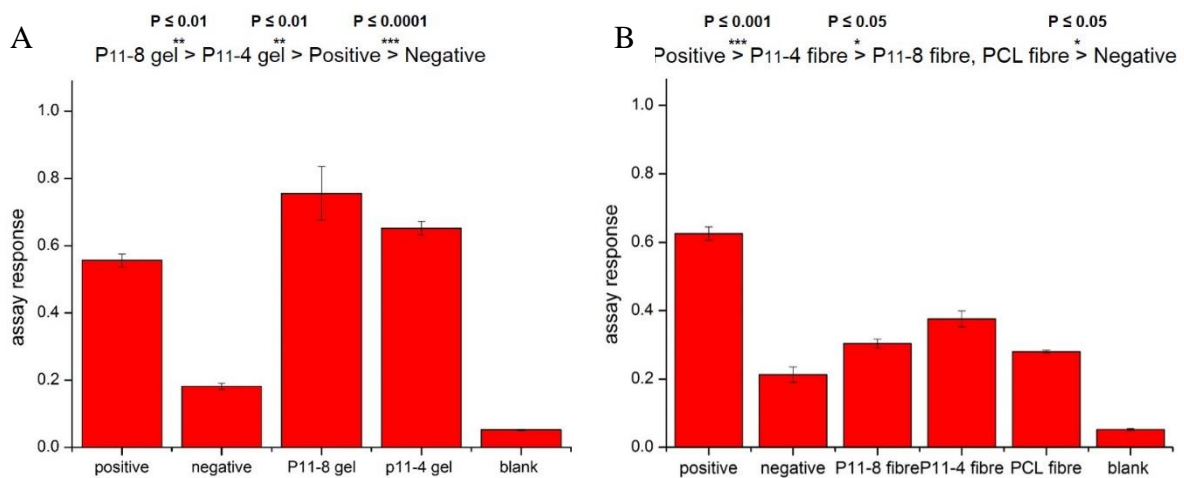


Figure 6-18. IVN assay response of (A) peptide hydrogel samples and (B) electrospun fibrous samples at peptide concentration of 8 mg mL⁻¹.

The relative ability of SAPs at a concentration of 8 mg mL⁻¹ in both fibrous and hydrogel form is shown in Figure 6-19. As can be observed, both the P₁₁₋₄ and P₁₁₋₈ samples performed significantly ($p \leq 0.0001$) better in hydrogel form than in fibrous form at the same concentration of 8 mg mL⁻¹.

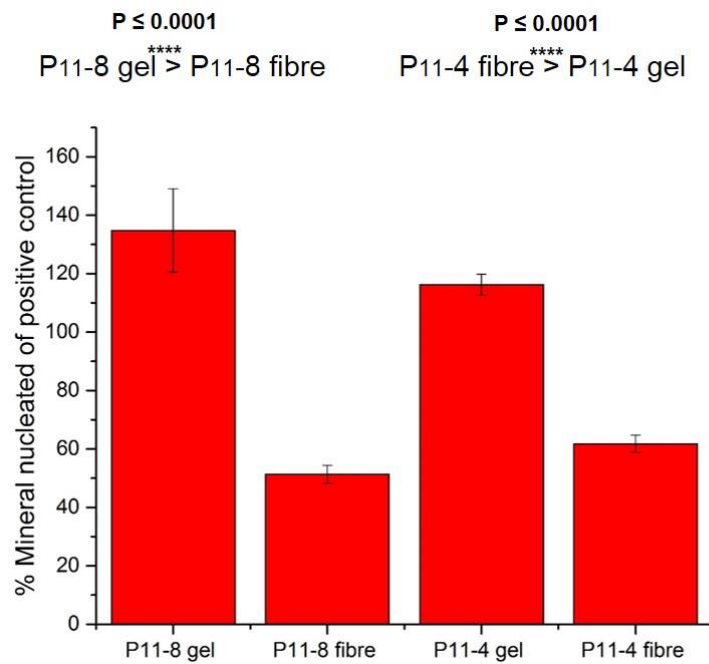


Figure 6-19. IVN assay response of P₁₁₋₄ and P₁₁₋₈ in both hydrogel and electrospun fibrous structure at peptide concentration of 8 mg mL⁻¹.

Figure 6-20 shows the combination of the determined assay response for all fibrous and hydrogel samples (together with the negative control and the PCL fibre control), at both concentrations of 4 and 8 mg mL⁻¹. The results are presented based on the percentage mineral nucleated compared to the positive control in each experiment. This overview of the data reveals that even though the increase in the concentration of peptide within the fibrous structure, does have a small effect on the nucleated mineral content, it is not comparable with the effect of SAP concentration in hydrogel form. This may be due to this specific assay and on the design of IVN apparatus (Section 3.2.16), since in the IVN method, even when the amount of SAP containing fibre present is doubled, the surface area of fibres exposed to nucleating buffer solutions does not change.

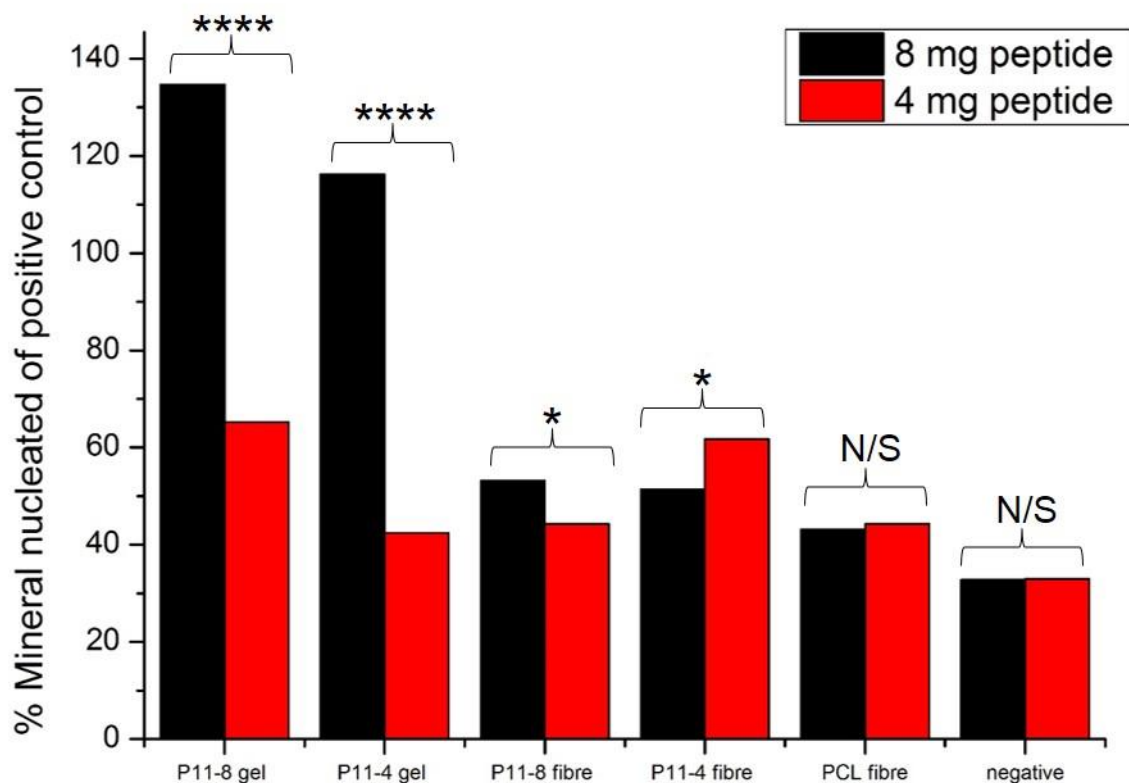


Figure 6-20. IVN assay response of fibrous and hydrogel together versus peptide concentration. (N/S)= $p \geq 0.05$, (*) = $p \leq 0.05$, (**) = $p \leq 0.01$, (***) = $p \leq 0.001$, (****) = $p \leq 0.0001$.

As indicated in the literature (53) (Section 2.4.5), mineralisation is nucleated on negatively charged surfaces (in this study P₁₁₋₄) due to the attraction of positively charged Ca²⁺ ions (224) and eventually super-saturation of the local environment in physiological conditions. It is known that glutamic acid side chains (in both P₁₁₋₄ and P₁₁₋₈) can play an important role in the mineralisation as well (225). Moreover based on the previous release behaviour study of incorporated SAPs within the fibres (results presented in Section 5.3.3), it is known that the peptides are released gradually by the fibres since many are encapsulated within the body of the fibre, and at least 40% is still present at day 7. Given that the duration of the present IVN assay is 5 days, it is likely that even when there is more peptide within the fibrous disk, the nucleating points of SAPs (negatively charged surface groups or glutamic acid side chains) do not have sufficient time to be available at the surface of the fibres to increase the mineral nucleation.

The IVN tank assay also showed that P₁₁₋₄ in fibrous scaffold performs slightly better than P₁₁₋₈ enriched fibres in terms of mineral nucleation. However in this assay, it was shown that P₁₁₋₈ in hydrogel form performs significantly ($p \leq 0.01$) better than P₁₁₋₄ hydrogel when the concentration of SAP in them is the same (both 4 and 8 mg mL⁻¹), which is consistent with the unpublished data of hydrogels analysed via the IVN method previously in Leeds (53).

In the IVN study, it was also interesting to note the extent to which a non-SAP enriched PCL fibre web was able to nucleate mineral using either one disk or two disks of PCL fibre webs. This is most likely due to the provision of solid surface area, at the interface between agarose gel and fibrous disks, within which nucleation could commence. This is in contrast with the results from the first method explained in Section 6.3.1 which was predictable, as this interface between fibres and hydrogel was not present in those samples.

The IVN data in particular was instructive in elucidating the effect of the SAP delivery vehicle on nucleation behaviour, and has implications in terms of the future design of clinical tools and therapies. In short, these data reveal that even if the peptide contents are comparable, the format of the delivery vehicle, i.e. a hydrogel or a fibre, will affect the rate at which it becomes available for apatite nucleation. In a porous gel, the peptide is immediately accessible in the IVN method, whereas in a 3D electrospun fibrous matrix, access to peptide is slower because of its encapsulation within a water-stable PCL polymeric matrix through which it must gradually diffuse. For the building of therapeutic devices for the clinic, this ability to deliver SAPs over a longer period than is likely to be possible with hydrogels, is potentially advantageous. By selecting an appropriate synthetic polymer carrier, such as PCL or other biodegradable polymers, delivery rates can be modulated. This is in addition to the advantage of a more mechanically robust delivery vehicle, as provided by an electrospun format compared to a fully hydrated hydrogel.

6.4 Summary

SEM, EDX and XRD analysis of the electrospun fibre webs incubated in SBF, revealed that PCL/SAPs fibres have considerable capability to nucleate hydroxyapatite and support crystal growth *in vitro*. This was evidenced by observed spheroidal growth of calcium phosphate crystals on the SAP enriched fibres in SEM micrographs. The EDX elemental analysis showed that the Ca:P ratios of the nucleated crystals on the PCL/P₁₁₋₄ fibres from week one, were very close to 1.67 which corresponds to that of hydroxyapatite. PCL/P₁₁₋₈ fibres displayed a Ca:P ratio of 1.65 after four weeks, which is comparable and very close to the stoichiometric Ca:P ratio for hydroxyapatite. XRD analysis also confirmed the diffraction peaks corresponding to hydroxyapatite crystals in both PCL/SAPs incubated fibres from week two.

A washing process carried out after incubation of fibres in SBF and before any analysis to remove unwanted precipitations that can affect the crystal content, which may be due to the instability of the crystals formed on the surface of the fragile nanofibres in the webs. However, this effect can only happen in *in vitro* studies and when *in vivo*, the crystals have more time to crystallise and become stable while the whole scaffold is *in situ*.

FTIR analysis of the fibres after incubation in SBF for one, two and four weeks confirmed the presence of SAPs within the fibres after four weeks, and even the presence of β -sheet self-assembled structure was evident to some extent after two weeks, although some transformation to monomeric form had taken place as well.

Within the constraints of the IVN tank system, enhancement in the mineral nucleation performance of electrospun fibres was confirmed when the SAPs are incorporated in them. At 4 mg mL⁻¹ SAP concentration, PCL/SAP fibre web mineral nucleation performance was comparable to that of SAP hydrogel. However, when the concentration of SAP was increased in the fibrous scaffold to 8 mg mL⁻¹, the ability of fibres to nucleate minerals or support their growth

did not significantly increase. This may be due to the unchanged interface area of the fibres exposed to nucleation buffers and also the additional SAPs in the fibres not having sufficient time (within the 5 d test period) to be available at the surface to promote nucleation.

The IVN tank assay may not have provided remarkable evidence to show the capability of nucleating hydroxyapatite in PCL/SAP fibre, however it does evidence one of the initial objectives of this study. The objective was to make SAPs more stable in biological conditions, by incorporation of the SAPs into PCL electrospun fibres. As indicated in Chapter 5, in an *in vivo* study by Burke et al. (53), SAP hydrogels will be diffused out by day seven when in biological conditions, which is insufficient time for bio-mineralisation to fully take place. Thus, in this study and specifically in the SBF assay, it has been established for the first time that nucleation and growth of hydroxyapatite can be further increased by at least four weeks, while the SAP remains stable and partially still in self-assembled form within the fibres.

The unsuitability of the IVN tank method to characterise fibrous scaffold structures can be addressed by the following modifications to the method:

- Increase in the incubation time beyond 5 d to facilitate the delivery of SAPs at the surface of fibres, and the creation of nucleation points.
- The design of apparatus could be changed to increase the contact area between the nucleating buffer and the interface of the fibres.

Both the SBF and IVN assays indicated that PCL/P₁₁₋₄ fibres generally performs better than PCL/P₁₁₋₈ fibres in terms of nucleation of hydroxyapatite and supporting its crystal growth *in vitro*, which is due in part to differences in the electrospun fabric structure produced by each.

CHAPTER 7

Conclusion

7.1 General Conclusions

Electrospun webs are promising structures for use as bone tissue engineering scaffolds due to their small mean fibre diameter and high surface area to volume ratio, which mimic structural features of natural bone ECM. These characteristics together with high porosity and pore interconnectivity are beneficial for cell attachment, proliferation and nutrient transport. Additionally, if bioactive materials known to promote nucleation and mineralisation of HAP can be incorporated into such scaffolds then there is an opportunity to produce advanced devices capable of assisting with mineralisation and the repair of damaged bone.

The self-assembling peptides P₁₁₋₄ (-2 charge) and P₁₁₋₈ (+2 charge) in the form of hydrogels have previously been shown to be non-cytotoxic to human and murine cells as well as to enhance bone tissue regeneration and remineralisation. However, in clinical practice despite their inherent biofunctionality, there are a number of challenges in using SAPs hydrogels because of their poor mechanical strength and lack of structural stability. This also complicates their handling and fixation during implantation, particularly in large load-bearing tissue defects. Whilst the biomineralisation properties of SAP hydrogels have been reported before, the incorporation of P₁₁₋₄ and P₁₁₋₈ peptides within synthetic electrospun fibres and their biofunctionality has not previously been reported in the literature. For the first time, this research

has demonstrated a means of delivering SAPs in a form that could extend the clinical uses of SAPs, by providing them in a novel format.

As a carrier material, PCL is a low-cost, non-toxic, biodegradable polymer and FDA approved devices containing PCL have previously been used in the human body. PCL has shown promise in regenerative bone therapies, and as such, it was selected as a means of delivering the SAPs of interest during this research. The feasibility of incorporating P₁₁₋₄ and P₁₁₋₈ into electrospun PCL scaffolds was explored, together with the resulting biological and mineralisation properties of the resulting fibres.

Initially, the production of electrospun fibres was investigated in Chapter 4 using a single spinneret needle electrospinning, and successful incorporation of P₁₁₋₄ and P₁₁₋₈ into PCL in a one-step manufacturing process was demonstrated. Firstly, a range of PCL concentrations in HFIP solution were examined to determine the optimum spinning solution. It was established that PCL at 6% (w/w) concentration, could be electrospun by governing process parameters, and smooth fibres, free from defects were produced. The smallest mean fibre diameter was achieved using a 1 mL h⁻¹ flow rate, a voltage of 20 kV and a tip to collector distance of 180 mm on an aluminium foil collector. SEM, TEM and CLSM analysis revealed a bimodal fibre diameter distribution of superimposed nano- (below 100 nm) and submicron (below 1µm) scale fibre networks of PCL/SAP fibres in contrast to the PCL control fibres, which were narrowly distributed and of submicron dimensions only. Adjusting the peptide concentration in the electrospinning solution was found to be the main parameter governing formation of the nanofibrous network and the nanofibres became more pronounced as the peptide concentration in solution increased from 10 to 40 mg mL⁻¹. This was most evident in the case of PCL/P₁₁₋₈ fibres. This observation provides a useful means of systematically customising the internal nanoscale structure of the webs, which provides a convenient way of controlling nonwoven architecture at the nanoscale during scaffold manufacture.

The presence of SAPs within the as-spun fibres was then confirmed by SEM/EDX, while TEM/EDX on the PCL/P₁₁₋₈ fibres revealed that both the superimposed nano- and submicron scale fibres contained peptides. This provided evidence that there was no phase separation between the PCL and the peptide components during electrospinning. Moreover, the uniform distribution of peptide within the fibres was investigated and confirmed by CLSM analysis.

It was important to determine how the secondary conformation of the SAPs changed during the spinning process. Analysis of the spinning solutions and the as-spun fibres by CD and FTIR revealed a switch from monomeric to β -sheet peptide conformation, though the β -sheet configuration was more predominant in the PCL/P₁₁₋₈ fibres compared to PCL/P₁₁₋₄. These results confirmed that the electrospinning process was able to successfully trigger the molecular self-assembly mechanism in the peptides, therefore inducing nanofibre formation among the submicron fibres.

Having successfully produced PCL fibres loaded with SAPs, the properties of the webs were further investigated. Scaffolds for bone tissue engineering must fulfil several criteria such as biocompatibility. Accordingly, the wettability and cytocompatibility of PCL/SAPs electrospun fibres were investigated. It was found that the hydrophilicity of PCL electrospun fibre webs in the presence of SAPs substantially increases. This was evidenced by measuring the contact angle of deionised water and DMEM on electrospun webs, which revealed a decrease from above 90° (hydrophobic) to 0°, when the peptide concentration in the electrospinning solution increased from 0 to 40 mg mL⁻¹.

Although there have been many studies confirming the cytocompatibility of 100% electrospun PCL fibres, none have considered extract cytotoxicity in the presence of P₁₁₋₄ and P₁₁₋₈ peptides. A preliminary experiment determined no toxic response in L929 cells cultured with PCL/SAPs electrospun sample extracts, although the cell viability in PCL/SAPs extract was slightly reduced

compared with the PCL control sample. It was reasoned that this could be due to peptide disassembly into monomeric form in aqueous solution during the extraction time which affects the metabolic activity of L929 mouse fibroblasts. Therefore, the direct cytotoxicity assay was conducted whereby L929 mouse fibroblasts were cultured in contact with PCL/SAPs electrospun fibres. This provided additional confirmation that the peptide loaded samples had no cytotoxic response (<90% cell viability) and the data confirmed that the PCL/SAPs fibres have potential as candidates for use as bone tissue scaffolds.

It is an important requirement for bone tissue scaffolds to maintain a stable structure, while the newly regenerated tissue can be formed and bone crystal mineralisation can take place. One aim of this study was to improve the stability of biofunctional SAPs when they are in a biological environment, by incorporating them into PCL scaffolds, as compared with their hydrogel structure. Therefore, a seven-day degradation study of the PCL/SAPs fibres was conducted in aqueous solutions at different pH. The percentage release of SAPs from PCL fibres was detected via mass loss analysis and it was demonstrated that at least 40% and 65% of the P₁₁₋₈ and P₁₁₋₄ respectively, are still available and stable within the electrospun fibres after 7 d. This was the case even at the least favourable pH for SAPs structural stability, at which their transformation to monomers can take place.

Using CD analysis, it was confirmed that the mass loss percentages were associated with peptide release into solution and not associated with PCL component degradation. At pH 7.5, which is close to biological pH, at least 75% of P₁₁₋₄ and 45 % of P₁₁₋₈ was still present within the fibres. This suggests that fibres containing SAPs could provide vehicles for delivery of the peptide over a longer period than is possible when they are delivered in the form of hydrogels. The difference in retained SAPs for the P₁₁₋₈ and P₁₁₋₄ peptides, could be partially explained by differences in the dimensions and morphology of PCL/P₁₁₋₈ fibres, which influences the length of the diffusion pathway. In the larger PCL/P₁₁₋₄ fibres, most of the SAPs are encapsulated within the submicron

fibres and therefore they will be slower to release than would be the case from the large number of nanoscale fibres present in the PCL/P₁₁-8 webs. Interestingly, in the degradation study, the morphology of the fibres remained essentially unchanged suggesting that the PCL was stable and that the diffusion of the peptides did not cause structural instability in the web. This also provides further evidence that the nanoscale fibres in the webs were not composed entirely of peptide, but rather a commixture of both PCL and peptide. By further analysis of the SEM images, an increase of 25% in diameter of the PCL control fibres and a 90-115% increase in the diameter of the PCL/SAP fibres was observed. This was due to water uptake during hydrolysis and the fact that the PCL/SAP fibres are more hydrophilic compared to the PCL fibres, thereby promoting swelling.

The apatite-forming ability of electrospun PCL/ SAPs fibres was then assessed to determine their suitability to promote mineral nucleation and support their subsequent growth. Firstly, the BS ISO 23317:2014 standard method was employed to determine if PCL/SAPs webs are able to nucleate HAP minerals. After incubation in SBF, spheroidal growth of calcium phosphate crystals confirmed considerable capability of PCL/SAPs fibres to nucleate and further grow HAP *in vitro*, compared with PCL only fibres. The Ca:P ratios of the nucleated crystals on the PCL/P₁₁-4 fibres were very close to that of hydroxyapatite from week one, whereas the PCL/P₁₁-8 fibres displayed the relevant Ca:P ratio to HAP after four weeks. XRD analysis also confirmed the diffraction peaks corresponding to hydroxyapatite crystals in both PCL/SAP incubated fibres from week two.

The stability of SAPs and their ability to remain within the fibres after four weeks incubation in SBF and even to remain in the β -sheet self-assembled form until after two weeks was evidenced via FTIR analysis. Moreover, the IVN tank method was used to determine apatite forming ability of PCL/SAP fibres and to determine whether their ability is comparable to hydrogel structures of the same SAP concentration. IVN tank studies had never previously been attempted using

fibre-based materials of the type produced in this research. Initial experiments with the IVN system revealed enhancement in the mineral nucleation performance of electrospun fibres when the SAPs are incorporated in them. At 4 mg mL⁻¹ SAP concentration, PCL/SAP fibre performance was comparable with SAP hydrogel of the same concentration. However, when the concentration of SAPs increased in the electrospun webs to 8 mg mL⁻¹, the ability of fibres to nucleate minerals or support their growth was not significantly increased compared to that of hydrogels. This was explained in terms of the accessibility of the peptides within the fibres, prior to their diffusion from the fibre surfaces or availability at the surface, when exposed to nucleation buffers. Since the duration of the assay did not exceed five days, the additional SAP present in the fibres did not have sufficient time to become available at the fibre surfaces to promote nucleation.

7.2 Recommendations for Further Work

To further understand the incorporation of P₁₁₋₄ and P₁₁₋₈ peptides into fibrous structures and provide greater understanding of their performance in biological environments and in nucleation of bone minerals and regeneration, the following additional areas of study can be identified:

- Use of different solvent systems in electrospinning, to establish the morphological characterisation of SAP enriched fibres and to see whether or not similar bimodal fibre diameter network are produced in different solvent systems when the SAPs are present.
- Use of different spinning techniques, which are not reliant on electrostatic forces such as force-spinning or wet-spinning to give further insight into the fibrous morphology and incorporation properties of SAPs into polymeric fibres.
- The peptide release study provided herein was conducted for only up to 7 d. This was mainly to understand stability of the SAPs in the aqueous solution at a particular pH. Clinically, bone tissue scaffolds could be used *in vivo* for up to nine months or more in spinal fusion or three to six months for cranio-maxillofacial applications, until the newly bone tissue is grown. Ideally, the bioactive component (SAPs in this study) should not be diffused or depleted too quickly, while the polymer carrier component (PCL in this study) should be degraded by this time. Therefore, a thorough degradation study of the scaffolds produced in this work could be employed in aqueous solution with an ion concentration close to that of body fluid (i.e. in cell culture medium), and based on the results, the suitability of the scaffold for use in specific bone applications can be identified. An enzymatic degradation of the SAP enriched fibres could be valuably explored to determine the effect of enzymes on the degradation profile of fibres, to reach to a more robust estimation of the scaffold degradation profile under simulated biological conditions.

- Further to the degradation profile, electrospinning of alternative polymer systems, which have potential to offer different degradation rates, enriched with SAPs, would be of interest in future studies to assist in customising the design of the scaffold for clinical use.
- Working with different concentrations of SAPs in electrospinning solutions may also provide a route to identify optimum concentrations of SAPs (min and max) needed to achieve certain fibre morphologies and to meet the intended biofunctionality (e.g. apatite forming ability of fibres in SBF).
- The current study provided a novel analysis of PCL/SAP fibres webs in the IVN system, and the minerals nucleation performance has been demonstrated. There is scope to further develop this method in order to be more compatible with fibrous rather than hydrogel structures. For example, since the encapsulated SAPs in fibres are more slowly released into the surrounding solution, a longer period is required for the assay, so that the SAPs can gradually become available as nucleation points. Moreover, the sample holders in the apparatus can be redesigned to provide more contact area at the interface of the fibres with nucleating buffers.
- Tensile testing of PCL/SAP fibres can be carried out in future studies to provide a useful insight into the mechanical properties of the scaffolds. This would further help in defining the suitability of these scaffolds for clinical bone tissue regeneration.
- Ultimately, evaluation of the PCL/SAP fibre webs in a bone remineralisation *in vivo* model would be instructive by implantation into rat/rabbit calvaria defects.

References

1. Kim, B.-S. and Mooney, D.J. Development of biocompatible synthetic extracellular matrices for tissue engineering. *Trends in biotechnology*. 1998, **16**(5), pp.224-230.
2. Fleischer, S. and Dvir, T. Tissue engineering on the nanoscale: lessons from the heart. *Current opinion in biotechnology*. 2013, **24**(4), pp.664-671.
3. Yang, S.F. and Leong, K.F. and Du, Z.H. and Chua, C.K. The design of scaffolds for use in tissue engineering. Part 1. Traditional factors. *Tissue engineering*. 2001, **7**(6), pp.679-689.
4. Economist. *Population explosion*. [Online]. 2014. [Accessed]. Available from: <http://www.economist.com/news/middle-east-and-africa/21612239-runaway-birth-rates-are-disaster-population-explosion>
5. Fougère, M. and Mérette, M. Population ageing and economic growth in seven OECD countries. *Economic Modelling*. 1999, **16**(3), pp.411-427.
6. Reginster, J.-Y. and Burlet, N. Osteoporosis: a still increasing prevalence. *Bone*. 2006, **38**(2), pp.4-9.
7. Sen, M. and Miclau, T. Autologous iliac crest bone graft: should it still be the gold standard for treating nonunions *Injury*. 2007, **38**(1), pp.S75-S80.
8. Rabkin, E. and Schoen, F.J. Cardiovascular tissue engineering. *Cardiovascular pathology*. 2002, **11**(6), pp.305-317.
9. Jang, J.-H. and Rives, C.B. and Shea, L.D. Plasmid delivery in vivo from porous tissue-engineering scaffolds: transgene expression and cellular transfection. *Molecular Therapy*. 2005, **12**(3), pp.475-483.
10. Chan, B. and Leong, K. Scaffolding in tissue engineering: general approaches and tissue-specific considerations. *European spine journal*. 2008, **17**(4), pp.467-479.
11. Gelinsky, M. and Welzel, P. and Simon, P. and Bernhardt, A. and König, U. Porous three-dimensional scaffolds made of mineralised collagen: Preparation and properties of a biomimetic nanocomposite material for tissue engineering of bone. *Chemical Engineering Journal*. 2008, **137**(1), pp.84-96.
12. Drosse, I. and Volkmer, E. and Capanna, R. and De Biase, P. and Mutschler, W. and Schieker, M. Tissue engineering for bone defect healing: an update on a multi-component approach. *Injury*. 2008, **39**, pp.S9-S20.
13. Czajka, R. Development of medical textile market. *Fibres & Textiles in Eastern Europe*. 2005, **13**(1), pp.13-15.
14. Bhardwaj, N. and Kundu, S.C. Electrospinning: a fascinating fiber fabrication technique. *Biotechnology advances*. 2010, **28**(3), pp.325-347.
15. Li, W.-J. and Tuli, R. and Okafor, C. and Derfoul, A. and Danielson, K.G. and Hall, D.J. and Tuan, R.S. A three-dimensional nanofibrous scaffold for cartilage tissue engineering using human mesenchymal stem cells. *Biomaterials*. 2005, **26**(6), pp.599-609.
16. Ortega, Í. and Ryan, A.J. and Deshpande, P. and MacNeil, S. and Claeysens, F. Combined microfabrication and electrospinning to produce 3-D architectures for corneal repair. *Acta biomaterialia*. 2013, **9**(3), pp.5511-5520.
17. Bulman, S.E. and Goswami, P. and Tronci, G. and Russell, S.J. and Carr, C. Investigation into the potential use of poly (vinyl alcohol)/methylglyoxal fibres as

- antibacterial wound dressing components. *Journal of biomaterials applications*. 2014, p.DOI: 10.1177/0885328214556159.
18. Haynie, D.T. and Khadka, D.B. and Cross, M.C. Physical properties of polypeptide electrospun nanofiber cell culture scaffolds on a wettable substrate. *Polymers*. 2012, **4**(3), pp.1535-1553.
 19. Khadka, D.B. and Haynie, D.T. Protein-and peptide-based electrospun nanofibers in medical biomaterials. *Nanomedicine: Nanotechnology, Biology and Medicine*. 2012, **8**(8), pp.1242-1262.
 20. Durham, E. and Tronci, G. and Yang, X.B. and Wood, D.J. and Russell, S.J. Nonwoven Scaffolds for Bone Regeneration. In: *Biomedical Textiles for Orthopaedic and Surgical Applications: Fundamentals, Applications and Tissue Engineering*. Elsevier, 2015, pp.45-66.
 21. Sun, B. and Jiang, X.-J. and Zhang, S. and Zhang, J.-C. and Li, Y.-F. and You, Q.-Z. and Long, Y.-Z. Electrospun anisotropic architectures and porous structures for tissue engineering. *Journal of Materials Chemistry B*. 2015, **3**(27), pp.5389-5410.
 22. Zhang, Y. and Ouyang, H. and Lim, C.T. and Ramakrishna, S. and Huang, Z.M. Electrospinning of gelatin fibers and gelatin/PCL composite fibrous scaffolds. *Journal of Biomedical Materials Research Part B: Applied Biomaterials*. 2005, **72**(1), pp.156-165.
 23. Khademhosseini, A. and Vacanti, J. and Langer, R. Progress in tissue engineering. *Scientific American Magazine*. 2009, **300**(5), pp.64-71.
 24. Li, W.J. and Laurencin, C.T. and Caterson, E.J. and Tuan, R.S. and Ko, F.K. Electrospun nanofibrous structure: a novel scaffold for tissue engineering. *Journal of biomedical materials research*. 2002, **60**(4), pp.613-621.
 25. Kim, K. and Yu, M. and Zong, X. and Chiu, J. and Fang, D. and Seo, Y.-S. and Hsiao, B.S. and Chu, B. and Hadjiargyrou, M. Control of degradation rate and hydrophilicity in electrospun non-woven poly (D, L-lactide) nanofiber scaffolds for biomedical applications. *Biomaterials*. 2003, **24**(27), pp.4977-4985.
 26. Qiao, X. and Russell, S.J. and Yang, X. and Tronci, G. and Wood, D.J. Compositional and in vitro evaluation of nonwoven type I collagen/poly-DL-lactic acid scaffolds for bone regeneration. *Journal of functional biomaterials*. 2015, **6**(3), pp.667-686.
 27. Cipitria, A. and Skelton, A. and Dargaville, T. and Dalton, P. and Hutmacher, D. Design, fabrication and characterization of PCL electrospun scaffolds—a review. *Journal of Materials Chemistry*. 2011, **21**(26), pp.9419-9453.
 28. Reed, C.R. and Han, L. and Andradý, A. and Caballero, M. and Jack, M.C. and Collins, J.B. and Saba, S.C. and Lobo, E.G. and Cairns, B.A. and van Aalst, J.A. Composite tissue engineering on polycaprolactone nanofiber scaffolds. *Annals of plastic surgery*. 2009, **62**(5), pp.505-512.
 29. Williams, J.M. and Adewunmi, A. and Schek, R.M. and Flanagan, C.L. and Krebsbach, P.H. and Feinberg, S.E. and Hollister, S.J. and Das, S. Bone tissue engineering using polycaprolactone scaffolds fabricated via selective laser sintering. *Biomaterials*. 2005, **26**(23), pp.4817-4827.
 30. Shor, L. and Güçeri, S. and Wen, X. and Gandhi, M. and Sun, W. Fabrication of three-dimensional polycaprolactone/hydroxyapatite tissue scaffolds and osteoblast-scaffold interactions in vitro. *Biomaterials*. 2007, **28**(35), pp.5291-5297.
 31. Kamath, M.S. and Ahmed, S.S. and Dhanasekaran, M. and Santosh, S.W. Polycaprolactone scaffold engineered for sustained release of resveratrol: therapeutic enhancement in bone tissue engineering. *International journal of nanomedicine*. 2014, **9**, p.183.

32. Danesin, R. and Brun, P. and Roso, M. and Delaunay, F. and Samouillan, V. and Brunelli, K. and Iucci, G. and Ghezzi, F. and Modesti, M. and Castagliuolo, I. Self-assembling peptide-enriched electrospun polycaprolactone scaffolds promote the osteoblast adhesion and modulate differentiation-associated gene expression. *Bone*. 2012, **51**, pp.851-859.
33. Powell, H.M. and Boyce, S.T. Engineered human skin fabricated using electrospun collagen–PCL blends: morphogenesis and mechanical properties. *Tissue Engineering Part A*. 2009, **15**(8), pp.2177-2187.
34. Van der Schueren, L. and De Meyer, T. and Steyaert, I. and Ceylan, Ö. and Hemelsoet, K. and Van Speybroeck, V. and De Clerck, K. Polycaprolactone and polycaprolactone/chitosan nanofibres functionalised with the pH-sensitive dye Nitrazine Yellow. *Carbohydrate Polymers*. 2012.
35. Agarwal, S. and Wendorff, J.H. and Greiner, A. Progress in the field of electrospinning for tissue engineering applications. *Advanced Materials*. 2009, **21**(32-33), pp.3343-3351.
36. Andukuri, A. and Kushwaha, M. and Tambralli, A. and Anderson, J.M. and Dean, D.R. and Berry, J.L. and Sohn, Y.D. and Yoon, Y.-S. and Brott, B.C. and Jun, H.-W. A hybrid biomimetic nanomatrix composed of electrospun polycaprolactone and bioactive peptide amphiphiles for cardiovascular implants. *Acta biomaterialia*. 2011, **7**(1), pp.225-233.
37. Hartman, O. and Zhang, C. and Adams, E.L. and Farach-Carson, M.C. and Petrelli, N.J. and Chase, B.D. and Rabolt, J.F. Biofunctionalization of electrospun PCL-based scaffolds with perlecan domain IV peptide to create a 3-D pharmacokinetic cancer model. *Biomaterials*. 2010, **31**(21), pp.5700-5718.
38. Gentsch, R. and Pippig, F. and Schmidt, S. and Cernoch, P. and Polleux, J. and Börner, H.G. Single-step electrospinning to bioactive polymer nanofibers. *Macromolecules*. 2011, **44**(3), pp.453-461.
39. Chow, L.W. and Armgarth, A. and St-Pierre, J.P. and Bertazzo, S. and Gentilini, C. and Aurisicchio, C. and McCullen, S.D. and Steele, J.A. and Stevens, M.M. Peptide-Directed Spatial Organization of Biomolecules in Dynamic Gradient Scaffolds. *Advanced healthcare materials*. 2014, **3**(9), pp.1381-1386.
40. Knapman, T.W. and Aggeli, A. and Ashcroft, A.E. Critical concentrations of β -sheet peptide self-assembly quantified directly by nanoelectrospray ionization mass spectrometry. *Rapid Communications in Mass Spectrometry*. 2008, **22**(10), pp.1611-1614.
41. Boekhoven, J. and Zha, R.H. and Tantalitti, F. and Zhuang, E. and Zandi, R. and Newcomb, C.J. and Stupp, S.I. Alginate–peptide amphiphile core–shell microparticles as a targeted drug delivery system. *RSC advances*. 2015, **5**(12), pp.8753-8756.
42. Maude, S. and Ingham, E. and Aggeli, A. Biomimetic self-assembling peptides as scaffolds for soft tissue engineering. *Nanomedicine*. 2013, **8**(5), pp.823-847.
43. Kyle, S. and Aggeli, A. and Ingham, E. and McPherson, M.J. Recombinant self-assembling peptides as biomaterials for tissue engineering. *Biomaterials*. 2010, **31**(36), pp.9395-9405.
44. Firth, A. and Aggeli, A. and Burke, J.L. and Yang, X. and Kirkham, J. Biomimetic self-assembling peptides as injectable scaffolds for hard tissue engineering. *Nanomedicine*. 2006, **1**(2), pp.189-199.
45. Brun, P. and Ghezzi, F. and Roso, M. and Danesin, R. and Palù, G. and Bagno, A. and Modesti, M. and Castagliuolo, I. and Dettin, M. Electrospun scaffolds of self-

- assembling peptides with poly (ethylene oxide) for bone tissue engineering. *Acta biomaterialia*. 2011, **7**(6), pp.2526-2532.
46. Maude, S. and Miles, D.E. and Felton, S.H. and Ingram, J. and Carrick, L.M. and Wilcox, R.K. and Ingham, E. and Aggeli, A. De novo designed positively charged tape-forming peptides: self-assembly and gelation in physiological solutions and their evaluation as 3D matrices for cell growth. *Soft Matter*. 2011, **7**(18), pp.8085-8099.
 47. Aggeli, A. and Bell, M. and Carrick, L.M. and Fishwick, C.W. and Harding, R. and Mawer, P.J. and Radford, S.E. and Strong, A.E. and Boden, N. pH as a trigger of peptide β -sheet self-assembly and reversible switching between nematic and isotropic phases. *Journal of the American Chemical Society*. 2003, **125**(32), pp.9619-9628.
 48. Carrick, L.M. and Aggeli, A. and Boden, N. and Fisher, J. and Ingham, E. and Waigh, T.A. Effect of ionic strength on the self-assembly, morphology and gelation of pH responsive β -sheet tape-forming peptides. *Tetrahedron*. 2007, **63**(31), pp.7457-7467.
 49. Kyle, S. and Aggeli, A. and Ingham, E. and McPherson, M.J. Production of self-assembling biomaterials for tissue engineering. *Trends in biotechnology*. 2009, **27**(7), pp.423-433.
 50. Kirkham, J. and Firth, A. and Vernals, D. and Boden, N. and Robinson, C. and Shore, R. and Brookes, S. and Aggeli, A. Self-assembling peptide scaffolds promote enamel remineralization. *Journal of dental research*. 2007, **86**(5), pp.426-430.
 51. Wilshaw, S. and Aggeli, A. and Fisher, J. and Ingham, E. The biocompatibility and immunogenicity of self-assembling peptides for use in tissue engineering and regenerative applications. *Tissue Engineering. Part A*. 2008, **14**(5), p.785.
 52. Burke, J.L. *In situ engineering of skeletal tissues using self-assembled biomimetic scaffolds*. thesis, PhD thesis, University of Leeds, 2011.
 53. Burke, J.L. and Aggeli, A. and Wilshaw, S. and Davies, R.P. and Firth, A. and Kang, J. and Yang, X.Y. and Brookes, S.J. and Kirkham, J. *Self-assembling Peptide Fibrillar Networks as Biomimetic Scaffolds in Bone Regeneration and Repair*. Unpublished, 2017.
 54. Semino, C. Self-assembling peptides: from bio-inspired materials to bone regeneration. *Journal of dental research*. 2008, **87**(7), pp.606-616.
 55. Brunton, P. and Davies, R. and Burke, J. and Smith, A. and Aggeli, A. and Brookes, S. and Kirkham, J. Treatment of early caries lesions using biomimetic self-assembling peptides—a clinical safety trial. *British dental journal*. 2013, **215**(4), pp.E6-E6.
 56. De Yoreo, J.J. and Vekilov, P.G. Principles of crystal nucleation and growth. *Reviews in mineralogy and geochemistry*. 2003, **54**(1), pp.57-93.
 57. Naka, K. and Chujo, Y. Control of crystal nucleation and growth of calcium carbonate by synthetic substrates. *Chemistry of Materials*. 2001, **13**(10), pp.3245-3259.
 58. Fornari, R. and Paorici, C. *Theoretical and Technological Aspects of Crystal Growth: Proceedings of the 10th International Summer School on Crystal Growth, ISSCG-10, Rimini, Italy, June 1998*. Trans Tech Publication, 1998.
 59. Markov, I.V. *Crystal growth for beginners: fundamentals of nucleation, crystal growth and epitaxy*. World Scientific, 2003.
 60. Mann, S. *Biomaterialization: principles and concepts in bioinorganic materials chemistry*. Oxford University Press on Demand, 2001.
 61. Brown, P.W. and Constantz, B. *Hydroxyapatite and related materials*. CRC press, 1994.
 62. Rey, C. and Combes, C. and Drouet, C. and Glimcher, M.J. Bone mineral: update on chemical composition and structure. *Osteoporosis International*. 2009, **20**(6), pp.1013-1021.

63. Bilezikian, J.P. and Raisz, L.G. and Martin, T.J. *Principles of Bone Biology: Two-Volume Set*. Academic Press, 2008.
64. Karsenty, G. and Wagner, E.F. Reaching a genetic and molecular understanding of skeletal development. *Developmental cell*. 2002, **2**(4), pp.389-406.
65. Parfitt, A. Osteonal and hemi-osteonal remodeling: the spatial and temporal framework for signal traffic in adult human bone. *Journal of cellular biochemistry*. 1994, **55**(3), pp.273-286.
66. Fukumoto, S. and Yamada, Y. Review: extracellular matrix regulates tooth morphogenesis. *Connective tissue research*. 2005, **46**(4-5), pp.220-226.
67. Burstein, A.H. and Zika, J. and Heiple, K. and Klein, L. Contribution of collagen and mineral to the elastic-plastic properties of bone. *J Bone Joint Surg Am*. 1975, **57**(7), pp.956-961.
68. Zachrisson, B.U. and Mjör, I.A. Remodeling of teeth by grinding. *American journal of orthodontics*. 1975, **68**(5), pp.545-553.
69. Zhong, B. and Peng, C. and Wang, G. and Tian, L. and Cai, Q. and Cui, F. Contemporary research findings on dentine remineralization. *Journal of tissue engineering and regenerative medicine*. 2015, **9**(9), pp.1004-1016.
70. Hansen, R. *The role of dentin in tooth fracture*. [Online]. 2008. [Accessed]. Available from: <https://str.llnl.gov/str/JanFeb08/kinney.html>
71. Amini, A.R. and Laurencin, C.T. and Nukavarapu, S.P. Bone tissue engineering: recent advances and challenges. *Critical Reviews™ in Biomedical Engineering*. 2012, **40**(5).
72. Baroli, B. From natural bone grafts to tissue engineering therapeutics: brainstorming on pharmaceutical formulative requirements and challenges. *Journal of pharmaceutical sciences*. 2009, **98**(4), pp.1317-1375.
73. Gazdag, A.R. and Lane, J.M. and Glaser, D. and Forster, R.A. Alternatives to autogenous bone graft: efficacy and indications. *Journal of the American Academy of Orthopaedic Surgeons*. 1995, **3**(1), pp.1-8.
74. Bhatt, R.A. and Rozental, T.D. Bone graft substitutes. *Hand clinics*. 2012, **28**(4), pp.457-468.
75. Payne, K.F. and Balasundaram, I. and Deb, S. and Di Silvio, L. and Fan, K.F. Tissue engineering technology and its possible applications in oral and maxillofacial surgery. *British Journal of Oral and Maxillofacial Surgery*. 2014, **52**(1), pp.7-15.
76. Yang, S. and Leong, K.-F. and Du, Z. and Chua, C.-K. The design of scaffolds for use in tissue engineering. Part I. Traditional factors. *Tissue engineering*. 2001, **7**(6), pp.679-689.
77. Drury, J.L. and Mooney, D.J. Hydrogels for tissue engineering: scaffold design variables and applications. *Biomaterials*. 2003, **24**(24), pp.4337-4351.
78. Fleischer, S. and Dvir, T. Tissue engineering on the nanoscale: lessons from the heart. *Current opinion in biotechnology*. 2012.
79. Vats, A. and Tolley, N. and Polak, J. and Gough, J. Scaffolds and biomaterials for tissue engineering: a review of clinical applications. *Clinical Otolaryngology & Allied Sciences*. 2003, **28**(3), pp.165-172.
80. Vasita, R. and Katti, D.S. Nanofibers and their applications in tissue engineering. *International journal of nanomedicine*. 2006, **1**(1), p.15.
81. Cooper, M.L. and Hansbrough, J.F. and Spielvogel, R.L. and Cohen, R. and Bartel, R.L. and Naughton, G. *In vivo* optimization of a living dermal substitute employing cultured human fibroblasts on a biodegradable polyglycolic acid or polyglactin mesh. *Biomaterials*. 1991, **12**(2), pp.243-248.

82. Cima, L.G. and Ingber, D.E. and Vacanti, J.P. and Langer, R. Hepatocyte culture on biodegradable polymeric substrates. *Biotechnology and bioengineering*. 1991, **38**(2), pp.145-158.
83. Evans, G. and Brandt, K. and Widmer, M. and Lu, L. and Meszlenyi, R. and Gupta, P. and Mikos, A. and Hodges, J. and Williams, J. and Gürlek, A. In vivo evaluation of poly (L-lactic acid) porous conduits for peripheral nerve regeneration. *Biomaterials*. 1999, **20**(12), pp.1109-1115.
84. Hutmacher, D.W. Scaffolds in tissue engineering bone and cartilage. *Biomaterials*. 2000, **21**(24), pp.2529-2543.
85. Simske, S. and Ayers, R. and Bateman, T. Porous materials for bone engineering. In: *Materials Science Forum*: Trans Tech Publ, 1997, pp.151-182.
86. Yilin Cao, M. and Clemente Ibarra, M. and Vacanti, C.A. Tissue engineering cartilage and bone. *Synthetic biodegradable polymer scaffolds*. 1997, p.199.
87. Regauer, M. and Jürgens, I. and Kotsianos, D. and Stütze, H. and Mutschler, W. and Schieker, M. [New-bone formation by osteogenic protein-1 and autogenic bone marrow in a critical tibial defect model in sheep]. *Zentralblatt für Chirurgie*. 2005, **130**(4), pp.338-345.
88. Bleiziffer, O. and Eriksson, E. and Yao, F. and Horch, R.E. and Kneser, U. Gene transfer strategies in tissue engineering. *Journal of cellular and molecular medicine*. 2007, **11**(2), pp.206-223.
89. Aibibu, D. and Hild, M. and Wöltje, M. and Cherif, C. Textile cell-free scaffolds for in situ tissue engineering applications. *Journal of Materials Science: Materials in Medicine*. 2016, **27**(3), pp.1-20.
90. Galler, K.M. and Eidt, A. and Schmalz, G. Cell-free approaches for dental pulp tissue engineering. *Journal of endodontics*. 2014, **40**(4), pp.S41-S45.
91. Chen, F.-M. and Wu, L.-A. and Zhang, M. and Zhang, R. and Sun, H.-H. Homing of endogenous stem/progenitor cells for in situ tissue regeneration: promises, strategies, and translational perspectives. *Biomaterials*. 2011, **32**(12), pp.3189-3209.
92. Li, S. and Sengupta, D. and Chien, S. Vascular tissue engineering: from in vitro to in situ. *Wiley Interdisciplinary Reviews: Systems Biology and Medicine*. 2014, **6**(1), pp.61-76.
93. Bell, J.H. and Haycock, J.W. Next generation nerve guides: materials, fabrication, growth factors, and cell delivery. *Tissue Engineering Part B: Reviews*. 2011, **18**(2), pp.116-128.
94. Bueno, E.M. and Glowacki, J. Cell-free and cell-based approaches for bone regeneration. *Nature Reviews Rheumatology*. 2009, **5**(12), pp.685-697.
95. Dvir, T. and Timko, B.P. and Kohane, D.S. and Langer, R. Nanotechnological strategies for engineering complex tissues. *Nature nanotechnology*. 2010, **6**(1), pp.13-22.
96. Hynes, R.O. The extracellular matrix: not just pretty fibrils. *Science*. 2009, **326**(5957), pp.1216-1219.
97. Chen, G. and Ushida, T. and Tateishi, T. Scaffold design for tissue engineering. *Macromolecular Bioscience*. 2002, **2**(2), pp.67-77.
98. Lutolf, M. and Hubbell, J. Synthetic biomaterials as instructive extracellular microenvironments for morphogenesis in tissue engineering. *Nature biotechnology*. 2005, **23**(1), pp.47-55.
99. Mooney, D.J. and Baldwin, D.F. and Suh, N.P. and Vacanti, J.P. and Langer, R. Novel approach to fabricate porous sponges of poly (D, L-lactic-co-glycolic acid) without the use of organic solvents. *Biomaterials*. 1996, **17**(14), pp.1417-1422.

100. Cima, L. and Vacanti, J. and Vacanti, C. and Ingber, D. and Mooney, D. and Langer, R. Tissue engineering by cell transplantation using degradable polymer substrates. *Journal of biomechanical engineering*. 1991, **113**(2), pp.143-151.
101. Hutmacher, D.W. Scaffold design and fabrication technologies for engineering tissues—state of the art and future perspectives. *Journal of Biomaterials Science, Polymer Edition*. 2001, **12**(1), pp.107-124.
102. Cohen, S. and Baño, M.C. and Cima, L.G. and Allcock, H.R. and Vacanti, J.P. and Vacanti, C.A. and Langer, R. Design of synthetic polymeric structures for cell transplantation and tissue engineering. *Clinical materials*. 1993, **13**(1), pp.3-10.
103. Whang, K. and Healy, K. and Elenz, D. and Nam, E. and Tsai, D. and Thomas, C. and Nuber, G. and Glorieux, F. and Travers, R. and Sprague, S. Engineering bone regeneration with bioabsorbable scaffolds with novel microarchitecture. *Tissue engineering*. 1999, **5**(1), pp.35-51.
104. Chiang, C.-Y. and Kyritsis, G. and Graves, D.T. and Amar, S. Interleukin-1 and tumor necrosis factor activities partially account for calvarial bone resorption induced by local injection of lipopolysaccharide. *Infection and immunity*. 1999, **67**(8), pp.4231-4236.
105. Groeneveld, E. and Burger, E. Bone morphogenetic proteins in human bone regeneration. *European Journal of Endocrinology*. 2000, **142**(1), pp.9-21.
106. Smoljanović, T. and Grgurević, L. and Jelić, M. and Kreszinger, M. and Hašpl, M. and Matičić, D. and Vukičević, S. and Pečina, M. Regeneration of the skeleton by recombinant human bone morphogenetic proteins. *Collegium antropologicum*. 2007, **31**(3), pp.923-932.
107. Glowacki, J. and Mizuno, S. Collagen scaffolds for tissue engineering. *Biopolymers*. 2008, **89**(5), pp.338-344.
108. Jerome, R. and Maquet, V. Design of macroporous biodegradable polymer scaffolds for cell transplantation. In: *Materials Science Forum: Trans Tech Publ*, 1997, pp.15-42.
109. Burg, K.J. and Porter, S. and Kellam, J.F. Biomaterial developments for bone tissue engineering. *Biomaterials*. 2000, **21**(23), pp.2347-59.
110. Choong, C.S. and Hutmacher, D.W. and Triffitt, J.T. Co-culture of bone marrow fibroblasts and endothelial cells on modified polycaprolactone substrates for enhanced potentials in bone tissue engineering. *Tissue engineering*. 2006, **12**(9), pp.2521-2531.
111. Thomas, V. and Jagani, S. and Johnson, K. and Jose, M.V. and Dean, D.R. and Vohra, Y.K. and Nyairo, E. Electrospun bioactive nanocomposite scaffolds of polycaprolactone and nanohydroxyapatite for bone tissue engineering. *Journal of nanoscience and nanotechnology*. 2006, **6**(2), pp.487-493.
112. Guarino, V. and Causa, F. and Taddei, P. and Foggia, M. and Ciapetti, G. and Martini, D. and Fagnano, C. and Baldini, N. and Ambrosio, L. Polylactic acid fibre-reinforced polycaprolactone scaffolds for bone tissue engineering. *Biomaterials*. 2008, **29**(27), pp.3662-3670.
113. Shor, L. and Güçeri, S. and Chang, R. and Gordon, J. and Kang, Q. and Hartsock, L. and An, Y. and Sun, W. Precision extruding deposition (PED) fabrication of polycaprolactone (PCL) scaffolds for bone tissue engineering. *Biofabrication*. 2009, **1**(1), p.015003.
114. Kyriakidou, K. and Lucarini, G. and Zizzi, A. and Salvolini, E. and Belmonte, M.M. and Mollica, F. and Gloria, A. and Ambrosio, L. Dynamic co-seeding of osteoblast and endothelial cells on 3D polycaprolactone scaffolds for enhanced bone tissue engineering. *Journal of bioactive and compatible polymers*. 2008, **23**(3), pp.227-243.

115. Van der Schueren, L. and De Schoenmaker, B. and Kalaoglu, Ö.I. and De Clerck, K. An alternative solvent system for the steady state electrospinning of polycaprolactone. *European Polymer Journal*. 2011.
116. Middleton, J.C. and Tipton, A.J. Synthetic biodegradable polymers as orthopedic devices. *Biomaterials*. 2000, **21**(23), pp.2335-2346.
117. Darling, A.L. and Sun, W. 3D microtomographic characterization of precision extruded poly- ϵ -caprolactone scaffolds. *Journal of Biomedical Materials Research Part B: Applied Biomaterials*. 2004, **70**(2), pp.311-317.
118. Engelberg, I. and Kohn, J. Physico-mechanical properties of degradable polymers used in medical applications: a comparative study. *Biomaterials*. 1991, **12**(3), pp.292-304.
119. Hutmacher, D.W. and Schantz, T. and Zein, I. and Ng, K.W. and Teoh, S.H. and Tan, K.C. Mechanical properties and cell cultural response of polycaprolactone scaffolds designed and fabricated via fused deposition modeling. *Journal of biomedical materials research*. 2001, **55**(2), pp.203-216.
120. Burg, K.J. and Porter, S. and Kellam, J.F. Biomaterial developments for bone tissue engineering. *Biomaterials*. 2000, **21**(23), pp.2347-2359.
121. Hubbell, J.A. Materials as morphogenetic guides in tissue engineering. *Current opinion in biotechnology*. 2003, **14**(5), pp.551-558.
122. Ma, P.X. and Elisseeff, J. *Scaffolding in tissue engineering*. CRC press, 2005.
123. McCarty, M. Life of bionics founder a fine adventure. *Dayton Daily News. Thursday, January*. 2009, **29**, p.2009.
124. Holzwarth, J.M. and Ma, P.X. Biomimetic nanofibrous scaffolds for bone tissue engineering. *Biomaterials*. 2011, **32**(36), pp.9622-9629.
125. Antebi, B. and Cheng, X. and Harris, J.N. and Gower, L.B. and Chen, X.-D. and Ling, J. Biomimetic collagen-hydroxyapatite composite fabricated via a novel perfusion-flow mineralization technique. *Tissue Engineering Part C: Methods*. 2013, **19**(7), pp.487-496.
126. Danishefsky, I. *Biochemistry for medical sciences*. Boston: Little Brown., 1980.
127. Elliott, W.H. *Biochemistry and molecular biology*. Oxford: Oxford University Press., 2005.
128. S., D. *Peptides and Proteins*. Royal Society of Chemistry, 2002.
129. Alazragi, R.S. *Self-assembling peptides as biofunctional component in medical fabrics*. thesis, University of Leeds, 2014.
130. Xiong, H. and Buckwalter, B.L. and Shieh, H.-M. and Hecht, M.H. Periodicity of polar and nonpolar amino acids is the major determinant of secondary structure in self-assembling oligomeric peptides. *Proceedings of the National Academy of Sciences*. 1995, **92**(14), pp.6349-6353.
131. Dobson, C.M. Protein misfolding, evolution and disease. *Trends in biochemical sciences*. 1999, **24**(9), pp.329-332.
132. Stephanopoulos, N. and Ortony, J.H. and Stupp, S.I. Self-assembly for the synthesis of functional biomaterials. *Acta Materialia*. 2013, **61**(3), pp.912-930.
133. Lim, Y.-b. and Lee, M. Nanostructures of β -sheet peptides: steps towards bioactive functional materials. *Journal of Materials Chemistry*. 2008, **18**(7), pp.723-727.
134. Whitesides, G.M. and Mathias, J.P. and Seto, C.T. *Molecular self-assembly and nanochemistry: a chemical strategy for the synthesis of nanostructures*. DTIC Document, 1991.
135. Dahlin, R.L. and Kasper, F.K. and Mikos, A.G. Polymeric Nanofibers in Tissue Engineering. *Tissue Engineering Part B: Reviews*. 2011, **17**(5), pp.349-364.
136. Holmes, T.C. Novel peptide-based biomaterial scaffolds for tissue engineering. *Trends in biotechnology*. 2002, **20**(1), pp.16-21.

137. Aggeli, A. and Bell, M. and Boden, N. and Carrick, L.M. and Strong, A.E. Self-Assembling Peptide Polyelectrolyte β -Sheet Complexes Form Nematic Hydrogels. *Angewandte Chemie International Edition*. 2003, **42**(45), pp.5603-5606.
138. Aggeli, A., Bell, M., Boden, N. and Keen, J.N., 1997. Responsive gels formed by the spontaneous self-assembly of peptides into polymeric beta-sheet tapes. *Nature*, 386(6622), p.259.
139. Maude, S. *Design and Characterisation of Functionalised Self-Assembled Peptide Nanostructures*. PhD thesis, University of Leeds, 2010.
140. Aggeli, A. and Nyrkova, I. and Bell, M. and Harding, R. and Carrick, L. and McLeish, T. and Semenov, A. and Boden, N. Hierarchical self-assembly of chiral rod-like molecules as a model for peptide β -sheet tapes, ribbons, fibrils, and fibers. *Proceedings of the National Academy of Sciences*. 2001, **98**(21), pp.11857-11862.
141. Chothia, C. Conformation of twisted β -pleated sheets in proteins. *Journal of molecular biology*. 1973, **75**(2), pp.295-302.
142. Kyle, S. and Felton, S.H. and McPherson, M.J. and Aggeli, A. and Ingham, E. Rational Molecular Design of Complementary Self-Assembling Peptide Hydrogels. *Advanced healthcare materials*. 2012, **1**(5), pp.640-645.
143. Kyle, S.A. and McPherson, M.J. and Ingham, E. The self-assembling peptide, p11-4 as a scaffold for use in regenerative medicine. *European Cells and Materials*. 2008, **16**(3), p.1.
144. Hartgerink, J.D. and Beniash, E. and Stupp, S.I. Self-assembly and mineralization of peptide-amphiphile nanofibers. *Science*. 2001, **294**(5547), pp.1684-1688.
145. Sargeant, T.D. and Guler, M.O. and Oppenheimer, S.M. and Mata, A. and Satcher, R.L. and Dunand, D.C. and Stupp, S.I. Hybrid bone implants: self-assembly of peptide amphiphile nanofibers within porous titanium. *Biomaterials*. 2008, **29**(2), pp.161-171.
146. Kretsinger, J.K. and Haines, L.A. and Ozbas, B. and Pochan, D.J. and Schneider, J.P. Cytocompatibility of self-assembled β -hairpin peptide hydrogel surfaces. *Biomaterials*. 2005, **26**(25), pp.5177-5186.
147. He, G. and Dahl, T. and Veis, A. and George, A. Nucleation of apatite crystals in vitro by self-assembled dentin matrix protein 1. *Nature materials*. 2003, **2**(8), pp.552-558.
148. Koopmans, R.J. and Aggeli, A. Nanobiotechnology—quo vadis? *Current Opinion in Microbiology*. 2010, **13**(3), p.327.
149. *Effect of P11-4 in patients with carious lesions* [Online]. Available from: <http://england.ukcrn.org.uk/StudyDetail.aspx?StudyID=9473>
150. Wright, J.T. and Carrion, I. and Morris, C. The molecular basis of hereditary enamel defects in humans. *Journal of dental research*. 2015, **94**(1), pp.52-61.
151. Eyre, D.R. and Weis, M.A. Bone collagen: new clues to its mineralization mechanism from recessive osteogenesis imperfecta. *Calcified tissue international*. 2013, **93**(4), pp.338-347.
152. Ma, Z. and Kotaki, M. and Inai, R. and Ramakrishna, S. Potential of nanofiber matrix as tissue-engineering scaffolds. *Tissue engineering*. 2005, **11**(1-2), pp.101-109.
153. Cui, W. and Li, X. and Xie, C. and Chen, J. and Zou, J. and Zhou, S. and Weng, J. Controllable growth of hydroxyapatite on electrospun poly (dl-lactide) fibers grafted with chitosan as potential tissue engineering scaffolds. *Polymer*. 2010, **51**(11), pp.2320-2328.
154. Gouma, P.-I. and Ramachandran, K. Electrospinning for bone tissue engineering. *Recent patents on nanotechnology*. 2008, **2**(1), pp.1-7.
155. Li, W.J. and Danielson, K.G. and Alexander, P.G. and Tuan, R.S. Biological response of chondrocytes cultured in three-dimensional nanofibrous poly (ϵ -caprolactone)

- scaffolds. *Journal of Biomedical Materials Research Part A*. 2003, **67**(4), pp.1105-1114.
156. Wutticharoenmongkol, P. and Sanchavanakit, N. and Pavasant, P. and Supaphol, P. Preparation and characterization of novel bone scaffolds based on electrospun polycaprolactone fibers filled with nanoparticles. *Macromolecular Bioscience*. 2006, **6**(1), pp.70-77.
 157. Nuansing, W. and Frauchiger, D. and Huth, F. and Rebollo, A. and Hillenbrand, R. and Bittner, A.M. Electrospinning of peptide and protein fibres: approaching the molecular scale. *Faraday discussions*. 2013, **166**, pp.209-221.
 158. Tayi, A.S. and Pashuck, E.T. and Newcomb, C.J. and McClendon, M.T. and Stupp, S.I. Electrospinning Bioactive Supramolecular Polymers from Water. *Biomacromolecules*. 2014, **15**(4), pp.1323-1327.
 159. Wu, X.F. and Salkovskiy, Y. and Dzenis, Y.A. Modeling of solvent evaporation from polymer jets in electrospinning. *Applied Physics Letters*. 2011, **98**(22), pp.223108-223108-3.
 160. Li, D. and Xia, Y. Electrospinning of nanofibers: reinventing the wheel? *Advanced Materials*. 2004, **16**(14), pp.1151-1170.
 161. Seeram Ramakrishna, K.F., Wee-Eong Teo, . *An introduction to Electrospinning and Nanofibers*. Singapore: world scientific publishing Co. Pte. Ltd., 2005.
 162. Ke, P. and Jiao, X.-N. and Ge, X.-H. and Xiao, W.-M. and Yu, B. From macro to micro: structural biomimetic materials by electrospinning. *RSC advances*. 2014, **4**(75), pp.39704-39724.
 163. Yu, D. and Branford-White, C. and White, K. and Chatterton, N. and Zhu, L. and Huang, L. and Wang, B. A modified coaxial electrospinning for preparing fibers from a high concentration polymer solution. *Express Polym Lett*. 2011, **5**, pp.732-741.
 164. Wannatong, L. and Sirivat, A. and Supaphol, P. Effects of solvents on electrospun polymeric fibers: preliminary study on polystyrene. *Polymer International*. 2004, **53**(11), pp.1851-1859.
 165. Tao, J. and Shivkumar, S. Molecular weight dependent structural regimes during the electrospinning of PVA. *Materials Letters*. 2007, **61**(11), pp.2325-2328.
 166. Cengiz, F. and Krucińska, I. and Gliścińska, E. and Chrzanowski, M. and Göktepe, F. Comparative analysis of various electrospinning methods of nanofibre formation. *Fibres & Textiles in Eastern Europe*. 2009, **17**(1), p.72.
 167. Ramakrishna, S. and Fujihara, K. and Teo, W.-E. and Lim, T.-C. and Ma, Z. *An introduction to electrospinning and nanofibers*. World Scientific, 2005.
 168. Choi, J.S. and Lee, S.W. and Jeong, L. and Bae, S.-H. and Min, B.C. and Youk, J.H. and Park, W.H. Effect of organosoluble salts on the nanofibrous structure of electrospun poly (3-hydroxybutyrate-co-3-hydroxyvalerate). *International Journal of Biological Macromolecules*. 2004, **34**(4), pp.249-256.
 169. Zhang, C. and Yuan, X. and Wu, L. and Han, Y. and Sheng, J. Study on morphology of electrospun poly (vinyl alcohol) mats. *European Polymer Journal*. 2005, **41**(3), pp.423-432.
 170. Uyar, T. and Besenbacher, F. Electrospinning of uniform polystyrene fibers: The effect of solvent conductivity. *Polymer*. 2008, **49**(24), pp.5336-5343.
 171. Zong, X. and Kim, K. and Fang, D. and Ran, S. and Hsiao, B.S. and Chu, B. Structure and process relationship of electrospun bioabsorbable nanofiber membranes. *Polymer*. 2002, **43**(16), pp.4403-4412.
 172. Lee, J.S. and Choi, K.H. and Ghim, H.D. and Kim, S.S. and Chun, D.H. and Kim, H.Y. and Lyoo, W.S. Role of molecular weight of atactic poly (vinyl alcohol)(PVA) in the

- structure and properties of PVA nanofabric prepared by electrospinning. *Journal of Applied Polymer Science*. 2004, **93**(4), pp.1638-1646.
173. Buchko, C.J. and Chen, L.C. and Shen, Y. and Martin, D.C. Processing and microstructural characterization of porous biocompatible protein polymer thin films. *Polymer*. 1999, **40**(26), pp.7397-7407.
 174. Deitzel, J.M. and Kleinmeyer, J. and Harris, D. and Tan, N.B. The effect of processing variables on the morphology of electrospun nanofibers and textiles. *Polymer*. 2001, **42**(1), pp.261-272.
 175. Downes, L.A.B.a.S. *Electrospinning for tissue regeneration* Cambridge: woodhead publishing limited, 2011.
 176. Kilic, A. and Oruc, F. and Demir, A. Effects of polarity on electrospinning process. *Textile Research Journal*. 2008, **78**(6), pp.532-539.
 177. Supaphol, P. and Mit-upatham, C. and Nithitanakul, M. Ultrafine Electrospun Polyamide-6 Fibers: Effects of Solvent System and Emitting Electrode Polarity on Morphology and Average Fiber Diameter. *Macromolecular Materials and Engineering*. 2005, **290**(9), pp.933-942.
 178. Jeun, J. and Kim, Y. and Lim, Y. and Choi, J. and Jung, C. and Kang, P. and Nho, Y. Electrospinning of Poly (L-lactide-co-D, L-lactide). *JOURNAL OF INDUSTRIAL AND ENGINEERING CHEMISTRY-SEOUL-*. 2007, **13**(4), p.592.
 179. Tambralli, A. and Blakeney, B. and Anderson, J. and Kushwaha, M. and Andukuri, A. and Dean, D. and Jun, H.W. A hybrid biomimetic scaffold composed of electrospun polycaprolactone nanofibers and self-assembled peptide amphiphile nanofibers. *Biofabrication*. 2009, **1**, p.025001.
 180. Sill, T.J. and Von Recum, H.A. Electrospinning: applications in drug delivery and tissue engineering. *Biomaterials*. 2008, **29**(13), pp.1989-2006.
 181. Yu, D.-G. and Zhu, L.-M. and White, K. and Branford-White, C. Electrospun nanofiber-based drug delivery systems. *Health*. 2009, **1**(2), pp.67-75.
 182. Bose, S. and Roy, M. and Bandyopadhyay, A. Recent advances in bone tissue engineering scaffolds. *Trends in biotechnology*. 2012, **30**(10), pp.546-554.
 183. Wirth, R. Focused Ion Beam (FIB) combined with SEM and TEM: Advanced analytical tools for studies of chemical composition, microstructure and crystal structure in geomaterials on a nanometre scale. *Chemical Geology*. 2009, **261**(3), pp.217-229.
 184. Saville, P.H.G.a.B.P. *Microscopy of Textile Fibres*. Oxford: BIOS Scientific Publishers Ltd., 1995.
 185. Gharaei, R. *Design of a Novel Nano-Fibrous Assembly of Poly ϵ -Caprolactone/Self-Assembly Peptide for Tissue Engineering Applications*. MSc thesis, University of Leeds, 2012.
 186. Williams, D.B. and Carter, C.B. *The Transmission Electron Microscope*. Springer, 1996.
 187. Gai, P.L. and Boyes, E.D. Environmental high resolution electron microscopy in materials science. In: *In-Situ Microscopy in Materials Research*. Springer, 1997, pp.123-147.
 188. Hutzler, P. and Fischbach, R. and Heller, W. and Jungblut, T.P. and Reuber, S. and Schmitz, R. and Veit, M. and Weissenböck, G. and Schnitzler, J.-P. Tissue localization of phenolic compounds in plants by confocal laser scanning microscopy. *Journal of Experimental Botany*. 1998, **49**(323), pp.953-965.
 189. Goldstein, J. and Newbury, D.E. and Joy, D.C. and Lyman, C.E. and Echlin, P. and Lifshin, E. and Sawyer, L. and Michael, J.R. *Scanning electron microscopy and X-ray microanalysis*. Springer, 2003.
 190. Drenth, J. *X-Ray Crystallography*. Wiley Online Library, 2007.

191. Introduction to Fourier Transform Infrared Spectrometry. *Thermo Nicolet Corporation*. 2001.
192. Amenabar, I. and Poly, S. and Nuansing, W. and Hubrich, E.H. and Govyadinov, A.A. and Huth, F. and Krutokhvostov, R. and Zhang, L. and Knez, M. and Heberle, J. Structural analysis and mapping of individual protein complexes by infrared nanospectroscopy. *Nature communications*. 2013, **4**.
193. Adochitei, A. and Drochioiu, G. Rapid characterization of peptide secondary structure by FT-IR spectroscopy. *Rev Roum Chim*. 2011, **56**(8), pp.783-791.
194. Sreerama, N. and Woody, R.W. Estimation of protein secondary structure from circular dichroism spectra: comparison of CONTIN, SELCON, and CDSSTR methods with an expanded reference set. *Analytical biochemistry*. 2000, **287**(2), pp.252-260.
195. STANDARD, B. *Biological evaluation of medical devices, Part 12: Sample preparation and reference materials* 2007.
196. STANDARD, B. *Biological evaluation of medical devices, Part 5: Test for in vitro cytotoxicity* 2009.
197. Promega, C. 96® Aqueous One Solution Cell Proliferation Assay. *Technical Bulletin*. 2005.
198. STANDARD, B. *Implants for surgery - In vitro evaluation for apatite-forming ability of implant materials*. 2014.
199. Poologasundarampillai, G. and Wang, D. and Li, S. and Nakamura, J. and Bradley, R. and Lee, P. and Stevens, M. and McPhail, D. and Kasuga, T. and Jones, J. Cotton-wool-like bioactive glasses for bone regeneration. *Acta biomaterialia*. 2014, **10**(8), pp.3733-3746.
200. Kayser, V. and Turton, D.A. and Aggeli, A. and Beevers, A. and Reid, G.D. and Beddard, G.S. Energy migration in novel pH-triggered self-assembled β -sheet ribbons. *Journal of the American Chemical Society*. 2004, **126**(1), pp.336-343.
201. Hunter, G.K. and Hauschka, P.V. and Poole, R.A. and Rosenberg, L.C. and Goldberg, H.A. Nucleation and inhibition of hydroxyapatite formation by mineralized tissue proteins. *Biochemical Journal*. 1996, **317**(1), pp.59-64.
202. Hunter, G.K. and Goldberg, H.A. Nucleation of hydroxyapatite by bone sialoprotein. *Proceedings of the National Academy of Sciences*. 1993, **90**(18), pp.8562-8565.
203. Hunter, G.K. and Goldberg, H.A. Modulation of crystal formation by bone phosphoproteins: role of glutamic acid-rich sequences in the nucleation of hydroxyapatite by bone sialoprotein. *Biochemical Journal*. 1994, **302**(1), pp.175-179.
204. Chen Jr, P. and Toribara, T.t. and Warner, H. Microdetermination of phosphorus. *Analytical chemistry*. 1956, **28**(11), pp.1756-1758.
205. Aggeli, A. and Bell, M. and Boden, N. and Keen, J. and Knowles, P. and McLeish, T. and Pitkeathly, M. and Radford, S. Responsive gels formed by the spontaneous self-assembly of peptides into polymeric β -sheet tapes. *Nature*. 1997, **386**, pp.259-262.
206. Davies, R. and Aggeli, A. and Beevers, A. and Boden, N. and Carrick, L. and Fishwick, C. and McLeish, T. and Nyrkova, I. and Semenov, A. Self-assembling β -sheet tape forming peptides. *Supramolecular Chemistry*. 2006, **18**(5), pp.435-443.
207. Nordén, B. *Circular dichroism and linear dichroism*. Oxford University Press, USA, 1997.
208. Adler, A.J. and Greenfield, N.J. and Fasman, G.D. [27] Circular dichroism and optical rotatory dispersion of proteins and polypeptides. *Methods in enzymology*. 1973, **27**, pp.675-735.
209. Greenfield, N.J. and Fasman, G.D. Computed circular dichroism spectra for the evaluation of protein conformation. *Biochemistry*. 1969, **8**(10), pp.4108-4116.

210. Johnson, W.C. Protein secondary structure and circular dichroism: a practical guide. *Proteins: Structure, Function, and Bioinformatics*. 1990, **7**(3), pp.205-214.
211. Castelletto, V. and Kirkham, S. and Hamley, I.W. and Kowalczyk, R.M. and Rabe, M. and Reza, M. and Ruokolainen, J. Self-Assembly of the Toll-like Receptor Agonist Macrophage-Activating Lipopeptide MALP-2 and of its Constituent Peptide. *Biomacromolecules*. 2016, p.doi: 10.1021/acs.biomac.5b01573.
212. Elzein, T. and Nasser-Eddine, M. and Delaite, C. and Bistac, S. and Dumas, P. FTIR study of polycaprolactone chain organization at interfaces. *Journal of colloid and interface science*. 2004, **273**(2), pp.381-387.
213. Barth, A. The infrared absorption of amino acid side chains. *Progress in biophysics and molecular biology*. 2000, **74**(3), pp.141-173.
214. Birjandi, F.C. and Sargolzaei, J. Super-non-wettable surfaces: A review. *Colloids and Surfaces A: Physicochemical and Engineering Aspects*. 2014, **448**, pp.93-106.
215. Kim, C.H. and Khil, M.S. and Kim, H.Y. and Lee, H.U. and Jahng, K.Y. An improved hydrophilicity via electrospinning for enhanced cell attachment and proliferation. *Journal of Biomedical Materials Research Part B: Applied Biomaterials*. 2006, **78**(2), pp.283-290.
216. Huang, F. and Wei, Q. and Cai, Y. and Wu, N. Surface structures and contact angles of electrospun poly (vinylidene fluoride) nanofiber membranes. *International Journal of Polymer Analysis and Characterization*. 2008, **13**(4), pp.292-301.
217. Meegan, J.E. and Aggeli, A. and Boden, N. and Brydson, R. and Brown, A.P. and Carrick, L. and Brough, A.R. and Hussain, A. and Ansell, R.J. Designed Self-Assembled β -Sheet Peptide Fibrils as Templates for Silica Nanotubes. *Advanced Functional Materials*. 2004, **14**(1), pp.31-37.
218. Adler-Abramovich, L. and Reches, M. and Sedman, V.L. and Allen, S. and Tendler, S.J. and Gazit, E. Thermal and chemical stability of diphenylalanine peptide nanotubes: implications for nanotechnological applications. *Langmuir*. 2006, **22**(3), pp.1313-1320.
219. Ito, Y. and Hasuda, H. and Kamitakahara, M. and Ohtsuki, C. and Tanihara, M. and Kang, I.-K. and Kwon, O.H. A composite of hydroxyapatite with electrospun biodegradable nanofibers as a tissue engineering material. *Journal of bioscience and bioengineering*. 2005, **100**(1), pp.43-49.
220. Rodríguez, K. and Renneckar, S. and Gatenholm, P. Biomimetic calcium phosphate crystal mineralization on electrospun cellulose-based scaffolds. *ACS applied materials & interfaces*. 2011, **3**(3), pp.681-689.
221. Liu, X. and Smith, L.A. and Hu, J. and Ma, P.X. Biomimetic nanofibrous gelatin/apatite composite scaffolds for bone tissue engineering. *Biomaterials*. 2009, **30**(12), pp.2252-2258.
222. Bittiger, H. and Marchessault, R. and Niegisch, W. Crystal structure of poly- ϵ -caprolactone. *Acta Crystallographica Section B: Structural Crystallography and Crystal Chemistry*. 1970, **26**(12), pp.1923-1927.
223. Baji, A. and Wong, S.C. and Liu, T. and Li, T. and Srivatsan, T. Morphological and X-ray diffraction studies of crystalline hydroxyapatite-reinforced polycaprolactone. *Journal of Biomedical Materials Research Part B: Applied Biomaterials*. 2007, **81**(2), pp.343-350.
224. Addadi, L. and Weiner, S. Control and design principles in biological mineralization. *Angewandte Chemie International Edition in English*. 1992, **31**(2), pp.153-169.
225. Hunter, G.K. and Kyle, C.L. and Goldberg, H.A. Modulation of crystal formation by bone phosphoproteins: structural specificity of the osteopontin-mediated inhibition of hydroxyapatite formation. *Biochemical Journal*. 1994, **300**(3), pp.723-728.

